Development of an *in-vitro* epithelial-myofibroblast intestinal model

Jamie Patient BSc

Thesis submitted to the University of Nottingham for the degree of Doctor of Philosophy

September 2015

Abstract

In vitro studies of drug permeability are traditionally carried out using cultured monolayers of epithelial cell lines grown on semi permeable membranes. Caco-2 cells, which are colon-derived, spontaneously form polarised cell layers when cultured in vitro which are akin to an epithelium of enterocyte-like cells. The Caco-2 model has been developed as a powerful *in vitro* tool in the early assessment of human drug permeability and is even approved by regulatory agencies for biowaver applications (i.e. *in vitro* tests in lieu of *in vivo* animal experiments).

As Caco-2 cells are derived from colon tissue they represent a more formidable barrier to drug absorption than the upper regions of the intestine which is where the majority of oral drugs permeate into the body. Whilst the Caco-2 model, alongside other *in vitro* methods, has provided a significant means to understand the mechanics of drug permeability. Many researchers have sought to improve upon the existing unicellular model; it is hoped that this will result in a more relevant and predictive model for researchers to test new drugs but also to dissect cellular cross talk and to probe cell-matrix interactions.

Myofibroblasts are a niche cell type located subjacent to epithelial tissues which regulate the integrity, growth and differentiation of the overlying epithelium. In this study the co-culture of human epithelial cell lines with a myofibroblast cell line, CCD-18co, were investigated to study how myofibroblasts influence the barrier integrity of epithelia in vivo. Additionally, nanofibre scaffolds produced by electrospinning were explored as 3-dimensional and topographically relevant cell scaffolds to support the growth of intestinal cells in vitro.

In a traditional transwell format, cultured epithelial lines Caco-2 (intestinal), HT-29 (intestinal) and Calu-3 (airway) in co-cultures with CCD-18co revealed cell-line specific response with respect to the modulation of barrier integrity. The mechanism of the

modulation was confirmed to be mediated through paracrine signalling by using myofibroblast conditioned media.

Fibre scaffolds which mimic the fibrillar nature of the extra cellular matrix and basement membrane were produced by electrospinning using the polymer, poly (ethylene terephthalate). Nanofibre scaffolds were characterised and further optimised for cell culture with surface coating with collagen to achieve adequate cell attachment and confluence. Work was also conducted to incorporate villi architectures into the fibre scaffolds; the potential of this ambition was investigated by using models produced by rapid prototyping. These models, which demonstrated good fidelity with the actual villi dimensions found *in vivo,* were used during the electrospinning process to shape the polymer scaffolds towards the geometry found in intestinal tissue.

A number of molecular tracers and model drug compounds were used to evaluate the permeability profiles of Caco-2 monocultures, Caco-2/CCD-18co co-cultures cultured on the two different culture substrates in addition to the assessment of resected porcine intestinal tissue sections. Caco-2 cells and Caco-2/CCD-18co co-cultures grown on nanofibre substrates were found to have lower electrical resistance and higher permeability properties than their transwell equivalents. Caco-2/CCD-18co co-cultures on conventional transwell inserts demonstrated a permeability profile closer to the resected porcine tissue and reported human tissue values than the conventional Caco-2 model whilst maintaining p-glycoprotein assay sensitivity.

This work forms a solid foundation for further research into the role of myofibroblasts in epithelial cell function and in the development of more predictive *in vitro* cell models for widespread scientific research.

Acknowledgements

Firstly I must acknowledge my university supervisors Felicity, Amir, Lisa, Phil and Clive. Your guidance and supervision have been essential in my development as a scientist and also as an individual. You have made my research experience exhilarating and demanding, in equal measure. I would also like to thank Kate, Christer and Bertil (AstraZeneca, UK & Sweden) for their input, training and guidance with this project. It has been invaluable to have some industrial perspective within this research. I would like to show immense gratitude and thanks to Denise Christie and Ian Ward of the School of Life Sciences Imaging Advanced Microscopy Unit, Queens Medical Centre for training and general day to day assistance in transmission electron and confocal microscopy. Thanks also to Dr David Scurr (Laboratory of Biophysics and Surface Analysis, School of Pharmacy, University of Nottingham) for help with ToF-SIMs data acquisition, subsequent data analysis and general discussion regarding my work. I would also like to thank Paul Cooling and Christy Grainger-Boultby (Boots Science Building) for all their assistance and training with HPLC and SEM over the years.

Thanks to all the members of the tissue engineering group, both the academic/ technical staff and students, past and present. It's been a hugely stimulating environment to work in and real pleasure to know you all. I'd also like to express my appreciation to Dr Joel Segal (Manufacturing Engineering group, University of Nottingham) and project student Sophie Luckhurst for their collaboration and hard work regarding the villi-former work and all the associated discussions (scientific or not!)

Members the Targeted Therapeutics Centre for Doctoral Training past and present for all the friendship, help and guidance over the years. Special thanks to Claudia Matz for all the organisation and support she has given me throughout my studies.

To my CDT colleagues (Naim, Lee, Kathryn, Andreea and Francesco) thank you for the friendship, the laughs and making the last 4 years. When is the next party? Very special thanks must go to my good friend and colleague Dr Saif Shubber for significant theoretical discussions regarding this work and also for help with confocal microscopy.

To all of my family and friends, thank you for being there, during the good times and the bad. Let the good times roll!

This thesis is dedicated to my father. Your thirst for knowledge and your perspective on life continue to and will always be a perpetual source of inspiration.

This work was funded by the EPSRC and AstraZeneca EP/I01375X/1.

“So in the end, was it worth it? Jesus Christ. How irreparably changed my life has become. It's always the last day of summer and I've been left out in the cold with no door to get back in. I'll grant you I've had more than my share of poignant moments. Life passes most people by while they're making grand plans for it. Throughout my lifetime, I've left pieces of my heart here and there. And now, there's almost not enough to stay alive. But I force a smile, knowing that my ambition far exceeded my talent. There are no more white horses or pretty ladies at my door”.

George Jung

Table of Contents

Figures

Tables

Equations

Abbreviations

AB/AM - Antibiotic/Antimycotic solution

ADME - Absorption, Distribution, Metabolism and Excretion

ALI - Air-Liquid Interface

α-SMA - Alpha- Smooth Muscle Actin

BCS - Biopharmaceutics Classification System

Caco-2 - Colorectal Adenocarcinoma Epithelial Cell

DAPI - 4'6-diamino-2-phenylindole

DMEM - Dulbecco's Modified Eagles Medium

DMSO - Dimethyl Sulfoxide

EDTA - Ethylenediamine-tetraacetic acid

FAE - Follicle Associated Epithelium

FBS - Foetal Bovine Serum

HBSS - Hanks Balanced Salt Solution

HEPES - 4-(2-hydroxyethyl)-1-piperazineethanesulfonic acid

HMDS - Hexamethyldisilazane

HTS- High Throughput Screening

MFCM- Myofibroblast conditioned media

MFs - Myofibroblasts

NBF - 10 % Neutral buffered formalin

IMS - Industrial Methylated Spirits (denatured ethanol)

MDCK - Madin-Darby canine Kidney Cells

PBS - Phosphate buffered saline

PET - Poly (ethylene terephthalate)

PFA - Paraformaldehyde

RPM - Revolutions per Minute

SEM - Scanning Electron Microscopy

TEM - Transmission Electron Microscopy

TEER - Trans-epithelial Electrical Resistance

TFA- Trifluroacetic acid

ZO-1 - Zona Occludens 1

1. General Introduction

The gastro-intestinal (GI) tract is a specialised organ that catalyses the breakdown of ingested material, absorbs nutrients and removes indigestible waste. By virtue of these functions the GI tract plays a fundamental role in the processing and absorption of orally administered therapeutics. It therefore stands to reason that understanding the anatomy and physiology of the barrier that the GI tract imposes on the external environment and how molecules are able to navigate across it is vitally important to aid the design and development of new medicines.

Given the growing cost of research and development for new drugs (Figure 1.1) there is an ever greater onus, where possible, for expediting the development of new medicines. It is widely acknowledged that a large proportion of compounds identified through high throughput screening (HTS) and rational drug design are poorly soluble in water or demonstrate poor permeability profiles[1]. Both the pharmaceutical industry and academia

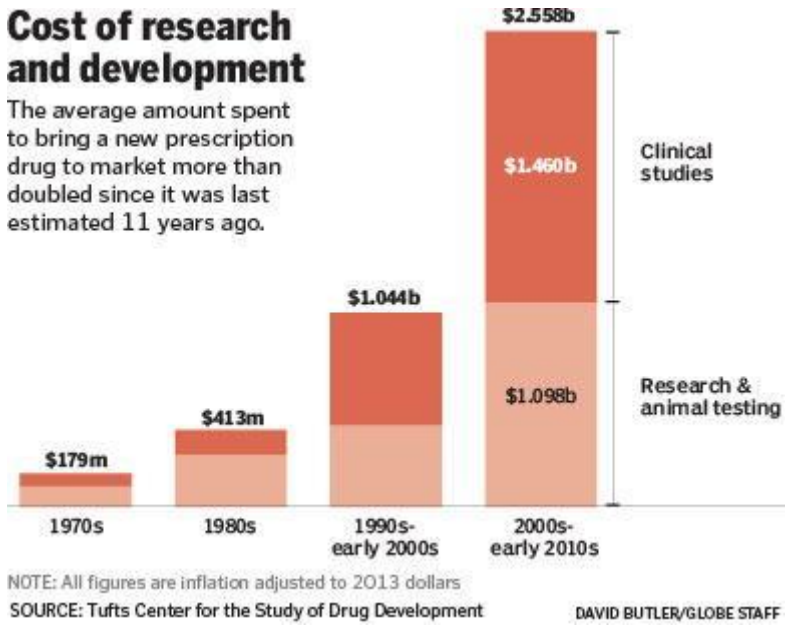

Figure 1.1The growing cost of bringing medicines to market. The cost of bringing new medicines to market has steadily increased over the last 40 years with a substantial amount of money being spent in the preclinical stages of development. Source BostonGlobe[2]

have sought to alleviate the problems encountered with absorption, distribution, metabolism and excretion (ADME) through advanced formulation and drug delivery strategies. It is hypothesised that should obstacles to solubility and permeability be overcome then this will help curb the rate of lead compound attrition during development. Despite considerable advances in alternative drug delivery technologies, orally formulated medicines remain dominant in the market; in 2014, 19 of 41 newly FDA approved drugs were formulated for oral delivery[3]. In light of this strategy it would be remiss not to ensure that *in vitro* assays to evaluate drug permeability and formulation performance as predictive as possible, allowing more informed decisions to be made in the early stages of pharmaceutical research.

The oral delivery of drugs has always been and will likely remain the most widely used route for the delivery of therapeutics. It is therefore not surprising that the pharmaceutical research and development process is structured for the development of drugs that are orally available. Several methods are used to assess oral drug permeability; the most widely used and cited method is the monolayer method using Caco-2 cells cultured on hanging inserts[4-7]. This method is blessed with simplicity and utility that has earned it widespread approval from industry, in academic circles and also by regulatory bodies as a useful *in vitro* tool to predict oral drug absorption in the GI tract[8-10]. Despite its obvious value, it has several drawbacks which will be discussed in detail later in this chapter. Much of the current research into this area focuses on manipulation and modulation of this model through co-culturing with different cell types and utilising new and architecturally relevant scaffold technologies[11-19]. In addition to these strategies there have also been some attempts to utilise new cell types (existing cell lines, genetically modified cell lines, primary cells and iPS cells) with mixed success[20-24].

1.1 Anatomy & Physiology of the Intestine

1.1.1 General anatomy and physiology

The primary function of the intestines is the continuation of digestion of ingested material, the selective absorption of nutrients across the epithelium and facilitating the removal of indigestible material. The small intestine is the foremost site for absorption of nutrients and drugs along the GI tract. The colon also plays a role in the absorption of drugs and for oral controlled release formulations colonic absorption is likely to be highly relevant[25]. From a physiological perspective however the colon functions primarily in the absorption of water. The small intestine itself is segmented into three major sections; the duodenum, the jejunum and the ileum. The intestinal tract has a relatively consistent cross sectional anatomy (Figure 1.2) with four defined tissue layers. The serosa is a visceral membrane found on the external surface of all organs found within body cavities. The muscularis propria is composed of dual layers of longitudinal and circular smooth muscle that are responsible for the peristaltic movements of the gut and also aid the mixing of the intestinal contents. The submucosa is a connective tissue layer that supports the mucosa and adjoins it to both the muscularis propria and serosa. The mucosa is the inner most layer which is exposed to the gut lumen and its contents. The mucosa can be further defined into the epithelium, the lamina propria and the muscularis mucosae.

As the contents of the stomach (known as chyme) is emptied into the duodenum it is mixed with secretions from both the liver and the pancreas. As the chyme moves through the jejunum and ileum it is subjected to further mixing and enzymatic degradation. The mixing of the chyme with enzymatic juices is encouraged by deep circular folds (known as plicae circulares) within intestinal wall. The spiralling actions caused by these deeps folds allow the chyme to have extensive interaction with the epithelium which facilitates the absorption process.

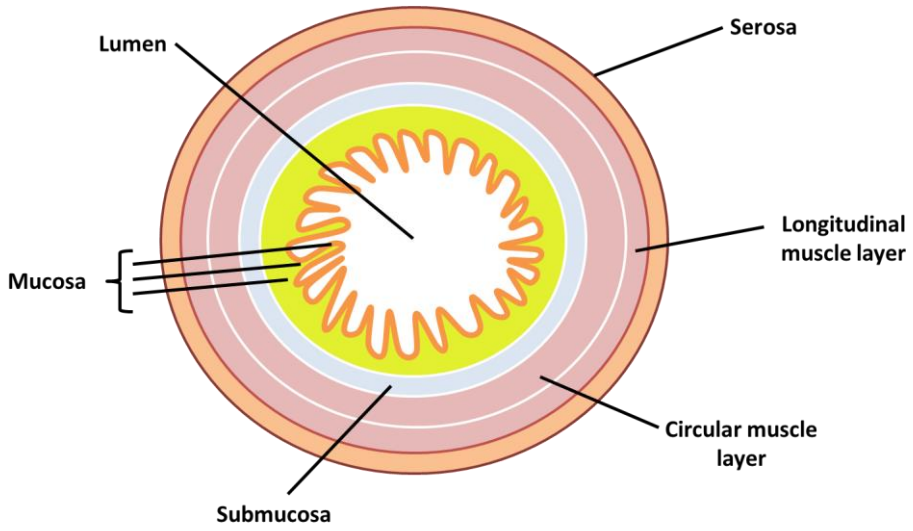

Figure 1.2 Anatomy of the intestinal tract. A cross sectional view of the intestinal tract reveals four distinct layers; The serosa, the muscularis propria (muscle layers), the submucosa and the mucosa. The folds (plicae) within the wall are depicted in orange.

The lining of the intestine has well defined morphological features which enhance absorption of the gut contents from the lumen across the epithelial barrier and into the body. The surface of the small intestine is covered in leaf-like projections called villi. These are approximately 0.5-1.5 mm in height depending on their location along the small intestine[26,27]. They dramatically increase the surface area of the small intestine which maximises the surface area available for absorption.

1.1.2 The villi-crypt axis

The villi-crypt unit can be considered as the individual functional unit of the intestinal mucosa (Figure 1.3). The crypts of Lieberkühn are the small cylindrical pits which can be found at the base of the villi which project into the gut lumen. Within the crypts resides the stem cell niche which is responsible for maintaining the rapid renewal of the intestinal epithelium, a process which takes place every 3-4 days[28]. Adjacent to the epithelium is the lamina propria where the supportive mesenchymal cells reside.

Mesenchymal cells, namely sub-epithelial intestinal myofibroblasts (ISEMFs) play a crucial role in supporting the epithelium through initial embryonic development and morphogenesis as well as during differentiation, inflammation and repair[30-37]. As cells migrate along the crypt towards the villus they are exposed to various gradients of cytokines, secreted factors and cell signalling pathways such as Notch, Wnt and BMP. These signalling pathways ultimately decide the fate of the cells as they migrate along the crypt-villous axis. As a result of this the epithelial cells which line the crypt and lower villi can be considered less differentiated than their villi-tip counterparts.

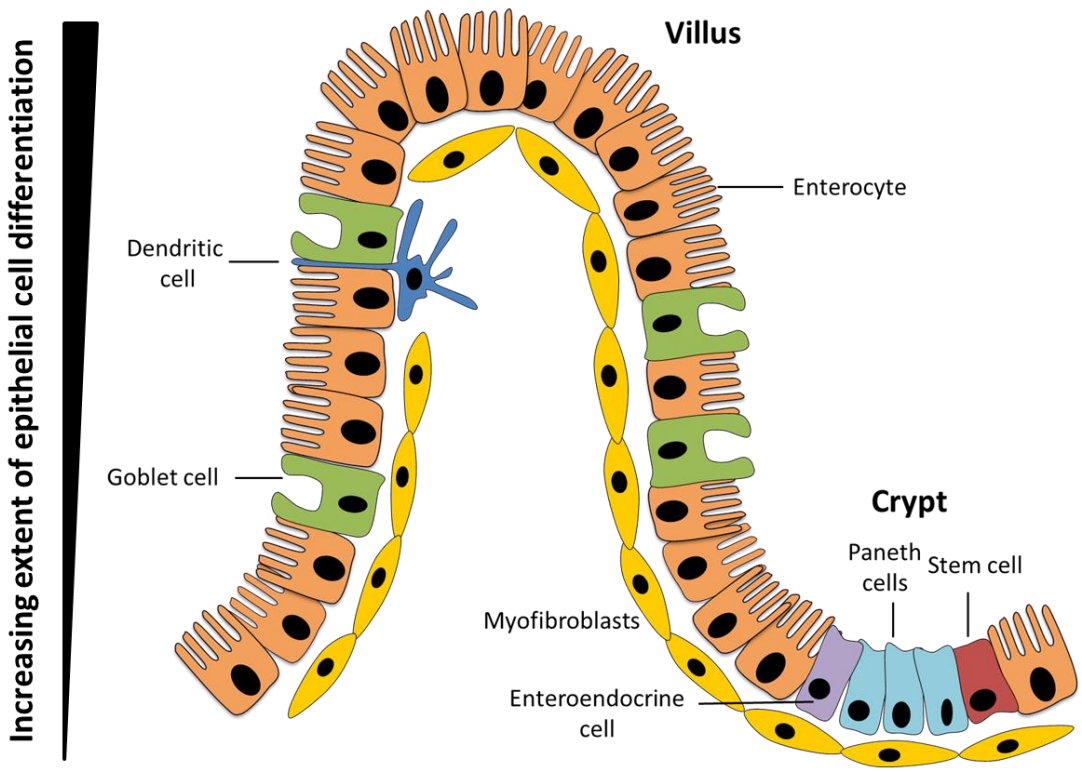

Figure 1.3 Longitudinal cross section of the villi-crypt axis.

The villi-crypt can be considered the funcitonal unit of the intestine. The epithelium is composed of several cell types which all contribute to the barrier functiuon of the tissue. The underlying lamina propria contains many supportive cell types, such as myofibroblasts, in addition to a rich vasclar and lymphatric network. Adapted from Abreu *et al*.,[29].

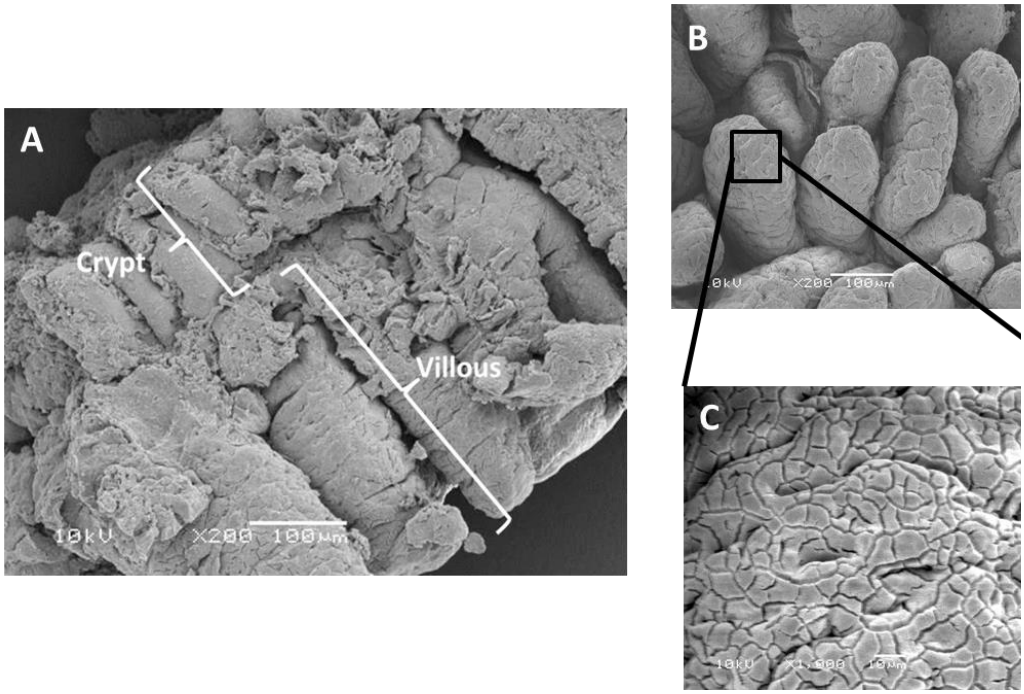

Figure 1.4 Intestinal villi architecture. Representative scanning electron micrographs of decellularised porcine intestine. (**A**) A cross section of the intestinal mucosa displaying the villi and crypt regions on the intestinal mucosa. (**B**) A birds- eye-view of the intestinal villi structures from the ileum showing the finger like structures which project into the lumen. (**C**) A surface view of the epithelium which covers the surface of the villi structures and forms a barrier to the gut contents.

1.1.3 Cell Types of the Intestinal Epithelium

The villi are clad with multiple epithelial cell types, the most abundant of which is the absorptive columnar epithelial cell or enterocyte. The second most prevalent is the goblet cell but in addition to these two core cell types there are also the enteroendocrine and Paneth cells. These four principal intestinal cell types are highly polarised cells which exhibit distinct apical and basolateral compartmentalisation of organelles. The cells arise from multipotent stem cell populations found near the bottom of the crypts of Lieberkühn (Figure 1.3). With the exception of Paneth cells all the other epithelial lineages differentiate as they migrate up the crypt, Paneth cells differentiate as they journey to the base of each crypt[38].

1.1.3.1. Enterocytes

Absorptive enterocytes are the fundamental cells of the intestinal mucosa responsible for absorption and are essential to the barrier integrity of the epithelium. The morphological

and functional markers of a well differentiated enterocyte include a microvilli-brush border, well defined structural cell hyperpolarisation with apical tight junction expression, high brush border enzyme activity (alkaline phosphatase, sucrase and aminopeptidase) in addition to functional transporter expression on both apical and basolateral membranes[28]. The absorption of molecules can occur through two primary routes, through the cell via the 'transcellular' pathway which includes several different transport mechanisms and the 'paracellular' route which is size and charge selective route between adjacent epithelial cells governed by the apical tight junctional complexes.

1.1.3.2. Goblet Cells

The second most prevalent cell type within the intestinal epithelium is the mucus producing goblet cell. Goblet cells produce a variety of mucins[39] which contribute to the protective mucous layer on the apical surface of the intestinal epithelium[40].

1.1.3.3. Enteroendocrine cells

Enteroendocrine cells are a population of various specialised endocrine cells found throughout the entire gastrointestinal tract. Their primary function involves the secretion of hormonal factors both as systemic mediators and locally acting agents which can initiate responses to the enteric nerve system[41].

1.1.3.4. Paneth cells

Paneth cells have secretory functionality and reside in clustered groups at the bottom of the crypts found exclusively in the small intestine[42]. Like goblet cells they contain large secretory granules however these granules contain a huge array of proteins and peptides, many of which have antimicrobial activity[43]. The antimicrobial proteins are either constitutively expressed or transcriptionally induced and form a crypt-protective secretion which helps contribute to the antimicrobial nature of the entire mucosal barrier[43]. Unlike

other cells which exfoliate from the villus, Paneth cells are removed after roughly 21 days by phagocytosis[44].

1.1.4 Cells of the lamina propria

The lamina propria is subjacent to the intestinal epithelium and is abundant in multiple cell types. It also contains a rich network of vascular and lymphatic vessels which absorb digested material. In the interest of being concise the focus of the following section will exclude the white blood cell and endothelial elements of the lamina propria. For an in depth evaluation beyond the scope of this thesis the reader is directed towards the reviews by Powell *et al*.,[33] and Hunyady *et al*.[45].

1.1.4.1. Myofibroblasts

Myofibroblasts (MFs) reside just below the basal lamina of the epithelium and can be found along the entire length of the GI tract, all the way from the oesophagus to the anus[46]. They exhibit fibroblast morphology and form a syncytial network underneath the overlying epithelium which communicates via gap junctions between neighbouring cells. Myofibroblasts are named as a result of displaying both the attributes and morphology of normal fibroblasts. This is coupled with the similarity in the expression of protein filaments akin to those of smooth muscle cells; specifically the expression of the actin isoform, alpha-smooth muscle actin (α-SMA)[30,32,46-48]. It has been suggested that MFs have multiple functions and play a crucial role in tissue organogenesis, differentiation, inflammation, repair and tumorigenesis.

Myofibroblasts secrete an extensive arsenal of chemical mediators in addition to expressing the complementary receptors for many of these secreted ligands[30]. This alone demonstrates a clear ability for MFs to signal in a paracrine fashion and that such communication can occur in both directions, between the underlying myofibroblasts network to the overlying

epithelium and also with other cells within the lamina propria[32]. This allows dynamic control over the entire mucosal microenvironment which can be controlled and propagated by MFs.

The MFs form a 3 dimensional cellular network within each villus (Figure 1.3), this anatomical location not only acts as a supportive skeleton to the villus structure but has also been proposed to influence the absorption and transportation of nutrients through coordinated contraction and shape conversion (from flat to stellate morphology)[46] in response to chemical and mechanical stimuli[49].

1.1.4.2. Pericytes

Pericytes are vascular, α-SMA positive smooth muscle cells which encase capillaries and were first described by Rouget in 1873[50]. The cells express proteins for the endothelial basement membrane and contribute to angiogenesis and revascularisation[33]. Like myofibroblasts, pericytes interact with surrounding cells through paracrine signalling and are able to elicit control over the contractility and permeability of the capillary network.

The relationship between pericytes and the endothelium is analogous to that of myofibroblasts and the epithelium. In addition to sharing similar molecular markers they also behave and respond to molecular signals in a comparable fashion. It has been suggested that they may have a common embryonic origin and are likely to have similar functions in both health and disease[33].

1.1.4.3. Fibroblasts

Fibroblasts are a huge and varied population of structural cell types found throughout the body. Their primary function is to produce extracellular matrix (ECM) for normal tissue function and also during damage and repair[51]. In addition to structural support for tissues they are also key players in tissue homeostasis, constantly sensing and responding to

physical and chemical stimuli within their environment and are thus intimately involved in almost all intestinal tissue functions.

1.2 Routes of intestinal absorption

It is generally accepted that drugs permeate the intestinal barrier via passive diffusion or through protein facilitated (carrier mediated) transport (Figure 1.5). There has been contention by leading scientists over the contribution of each particular type of drug transport process (i.e. passive diffusion versus any protein mediated transport across lipid bilayers) to the overall drug absorption process[52-57]. It is widely accepted that drugs permeate cellular barriers via these two aforementioned pathways but the contribution (or lack thereof) of passive diffusion has since become a matter of controversy. The traditional belief is that molecules, based mainly on their physicochemical properties (such as lipophilicity, pKa, molecular size, shape or flexibility), are able to traverse epithelial barriers via passive permeability by either partitioning through the cell lipid bilayer or navigating via the paracellular spaces between adjoining cells. The ability of drug to move directly

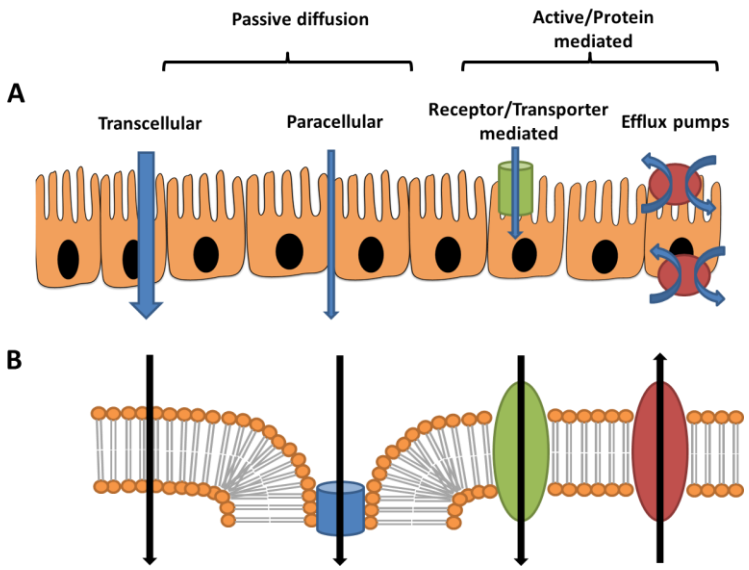

Figure 1.5 Routes of absorption across epithelial tissues. (A) Cellular view and (B) membrane view of the various parallel pathways involved in absorption of molecules across the intestine. Passive diffusion can occur via transcellular and paracellular routes which are usually governed by the physicochemical properties of the drug. Active (carrier or endocytosis mediated) transport is also plays a significant role in the movement of drugs, especially in active efflux processes.

through cell membrane bilayers can be based not only on its lipophilicity but also whether it is in an ionised form or not (as determined by the environment pH and the pKa of the molecule). Ionised or very hydrophilic drugs therefore demonstrate poor transcellular permeability profiles due to their inability to distribute into the lipid bilayer. Hydrophilic small molecule drugs are absorbed via the paracellular route between neighbouring epithelial cells, a process regulated by apical tight junctions. These protein complexes, which seal the entrances to the intracellular space, are fundamental to the barrier performance of epithelial tissues in addition to acting as a physical separation of apical membrane components from those found on the basolateral side of polarised epithelial cells[58,59].

1.2.1 Tight junctions and the paracellular pathway

Tight junctions (TJs) constitute the major barrier to the movement of ions and molecules via the paracellular pathway of absorption[60]. At a molecular level the apical TJ is composed of three families of transmembrane proteins; occludins, claudins and junctions adhesion

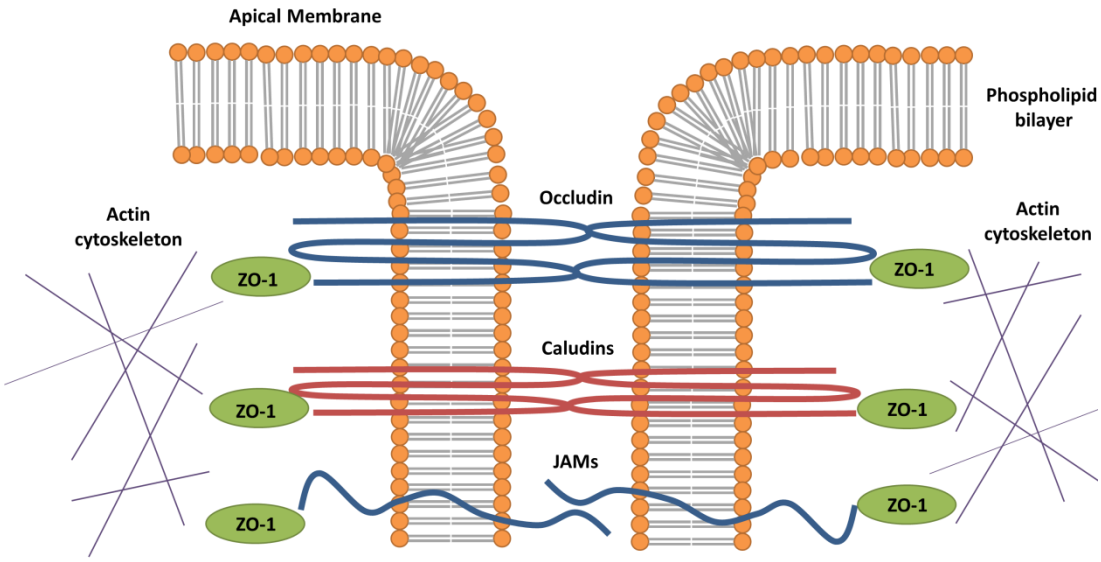

Figure 1.6 Simple molecular representation of the apical tight junction. Molecular components of the apical tight junction can be divided into 3 families. The three families of tight junction transmembranes domains are the occludins, claudins and junction adhesion molecules (JAMs). Zona Occludens (1, 2 and 3) alongside other proteins such as cingulin, MAG-1 and PATJ act as scaffold proteins which anchor the transmembrane proteins with the intercellular actin cytoskeleton. Adapted from Chiba *et al.*,[61].

molecules (JAMs)[61] (Figure 1.6). The TJ forms the most apical adhesion point between neighbouring epithelial cells and form 'kissing points' at which the intercellular space is diminished into small, size and charge restrictive pores in the extracellular loops of the transmembrane domains[61]. The sealing of the paracellular space by various contact points produced by the protein interactions is thought to be in part responsible for the variation in the barrier properties of different epithelial tissues. Specifically the type of claudins expressed in the tight junction[58,61] and the number of junctional strand contact points[60,62,63] are proposed to alter the pore size and resistance of the junctional complex. Differential expression of claudins along villi-crypt axis of the small and large intestine in mice with specific expression profiles demonstrated for the villi compared to the crypt regions[61] as well as across different epithelial tissues[58]. Different claudin compositions found in the TJs results in changes in the size and charge selectivity (as a result of variation in amino acid side chains) of the exposed extracellular loop domains which serve as the pores that enable the semi-permeable function of the TJ.

In addition to the membrane spanning proteins there are a variety of scaffold proteins which anchor the transmembrane proteins of the TJ complex to the intercellular actin cytoskeleton[64]. These include but are not limited to ZO-1, 2 and 3 and also cingulin, MAG1 and PATJ[60,64]. Collectively these proteins are key intracellular players in the formation and regulation of the tight junction.

1.2.2 Tight junction pore size

Different researchers have reported experimentally calculated pore sizes (often as ranges) for intestinal tissue and also intestinal cell lines based on the permeability of molecular tracers and mathematical modelling. Using a series of different molecular weight poly ethylene glycols Watson *et al.*, determined TJ pore size in Caco-2 and T84 (a metastatic lung-derived colonic epithelial cell) cultured epithelial cell lines to be biphasic in nature. They proposed a restrictive pore pathway dominating the paracellular pathway limiting molecules with a

radii of < ~4 Å [65] (4.5 Å and 4.3 Å for Caco-2 and T84 respectively). Their work also suggested a second pathway, a potentially non-specific 'leak' route, which enable molecules with radii >7.4 Å to permeate the paracellular route. This is in general agreement with other literature reporting T84 pore radii between 3.6-15 Å[66]. Knipp et al., calculated a Caco-2 pore radii of ~5.2 Å rising up to 14.6 Å in cell monolayers treated with TJ modulators palmitoyl-DL-carnitine (PC) (unknown mechanism) and the calcium chelator ethyleneglycol-*bis*-(*β*-aminethyl ether) -N, N, N', N'- tetraacetic acid (EGTA). Both of which are thought to 'open' the TJs without inducing damage/disruption. It was Philipa Claude who first suggested that TJs may exist in 'open' and 'closed' states, a hypothesis which might also explain overall TJ permeability[62].

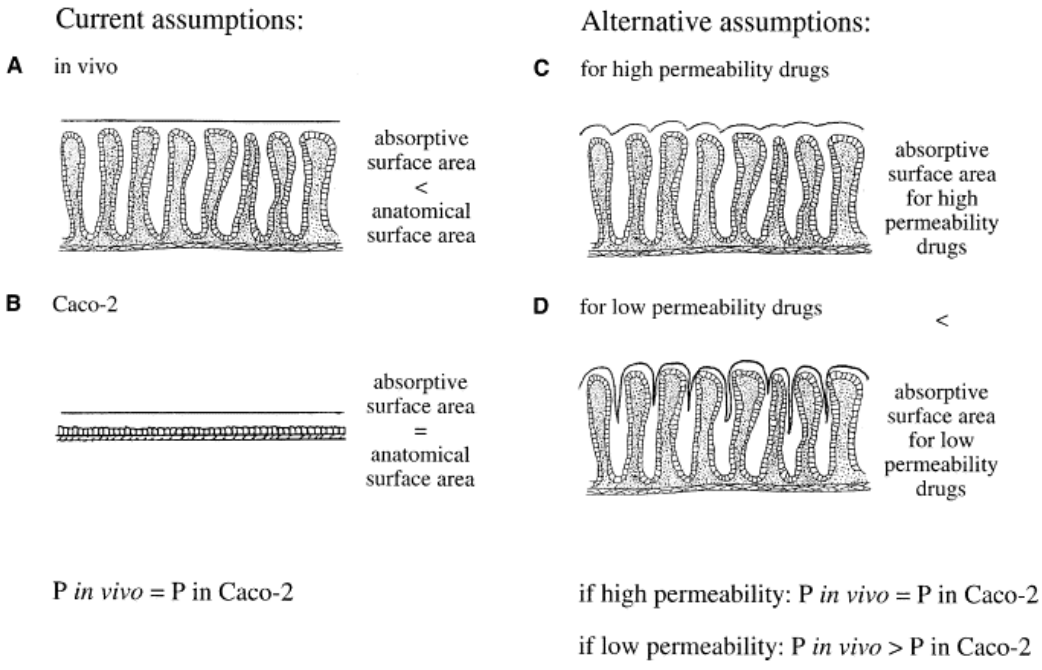

Figure 1.7 Comparing the absorptive surface area in Caco-2 versus the in vivo intestinal tissue for high and low permeability drugs

Artusson *et al*., proposed that variation observed between in high and low permeability drugs in Caco-2 monolayers and intestinal tissue was a direct result of the differences in anatomical surface area. (C) For high permeability drugs which permeate most via the villi tips a good correlation is observed between Caco-2 and intestinal tissue. (D) For low permeability drugs, which spend more time in the villi environment, are able to permeate 'leakier' regions on the villi and thus will demonstrate higher permeability *in vivo* than in Caco-2 monolayers. Taken from Artusson *et al*.,[7]

All of the calculated pore size values are comparable to proposed rat colon tissue paracellular pore radii of >11 Å[67] and human and rat perfusion models with TJ pore radii calculated as ~13 Å[68,69]. There is also *in vivo* evidence that the pore size increases down the villi-crypt axis with basal villi tight junctions representing the larger size pores (i.e. 10-15 Å), the villi tips having mainly small pores (< 6 Å) and the crypts (although mainly inaccessible to luminal contents) having pore sizes up to 60 Å[69]. This is in agreement with the postulation regarding the anatomical surface areas of cultured monolayers versus the *in vivo* tissue when explaining the correlation between high and low permeability drugs[7] (Figure 1.7).

1.2.3 Trans-epithelial Electrical Resistance (TEER) measurement of TJ integrity and barrier properties

Trans-epithelial electrical resistance (TEER) is a widely utilised quantitative technique to measure the barrier integrity of epithelial and endothelial tissues and cell monolayers. It can be used throughout the differentiation period of cells cultured on hanging well inserts to quantitatively measure the development of the barrier function of epithelial/endothelial tissues and TJ formation in cell monolayers. It is also utilised as an acceptance criteria for *in vitro* model assays, such as the Caco-2 permeability assay, to ensure consistency and assay quality control before experimental procedures. It can also be used as a non-invasive tool to continually monitor changes to barrier integrity throughout an experiment. In addition to monitoring the development of barrier tissues, changes in TEER are often used to characterise and quantitate damage to and restitution of, barrier integrity for *in vitro* toxicology and drug permeability studies of barrier tissues (e.g. skin[70,71], airway[70,72], gastrointestinal[5], blood brain barrier[73]).

The technique measures the electrical resistance of the tissue/monolayer by applying an alternating current across the tissue (to avoid cellular damage). The electrical resistance is measured in ohms (Ω) and usually recorded using chopstick style electrodes (Figure 1.8).

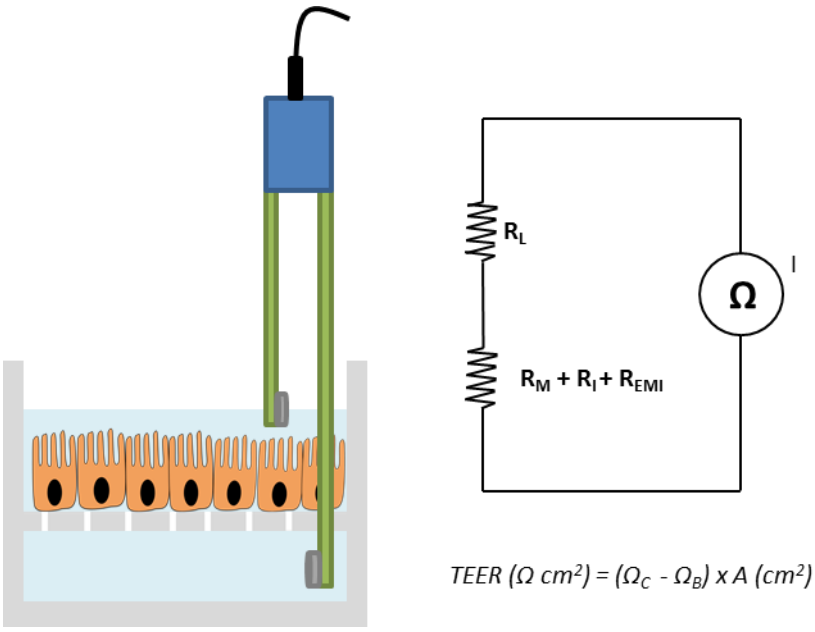

Figure 1.8 Trans-epithelial electrical resistance (TEER) of transwell inserts with chopstick electrodes. Electrical resistance is measured as the total resistance of the entire set-up; the resistance of the cell layer (R_L), the cell culture medium (R_M), the semipermeable membrane (R_I) and the electrode-medium interface (R_{EMI}). Adapted from Srinivasan *et al.*,[74] TEER is calculated by subtracting the resistance of a blank filter (Ω_B) from the resistance of the cell monolayer (Ω_C). This value is then multiplied by the exposed surface area (A).

The chopsticks are placed in the apical and basolateral chambers of a hanging insert which has been filled with a pre-heated blank medium (such as Hank's Balanced Salt Solution). The TEER can then be recorded when a steady reading is achieved. The resistance of a blank insert is then subtracted from the value and multiplied by the surface area of the semipermeable membrane.

TEER is used, like molecular permeability, to assess the barrier properties of *in vitro* model systems, such as Caco-2, and relate the barrier integrity to human tissues. TEER has been used extensively throughout the literature but what does it actually tell us about the barrier properties of a given tissue? TEER reflects the conductance of ions across the tissue/monolayer; this however is quite different from the flux of molecules down the paracellular route which is primarily governed by the TJs. Artusson was one of the first to caution any definitive relationship between TEER and molecular flux; he demonstrated that two clones of Caco-2 with significantly different TEER readings demonstrated no significant difference in the permeability coefficients for the paracellular permeant, mannitol[75]. Clearly

TEER readings displayed by *in vitro* systems can be compared to *ex vivo* tissue specimens as a measure of physiological similarity but as a stand-alone technique it cannot definitively conclude the permeability properties of a monolayer/tissue.

1.3 The Biopharmaceutics drug Classification System (BCS)

The Biopharmaceutics drug classification system (BCS) was proposed in 1994 and was used to estimate *in vivo* drug absorption[76]. The system recognised that drug dissolution and gastrointestinal permeability were the fundamental parameters controlling the rate and extent of drug absorption. By combining data collected from *in vitro* drug dissolution testing with intestinal membrane permeability (P_{eff}) (both animal[77,78] and human[79,80] were being explored at the time), a clear scientific basis was established for a scientific framework to classify drugs to set standards for *in vitro* evidence required for regulatory assessment. The BCS has since been widely accepted by industry, academic and regulatory bodies for the classification of oral medicines based on their aqueous solubility and intestinal permeability[81].

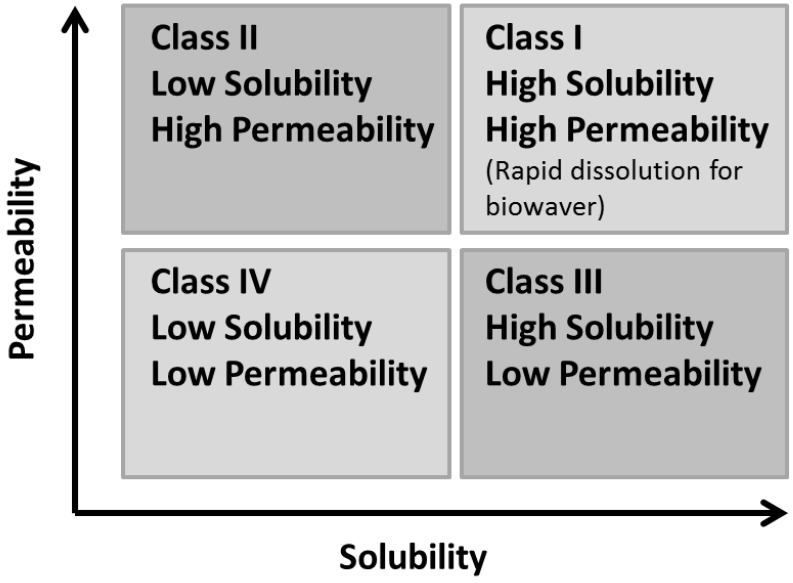

Figure 1.9 The biopharmaceutics classification system permeability-solubility classes.

The framework divides drugs into high/low solubility-permeability classes for immediate release products (Figure 1.9) and establishes conditions under which no in *vitro-in vivo* (IVIV) correlation can be expected (e.g. for low permeability drugs which display rapid dissolution). It can also indicate whether a simple dissolution test might be sufficient to ensure adequate bioavailability of a drug compound (e.g. where a drug reaches >85% dissolution in less than 15 mins – for very rapidly dissolving high solubility drugs). Each class has an associated "correlation expectation" which can guide researchers as to the IVIV correlation. The BCS has enabled a scenario whereby biowavers and bioequivalence studies for certain drugs can be approved from *in vitro* data[81,82]. This essentially means some *in vivo* tests can be avoided during the drug development process saving time, cost, and reducing animal experiments.

1.4 Current *In vitro* cell models of the intestine

Several models that aim to simulate the anatomy and physiology of the small intestine are have already been developed, ranging from the very simple artificial cell membranes and multicellular co-cultures to labour intensive *ex* and *in vivo* models. The overwhelming majority of models are concerned with drug permeability determination due to the key role the intestine plays in drug absorption in humans. A great deal has been learned from these models which in addition to functioning as predictive models of drug absorption have also furthered scientific knowledge of many of the poorly characterised biological process within the intestine. There is little doubt that further work in model and assay development within this area will allow us to explore cell biology and cellular interactions/crosstalk to greater depths and hopefully elucidate misunderstood and controversial biological processes.

Cell based models are probably the most widely utilised models of the small intestine. Models based on human primary cells/cell lines are preferable than cell lines derived from animals as there is quite often a lack biological relevance to humans.

The gold standard in in vitro cell based models is the Caco-2 monolayer. It is used primarily for the assessment of oral drug permeability *in vitro* and is a mainstay of both academic and industrial pharmaceutical research in oral drug permeability. In addition to the Caco-2 line there are various other cells lines which display appropriate morphology and physiology for drug permeability studies; these include but are not limited to; HT-29, MDCK and 2/4/A1 cells.

1.4.1 Epithelial cell lines

1.4.1.1. Caco-2

The Caco-2 cell line was originally isolated from a colon adenocarcinoma and established in culture by Fogh, Zweibaum and colleagues. They noted its unique spontaneous differentiation into enterocyte-like cells both in terms of morphology and functionality and were also capable of forming confluent monolayers when cultured *in vitro*[83]. Borchardt and colleagues postulated and demonstrated that the Caco-2 cell line could be used as a viable model to assess the intestinal permeability of drugs[84]. This work was then further elaborated upon namely by Per Artusson, amongst others, who established a correlation between Caco-2 drug permeability and oral drug absorption in humans[6].

The model requires culturing Caco-2 cells on transwell-style permeable supports for up to 15-21 days; by this time the cells have become polarised, fully confluent and express tight junctions, apical microvilli, brush border enzymes and protein transporters capable of some of the transportation processes akin to their *in vivo* counterparts[84]. Once the cells have matured to this extent then transport experiments can be conducted by the addition of a

compound into the apical chamber whilst sampling at the basolateral side over time (or vice versa). Whilst the Caco-2 model is regarded as the gold standard for drug permeability studies there are many limitations associated with this specific cell line.

The Caco-2 cell is very much like an absorptive enterocyte when cultured *in vitro*; however like other cell lines which have been immortalised, the responses observed from these cells may not be truly comparable to that of native cells *in vivo*. Furthermore the colonic epithelium is quite different to the small intestinal epithelium both functionally and morphologically, for example colonic epithelia demonstrate enhanced barrier integrity (as demonstrated by higher TEER values in cultured Caco-2 cells versus colonic & jejunal excised tissue segments[75] and other cell lines of different organ origin[8,20,85]). The expression of pharmaceutically relevant drug transporters in Caco-2 cells has been demonstrated[9,86], however it is generally conceded that the expression profiles for certain transporters, such as the apically expressed efflux transporter BCRP, are different in Caco-2 monolayers compared to the human jejunum[8,86]. This can limit the ability to predict whether drugs are substrates for efflux transporters and whether they have the potential for drug-drug interactions *in vivo*. It has also been shown that poorly permeating compounds, some actively transported drugs and low molecular weight hydrophilic compounds do not show ideal correlation in Caco-2 permeability studies compared with human absorption observed *in vivo*[9]. For example, poly (ethylene glycols) of varying molecular weight (which permeate via the paracellular route) demonstrate almost a 100-fold lower permeability in Caco-2 monolayers when compared with human absorption[7,75].

1.4.1.2. HT29

Many, if not all of the cell lines currently utilised for *in vitro* models of the small intestine are phenotypically absorptive, enterocyte like cells. Whilst they are the most abundant cell type within the intestinal epithelium, the absence of other cell types disregards their contribution to the integrity of the epithelial barrier.

The HT29 cell line, also derived from a human colorectal adenocarcinoma, is one of very few mucus producing goblet cell-like cell lines available to researchers. They can be investigated to help understand the importance of the mucus layer and glycocalyx (a layer of oligosaccharides and membrane glycoproteins which coats the cells) in drug absorption and disposition. Various sub clones of the HT29 cell line have been isolated, some of which have shown more favourable phenotypic traits such as a greater degree of cell homogeneity and high levels of mucus secretion. Wilkman et *al.,* noted that the HT29-H clone developed monolayers of multiple phenotypes, however the dominating cell type had a goblet cell morphology (approx. 80%) with apical mucin granules easily visualised by electron microscopy. The average thickness of the mucus layer was between 40-60 µm however it varied between 0-100 µm across the monolayer [87]. The authors also noted low TEER values (~50 Ω cm^2) and lower P_{app} (apparent permeability) values for the lipophilic drug testosterone (6 x 10^{-6} cm s^{-1} for the HT29-H monolayers compared to 35.3 x 10^{-6} cm s^{-1} for Caco-2). The low permeability of testosterone is significant because of the retardation of an otherwise highly permeable drug; this demonstrates the impact of the hydrophilic mucus layer on lipophilic drug disposition. Further attempts to select clones of the HT29 cell line which demonstrate more favourable characteristics has led to the development of methotrexate induced lineages which show increased mucus secretion. Two HT29-MTX clones produced increased TEER over the parent HT29 line (279 and 169 Ω cm^2 versus 15 Ω cm^2, respectively). More importantly both clones expressed MUC2[88] which is absent in the parent HT29 and is the major intestinal mucin [89].

1.4.1.3. 2/4/A1

2/4/A1 is a transformed cell line that originates from a foetal rat intestine. It was initially projected to help assess compounds that transport primarily through the paracellular transport route due to the fact that the 2/4/A1 monolayers form leakier monolayers, compared to Caco-2, when cultured *in vitro* [85]. The leakiness of the 2/4/A1 monolayer was

demonstrated by a low observed TEER reading (a plateau value of 25 ± 2.9 Ω cm^2) and the permeability of paracellular hydrophilic markers that more closely resembled that of a human intestine than the Caco-2 model[20]. Another benefit of this cell line is the relatively short cultivation time compared to Caco-2 cells (4 vs. 15-21 days). Despite these promising features over the conventional Caco-2 model it does not seem to have taken a foothold in mainstream research. It could be due to the fact that it displays less developed morphological characteristics (small and sparse microvilli, cuboidal cell shape etc.) as well as lacking some important drug transporters. These caveats have been attraibuted to the fact that the cell line was isolated from a foetal rat at a point when full intestinal differentiation had not occurred. Therefore other cell lines that are isolated from rats may offer a promising alternative to Caco-2 should they display the relevant features that are absent in in the 2/4/A1 line.

1.4.1.4. MDCK

Like 2/4/A1 cells, Madin-Darby Canine Kidney cells (MDCK) are of non-human origin. In addition to this they are also not intestinally derived. Despite this they differentiate into columnar epithelial cells when cultured on semi permeable membranes and share many of the common epithelial characteristics of the other aforementioned cell lines[90]. There has been a reported similarity in the apparent permeability values between the Caco-2 and MDCK cell lines, especially for passively absorbed compounds that showed high P_{app} values[91]. Like 2/4/A1 cells, the MDCK cell line has a short cultivation time, providing reliable results within 3 days of culture following an initial high seeding density[91]. Whilst the MDCK cell line provides a faster alternative to Caco-2 their non-human, non-organ specific origin is quite likely to make the expression profiles of pharmaceutically relevant transporters significantly different.

1.4.1.5. Intestinal primary and stem cells

The use of primary and stem cells in routine intestinal cultures, specifically for drug permeability studies, remains limited. Some reports have shown improved culture

conditions and characterisation of primary human intestinal cells[23,24] but the reported use for any kind of permeability studies are minimal[22,92,93]. In a recent paper Yin *et al*., developed a method for producing high purity intestinal stem cell populations[21] which will certainly drive forward intestinal research and may help future research into intestinal *in vitro* modelling.

Mitzutani *et al*., and Takenaka et al.; both present primary cell based or stem cell derived cell models which show significant promise for the future. Mitzuani *et al*. tested two commercially available primary intestinal cells and conducted some simple characterisation and comparison with Caco-2 demonstrating good functional activity of p-gp and high TEER readings (>1000 Ω cm^2). Takenaka and colleagues went further and developed a model using similarly derived human intestinal epithelial cells and evaluated the absorption of a number of compounds. With their model they were able to demonstrate a better correlation between experimental permeability (P_{app}) and reported human fraction absorbed values for 10 compounds than that established with Caco-2 monolayers[22]. This means the model should be more predictive as a predictive oral drug permeability tool. Despite this, experimental P_{app} values were still significantly lower than those obtained with human tissue segments and from perfuse loop systems[94-96].

Whilst the use of either primary or stem cell derived cultures may well prove to yield more relevant *in vitro* models in the future there are a myriad of issues that make their routine use very difficult such as high costs and labour intensive culture methods (including tridaily cell feeding[21]). Cell lines currently offer a far easier and inexpensive tool for high throughput *in vitro* modelling with comparable predictive power to the primary cell based models that have been currently developed.

1.4.2 Emerging cell models of the intestine

There are several emerging cell models of the intestine which epitomise the current attempts within the research field to recreate more sophisticated cell models of the intestine. The

following examples provide an insight into three different approaches; directed self-assembly, structural biomimicry and multi-cell co-cultures in 3D environments. Other cell models will be discussed in more detail throughout the thesis in the relevant experimental chapters.

The gut-on-a-chip model from the Ingber group[17,18] forms a part of the organs-on-chips project which aims to mimic the entire human physiology with connected, micro-engineered chip based 'organ's[97]. Kim *et al*., developed a Caco-2 based chip system which was capable of fluid flow across the apical and basolateral surface and also able to exert peristaltic-like strain upon the cells[18].

What is most significant is that Caco-2 cells appeared to undergo villi-like differentiation under these conditions and the authors were able to co-culture bacteria with Caco-2 without damage to the barrier integrity[18]. The authors report an increase in cell size compared to transwell cultures more akin to their *in vivo* counterparts (10µm versus 20-30µm in height)[18], improved mucus production (specific expression of MUC2, 3 & 17), villi-like structures with villi-crypt axis reconstitution (proliferative crypts and villi-crypt differentiation marker expression of Villin, KRKT20 & CEACAM1) and increased aminopeptidase and CYP450-3A4 expression[17]. The idea that Caco-2 is capable of undergoing 'villi-like' is slightly illogical considering that Caco-2 originate in the colon where there are no villi.

However given the drastically altered phenotype (enzyme expression, morphological changes and villi tissue markers) and villi-like organisation it appears to demonstrate the importance of environmental cues, specifically fluid flow (the authors note that the cyclic strain has little added benefit). It is possible that they have observed one of two phenomena common to Caco-2 and cultured epithelial cell lines. Epithelial cells in culture can experience a process called 'doming' whereby the cells, upon full differentiation into a tight and confluent epithelium, actively pump fluid into the basolateral space.

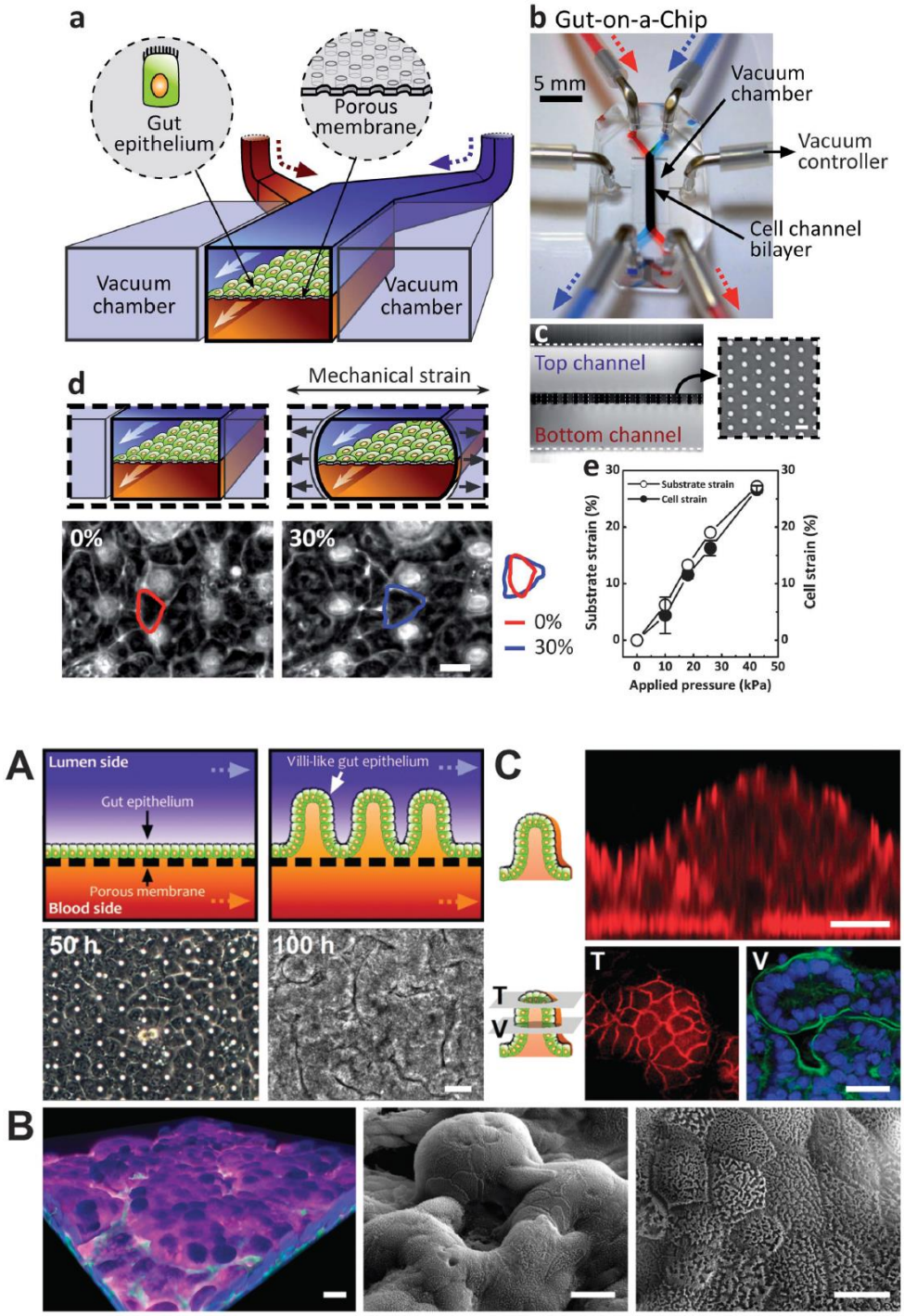

Figure 1.10. Human 'gut-on-a-chip' displays villi-like differentiation under perfused culture. Overview of the 'Lab-on-a-chip' gut project aiming to mimic the small intestinal epithelium. (a) The system uses micronized chip technology to produce intestinal models that utilise Caco-2 cells but exposes them to environmental cues such as apical & basolateral perfusion and vacuum chambers to mimic gut peristalsis. (A, B & C) Under these conditions Caco-2 cells have been shown to demonstrate 'villi-like' differentiation appearing to form the macroarchitectures of the small intestine in addition to altered expression profiles more akin to the small intestinal epithelium. Taken from Kim *et al*.,[17,18]

This results in the cells detaching from the surface and forming into dome structures[83,98]. However considering they use semi permeable supports within their chips (Figure 1.10) it is perhaps unlikely that this is the case, although pore size has been demonstrated to be an important factor in dome formation on permeable supports[99]. The other potential explanation (other than actual villi-like differentiation) is simply multi-layering of the cells, which is very common in epithelial cells from tumorigenic origin[5,100].

Research from the March group presents another attempt to recreate the small intestinal epithelium whilst still utilising Caco-2 (Figure 1.11). Using a sacrificial moulding process in series the authors produced a 3D hydrogel with accurate villi dimensions which could be seeded with Caco-2 epithelial cells to mimic the small intestinal mucosa. The authors observed lower TEER (~50 Ω cm^2) and more physiologically relevant permeability for one model drug, atenolol (The reported P_{app} value of ~8 $x10^{-6}$ cm s^{-1} using the 3D villous model compared with 15 $x10^{-6}$ cm s^{-1} for reported human P_{eff} values[94,95]). Whilst this was very promising they noticed in the case of rapidly absorbed drugs (in this case antipyrine) the hydrogel was a limiting barrier to permeability. The model in its current state is not compatible for all drugs and has not become established even though it perhaps represents a more predictive model for paracellular permeability. The current developments with this work has focused on the understanding of intestinal cellular behaviour and differentiation with Caco-2/HT-29 MTX co-cultures[101] and cultures for studying host-microbial interactions[102] rather than further developing the model for drug permeability screening. To that end they have been able to culture established microbial niches along a pseudo crypt-villous axis using their 3D hydrogel villous model to try and mimic the natural microenvironment found in the intestine *in vivo*.

In a very similar piece of work Kim *et al*., used the same technique as the March group to produce similar Caco-2 based models but were able to further demonstrate enhanced protection from bacterial infection through the expression of intestinal mucin, MUC17[103].

Pereira *et al*., present an example of *in vitro* multi-culture 3D model in an attempt to dissect the importance of stromal-epithelial interactions[14]. They present several iterations of a Caco-2/HT-29 MTX/CCD-18co model using transwell inserts and matrigel (a gelatinous mixture of proteins secreted by murine sarcoma cells) to make the model 3-dimensional (Figure 1.12). In all of their model iterations they present the epithelial cell component was seeded directly onto CCD-18co or onto CCD-18co embedded within matrigel. The authors noted decreased TEER when Caco-2 and co-cultures of Caco-2/HT-29 MTX were cultured with CCD-18co, which they attributed to direct interspacing of CCD-18co in-between the overlying epithelium. The observations of TEER changes were coupled with increased permeability to insulin compared to Caco-2 transwell cultures.

Research, both past and present, demonstrates a clear need to delve deeper to further understand the important roles each of the cells contribute to the intestinal tissue function the complex interplay that occurs between them. Cell models provide an important means to enable this and also, at the same time, facilitate the development of analytical tools to use for drug development

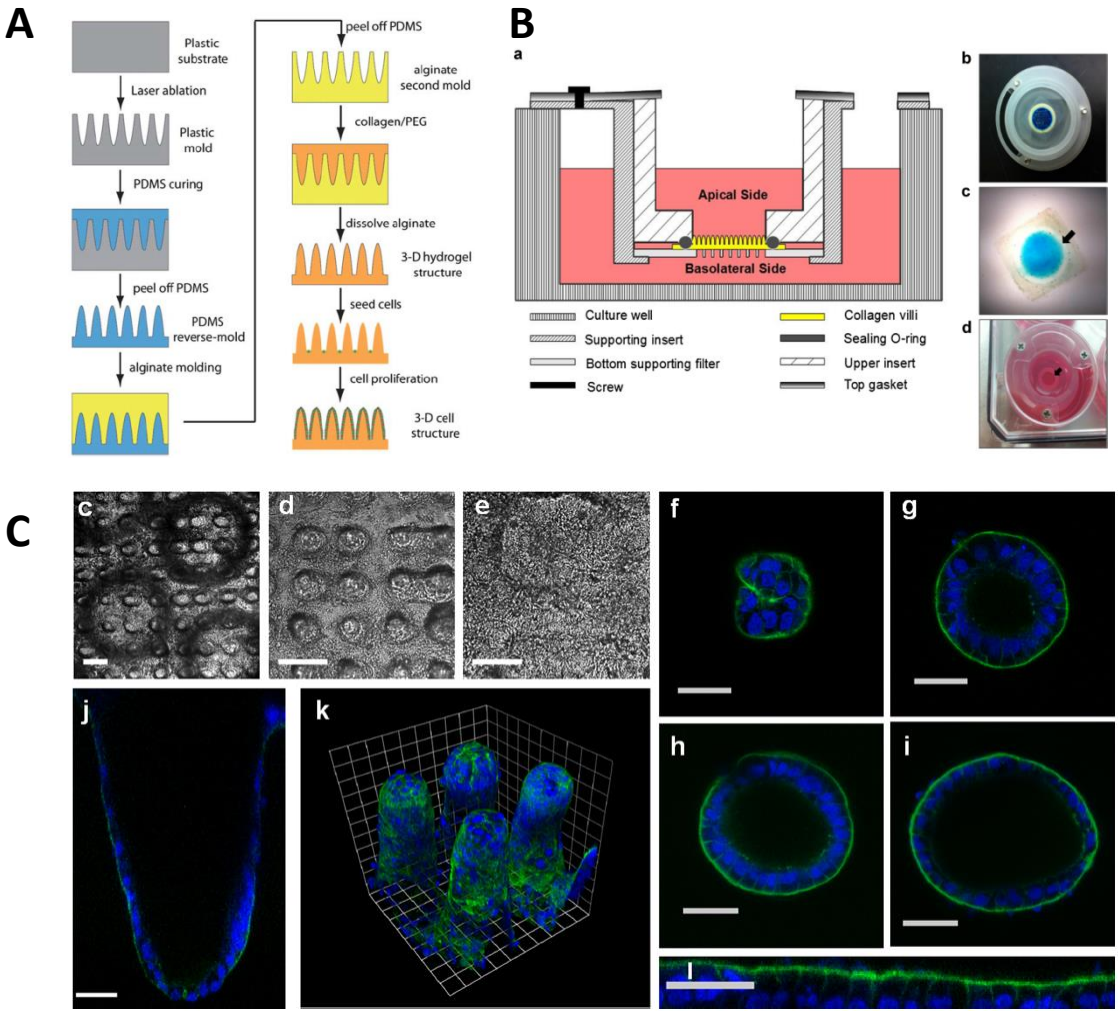

Figure 1.11. ***In vitro*** **3D human small intestinal villous model for drug permeability determination.** (A) The sacrifical molding process; a polymethacrylate (PMMA) mold is used to produce a polydimethysiloxane (PDMS) mold which is then used to create an alginate one which is subsequently used to create the collagen hydrogel. (B) The in house gasket for housing the 3D hydrogels. (C) (c-e) Phase contrast and (f-l) immunofluorescence images of the hydrogel based *in vitro* villous model which utilises Caco-2 on a hydrogel substrate produced by a sacrificial moulding process. The intricate villi structures are seeded with Caco-2 cells which can then be used with an in-house gasket system to study drug permeability. Cell nuclei (blue) and F-actin (green) can be visualised on the villi hydrogel. Taken from Sun *et al.*,[15] and Yu *et al.*,[12].

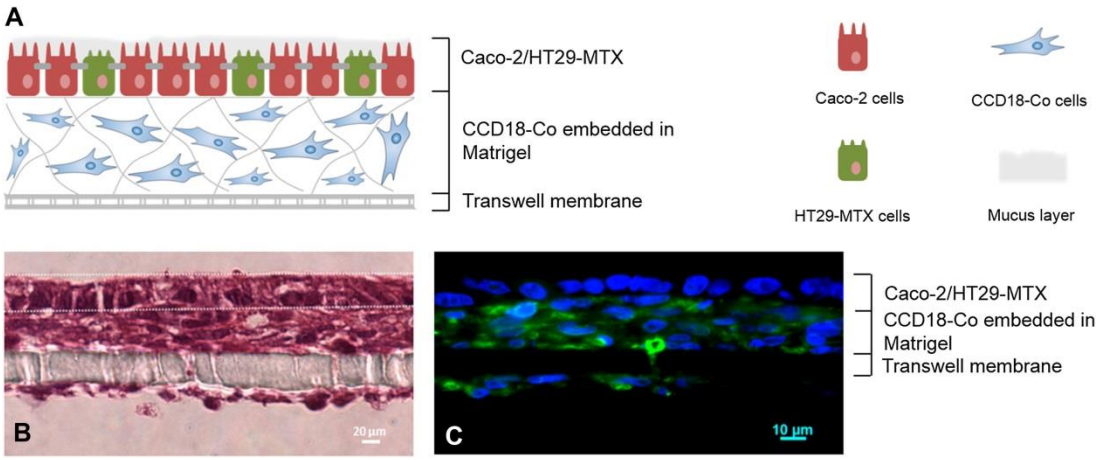

Figure 1.12. Dissecting stromal-epithelial interactions in a Caco-2/HT-29 MTX/CCD-18co tri-culture model. (A) Schematic representation of the triple-culture 3D model. (B) Haematoxylin and eosin stained paraffin embedded cross section. (C) Fibronectin expression (green) in a paraffin embedded immunostained cross section. Cell nuclei are stained with DAPI (blue).

.

2. General Materials and Methods

2.1 Materials

2.1.1 Cells and cell culture media components

Caco-2 (passage 10-30), Calu-3 (p34-50) and HT-29 (p11-35) cells were obtained from the Clinical Pathology laboratory, Queens Medical Centre, Nottingham. CCD-18co myofibroblasts (CRL-1459) were acquired from LGC Standards/American Type Culture Collection and used from passage 7-30.

Hanks balanced salt solution (HBSS, #H8264), foetal bovine serum (FBS, F9665) nutrient mixture F12 (HAMS-F12, #N6658), MEM non-essential amino acids (NEAA's, #M7145), antibiotic/antimycotic solution (10,000 U/mL penicillin, 10 mg/mL streptomycin and 25 ug/mL amphotericin B, #A5955), trypsin (#T4549), dimethyl sulphoxide (DMSO, #D2650) were all obtained from Sigma-Aldrich, UK.

Dulbecco's modified eagles medium (DMEM, #VX42430025), minimum eagles medium (MEM, #11095-080), penicillin/streptomycin (10,000 U/mL and 10 mg/mL respectively, #VX15070063), phosphate buffered saline (PBS, BR014G) were obtained from Gibco, Life Technologies.

2.1.2 Plastic ware

Transwell® (12-well) and Snapwell® (6-well) inserts, 12 mm diameter and 0.4 μm pore size polyester membranes (#3460 and #3470 respectively) and 6,12 & 24 well non-tissue culture treated plates were obtained from Corning Life Sciences, Netherlands. CellCrowns™ (24 well – 0.8 cm^2 exposed surface area) were purchased from Scaffdex, Finland.

T-75/25 culture flasks (75/2 $cm^{2,}$ canted neck and vented caps), and multi-well plates were acquired from Nunc, Thermo Scientific. Cryovials and centrifuge tubes were obtained from Fisher.

2.1.3 Antibodies

Mouse monoclonal primary tagged human anti-Zona Occludens-1 Alexa Fluor 488, goat anti mouse, goat anti rabbit IgG secondary Alexa Fluor 488, Rhodamine red, 4'-6'-diamino-2-phenylindole (DAPI) and Hoescht 33342 were purchased from Invitrogen, Life technologies. Rabbit polyclonal primary human anti-desmin, mouse monoclonal human anti-vimentin and goat serum were purchased from Sigma Aldrich, UK. Mouse monoclonal primary anti-Alpha smooth muscle actin was purchased from Abcam, UK. Mouse monoclonal human fibroblast activation protein was purchased from R & D Systems, Bio-techne, USA.

2.1.4 Chemicals and other materials

Harris haematoxylin, atenolol, propranolol, verapamil, FITC-dextran 4 kDa, 10 % neutral buffered formalin, 2.5% (*v/v*) trypsin/ethylenediaminetetraacetic acid, industrial methylated spirit (IMS -denatured ethanol), allylamine monomer, hexamethyldisalizane (HMDS), alcian blue (pH 2.5), xyelene, trifluoroacetic acid (TFA), L-alanine-4-nitroanilide hydrochloride, 4-nitroaniline were purchased from Sigma Aldrich, UK. Rhodamine 123 and lucifer yellow (potassium salt) were obtained from Biotium, CA. HPLC gradient grade Acetonitrile, dichloromethane and Sartorius minisart (0.2 µm) were purchased from Fisher. Eosin Y, Osmium Tetroxide 1% (*v/v*) and glutaraldehyde (50% *v/v*) were purchased from TAAB laboratories. HPLC column and guard cartridges were obtained from Phenomenex, UK.

Poly (ethylene terephthalate) (PET) pellets were purchased from Sigma Aldrich, UK. PET flakes were procured from recycled plastic bottles and processed in house. Blunt fill 18G

needles (0.84mm internal diameter) and disposable syringes were purchased from Beckton Dickinson, USA.

2.2 General Methods

2.2.1 Cell culture

2.2.1.1. Routine flask culture

All cells were routinely cultured in T75 flasks (75 cm^2 growth area) at 37°C, 5% CO_2 in 95% relative humidity. Cells were cultured to around 80% confluence before harvesting cells and passaging. Cell culture medium was replaced every 2 days (unless otherwise stated) after pre warming the relevant medium in a thermostatically controlled water bath for a minimum of 30 minutes. Cell growth and general morphology was visually monitored daily for signs of abnormal growth and contamination. Cells were also tested every quarter for mycoplasma contamination.

2.2.2 Passaging

All cells were harvested using the following protocol (unless otherwise stated). At approximately 80% confluence cell medium was aspirated and cultures were washed with 10 mL PBS (pre warmed to 37°C). Strongly adherent epithelial cells (Caco-2 and Calu-3) were often washed multiple times to ease their detachment from culture surfaces as minor amounts of serum containing cell medium inhibits the enzymatic harvesting process. Following aspiration of the PBS, 3 mL of 2.5% (*v/v*) Trypsin/EDTA was added and incubated at 37°C. Typically, flasks were incubated for 4 minutes and then checked for detachment using a microscope. For tightly adherent epithelial cells and more confluent cultures longer enzyme incubation times were often required (e.g. 5-10 minutes). Following cell detachment the enzymatic action of Trypsin was neutralised by the addition of relevant pre-warmed complete medium. The trypsin/EDTA/media cell suspension was gently mixed

and rinsed over the growth area of the flask with a serological pipette to pick up all the detached cells and dispensed into a centrifuge tube. The cells were centrifuged at 200 g for 5 minutes at ambient temperature. The supernatant was aspirated and replaced with fresh medium before re-suspending the pelleted cells by gentle mixing with a pipette.

2.2.3 Frozen storage of cells

Cells were passaged as previous. Following centrifugation the cell pellet was re-suspended in complete medium and the cells counted using a haemocytometer. Cells were centrifuged again and the supernatant aspirated. The cell pellet was then re-suspended in foetal bovine serum containing 10% (*v/v)* dimethylsulphoxide (DMSO) at a cell density of 1 $x10^6$ cells/ mL. The resulting cell suspension was dispensed into cryo-vials as 1 mL aliquots. Cryo-vials were then stored in a CoolCell® (BioCision, CA) at -80°C for a minimum of 24 hours. The vials were then stored in liquid nitrogen vapour.

2.2.4 Cell revival from frozen storage

Cryo-vials were removed from cold storage and quickly thawed in a thermostatically controlled water bath at 37°C. The cell suspension was gently mixed using a pipette and dispensed into flask containing the relevant pre-warmed medium. Cells were then allowed to attach for 4-24 hours before the medium was changed to remove any remaining DMSO.

2.2.5 Trans-epithelial electrical resistance (TEER) integrity measurements

Epithelial barrier formation and integrity was measured throughout culture on hanging inserts by measuring the resistance to an ion current across the epithelium. TEER measurements were taken using the Evom2 Voltohmmeter with STX2 chopstick electrodes (World Precision Instruments, Florida). Cell inserts were washed with PBS before the addition of pre-warmed HBSS. Cells were left to equilibrate at 37° C, 5% CO_2 for 30 minutes prior to resistance measurements. As resistance is inversely proportional to the area

of the tissue the product of the tissue resistance and the surface area are calculated to allow for comparison with other reported TEER data. TEER (Ω cm^2) values were calculated by the following equation:

Equation 2-1

$$TEER\ (\Omega\ cm^2) = (\Omega\ cell\ layer - \Omega\ blank\ filter) \times filter\ surface\ area\ (cm^2)$$

2.2.6 Immunocytochemistry

Cells were washed in PBS (x3) before being fixed in 3.7% (*v/v*) paraformaldehyde for 15 minutes. Samples were then washed in PBS and permeabilised with 0.5% (*v/v*) Triton-X for 5 minutes at 4° C. Following a PBS wash non-specific protein interactions were blocked in a 3% BSA, 1% glycine (*v/v*) solution for 30 minutes at ambient temperature. Samples were then washed and in the case of indirect immunochemistry, blocked further in 10% (*v/v*) serum (of the donor of the secondary antibody) for 30 minutes at ambient temperature. The cells were then incubated with the primary antibody for a minimum of 1 hour at ambient temperature or overnight at 4° C. Following another PBS wash, for indirect immunochemistry samples were incubated with a secondary fluorescently tagged antibody for 45 minutes. Samples were protected from sources of light from this point onwards to limit photo bleaching. Following this the samples were washed and incubated with a nuclear stain, either DAPI/Hoechst 33342 for 5 minutes. Transwell/snapwell samples were removed from their insert housing using a scalpel and then all samples were mounted on glass slides with a small drop of fluorescent mounting media. For transwell/snapwell samples a glass coverslip was mounted over the top before sealing the samples with nail varnish.

For indirect immunocytochemistry, negative controls were included in every staining procedure (secondary antibody treatment without pre-incubation with the primary antibody) as standard. Positive controls were used where relevant cell lines were available.

2.2.7 Histology and Haematoxylin and Eosin staining

Tissue and cell samples were fixed in 10% (*v/v*) formalin solution for 20 minutes. After washing in PBS, the samples were dehydrated in a series of ethanol solutions 25-100% (*v/v*) for 30 minutes in each solution followed by xylene for 1 hour (x2) and then finally in paraffin wax for 1 hour (x2) in a tissue processor (Leica TP1020, Milton Keynes, UK). Samples, embedded in paraffin, were cut into 8 µm sections (Leica RM 2165 microtome) before mounting on glass slides in preparation for staining. Samples were paraffin-stripped in xylene and rehydrated in 100-25% (*v/v*) IMS and then into tap H_2O for 1 minute each. Samples were then placed in Harris haematoxylin for 5 minutes to stain cell nuclei. Excess stain was then removed and allowed to develop in slowly running tap H_2O for 5 minutes. Samples were then re-dehydrated before being stained in 1% w/v alcoholic eosin to stain the cell cytoplasm. The completely stained samples were then further dehydrated through 100% (v/v) IMS and xylene. Slides were then allowed to air dry overnight at room temperature before mounting with DPX mounting media and a coverslip. Images were obtained using an inverted Nikon Eclipse TS100 microscope.

2.2.8 Scanning electron microscopy (SEM)

For acellular Transwell and nanofibre scaffolds, samples were simply sputter coated (Leica EMSCD005) with gold for 4-5 minutes prior to microscopy. Biological samples were fixed in 3% (*v/v*) glutaraldehyde overnight at 4°C adhering to standard tissue infiltration times of 0.5 mm^3/hour[104]. Sample were washed with PBS (x3) and dehydrated through a series of IMS steps (25-100% *v/v* ethanol) for 10 minutes in each solution. Following dehydration, hexamethyldisilazane (HMDS) was added to chemically dry the samples, this process was then repeated and the samples were left to air dry overnight before sputter coating with gold. Scanning electron microscopy was carried on a JEOL JSM-6100 (JEOL, UK). Where necessary, images were processed using ImageJ software. (W. Rasband, National Institute of Health, USA).

2.2.9 Transmission electron microscopy (TEM)

Samples were fixed in 3% (*v/v*) glutaraldehyde in 0.1M cacodylate buffer overnight at 4°C before post fixation in 1% (*v/v*) aqueous osmium tetroxide for 30 minutes. Samples were washed in water for 5 minutes before dehydration in 50% (*v/v*) ethanol for 2x 5 minute steps. Cell scaffolds were removed from their inserts and stored in 70% (*v/v*) ethanol before further dehydration in 90 and 100% (*v/v*) ethanol and subsequently 100% propylene oxide. Samples were infiltrated with araldite CY212 resin for 30 mins (in a 1:3 resin acetone mix), followed by 1 hour (1:1 resin acetone mix) and finally 3x 1 hours in pure araldite resin. Samples were then embedded in resin for at least 48 hours at 60° C. Ultra-thin (90 nm) sections were cut using a diamond knife and were negatively stained with uranyl acetate and lead citrate. The sections were then viewed using a FEi Tecnai G2 TEM.

2.2.10 Drug/marker permeability

Transport studies were conducted using the standard, widely accepted protocol[5]. Transport markers were prepared in transport buffer (HBSS, 25 mM HEPES, pH 7.4, referred to simply as transport buffer throughout). Dimethyl sulphoxide (DMSO) was used to aid solubilisation of poorly soluble drugs at a maximum final concentration of 0.1% (*v/v*) used in all transport experiments. Cell samples were washed with PBS before being incubated with pre-warmed transport buffer with rotation at 150 r.p.m (Stuart Scientific, Orbital shaker S03), 37°C for 45 minutes. TEER was measured before and after each experiment to ensure barrier integrity during the experiments and as a control measure of experimental validity. Inserts were transferred to fresh plates containing transport buffer (apical/basolateral volumes were 0.4/1.2 mL and 0.5/6 mL for transwells and snapwells inserts respectively). Donor solutions were added to the relevant compartments (depending on transport direction; apical to basolateral - AB - and basolateral to apical - BA) of the inserts and a t=0 sample of the donor chamber was immediately taken. The inserts were then incubated at 37°C with shaking at 150 rpm and sampled at intervals of 30 mins or 1 hour for 1-2 hours. Apparent permeability coefficients (Papp) were calculated according to the equation:

Equation 2-2

$$Papp = (dQ/dt)(1/AC_0)$$

Where d*Q*/d*t* is the flux of the compound being investigated (μM s^{-1}), A is the exposed surface area of the insert/scaffold (cm^2) and C_0 is the concentration in the apical compartment at t=0 (μM).

2.2.11 Basic electrospinning protocol

Briefly, PET flakes were dissolved in a 1:1 mixed solution of dichloromethane and trifluoroacetic acid overnight with stirring at room temperature. The polymer solution was loaded into a graduated plastic syringe fitted with a needle (spinneret). The loaded syringe was securely fixed to a syringe pump (Harvard Apparatus, UK) and a voltage (Glassman High Voltage Inc, Series EL, Glassman Europe Ltd, UK) was applied to the spinneret. The polymer solution was passed through the spinneret at a set flow rate (mL/hr) and collected on a grounded static plate or rotating collector (in house design). The scaffolds were removed with the aid of 70% (*v/v*) IMS spray and were allowed to air dry to permit any remaining solvent to evaporate prior to use.

2.3 Statistics

Statistics analysis was carried out using Graphpad Prism 6.0. Specific statistical tests performed are quoted in figure captions. All data analysis were judged to be normal (Gaussian) using the normality test on Graphpad Prism. As a result parametric analyses were used entirely throughout this thesis. Where comparison of two groups was conducted (for unpaired groups) Student's t-test was used, for comparisons of three or more group's one-way ANOVA analysis was employed. For analysis by Student's t-test, Welch's correction was used where the variance (SD) was found to be significantly different for the two groups under analysis (calculated by means of the F-test in the Graphpad Prism software). One-way

ANOVA analysis post-tests were dependent on the type of analysis being performed. For multiple comparisons of all the data sets with one another, Tukey's post-test was used. For analysis of data with a control column where groups were selected for comparison, Šidaks post-test was used.

For clarity, n numbers exclusively refer to the sample numbers (i.e. total number of technical replicates from a number of experimental replicates). The number of independent experiments (experimental replicates) conducted is referred to separately in each figure caption. Where possible all experiments were conducted in triplicate (technical replicates) on 3 independent occasions (experimental replicates). Any deviation from this is reported in the specific figure caption. P values ≤ 0.05 were considered statistically significant and are represented by asterisks and obey to the following format throughout; * $p \leq 0.05$, ** $p \leq 0.01$, *** $p \leq 0.001$, **** $p \leq 0.0001$.

3. Development of intestinal cell co-cultures

3.1 Introduction

Significant ground is being made in the ability to culture multiple cell types together to reconstitute more realistic tissue function in the lab, the applications of which go beyond *in vitro* models, and support the future development of tissue implants and grafts for medical interventions. Attempts to better recapitulate the intestinal tract, more specifically the intestinal epithelial mucosa, is no exception to this trend and such models have immense relevance first and foremost to the pharmaceutical industry but also in understanding cancer pathogenesis. Testing the pharmacokinetics of novel drugs during pre- clinical drug development plays a substantial role in early drug discovery and can be a significant factor in the success of drug. Current models which have approval of major regulatory bodies not only reduce the burden on labour intensive animal models, which can often have poor correlation to humans[105,106], but also help in the early decision processes. Making decisive, well informed judgments based on sound experimental evidence early on in the drug development process enables the streamlining of new drug candidates and will hopefully result in faster and more efficient development of new medicines.

Scientists in the past have not neglected the simple fact that the intestinal mucosa is a complex, multi-cellular tissue when developing *in vitro* models. Many researchers have contributed to the development of currently utilised Caco-2 model however, it has been widely acknowledged that the lack of complexity in the model is central to some of the issues regarding correlations to the *in vivo* reality[75,84].

Despite the fact the Caco-2 cell line was first investigated in 1983[83] it was not until the 1990's that a fully characterised model was fully developed[6,84,107]. Even at this early stage of model development researchers were keen to improve upon the simple unicellular model by

culturing Caco-2 cells with goblet cell-like HT-29[108] and later HT-29-MTX[109] in an attempt to reconstitute a mucus component in the model. Although this marked a clear improvement, the simple unicellular Caco-2 model remains the go-to assay for *in vitro* models of the intestine and almost every new development in this field of research still utilises the Caco-2 line[11,12,14,17,18,110,111].

Various strategies have been attempted with the aim of manipulating and modulating the function of epithelial monocultures. Whilst the introduction of a goblet-like cell population has always been a central development strategy the importance of other cell types is beginning to be appreciated. Cells of the lamina propria such as myofibroblasts are increasingly becoming a focal point of interest. Myofibroblasts have been shown to influence the barrier integrity of the overlying epithelium[34], supporting the growth of the epithelium[47] and have been implicated in development and repair processes via cellular cross talk [32,112]; mediated not only by secreted soluble paracrine factors but also as a result of their intimate connection with the ECM, through its production and constant remodelling. In addition to this it is generally considered that myofibroblasts form an underlying syncytium[113] which in itself acts as a contractile barrier which can be modified through shape conversion in response to local mediators[46]. Furthermore this network provides a physical frame to the villi structures of the intestine and aids in the villi motility[46].

In the study by Beltinger *et al.,* myofibroblasts were shown to increase the TEER of HCA-7 monolayers cultured on microporous filters in co-culture[34]. This upregulation was observed also through 24 hour incubation with fibroblast conditioned media. Furthermore this effect could be ablated with a pan-specific anti-TGF-β antibody implicating TGF- β in this upregulation of TEER. Although the precise mechanism of the TGF-β induced effect upon the epithelial line was not elucidated it clearly supports the hypothesis of a significant role of myofibroblasts in epithelial barrier regulation.

In contrast to this finding CCD-18co myofibroblasts in direct co-culture with T84 epithelial cells (that is T84 cells seeded directly on top of a CCD-18co cell layer) displayed no significant increase in barrier integrity (TEER) in standard culture[114]. The study did however reveal a regulatory role for myofibroblasts in immune related epithelial damage and restitution of barrier function following disruption.

A very recent study into co-cultures of Caco-2 and CCD-18co demonstrated difference from the previously reported result. Co-cultures in three different sets ups were engineered; a direct co-culture of Caco-2 and CCD-18co, a CCD-18co layer embedded in matrigel with Caco-2 seeded on top and lastly a direct co-culture separated by a matrigel layer. All these set ups resulted in TEER values approximately half of that seen in Caco-2 monocultures[14]. The authors attributed this reduction in electrical resistance to the CCD-18co cells interspacing between the Caco-2 cells. Despite this observed change in TEER no significant change in insulin permeation was observed in the direct co-culture to the Caco-2 monocultures (the results for the matrigel 3D set ups were not compared by the authors). Changes in TEER were observed within the permeability experiments, suggesting changes to the monolayer integrity during the experiment, but no significant changes in the rejection of FIT-dextran 4 kDa were observed afterwards.

The cross talk mechanisms and the physiological rapport between mesenchymal cells and the overlying epithelium are complex. In studies with Calu-3 cells (airway epithelial cells) and supportive MRC-5 fibroblasts, electrical resistance is almost always increased in comparison with Calu-3 monocultures[115,116]. This increase in TEER was also shown to influence molecular flux in the early stages of culture[116]. This may be a result of tissue or cellular specific differences in response to secreted chemical mediators. Considering the homogeneity of the epithelial-myofibroblast anatomical arrangement in epithelial tissues throughout the body, different epithelial-fibroblast relationships may help shed light and add discussion to evidence derived from tissue specific cell experimentation. As scientists strive

to close the gap between the lab and the *in-vivo* situation it is vital to understand the underlying molecular interactions between specific cells and how they contribute to the tissue function. Furthermore, the mechanisms of co-culture related changes and the relevance of any modulation (especially with respect for specific downstream applications) need to be clearly understood. Without this the inertia and reliance upon simple methodologies will not be overcome.

3.2 Aims

The main aims of this chapter were to investigate the interaction of CCD-18co myofibroblasts with commonly used epithelial cell lines to study the influence they have upon epithelial function and barrier properties. CCD-18co cells have been shown to express the morphological and functional characteristics of primary myofibroblasts and have been widely used within the literature as cell lines for myofibroblast based investigations. Co-cultures of HT-29 and Caco-2 were also investigated to investigate the potential of a mucus element within a proposed *in vitro* model. Conventional transwell inserts were used as the platform for all of these investigations.

- Characterise the CCD-18co cell line to confirm key myofibroblasts filament marker expression
- Preliminary assessment of barrier integrity of epithelial-myofibroblast co-cultures in transwell inserts
- Morphological characterisation of epithelial-myofibroblast co-cultures in transwell inserts
- Investigate mechanism of altered epithelial barrier modulation in co-culture set ups
- Explore further changes to epithelium as a result of co-culture
- Investigate HT-29/Caco-2 co-cultures

3.3 Methods

3.3.1 CCD-18co intermediate filament expression characterisation by immunochemistry

CCD-18co myofibroblasts were seeded on glass coverslips and transwell inserts at 50,000 cells/well and cultured for 2-3 days in well plates. The cells were then fixed according to the previously mentioned immunochemistry protocol (Section 2.2.6) and stained for Vimentin, a typical intermediate filament protein expressed by all mesenchymal cells; Desmin, a muscle specific intermediate filament protein and alpha smooth muscle (α-SMA) actin, another intermediate filament which is a commonly used marker of myofibroblastic cells[46,117]. Stained cells were imaged using a Leica SP2 confocal microscope and images processed using ImageJ.

3.3.2 Co-culture TEER and PrestoBlue assessment of barrier integrity and cell viability

3.3.2.1. Myofibroblast cell seeding

Cells were detached from flasks as previously described and counted using a haemocytometer. A cell suspension containing 50,000 cells in 200 µL (i.e. 42,000 / cm^2 growth area) was used to seed cells onto the basolateral surface transwell inserts (Figure 3.1). The upturned inserts were placed in a petri dish and incubated at 37 °C, 5% CO_2 to allow the cells to adhere for a minimum of 4 hours. The inserts were then moved to a relevant well plate and fresh medium added to the well to submerge the insert.

3.3.2.2. Epithelial cell seeding

Cells were detached from flasks as previously described and counted using a haemocytometer. For Caco-2 and Calu-3 a cell suspension containing 200,000 cells per 500 µL (i.e. 179,000 / cm^2 growth area) was used to seed cells onto the apical side of the transwell inserts. The basolateral compartment was submerged with 1.5 mL of relevant

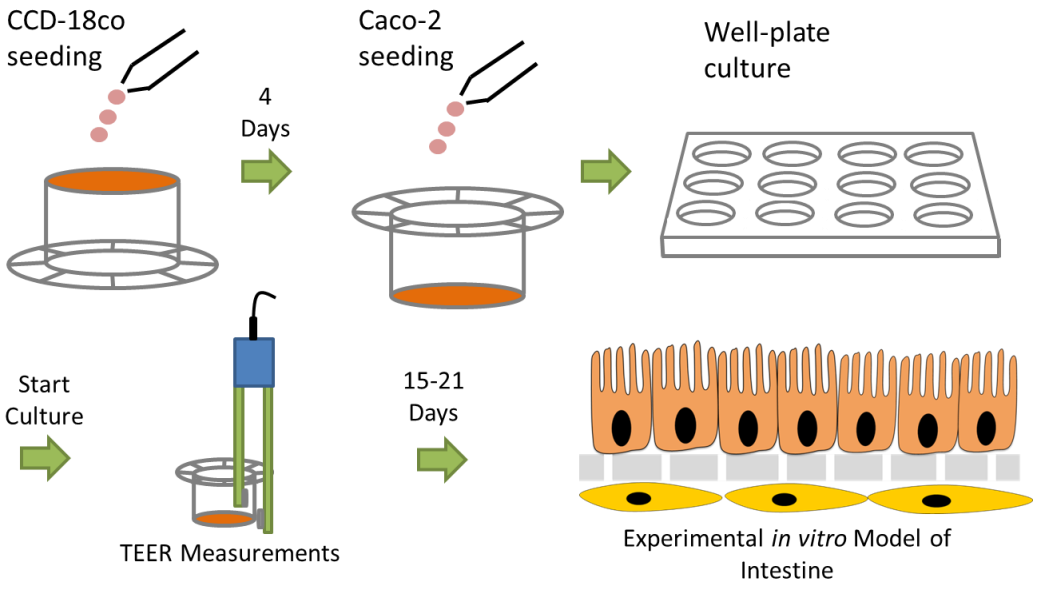

Figure 3.1. Schematic of Caco-2/CC-18co co-culture model set up. CCD-18co myofibroblasts were seeded onto the basolateral surface of transwell inserts and allowed to attach for up to 4 hours. Following attachment the cells are cultured for at least 4 days prior to epithelial cell seeding. Cells were then cultured for 15 to 21 days before being used for experiments. Barrier integrity (TEER) and viability measurements can be conducted during the culture period.

complete medium. For HT-29 cells a cell suspension containing 100,000 cells per 500 µL (i.e. 90,000 / cm2 growth area) was used.

Following epithelial seeding, cells were allowed to attach for between 4-16 hours before the apical medium was aspirated and replaced with fresh media. This minimises the formation of cell multi layers common in epithelial cell line cultures. Cell medium was changed in both the apical and basolateral compartments every other day. For Calu-3 cells, after day 6 of culture the cells were raised to the air liquid interface (ALI). The culture medium was aspirated from the apical compartment and 0.5 mL of media (a 50:50 mix of each respective cell media) was used in the basolateral chamber through the remaining culture period.

3.3.2.3. HT-29/Caco-2 Co-cultures

HT-29 and Caco-2 cells were seeded into transwell inserts at ratios of 1:1 and 1:9 at a total cell density of 200,000 cells/well. As both cells were routinely cultured in DMEM, no

specific medium alterations were required. TEER measurements and lucifer yellow permeability assays (AB direction only) were conducted as previously described (Sections 2.2.5 and 2.2.10 respectively). Donor concentrations of lucifer yellow were 50 µM with 30 minute sampling intervals for a total of 1 hour. Aliquots of 100 µL were transferred into a black 96-well plate and the fluorescence was detected using a plate reader at 427/535 nm (excitation/emission). Concentrations were calculated from the linear regression of a calibration curve using the equation of the trend line. Fresh calibration curves ranging from 100 µM to 1 nM were prepared for each separate experiment. The theoretical resistance and permeability values for HT-29/Caco-2 cultures were calculated using the following equation:

Equation 3-1

$$R_{Theor} = 1/(f_H/R_H + (1-f_H)/R_C)$$

where f_H is the fraction of the cell seeding density of HT-29 to Caco-2, R_H the resistance the HT-29 monolayer and R_C the resistance of the Caco-2 monolayer. Since P_{app} is the reciprocal of R, then the same equation can be used to calculate theoretical P_{app} values[108].

3.3.2.4. TEER and PrestoBlue viability measurements

The integrity and the viability of epithelial/myofibroblasts co-cultures were assessed over a 12 day culture period. Barrier integrity was measured by TEER according to the standard protocol (Section 2.2.5). Following TEER measurements the samples were assessed for cell viability. A working solution of 10% (*v/v*) was prepared from the stock PrestoBlue solution in HBSS (without phenol red) was sterile filtered using a 0.2 µm pore filter. Samples were washed three times with pre warmed PBS and the working solution of Prestoblue solution applied to the apical compartment of the inserts. Following a 30 minute incubation period at 37 °C, 5% CO_2 with shaking at 150 rpm 100 µL aliquots were taken from each sample and dispensed in triplicate into a black 96-well plate. The fluorescence of the samples was

determined using a plate reader (Tecan Infinite 200, Tecan UK) at 530/590 nm (excitation/emission wavelengths).

3.3.3 The development of tight junctions in epithelial monocultures and CCD18-co co-cultures by immunostaining for Zona Occludens-1 (ZO-1).

Tight junction expression was investigated in monocultures and co-culture set ups by immunochemistry using the TJ protein Zona Occludens-1 (ZO-1) to identify the tight junctions. Epithelial monocultures and co-cultures were cultured and the formation of tight junctions assessed at day 3, 6 and 9. Samples were fixed and stained according to the previously mentioned protocol (Section 2.2.6) and the ZO-1 antibody used at the manufacturers recommended dilution (5 µg / mL). Samples were imaged using a Leica confocal SP2 laser scanning microscope and images processed using ImageJ.

3.3.4 Investigating the mechanism of barrier integrity modulation using myofibrolast conditioned medium (MFCM)

The mechanism of barrier integrity modulation was assessed in Caco-2 and Calu-3 epithelial cell lines. Confluent flasks of CCD-18co cells were rinsed with PBS (x3) and replenished with the respective complete media. The medium was incubated with the myofibroblasts for 24 hours. The conditioned medium was then filtered through a 0.2 µm filter and used immediately in a 1:1 mix with respective pre-warmed complete medium. Any left-over conditioned media was refrigerated and used within 24 hours of the conditioning process. Conditioned medium was changed every other day and TEER measured every 3 days. At day 15 of culture the barrier formed by the monolayers was assessed by the permeability paracellular marker lucifer yellow (Section 2.2.10).

3.3.5 Measurement of aminopeptidase activity in Caco-2 and Caco-2/CCD-18co cultures

The expression of aminopeptidase, an epithelial brush border enzyme expressed in intestinal epithelial cells, was calculated from the catalysation of the substrate L-alanine-4-nitroanilide

hydrochloride (A4N) into 4-nitroaniline. A volume of 0.5 mL A4N at 1.5 mM in pre warmed complete media was incubated in the apical chamber of transwell mono and co-cultures for 1 hour (Basolateral chambers were aspirated for the duration of the experiment to ensure only the apical cells had access to the substrate). 100 µL of the apical solution was transferred to a clear 96-well plate where the cleavage product 4-nitrolaniline was quantified at 405 nm using a plate reader (Tecan Infinite 2000). The intrinsic activity (i.e. the amount of cleavage product produced in a blank well was subtracted from the specific enzyme activity). The concentration of 4-nitroaniline was calculated from the linear regression of a calibration curve. The specific activity of aminopeptidase (fmol/min/cell) was calculated as the total enzyme activity (total amount of 4-nitroaniline produced, fmol/min) divided by the cell number. Cells were removed by trypsinisation, gentle pipetting over the monolayers was required to remove all the cells. Cells were trypan blue stained for viability before counting however, all harvested cells were assumed to be viable prior to the trypsinisation process.

3.3.6 Investigation of CCD-18co aminopeptidase activity by immunochemistry for fibroblast activation protein (FAP)

CCD-18co were seeded as previously mentioned (Section 3.3.2.1) and cultured for 10 days. The cells were then fixed and stained by indirect immunostaining (Section 2.2.6) with mouse anti-human fibroblast activation protein primary antibody at a concentration of 2 µg /mL. The cells were then imaged on a Lecia DM IRB microscope.

3.3.7 Alcian blue and Periodic Acid Schiff Staining

Regional sections of porcine jejunum were obtained and dissected as mentioned in section (Section 5.3.3). Samples were cut into small pieces and fixed in 10 % neutral buffered formalin (NBF) overnight. Following fixation tissue samples were processed as previously mentioned using a tissue processor (Section 2.2.7) with the exception that samples were immersed for 2 hrs in each dehydration solution and subsequent wax infiltration steps. For

cell monolayers inserts, samples were fixed in 10 % NBF for 15 minutes. Samples were then washed three times in PBS prior to the staining procedure.

Samples were exposed to alcian blue (pH 2.5) for 30 minutes each. Mounted samples were washed in tap water and subsequently were cross stained in haematoxylin for 1 minute. Samples were then rinsed in tap water before dehydration before being mounted and sealed. Cell inserts were rinsed several times with water until no remaining stain was being removed.

For periodic acid Schiff (PAS) staining samples were fixed and washed as described above. Samples were then oxidised in 0.5 % (*v/v*) periodic acid solution for 5 minutes. After rinsing in distilled water Schiff reagent was added to each sample for 15 minutes. The samples were then washed in luke-warm tap water for 5 minutes until no remaining stain could be removed.

3.4 Results

3.4.1 Routine morphological analysis of cell lines

Epithelial cell lines HT-29, Caco-2 and Calu-3 were cultured in conventional tissue culture treated well plates. Epithelial cells exhibited a very typical morphology which is a cobblestone-like monolayer of cells which form confluent sheets (Figure 3.2. A-C). It is clear from the microscope images that Caco-2 and Calu-3 cells (Figure 3.2. B & C) form better and well defined monolayers with cell boundaries being more evident. CCD-18co myofibroblasts on the other hand mostly exhibit a flattened stellate morphology when cultured on tissue culture treated polystyrene (Figure 3.2. D).

3.4.2 Myofibroblast characterisation by intermediate filament expression on glass and Transwell substrates

CCD-18co cells were screened for the specific expression of key intermediate filaments used in the characterisation of myofibroblasts on glass coverslips and on porous tissue culture treated transwell inserts. CCD-18co stained positively for general mesenchymal intermediate filament marker vimentin and also for desmin, a muscle specific marker, on both substrates tested (Figure 3.3 A, B, D & E). With respect to α-SMA staining, CCD-18co cells appeared to demonstrate more significant positive staining for the myofibroblast-specific marker on the porous transwell substrate than on the glass coverslips. Some low level staining however was observed on the glass substrate (Figure 3.3. C - Inset image). In addition to characterisation of the intermediate filament markers some clear morphological differences could be observed through immunostaining. For CCD-18co cells cultured on glass substrates clear cell spreading is observed resulting in a ‘flat-shaped’ morphology (Figure 3.3. A-B). In contrast, cells cultured on transwell inserts appear to have a more elongated, spindle-like morphology with a quite apparent directional alignment (Figure 3.3. D-E).

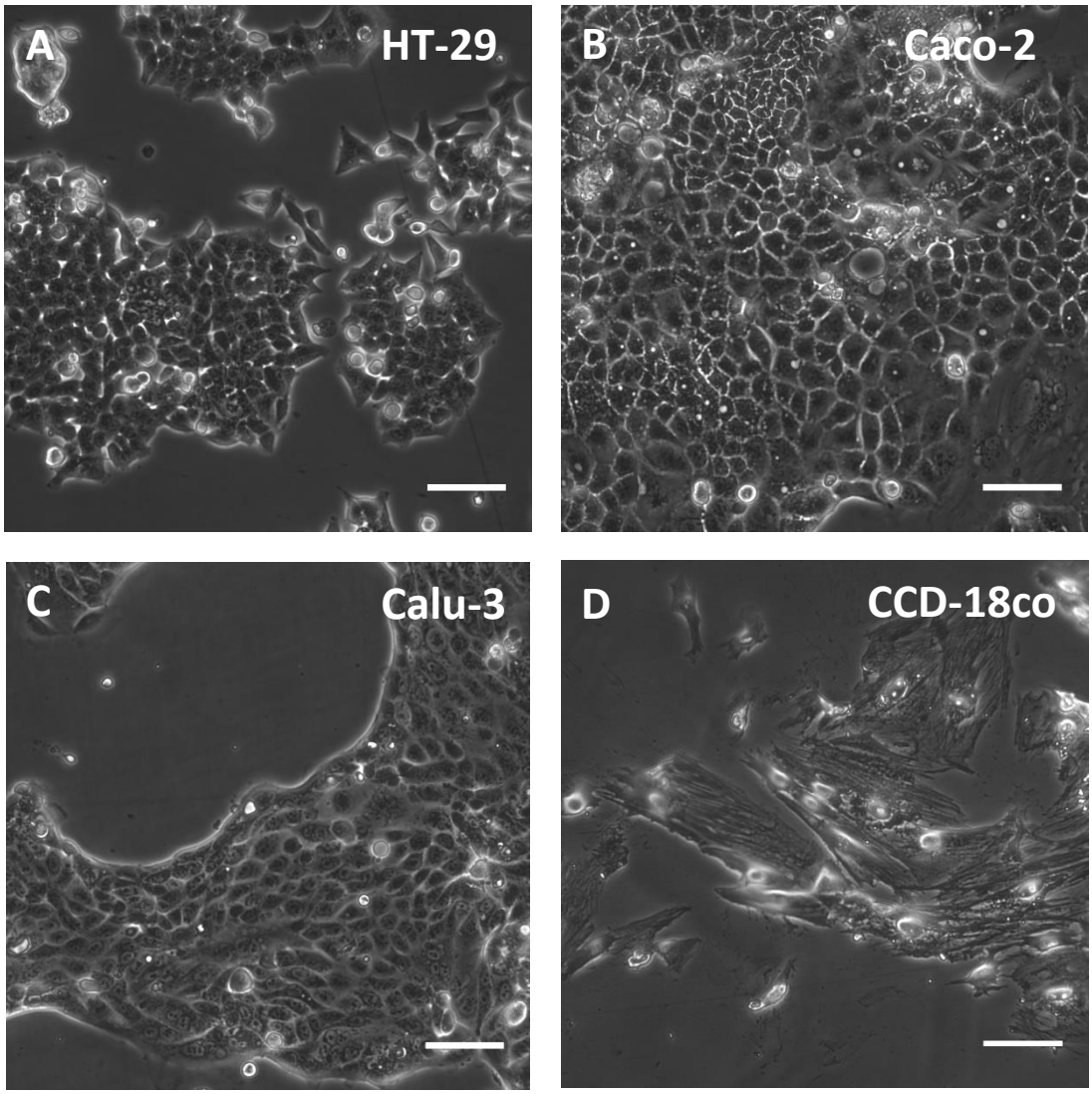

Figure 3.2 Representative bright field photomicrographs of epithelial and myofibroblasts cells Representative bright field images of cells grown on tissue culture treated polystyrene (A) HT-29 colonic epithelial cells. (B) Caco-2 colonic epithelial cells. (C) Calu-3 airway epithelial cells. (D) CCD-18co colonic fibroblasts. Scale bars equal 150 µm.

3.4.3 Trans-epithelial electrical resistance of epithelial-myofibroblast mono & co-cultures

The effect of co-culturing different epithelial cell types with the CCD-18co myofibroblast line was examined to investigate any significant effects upon the barrier integrity of the overlying epithelial layer. With respect to Caco-2 cells co-cultured with the myofibroblasts the results showed a plateau early on in culture and in general demonstrate lower TEER from day 12 of culture onwards compared to Caco-2 monocultures (Figure 3.4.A). Caco-2 cells in monoculture continue to increase in TEER throughout the culture period with a sharp increase in resistance observed from day 12 onwards; peak TEER values in excess of 800 Ω cm^2 were observed after 21 days. Caco-2/CCD-18co co-cultures in contrast demonstrate a much slower increase in TEER throughout an identical culture period. The steepest increase occurs between day 1 to 6 and peak TEER values reach ~240 Ω cm^2. Significant differences between the two culture set-ups can be observed from day 9-21. In contrast to this, monocultures of HT-29 demonstrated no significant difference in TEER values throughout culture, compared to co-cultures, with the exception of day 15 where a slight decrease is observed (Figure 3.4 B). Peak TEER values were much lower in HT-29 monocultures compared to the Caco-2 cell line. Peak TEER values of ~ 60 Ω cm^2 were observed for both HT-29 monocultures and HT-29/CCD-18co monocultures (Figure 3.4 D).

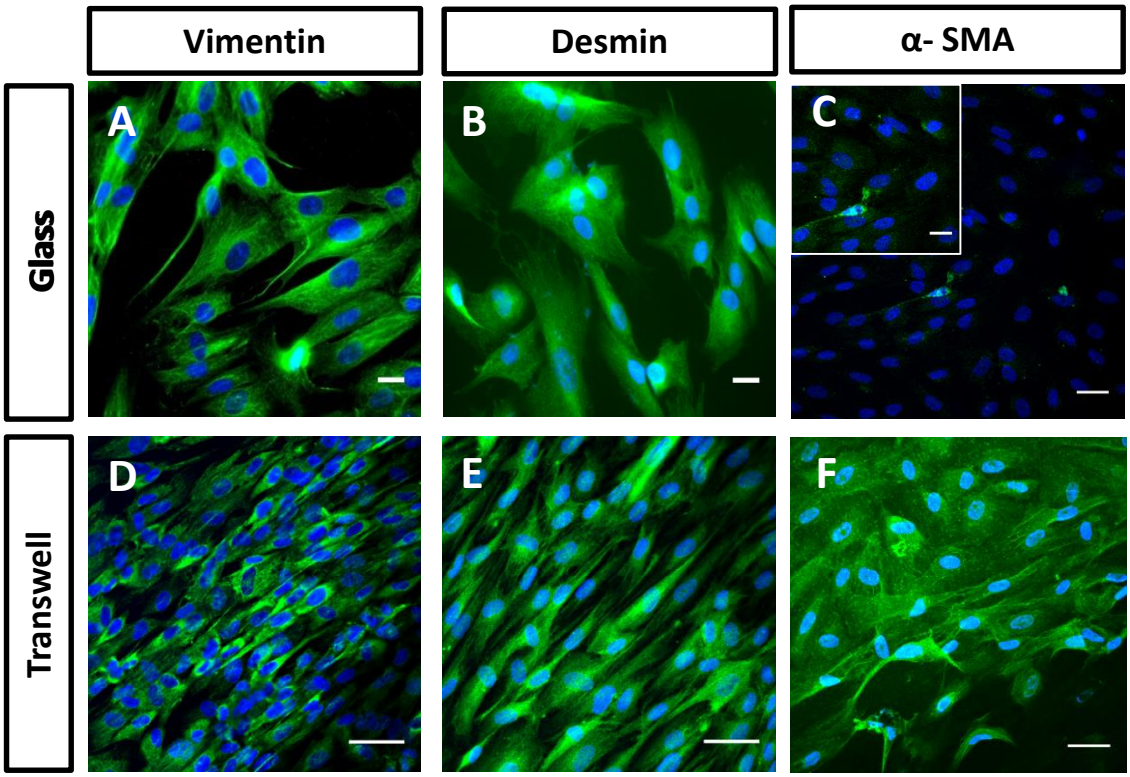

Figure 3.3 Substrate-specific myofibroblast intermediate filament expression in CCD-18co cells Characterisation of CCD-18co cells for key myofibroblast markers (A & D) Vimentin, Desmin (B & E) and α-smooth muscle actin (C & F) on different growth substrates. Blue = cell nuclei, green = intermediate filaments. Scale bars = 50 µm, inset images (C) scale bars = 20 µm.

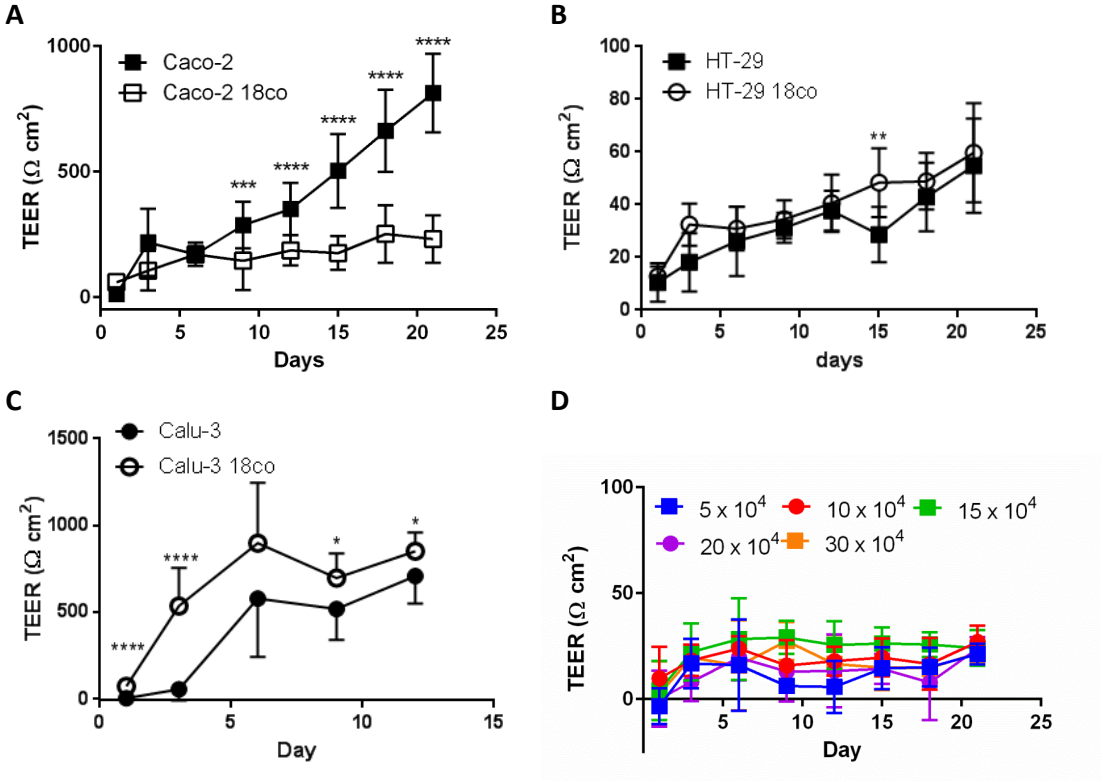

Figure 3.4. Electrical resistance of epithelial-myofibroblast co-cultures cultured on transwell inserts. Monocultures and CCD-18co co-cultures with epithelial cells (A) Caco-2, (B) HT-29 and (C) Calu-3. (D) TEER measurements for monocultures of CCD-18co cultured on transwell inserts at different initial seeding densities. Values expressed as means ± 1 S.D, (A-C) n=9-15 (inserts) from a minimum of 3 independent experiments, (D) n=6 (inserts) from 2 independent experiments. Significance determined by Students t-test, ***p ≤ 0.001, ****p≤0.0001.

The final investigation of epithelial-myofibroblast interactions was between the airway epithelial line, Calu-3, and CCD-18co. In this case co-cultures demonstrated increased TEER compared to monocultures throughout 12 days of culture (Figure 3.4 C). Peak TEER values reached ~900 Ω cm^2 at day 6 for Calu-3/CCD-18co co-cultures whereas Calu-3 monocultures did not reach peak TEER until day 12 demonstrating resistance values of ~700 Ω cm^2. Despite the difference in achieving peak TEER at different rates, both set-ups showed similar trends throughout the culture period; the steepest increase was observed from day 1-6 with any further increases from day 6 onwards occurring at a much slower rate.

Monocultures of CCD-18co were also evaluated for any intrinsic impact on TEER. At varying densities CCD-18co showed minimal electrical resistance through the culture period. Peak TEER values reached ~30 Ω cm^2 and showed no time dependent effect in terms of TEER. Maximal TEER values were reached after 6 days in culture and were relatively linear throughout the remaining culture period (Figure 3.4 D).

3.4.4 Epithelial-myofibroblast monoculture vs co-culture cell viability

In addition to monitoring epithelial barrier integrity through TEER both culture set-ups for each epithelial cell line were assessed for cell viability over the first 12 days of culture. For Caco-2 and Calu-3 cultures no significant difference in epithelial cell viability between those cultured alone and those in co-culture could be observed throughout the 12 day culture period under analysis (Figure 3.5 A & C). In the instance of HT-29 cultures, some deviation of the HT-29-18co co-cultures can be seen from day 6 onwards with increasing cell viability demonstrated over the HT-29 monocultures but this was not found to be statistically significant (Figure 3.5 B).

3.4.5 Development of the epithelial tight junction

The development of the tight junction protein ZO-1 was investigated throughout the first 9 days of culture. In all monocultures and respective co-cultures the expression of ZO-1 was observed in as early as 3 days following cell seeding. In many of the cultures, despite the clear expression of the ZO-1 protein, the organisation of the protein into clearly defined junctional complexes had not yet occurred; staining appeared disorganised and indistinct (Figure 3.6 A-F). in contrast, for Calu-3/18co co-cultures (Figure 3.6 D), at the same time point, ZO-1 staining appeared more concentrated along defined cell borders compared to the Calu-3 monoculture and the other cell cultures at the same time point.

By day 6, tight junctions appeared to be forming more definite boundaries with localisation between adjacent cells becoming more apparent (Figure 3.6 G-J). Interestingly, for Caco-2 and HT-29 (Figure 3.6 G-H &K-L), the co-culture set-ups appear to have developed faster into sharp, cobblestone-patterned staining compared with their monoculture counterparts. Calu-3 cells again tell a different story with both the monocultures and CCD-18co co-cultures displaying the typical, clear and organised staining along individual cell boundaries (Figure 3.6 I & J).

By day 9, all culture set-ups exhibited well defined ZO-1 staining typical of boundary epithelia (Figure 3.6 M-R). There appears to be little difference between the mono and co-cultures with respect to Caco-2 and Calu-3. HT-29/CCD-18co cultures however appear to display a greater degree of well-arranged intercellular staining compared with the HT-29 monoculture (Figure 3.6 Q & R).

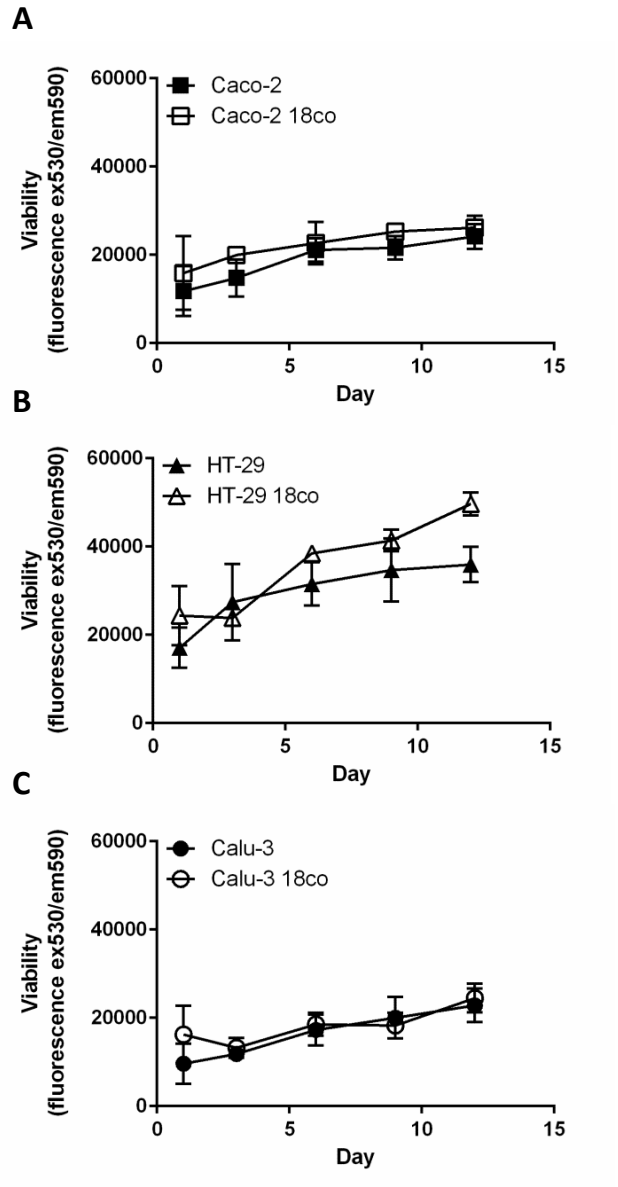

Figure 3.5. PrestoBlue cell viability in epithelial monocultures and epithelial-myofibroblast co-cultures. Cell viability was assessed by the PrestoBlue assay in monocultures and CCD-18co co-cultures of (A) Caco-2, (B) HT-29 and (C) Calu-3. Values represent means ± 1 S.D, for (A) & (C) n=7-9 from a minimum of 3 independent experiments. For (B) n=3-9 from at least 1 experiment.

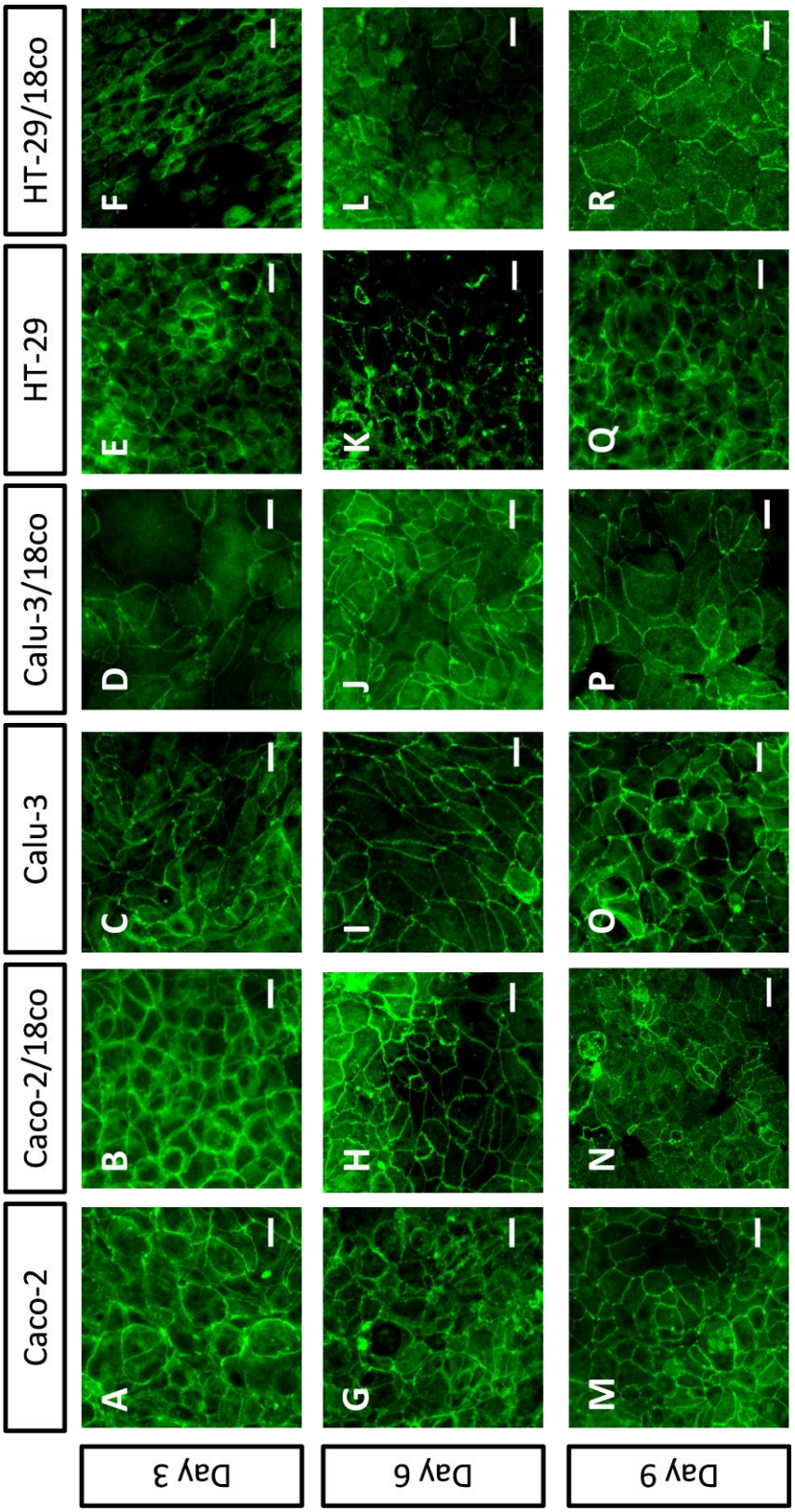

Figure 3.6 Tracking the development of the epithelial tight junction. Representative immunostained micrographs for tight junction protein Zona Occludens-1 in Caco-2, Calu-3 and HT-29 monocultures and their respective CCD-18co co-cultures over the first 9 days of culture. Scale bars equal 20 µm.

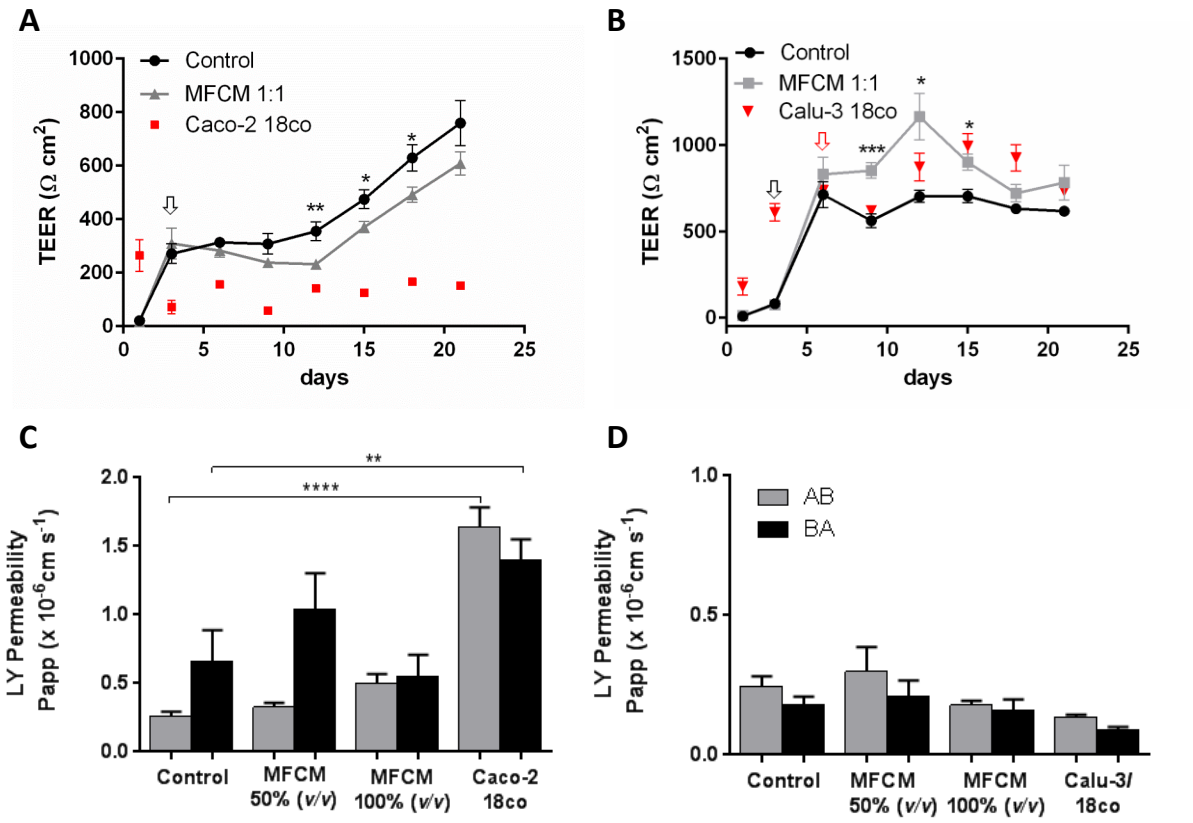

Figure 3.7 Electrical resistance and lucifer yellow permeability in myofibroblast conditioned media treated Caco-2 and Calu-3 monolayers. TEER measurements over a 21 day period and lucifer yellow permeability in (A & C) Caco-2 and (B & D) Calu-3 monolayers when treated with media conditioned by CCD-18co myofibroblasts. 100% MFCM treated monolayers were omitted for clarity. (A & B) Epithelial-myofibroblast co-culture values shown for comparison (red). Black arrow indicates commencement of conditioned media treatment. Red arrow indicates start of air-liquid interface culture. Values represent means ± 1 SEM, n=4-9 inserts from a minimum of 2 independent experiments. Significance determined by Student's t-test (A & B), One-way ANOVA with Sidak's multiple comparisons (C&D). * $p \leq 0.05$, ** $p \leq 0.01$, ***$p \leq 0.001$.

3.4.6 The effect of myofibroblast conditioned medium on Caco-2 and Calu-3 monolayers

Treatment of Caco-2 monolayers with CCD-18co conditioned medium (MFCM) was able to produce a significant decrease in electrical resistance of the monolayer between day 12-18 of culture (Figure 3.7A). Both cultures display identical TEER up to day 3 of culture but following day 3 (and the commencement of MFCM treatment) TEER plateaus slightly and begins to gently decrease until day 12. The effect was most pronounced at day 12 of culture but a steep increase, similar to that seen in the monoculture control from the same time point, was then observed from day 12 onwards. Peak TEER values reached ~750 Ω cm^2 and ~600 Ω cm^2 for the monoculture control and the MFCM treated monolayers respectively.

With respect to Calu-3, MFCM treated monolayers showed increased electrical resistance from day 9-15 of culture with the most significant change occurring on day 9 (850 Ω cm^2 versus 561 Ω cm^2) (Figure 3.7.B) which was also the peak TEER observed throughout the culture period. After day 12 of culture TEER began to plateau on the Calu-3 control monolayer whereas a decrease was observed in the MFCM treated monolayers (1163 Ω cm^2 at day 12 to 720 Ω cm^2 by day 18); by day 18 no significant difference was observed between the two cultures.

In addition to measuring the electrical resistance the monolayers were assessed for the permeability of lucifer yellow in both apical to basolateral (AB/absorptive) and basolateral to apical (BA/secretory) directions. With regards to Caco-2 cultures, no significant differences were observed between control Caco-2 monolayers and the 50 and 100% (*v/v*) MFCM treated monolayers; all mean values demonstrated permeability below 1 $x10^{-6}$ cm s^{-1}. Caco-2/CCD-18co co-cultures revealed increased permeability in both absorptive and secretory directions by 6-fold and 2-fold, respectively (0.26 $x10^{-6}$ versus 1.64 $x10^{-6}$ cm s^{-1} from A to B and 0.66 $x10^{-6}$ versus 1.4 $x10^{-6}$ cm s^{-1} from B to A). For Calu-3 cultures no significant differences were observed in the permeability of lucifer yellow for any of the

MFCM treated cultures and also the Calu-3/CCD-18co co-cultures compared to the Calu-3 control monolayers.

3.4.7 Transmission electron microscopy of epithelial-myofibroblast co-cultures

Cross sections of all epithelial-myofibroblast cultures were analysed using transmission electron microscopy. Highly detailed micrographs can reveal the cellular structures not evident in microscopy and confirm expression of characteristic cellular features. Caco-2 and Calu-3 samples exhibited expected simple single epithelial monolayers (Figure 3.8 A & B). Higher magnification images of both samples revealed plentiful apical microvilli (MV) and apical expression of tight junctional complexes (white arrows) (Figure 3.8 D & E).

Unlike Caco-2 and Calu-3, HT-29 cultures formed multi layers of poorly differentiated cells in culture (Figure 3.8 C). Closer inspection revealed poorly formed apical microvilli but clear expression of apical tight junctions (Figure 3.8 F – white arrow). Due to poor adhesion to the transwell insert after fixation and during sample processing no image was acquired which included the underlying CCD-18co myofibroblasts and the overlying epithelial layer in the same frame. The presence of CCD-18co on the underside of the transwell inserts was subsequently confirmed by confocal electron microscopy (Figure A-1).

3.4.8 Brush border enzyme expression in Caco-2 and Caco-2/CCD-18co myofibroblasts co-cultures

Caco-2 cultures were specifically investigated for the expression of brush border enzyme aminopeptidase expression and for the impact of co-culture with CCD-18co myofibroblasts on the enzyme expression profile.

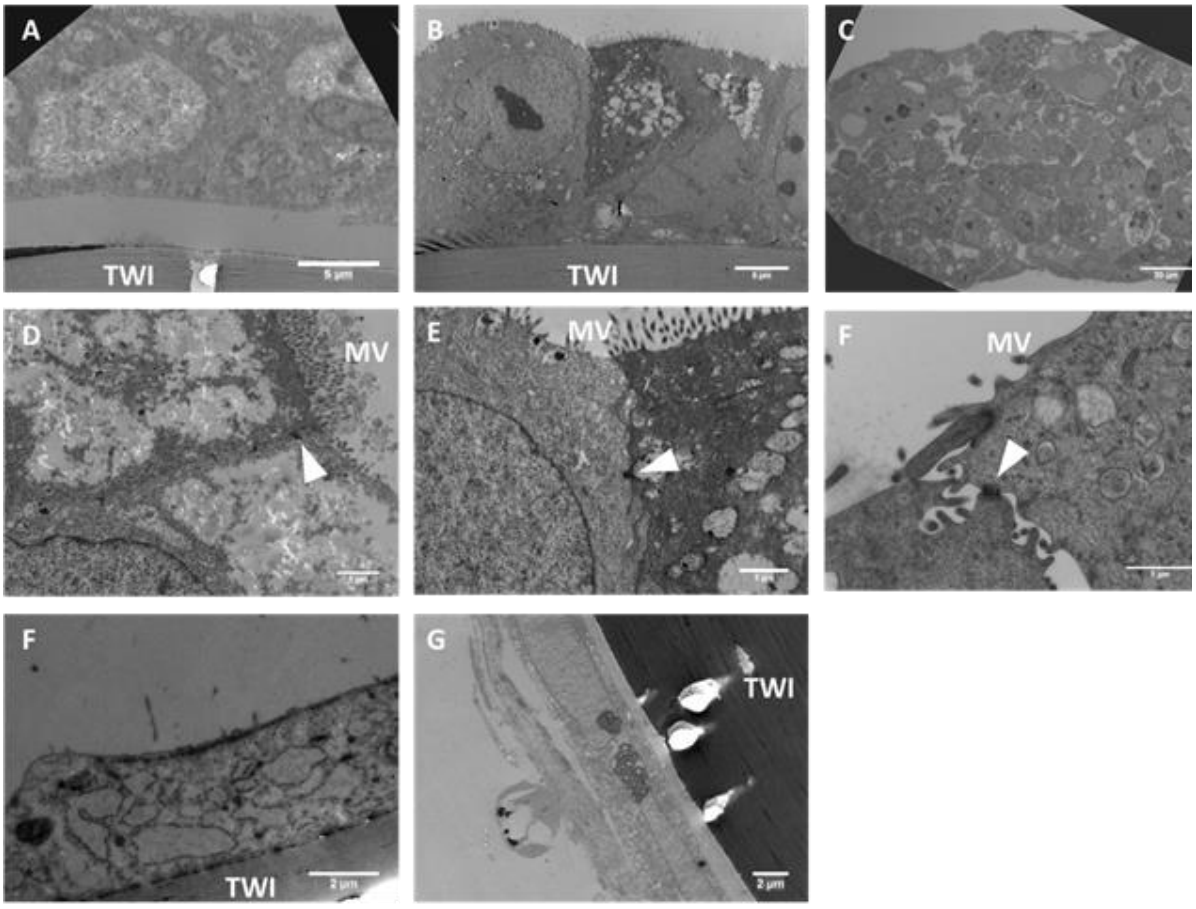

Figure 3.8 Transmission electron micrographs of epithelial-myofibroblast co-cultures. Epithelial-myofibroblast co cultures were sectioned and imaged to reveal cellular morphology and characteristic features. Overview of each respective epithelium; (A) Caco-2, (B) Calu-3 & (C) HT-29. (D, E & F) Higher magnification images of the epithelial layer reveal apical microvilli expression (MV) and tight junctions (white arrows). (F & G) CCD-18co myofibroblasts on the underside of the transwell inserts (TWI) in the respective co-cultures. For HT-29/CCD-18co significant cellular dissociation from the insert prevented image acquisition.

Monocultures of Caco-2 displayed a stepwise increase in expression of aminopeptidase throughout the culture period exhibiting an activity of 7.75 fmol/min/cell (Figure 3.9 A). Caco-2/CCD-18co co-cultures showed a delayed expression of aminopeptidase with a significant difference in enzyme activity at day 10 of culture compared to Caco-2 monocultures. The difference in enzyme activity after 21 days however had been diminished with no significant difference observed between the two culture set-ups at this time point. CCD-18co cells were initially used as a negative control within this experiment but interestingly the cell line demonstrated the ability to cleave the L-alanine- 4-amino-nitroanilide substrate. To elucidate this unexpected singularity, CCD-18co cells were checked for the expression of fibroblast activation protein. FAP is a membrane protein expressed in reactive stromal fibroblast cancers which is known to have serine protease function and might explain the observed protease activity. Composite microscope imaging (bright field, nuclear and FAP staining) showed CCD-18co were negative for the FAP protein (Figure 3.9 B). It should be noted that no positive control was available for this experiment.

3.4.9 Alcian blue and PAS staining of mucopolysaccharides

Alcian blue and PAS staining reveals the presence of polysaccharides, glycoproteins and glycoplipids such as those which compose the cell surface glycocalyx and mucus found on the intestinal epithelium. Microscope images of porcine intestinal segments revealed richly stained epithelial mucous layers for the duodenal section (Figure 3.10 A). Other sections did not display the same significant mucus layer but dense intercellular vesicular staining in the goblet cell population of the epithelium can be seen in all sections (Figure 3.10 B-F).

CCD-18co myofibroblasts, Caco-2 and HT-29 cells were subsequently stained with alcian blue and periodic acid schiff to visually detect variation in mucus secretion by each cell line. CCD-18co displayed minimal staining by either staining method (Figure 3.11 A & B). Caco-

2 cells showed more intense staining than CCD-18co cells with regional variation apparent within both samples where different staining intensity can be observed (Figure 3.11 C & D). HT-29 monocultures demonstrated the most significant staining by both alcian blue and PAS staining; dark blue and intense pink-red staining can be observed, respectively (Figure 3.11 E & F).

3.4.10 TEER and permeability evaluation of HT-29/Caco-2 Co-culture

HT-29 and Caco-2 co-cultures were evaluated for the barrier properties by TEER and lucifer yellow permeability. Co-cultures of HT-29 and Caco-2 displayed TEER values proportional to the two parent cell populations (Figure 3.12 A). Unlike Caco-2 monocultures, HT-29 monocultures exhibit very low TEER values and co-cultures of both cell types result in resistance values proportional to the fractions of the original cell seeding density. TEER values at day 15 and day 21 for both cell seeding ratios showed reasonable correlation to the calculated theoretical values with the exception of the 1:1 co-cultures at day 21; the experimental value was nearly half of the expected theoretical value (Table 3-1). It is notable that for the 1:9 co-cultures substantial variation was observed at day 21 (300 ± 217 Ω cm^2) compared to the other cultures. Despite this, significant differences were observed at day 15 and 21 between all the investigated combinations with the exception of HT-29 monocultures and 1:1 HT-29/Caco-2 co-cultures at day 21(Figure 3.12 B).

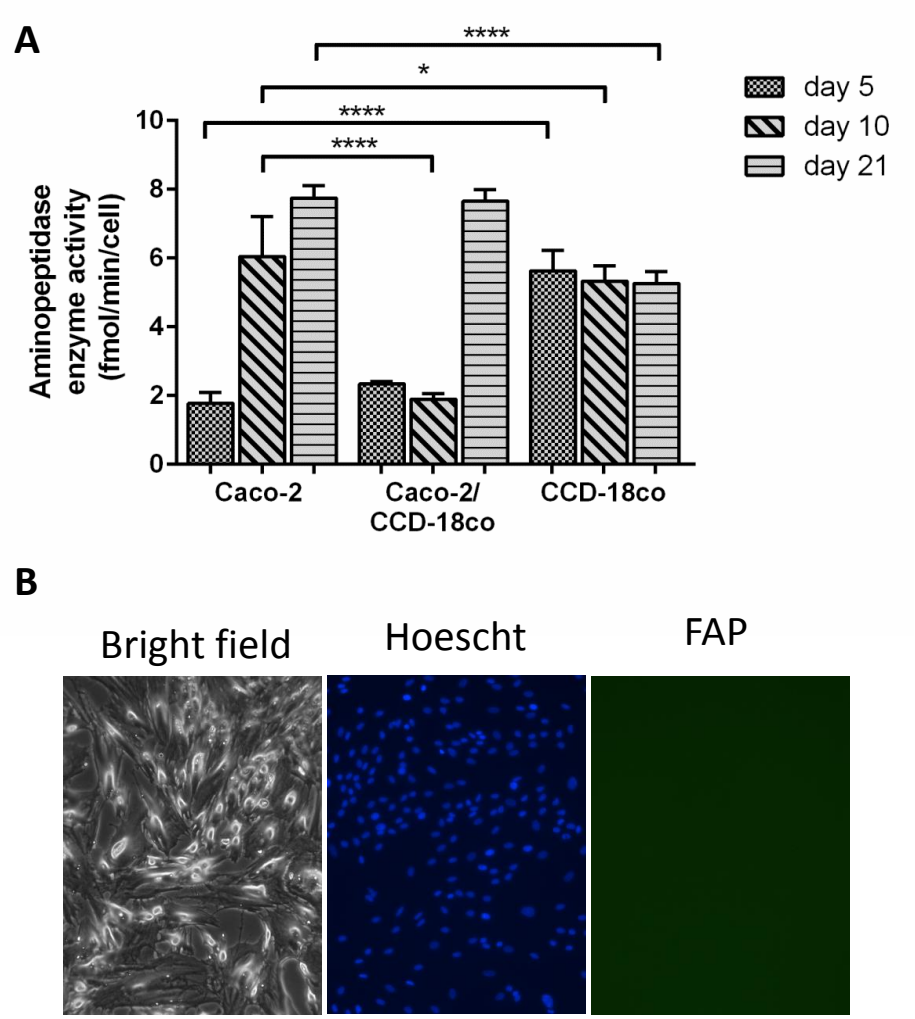

Figure 3.9.Investigating aminopeptidase enzyme activity in Caco-2 monocultures, Caco-2/CCD-18co co-cultures and CCD 18co. (A) Aminopeptidase enzyme activity at day 5, 10 and 21 of culture. (B) Immunostaining of CCD-18co myofibroblasts for fibroblast activation protein (FAP). Values represent mean ± 1 S.D, n=5-12 from a minimum of 3 independent experiments. Significance determined by one-way ANOVA with Sidak's multiple comparisons, * $p \leq 0.05$, ** $p \leq 0.001$, **** $p \leq 0.0001$.

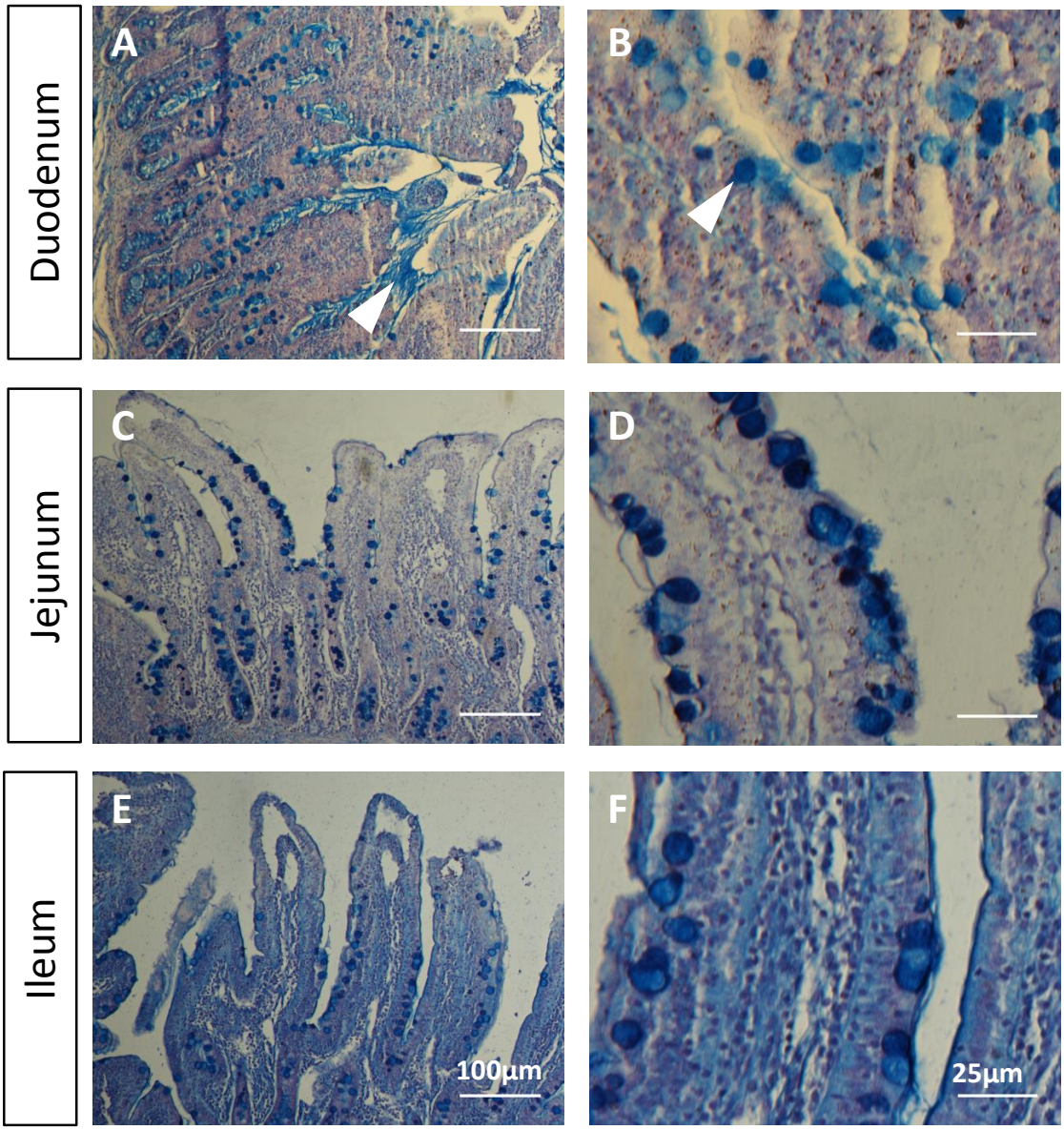

Figure 3.10 Alcian blue stained sections of regional porcine intestinal segments Regional (A & B) Duodenal, (C&D) Jejunal and (E &F) ileal porcine intestinal segments were stained for mucopolysaccharides using alcian blue (pH 2.5). Significant mucus layers can be visualised on the epithelial surface (A - white arrow) as well as concentrated compartmentalised mucus containing vesicles (white arrow-B) in all sections.

Permeability of lucifer yellow was also assessed at day 21 of culture (Figure 3.12 C). A stepwise decrease in permeability was observed from HT-29 ($5.98 \pm 1.35 \times 10^{-6}$ cm s^{-1}) through to Caco-2 ($0.31 \pm 0.04 \times 10^{-6}$ cm s^{-1}) although there was no significant difference in permeability between 1:9 cultures ($0.74 \pm 0.33 \times 10^{-6}$ cm s^{-1}) and Caco-2 monocultures.

Table 3-1. Comparison of actual and theoretical HT-29/Caco-2 co-cultures. Theoretical and actual TEER values (mean) at day 15 and day 21 of culture for HT-29/Caco-2 co-cultures at ratios of 1:1 and 1:9 (HT-29 to Caco-2).

	TEER (Ω cm^2)				Permeability (P_{app} x 10^{-6} cm s^{-1})	
Day	**15**		**21**			
	Actual	**Theoretical**	**Actual**	**Theoretical**	**Actual**	**Theoretical**
HT-29	37		55		5.98	
1:1	60	69	67	103	3.26	2.11
1:9	213	229	300	351	0.74	0.59
Caco-2	540		885		0.31	

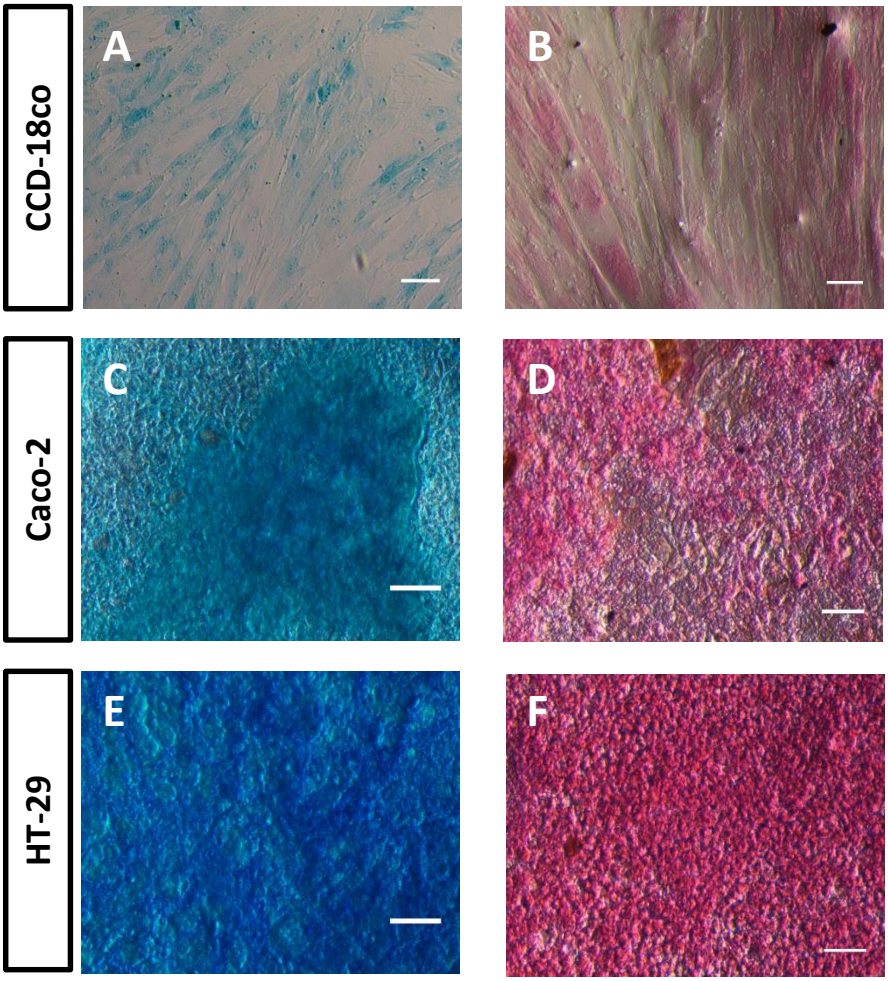

Figure 3.11 Alcian blue and PAS stained cell layers Mucopolysaccharides from apically secereted mucus can be stained with (A, C & E) alcian blue or (B, D & F) periodic acid schiff. (A-B) CCD-18co, (B-C) Caco-2 and (E-F) HT-29. Scale bars equal (A&B) 10 µm and (C-F). Scale bar equals 50 µm.

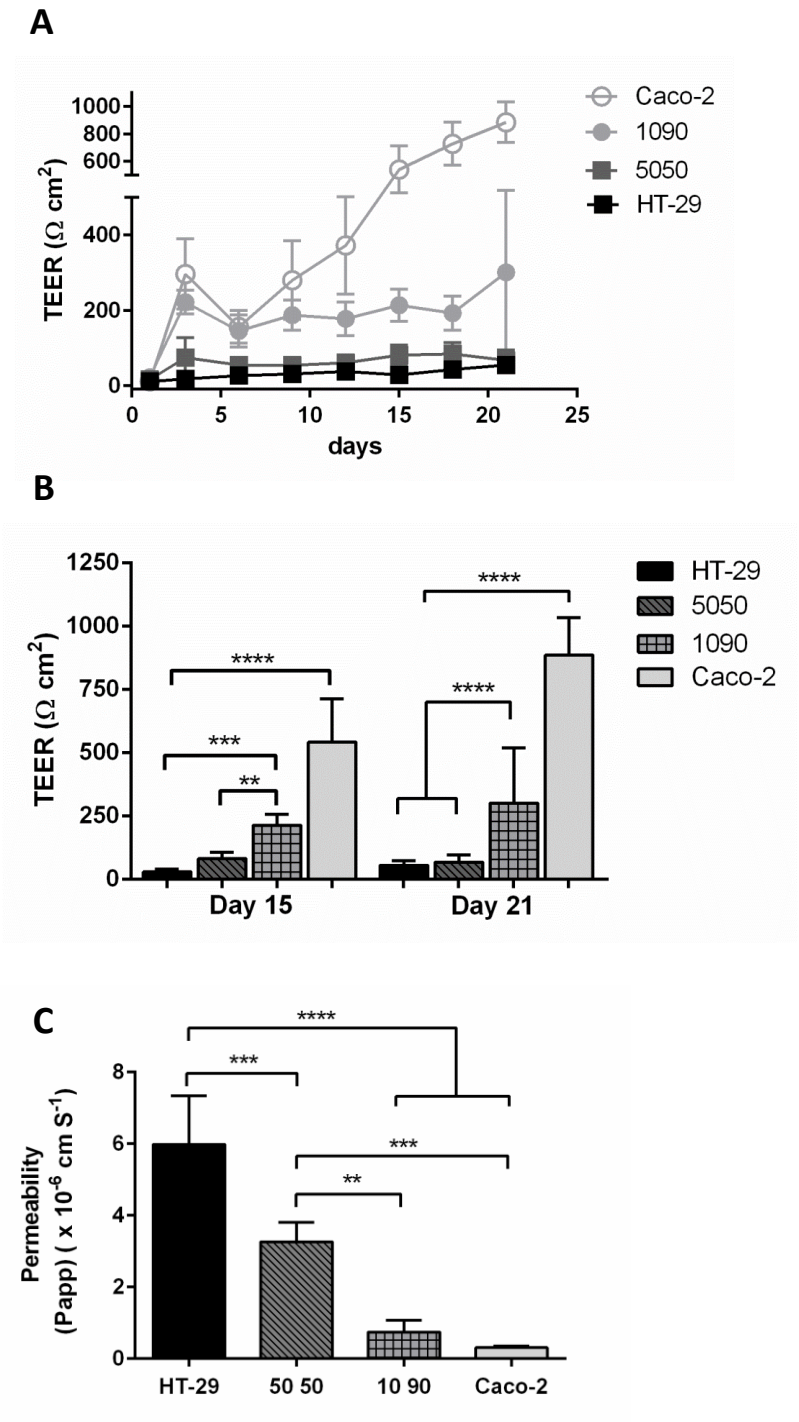

Figure 3.12 Electrical resistance and lucifer yellow permeability of HT-29 and HT-29/Caco-2 co-cultures (A) Electrical resistance in HT-29/Caco-2 co-cultures at initial seeding ratios of 50:50 and 10:90 during 21 days of culture compared to comparative monocultures. (B) Comparison of TEER at day 15 and day 21 of culture. (C) Permeability of lucifer yellow in each respective culture set up at day 21 of culture. Values represent means ± 1 S.D, (B) n=9-14 inserts from a minimum 3 independent experiments. (C) n= 6-13 inserts from a minimum of 2 independent experiments. One-way ANOVA with Tukey's multiple comparisons, ** $p \leq 0.01$, ***$p \leq 0.001$, ****$p \leq 0.0001$.

3.5 Discussion

The aim of this chapter was to evaluate CCD-18co as a cell line which could be used in lieu of primary MFs for an *in vitro* epithelial-myofibroblast intestinal model. Furthermore CCD-18co cells were assessed in co-cultures on conventional transwell inserts with common epithelial cell lines. The mechanism of the barrier modulation was also briefly investigated in addition to further consideration of other potential myofibroblast induced changes. Finally HT-29/Caco-2 co-cultures were explored as a potential addition to the development of an epithelial-myofibroblast model.

Myofibroblasts are acknowledged for their plasticity; their ability to change shape and expression profiles in response to external stimuli[30,48]. CCD-18co cells are described as normal colon fibroblasts by the ATCC (American Type Culture Collection) and were derived from a neonate (2.5 months old). Characterisation of intermediate filament markers by immunochemistry revealed CCD-18co cells exhibit the expected stellate or spindle morphology of fibroblasts[118,119] and express the intermediate filament markers of myofibroblast cells, significantly they are α-SMA(+). It is generally believed that although myofibroblasts are phenotypically halfway between fibroblasts and smooth muscle cells they only express α-SMA and not the smooth muscle marker, desmin[32,47,120,121]. It has been previously demonstrated that ISEMFs, in some cases, can be faintly desmin(+)[117] however, significant expression was observed in CCD-18co cells in this study on both growth substrates.

Furuya and Furuya conflictingly suggest that MFs in the tip region of the villus are actually desmin (+)[46], a hypothesis to the contrary of the aforementioned experimental evidence regarding the expression profiles of ISEMFs. Furthermore, the fact that CCD-18co cells stain strongly for vimentin, a potent indication they are not smooth muscle cells[122], only adds further ambiguity to the finding. CCD-18co have been shown to exhibit all the known

characteristics of myofibroblasts[48] and as a result have been used extensively as a myofibroblast cell line for *in vitro* studies[14,48,112,114,123]. However, no study has published data regarding desmin expression in CCD-18co.

Mifflin *et al*., have suggested that the sub-epithelial component of the small intestinal villus is potentially composed mainly of pericytes rather than purely ISEMFs[124]. Furthermore they suggest that true ISEMFs, that is the fibroblast population that is α-SMA(+), vimentin(+) and desmin(-), actually line the crypt epithelium of the small and large intestine. Given the close morphological and phenotypical similarity (intermediate filament expression) of the cells of the lamina propria, the classification of the cells is convoluted. It is agreed these cell types are likely to share mutual functions but at the same time are also are clearly distinct lineages in their own right. Given CCD-18co cells are α-SMA(+), vimentin(+) and also desmin(+) it is quite possible that instead of being true ISEMFs that they are in fact pericytes. It would not be surprising considering the similarity of the two cell types in function and morphology that they have been misrecognised until now. The intermediate expression profile of CCD-18co matches that of intestinal pericytes more than that of ISEMFs[124,125]. Furthermore pericytes, unlike ISEMFs, have been shown to express aminopeptidase[125-127]which adds weight to this argument and is an important distinction which will be argued later in this discussion. There are examples of *in vitro* studies of lung pericytes modulating endothelial monolayer TEER[128] and also numerous instances of similar modulation observed in comparable *in vitro* studies using brain derived pericytes and endothelial cells (blood brain barrier)[129-131].

There was also some indication that the culture substrate plays a role in α-SMA expression. Some weak α-SMA staining was observed on glass but it appeared reduced compared to transwell cultures. Culture substrate is known to play significant role in cell response and behaviour and this type of plasticity has been demonstrated before even in cell lines[132]. The morphology of CCD-18co on the two culture substrates was markedly different. CCD-18co

cultured on glass had a more flattened and stellate morphology whereas they formed spindle –like shapes with quite well defined directional growth patterns on transwell surfaces. Arguably both stellate and spindle-like shape morphologies are equally characteristic of fibroblastic cells so perhaps this observation is not entirely indicative of anything significant[118]. Considering cell shape has intimate connection to function it is perhaps important that simple differences in culture substrates can have a fundamental effect on cellular gene and protein expression.

The gradual increase in electrical resistance during epithelial cell culture is indicative of cellular confluence and also the expression of tight junctional complexes between neighbouring cells[133]. The TJs selectively regulate the movement of solutes across the epithelium; TJ expression in cell monolayers, on inserts such as transwells, can be monitored simply by measuring the TEER. Considering the huge variation in published TEER values for Caco-2 monolayers, the reasons for which are several-fold, it is difficult to compare from one lab to another even when the exact cell line clones and protocols are used[134]. It is generally considered that due to the colonic origin of Caco-2 these cells exhibit higher TEER values than is physiologically relevant to the upper regions of the GI tract regardless of the plethora of other factors involved in observed variation in TEER. In this work, Caco-2 monocultures reached ~500 Ω cm^2 from day 15 and up ~1000 Ω cm^2 at day 21 and beyond. Artursson and colleagues regularly achieve TEER values of ~260 Ω cm^2 [5] whereas it is not unheard of for groups to report values in excess of 1000 Ω cm^2 [18,19,65] and some have been reported even as high as 1600 Ω cm^2 [14].

CCD-18co, which only form gap junctions between adjoining cells[48], display a negligible TEER reading throughout culture and thus are not considered to directly contribute to overall TEER during co-culture. Caco-2 and CCD-18co co-cultures of display similar TEER values to Caco-2 monocultures up to day 6 but Caco-2 monocultures continue to rise throughout later periods of culture; Caco-2/CCD-18co co-culture TEER values remain

comparatively low from day 10-21 (between 150-250 Ω cm^2). This result is particularly striking given HT-29, another colon derived epithelial cell line, shows almost no change in TEER when co-cultured with CCD-18co compared to monocultures. Calu-3 airway epithelial cells, unlike the colonic epithelial lines, displayed a marked increase in TEER, most significantly in the early stages of culture (day 1-3) but also in later stages (days 9-12). This enhancement of Calu-3-myofibroblast TEER in co-culture is in agreement with other studies[115,116]. Whilst this might suggest a tissue-specific (perhaps even cell-specific) response (i.e. gut versus airway) Beltinger *et al*., whilst using primary myofibroblasts, proved a similar increase in TEER in HCA-7 cells[34] (a weak barrier forming colonic derived epithelial line) to that observed for Calu-3 in this study. Clearly these results suggest that the mechanism of myofibroblast-mediated epithelial barrier modulation is cell-specific. It might be that the pathways and signalling systems involved in the modulation process can be acquired or lost by cells (aberrant cellular signalling is a well-described process which can occur in a variety of situations); through events that occur during extended periods of culture (i.e. passage induced), as a result of the original oncogenesis (i.e. for tumour derived lines) or the immortalisation process.

Interest in the HT-29 line (and its various clones) as a model of intestinal enterocytes is born from the fact that it demonstrates a lower TEER than Caco-2, increased permeability to molecules permeating via the paracellular pathway and is also known to produce mucus[19,108,109,135,136]. This was further confirmed in this work with comparable TEER's observed for HT-29 to those reported in literature (<100 Ω cm^2), increased permeability to hydrophilic paracellular permeability marker lucifer yellow in addition to intense apical alcian blue and PAS staining. This low TEER, high permeability phenotype is unusual considering TEM imaging revealed that HT-29 cultures grew as dense multi layers, unlike Caco-2 and Calu-3. Given the significant degree of multi layering, which can be common in epithelial cultures[5,100] one might expect paracellular permeability to be retarded in some way due to the tortuous pathway that would presumably exist in such a situation. The

permeability of lucifer yellow in this study is similar to mannitol permeability observed by Wikman-Larhed for HT-29 monocultures[108]; both of which are commonly used as low permeability, paracellular markers for *in vito* monolayer studies.

The characteristics of HT-29 can be further utilised by physically mixing them with Caco-2 to achieve intermediate barrier properties with more relevant reconstitution of tissue function (i.e. through added mucus production and a more permeable barrier phenotype). As Wikman-Larhead and Artursson previously postulated, the two cell types can be considered as resistors acting in series; as such TEER and permeability values for intermediate HT-29/Caco-2 co-cultures could be calculated theoretically, with a relative degree of accuracy, from the prospective experimental results derived from each of the respective monocultures[108].

The TEER results obtained for Caco-2 and Calu-3 could , albeit to lesser extent than direct CCD-18co co-cultures, be reproduced using CCD-18co conditioned medium (MFCM), replicating the observations of Beltinger *et al.*,[34]. However, these changes did not correlate to changes in paracellular permeability; no change to lucifer yellow permeability in Calu-3/CCD-18co and MFCM treated Calu-3 monolayers was observed compared to Calu-3 control monolayers. Caco-2/CCD-18co co-cultures however showed increase permeability in both absorptive and secretory directions compared to Caco-2 control monolayers although this did not translate through to MFCM treated Caco-2 monolayers. Changes in TEER have previously been demonstrated to not readily translate into functional permeability changes in cultured monolayers[75], the difference in TEER between the respective co-cultures and the monoculture equivalents was larger for Caco-2 than Calu-3. In that respect the observed difference in permeability could be intuitive in light of the changes observed in TEER.

Any potential CCD-18co mediated inhibitory or negative effect upon epithelial viability/growth was abrogated through the viability assessment using PrestoBlue. No

significant changes were detected in cell viability over an initial 12 day culture period and also comparable expression of tight junction (TJ) protein ZO-1was observed in all cultures. Whilst the viability assessment rules out any growth inhibition or impact on epithelial cell viability no clear changes in ZO-1 expression were immediately obvious that would help explain the experimental differences in TEER. ZO-1 is one of at least 40 different proteins involved in in the TJ complex and any potential alterations to the permeability of these cell-cell contact points may be through the alteration of any one of these proteins. It is believed that the claudin family of proteins are most likely the main players in determining overall tight junction 'leakiness'[58,133]. That the claudin composition can be varied in tight junctional complexes which, in turn, defines the permeability properties of the given junction has been suggested to explain variation of tight junction permselectivity in different endothelial and epithelial tissues through the body[58]. If myofibroblasts have a modulatory effect upon tight junction composition in the investigated cell lines then alteration in their claudin composition may perhaps be a mechanism for this and subsequently an explanation of the observed changes.

In a recent paper from Pereira *et al*., where Caco-2 cells were cultured in either direct contact with CCD-18co or CCD-18co cultured within matrigel, the authors proposed the reduction in TEER observed was a result of interspacing of CCD-18co between the overlying Caco-2 epithelial layer[14]. In general their published results are in agreement with the reported data herein, they too observed reduced TEER in Caco-2/CCD-18co co-cultures. However data reported herein suggests that paracrine mediated changes are more likely the reason for observed changes in TEER, especially considering the two cell types are physically separated by the transwell insert in our model which would restrict any possibility of direct interspacing, as suggested by Pereira *et al*.,. Furthermore, the only permeability assessment conducted in their study was using insulin; the permeability of which across epithelial boundaries is controversial especially given peptide and dietary handling by

enterocytes is a matter of debate[137]. Insulin permeability could be facilitated via receptor mediated transcellular mechanisms in addition to any paracellular flux.

The effect on epithelial brush border enzyme expression in Caco-2/CCD-18co co-cultures was also investigated to ascertain whether CCD-18co have any further regulatory effect on epithelial function. Enzyme expression seemed to be delayed in co-cultures compared to the monoculture equivalents although results were comparable by day 21 of culture. CCD-18co cells demonstrated significant and most unexpected aminopeptidase activity. It has been shown that activated, tumour associated fibroblasts are functionally different to normal fibroblasts and have been shown to express, amongst other things, fibroblast activation protein (FAP)[138,139]. FAP is a membrane-bound, 95 kDa cell surface glycoprotein which is integral to matrix remodelling and contributes to tissue invasion during tumorigenesis. Specifically it has been shown to have dipeptidyl peptidase and collagenase activity and could have been an explanation for this unexpected observation. Immunostaining against FAP however was negative. Another explanation to this data is that to which has previously been alluded to; that CCD-18co is in fact of pericyte lineage and not a true ISEMF. Perciytes, which have already been discussed, share many traits with ISEMFs. The exception to this being that pericytes are desmin (+) and also have been shown to express aminopeptidase[125-127]

This work identifies further the influence of stromal cells, such as myofibroblasts, on epithelial barrier function and also on the permeability of hydrophilic molecules which permeate via the paracellular pathway. Most significantly the mechanism of epithelial modulation appears both cell and tissue specific. Further elucidation of the exact mechanism of barrier modulation and potential downstream consequences (e.g. tight junction remodelling) would be of considerable interest. Of most significant interest is the exact identification of the CCD-18co phenotype. As this work is not presented in chronological order, further elucidation and additional confirmation of CCD-18co cells was

not achieved within this thesis work. The knowledge gained from this work was drawn together with work from the next experimental chapter, design and production of an architecturally mimetic scaffold produced by electrospinning, to work towards the aim of producing an epithelial-myofibroblast *in vitro* cell model.

4. Design and production of a architecturally mimetic cell scaffold produced by electrospinning

4.1 Introduction

Cells are intuitively connected to their environment through specific receptor mediated contact with the protein rich extracellular matrix (ECM). Cell fate, whether that is cell division, differentiation down a specific specialised lineage or death by apoptosis, is prompted by internal cellular processes which in turn can be a consequence of external signals. Cell-cell contact, the secretion of chemical mediators by neighbouring cell populations and signals delivered through the supportive ECM, is crucial to regulating basic cell behaviour[140]. Many of the standard materials currently used in cell culture fail to recreate the complex structural, chemical and multicellular milieu which cells experience in the body.

Within epithelial tissues, such as the intestinal mucosa, the overlying epithelium is physically separated from the underlying stroma by a basement membrane (BM). The basement membrane is a dense sheet-like structure that acts as a barrier between the two distinct compartments of the tissue[141] and in several tissues the BM also acts as a filter with selective permeability[142]. BMs can be considered a specialised form of ECM and although it shares similarities with interstitial ECM their structures are quite unique (Figure 4.1) and very often tissue specific[143,144]. The BM is composed of three distinct layers; the lamina lucida which is adjacent to the apical cell surface; the lamina densa (an electron dense layer) and the lamina fibro reticularis. The underlying ECM of the stroma is a more porous fibrillar structure which physically surrounds the cells and can be constantly remodelled by the cells which inhabit it. Given the complex chemistry and geometry of the ECM it is quite difficult to synthetically mimic it *in vitro*. It could be argued the most effective way to

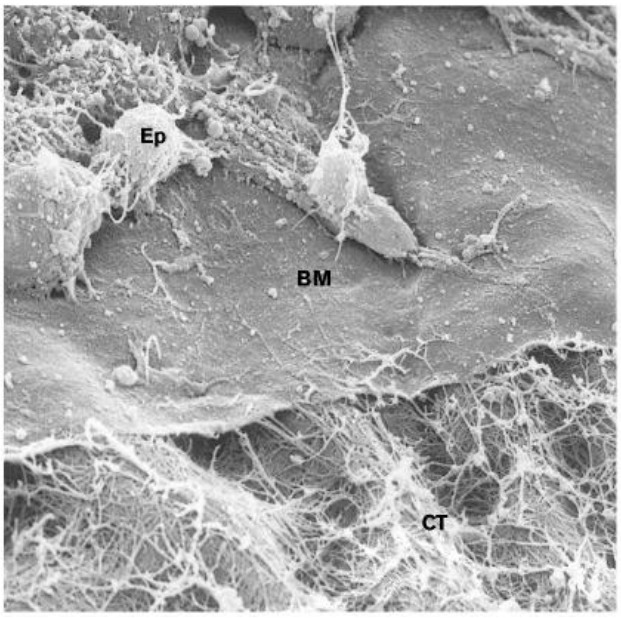

Figure 4.1 Representative scanning electron micrograph of corneal epithelium. Epithelial cells (Ep) grow on specialised dense extra cellular matrix sheets known as basement membrane (BM). The BM membrane supports the adhesion and growth of epithelial cells and importantly separates the epithelium from the underlying stroma. The connective tissue ECM (CT) can be seen as a more porous fibrillar structure underneath the BM. Taken from Schwarzbauer [141]

reproduce such structures in the lab would be to initially provide minimal structural support to cells and then allow the self-assembly of the BM and ECM structures by the cells themselves. For example it has been previously demonstrated that CCD-18co cells produce fibronectin *in vitro*, a major component of ECM *in vivo*[14]. However, initial supportive structures are required to assist the production and self-assembly of cell produced ECM. Permanent supportive structures are likely to be necessary as a physical support, especially where cells are cultured for many weeks. Electrospinning is one technique which can used to bridge the gap between currently utilised flat, two-dimensional culture materials and the *in vivo* environment. Scaffolds produced by electrospinning more closely reflect the three-dimensional, porous fibrous structures of the ECM[141,145] and can help promote more realistic environmental conditions for cell culture[116,146,147].

The process of producing fibrous material by electrospinning enables the manufacture of micro and nano sized material which can support cell growth *in vitro*. The aim of utilising this technique is to better mimic the physical architecture of the nanofibres that compose the BM and ECM structures[145] whilst preserving functional characteristics desirable for cell culture. This can include a high degree of porosity and permeability. Electrospun matrices also have the added potential to be produced on large scale with relatively simple manufacturing techniques[148] which is why they are of significant interest in scientific research.

Other materials and scaffold types have been used for the support of multiple cells for *in vitro* models, such as hydrated fibrillar structures (hydrogels), with mixed success. Hydrogels are a subject of immense interest for cell culture due to their nanofibrillar structures and biocompatibility. Yu *et al.*, noted that in their *in vitro* villous model, which utilised collagen hydrogels, the hydrogel itself became the limiting barrier to permeability for rapidly transported drugs[12]. Furthermore due to the inherent characteristics of hydrogels (e.g. their high water content) their use in research can be prohibitive during certain processing steps for some experimental techniques (e.g. where dehydration with alcohols is required), which can further limit their use.

Pusch *et al.*, used decellularised porcine jejunum sections as a supportive matrix for Caco-2 cultures which displayed some promising tissue phenotypes. However, as the scaffolds are sourced from porcine donors it is quite an intensive and expensive process and not immediately suitable for high throughput[11]. Kim et al., used in-house produced polydimethylsiloxane (PDMS) membranes in their "gut-on-a-chip" which mimics semipermeable membranes (much like transwell inserts) and simply coated the material with collagen for compatibility[17,18]. Pereira *et al.*, and Leonard *et al.*, both used transwell inserts in conjunction with hydrogels (Matrigel and Collagen, respectively) to make a 3D construct to support co-cultures.

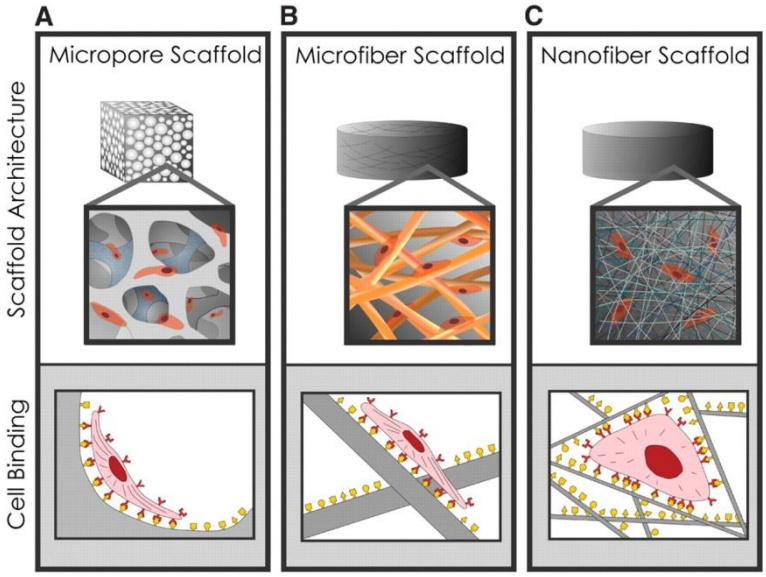

Figure 4.2.The effect of scaffold architecture on cell-matrix interactions. The extent of cell attachment and spreading on surfaces can be dependent upon nanoscale features of the cellular microenvironment. (A) Microporous and (B) microfibre scaffolds display lower surface areas for protein absorption and subsequent cell attachment. (C) Nanofibrous scaffolds have a higher surface area for increased cell-matrix interactions which is more closely related to the in vivo environment. Taken from Stevens & George[145].

Electrospinning as a technique is historically entrenched in the textiles industry where it was used in the production of fabrics. It has since garnered interest with several potential biomedical applications. The high degree of porosity and surface area in addition to the morphological similarity to ECM, make fibre scaffolds an interesting prospect for cellular scaffolds. The high surface area allows for more significant protein absorption than two-dimensional constructs and thus allows significantly greater interaction of cells with matrix components (Figure 4.2). It is proposed that additional binding sites offered by nanoscale architectures should be more realistic than traditional microscale geometries[148]. Many materials can be used for electrospinning and the ability to functionalise the materials before and after electrospinning is a further advantage[149-152]. It has also been demonstrated that electrospinning can be employed alongside Rapid Prototyping (RP) techniques (such as VAT photopolymerisation). RP describes a number of technologies which can be used to produce models in a layer by layer fabrication process using digital data. RP enables the manufacture of freeform geometries that are not possible with other fabrication properties

providing scope to construct physiologically relevant shapes to tailor extra dimensions of design to fibre scaffolds[153] in the aim of creating tissue-specific structures.

The production method of non-woven fibre scaffolds (i.e. randomly orientated fibre meshes) is relatively simple. A polymer dissolved in an appropriate solvent is passed through a spinneret with an applied electrical current. The applied current creates an electric field between the spinneret and a grounded collector plate or mandrel. A droplet of charged polymer solution at the tip of the spinneret begins to elongate as the surface tension of the solution is overcome by the electrostatic force. A conical shape (known as the Taylor cone) begins to form in the polymer droplet and a liquid fibre jet erupts from the surface. Provided the cohesive property of the solution is sufficiently high, a constant fibre is emitted from the Taylor cone. The projected fibre is elongated by a whipping motion, which occurs as a result the instability of the jet beyond a certain distance from the spinneret, drying the fibre (in addition to evaporation of the solvent within the liquid jet) before the finally depositing on the collector (Figure 4.4).

The process of electrospinning and the resulting properties of the fibre meshes are governed by several factors. It is generally agreed within the literature that polymer concentration, flow rate, applied voltage and tip-collector distance are the most significant process variables[154-156]. The properties of the polymer solution play an important role in the process (e.g. solubility, molecular weight and conductivity). Environmental factors, such as humidity, can also influence the final fibre morphology. This is usually as a result of changes in solvent evaporation from the polymer jet which can be more or less significant depending on properties of the polymer[157,158].

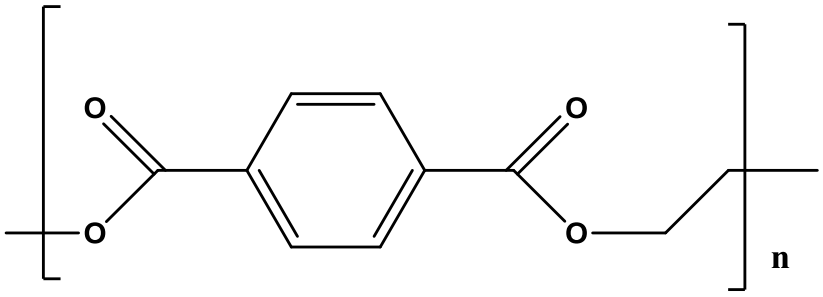

Figure 4.3. Molecular structure of the repeating subunit of poly (ethylene terephthalate).

Poly (ethylene terephthalate) (PET) is a widely used polymer for commercial applications (drinks bottles, containers and clothing fibres) in addition to its significant use in cell culture products (traditional porous filters, such as transwell inserts, can be made from PET). As a result this material allows us to investigate the effect of scaffold topography (with respect to the nanofibre morphology) whilst using a familiar material. It benefits from being durable; its resistance to organic solvents lends itself to simple processing for many microscopic techniques (e.g. SEM/TEM). Furthermore it is inexpensive, relatively inert and non-toxic[159] and also non-degradable. All these factors make it a useful material for long term cell culture. There are also many previously cited examples of its use in the literature for tissue scaffolds for *in vitro* models[72,115,116] in addition to transplantable graft constructs[159,160].

4.2 Aims

The aims of this chapter were to investigate electrospinning as a method to produce fibre scaffolds akin to the BM and ECM structures. To optimise the scaffold processing parameters based on their morphological features (i.e. fibre diameter, interfibre distance etc.) and explore the amenability of the scaffolds to cell culture. The final aim was to investigate rapid prototyping as a production method to produce 3D formers, replicating the villi architecture, which are amenable to the electrospinning process.

- Optimise conditions to produce consistent nanofibre PET scaffolds for cell culture
- Characterise scaffold morphology (fibre diameter, pore size, thickness)
- Investigate cell compliance with PET scaffolds
- Explore the use of resin formers to confer 3D macroarchitecture to the scaffolds structures

4.3 Methods

4.3.1 Electrospinning

Electrospinning was conducted as previously mentioned (2.2.11). Particular processing conditions (e.g. flow rate, collection method and polymer concentrations) are mentioned in the results section. Unless otherwise stated, the processing parameters were a solvent ratio of 1:1 (TFA to DCM), an applied voltage of 14kV, a tip-collector distance (TCD) of 15 cm and an 18 gauge spinneret. Electrospinning was conducted at ambient conditions in a ducted fume hood. For static-collection electrospinning, the original aluminium collector plate dimensions were 15 x 10 cm and spinning conducted for 4 hours with the plate rotated half way through (to ensure homogenous coating of the collector surface). Subsequently the collector plate dimensions were re-defined with area 12 x 7 cm and the total spinning time reduced to 2 hours with rotation half way through spinning (1 hour). For rotating drum collection, the dimensions of the collection surface were 10.8 x 22 cm. All samples were imaged by SEM for morphology prior to use for cell culture.

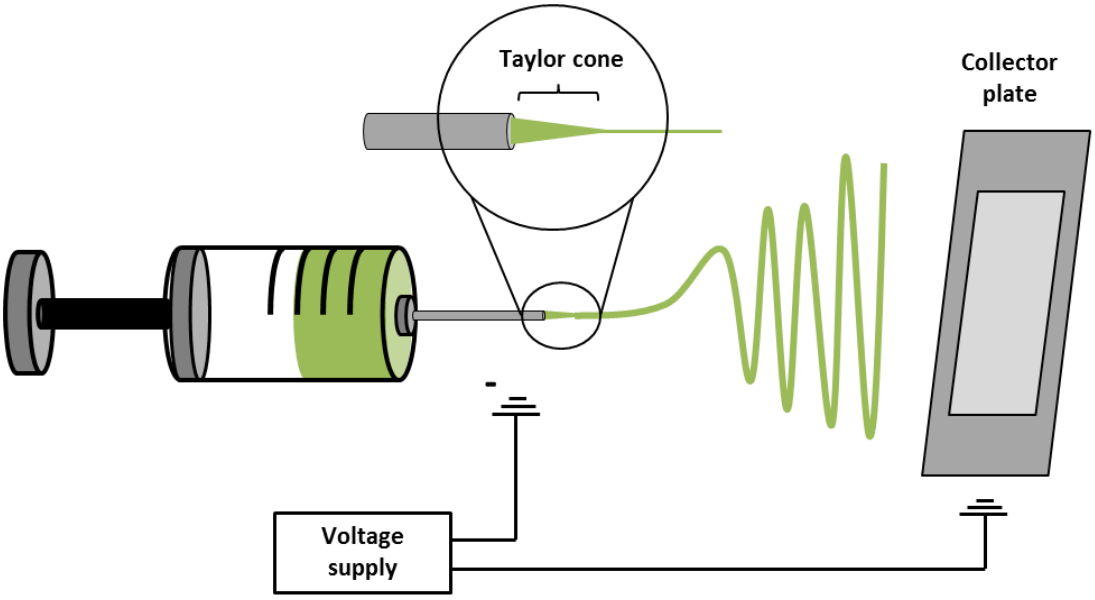

Figure 4.4. A typical example of an electrospinning set up. A polymer solution is passed through a syringe with the aid of an automated syringe pump. At the end of the spinneret, which has a voltage supply applied to it, a structure known as the Taylor cone forms. At high enough voltages the surface tension is overcome and this results in the eruption of a polymer jet from the Taylor cone and the fibre undergoes whipping motion prior to deposition on a grounded collector plate.

4.3.2 Image analysis

ImageJ was routinely used to analyse scanning electron micrographs to determine general scaffold morphology, fibre diameter and inter-fibre distances (as a gauge of scaffold pore size) and scaffold thickness (measured from histological cross sections).

4.3.3 Surface Treatment of PET nanofibre scaffolds

Nanofibre scaffolds were surface functionalised with either allylamine monomer using plasma deposition or surface coated with type I bovine collagen. Plasma deposition of ultra-thin polymer films is a method for functionalising material surfaces to change its physical and/or chemical properties. Electrically exciting a plasma polymer to the gas phase allows for the coating of complex surface geometries and has a variety of applications. For an excellent review of plasma deposition technology the reader is referred to Michelmore *et al.*,[161].

For plasma deposition the glass reactor chamber was initially wiped down with acetone to remove any remaining monomer. Subsequently the chamber was cleaned further by oxygen plasma struck at a pressure of 300 mTorr for 5 minutes. Following this, sections of nanofibre PET scaffold were placed in the reactor chamber and struck with allylamine plasma at a pressure of 300 mTorr at an input power of 10 Watts for 5 minutes. Scaffold samples were then prepared for use in cell culture by cutting them into circular discs (21 mm diameter) using a using an in-house designed punch/borer. The discs were then sterilised in 70% (*v/v*) IMS for 15 minutes before extensive washing with sterile dH_20 and subsequently PBS. For type I bovine collagen coated samples, 150 µL of collagen solution was gently pipetted on the surface ensuring adequate coverage of the entire scaffold. Samples were allowed to air dry in a microbiological safety cabinet for 1-2 hrs. Any remaining collagen solution was aspirated and the scaffolds were rinsed lightly with PBS before cell seeding.

4.3.4 Comparison of surface treatment improvement on initial cell attachment and proliferation by the PrestoBlue assay

Collagen type I, plasma allylamine etched and untreated nanofibre scaffolds were mounted in CellCrown culture inserts. The mounted inserts were then placed in 12-well culture plates and seeded with cells (50,000 cells/insert) in their respective culture medium. Following 24 hours of culture at 37°C, 5% CO_2 the PrestoBlue viability was carried out according to previous mentioned protocols (Section 3.3.2.4). Subsequent viability assays were conducted on day 3 and day 6 of culture to provide an initial assessment into the benefit of the surface treatments.

4.3.5 Sessile water contact angle measurement of type I collagen coated nanofibre scaffolds

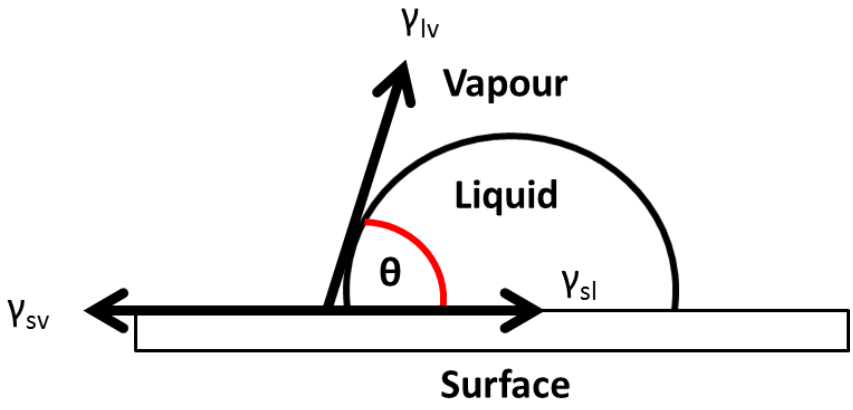

Figure 4.5. Water contact angle measurement by the sessile water drop technique. A droplet of water spread upon the substrate surface allows for a contact angle to be measured. The contact angle is that between the tangent drawn between the three phases (solid, liquid and vapour). Adapted from Kumar & Prabhu[162].

The water contact angle can be used to measure the surface energy, wettability and adhesion properties of a material. A small drop of water is dispensed upon the surface and the angle (θ) where the three phase line (where the droplet interfaces the sample surface and the external environment) is measured. Following surface treatment the substrate can become more or less hydrophilic/hydrophobic.

The angle is calculated by Young's equation which describes the surface tension and the contact angle.

Equation 4-1

$$\gamma_{lv}\cos\theta = \gamma_{sv}-\gamma_{sl}$$

Where γ_{lv}, γ_{sv}, γ_{sl} are the surface tensions of the three interfaces (liquid-vapour, solid-vapour and solid-liquid, respectively).

Strips of nanofibre PET scaffold (10% *w/v*) were attached to glass slides until taut and secured in place with tape on the underside of the slide. Samples were subsequently treated with type I bovine collagen at stock and working concentrations (3.1 mg/mL and 31 µg/mL, respectively) (Section 4.3.3) or left untreated. Samples were then washed with dH_20/PBS and the water contact angle was then measured using a contact angle optical tensiometer (CAM 200, KSV Instruments). A single, 10 µL drop of 18.2 MΩ de-ionised water (MilliQ water) was dispensed onto the surface and twelve one second frames recorded. Water contact angles were recorded from the average of left and right contact angles from 10 frames (first and last frames were discarded).

4.3.6 Time of Flight Secondary Ion Mass Spectrometry (ToF SIMS) analysis of collagen type I adsorption to nanofibre surface

ToF-SIMS is a technique which can be used to detect the chemistry of a surface. The sample is bombarded with a primary ion source to remove molecules from the outer surface of the sample. The secondary ions which fragment from the surface are accelerated and processed by their mass to charge ratio in a detector and mass spectra are generated detailing the secondary ions and ion fragments from the sample surface. The data can be analysed to detect sophisticated surface chemistries at high resolution[163].

Samples of nanofibre scaffold were treated with type I bovine collagen as mentioned before (Section 4.3.3). Effective surface adsorption of collagen was investigated by examining the difference in collagen deposition on the nanofibre scaffolds by ToF-SIMs with and without washing steps using 18.2 MΩ de-ionised water (MilliQ water) washes compared to untreated PET scaffolds.

ToF-SIMS was conducted using a TOF-SIMS IV from ION-TOF GmbH. Samples were mounted in the sealed chamber and spectra were obtained using a Bi^{+3} primary ion source. A flood gun was used during the acquisition of spectra to prevent surface charging. Data acquisition was courtesy of Dr David Scurr (University of Nottingham). Secondary ion images were generated from sample spectra and normalised to the total ion count for each sample. All data was analysed using SurfaceLab 6.4.

4.3.7 Design and manufacture of villi formers for electrospinning

Villi-like formers were designed using CAD software by Sophie Luckhurst. Original dimensions were based on literature sources for physiological sizing and spacing of human small intestine (starting dimensions; 25 villi/mm^2, ~500 µm villi height, 32 µm villi tip diameter and 90 µm vili base diameter)[12,13,164]. Two distinct styles were initially designed, a protruding model with the villi structures protruding from a base and an intruded model, with the villi projecting into the base structure.

The ‘formers’ (that is the structures produced which were used for electrospinning) were manufactured using projection micro-stereolithography (using The Prefactory® 4 Standard with ERM, envisiontec, USA). Briefly, a designed structure is built in a layer by layer approach using a photo curable resin (R5, envisiontec, USA). Each layer of resin is cured with UV light after it is deposited on a build plate and the three-dimensional structure is constructed.

Following former construction it was briefly washed and dried before post-curing to ensure complete polymerisation of the polymer using UV light. To make the formers more amenable to the electrospinning process the formers were sputter coated with gold to add a conductive coating. The polymer scaffolds were examined by SEM to assess the morphology of the resultant scaffold following removal from the former.

4.4 Results

4.4.1 Analysis of nanofibre scaffold production

Observations in the lab identified significant issues with commercially procured granular PET (referred to as PET pellets); as a result, food grade PET (referred to as PET flakes) sourced from recycled bottles was also investigated as a source of PET for electrospinning. A high extent of beading (agglomeration of polymer in droplets along fibres) was observed for the PET pellets (which is stabilised by glass) at various processing conditions, especially low polymer concentrations (Figure 4.6). PET flakes, under the same solution concentrations and processing conditions, demonstrated superior fibre meshes with little or no visible defects. Polymer solutions made from PET pellets displayed poor dissolution of the polymer; the polymer solution appeared cloudy and significant particulates were present in solution even after 24 hours (Figure 4.7). In contrast the flakes of PET dissolved quickly as clear polymer solutions, free from particulates, even at comparative and higher concentrations.

4.4.2 Production and characterisation of nano and microfibres

Uniform fibres were produced by electrospinning of PET (under static collection conditions) to achieve fibres of varying diameter. By reducing the initial polymer solution concentration and flow rate the fibres with much smaller diameter could be produced (Figure 4.8).

Microfibres were produced at polymer concentrations of 20 and 30% (*w/v*) with average fibre diameters of 1.1 (± 0.4) µm and 2.5 (± 0.4) µm, respectively. Nanofibres could be produced at 10% (*w/v*) (albeit with a lower flow rate of 0.5 mL/hr) with average fibres of <0.5 (± 0.2) µm in diameter (Table 4-2). 30% (*w/v*) polymer solutions exhibited thicker fibres (Figure 4.8) with larger pore sizes (Figure 4.9) measured by analysis of scanning electron micrographs. Although the fibre scaffolds produced by electrospinning are porous they do not have well defined and discrete pore distribution. Inter-fibre distances were used as a measure of pore size when comparing the differences in nanofibrous and microfibrous PET scaffolds. Mircrofibre scaffolds had a mean inter-fibre distance of 15.8 (± 8.0) µm compared to 1.3 (± 0.5) µm for nanofibre scaffolds.

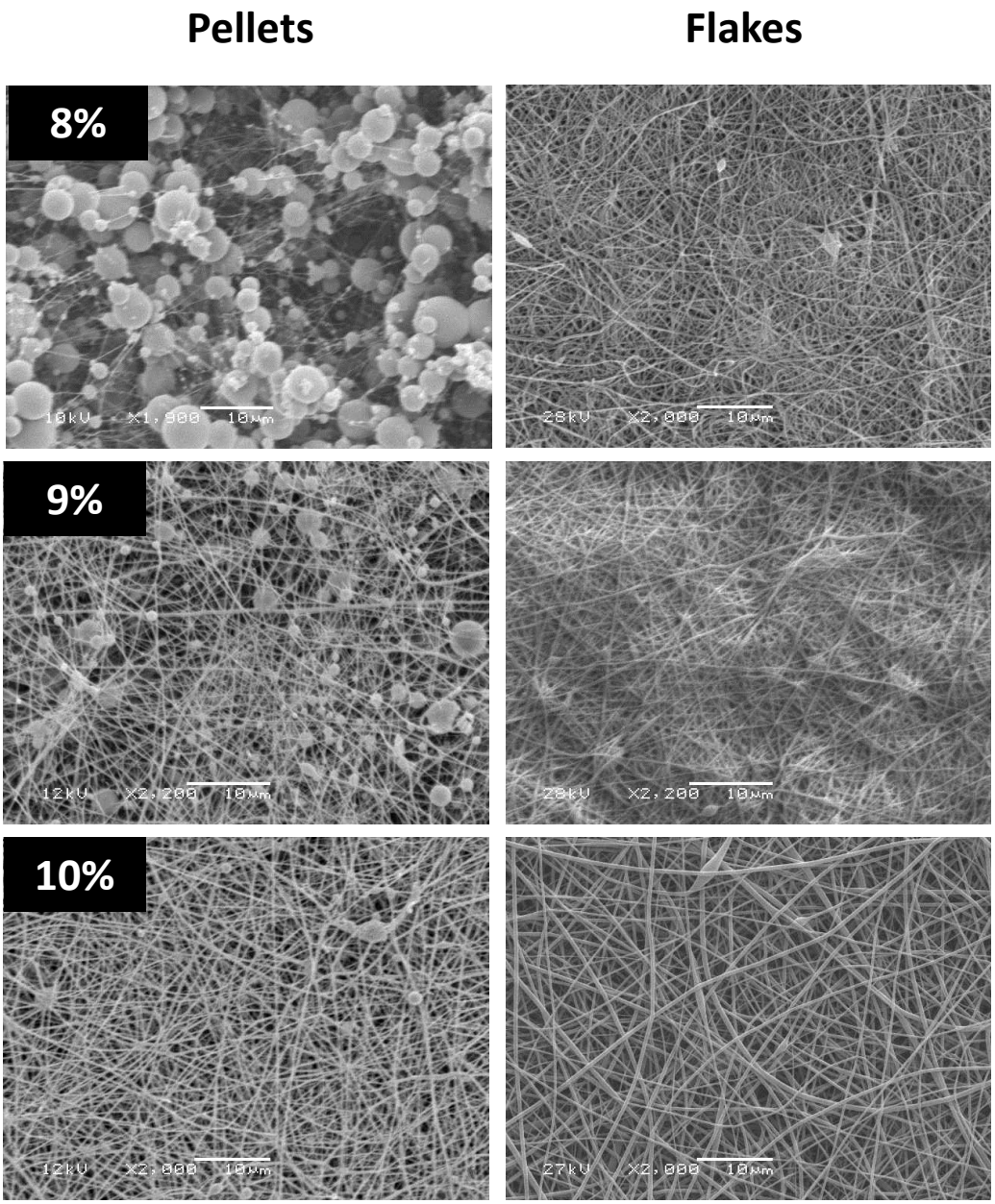

Figure 4.6. Representative scanning electron micrographs comparing fibre scaffolds produced using two different sources of PET. Polymer solutions of PET pellets and flakes were electrospun under the same processing conditions (14 kV, 15 cm tip to collector distance and 0.5 mL/hr) and the resulting scaffolds were examined by SEM. Concentrations are expressed as % (*w/v*).

Table 4-1. Scaffold thickness measurements under static and rotating collection conditions. Scaffold thicknesses were determined from histological cross sections and measured using imageJ. n= 20-30 measurements from 3 separate batches of scaffolds for each condition. Values are mean ± SD.

Scaffold thickness (µm ±SD)			
	Static collection		Rotating Collection (50 rpm)
Spinning time (mins)	240	120	240
	62.4 (15.7)	34.1 (7.0)	16.3 (6.0)

4.4.3 Changes in scaffold morphology in static versus rotating collection

Due to observations of poor uniformity in nanofibre scaffold thickness following histological cross-section analysis, a rotating collector drum was employed in the electrospinning process for collection of the scaffolds. Although no changes in processing conditions were required to transfer the process from static to rotating collection a brief assessment of any potential impact on the resulting scaffolds was carried out. The fibre diameter distribution was relatively similar but a reduction in the average fibre diameters was observed from 432.1 (± 147.7) µm to 375.6 (± 177.2) µm for static and rotating collection respectively (Figure 4.10). Due to the electrostatic nature of the scaffolds the duration of spinning was based on the need to produce thick enough scaffold to make the resulting fibre mesh easy to handle. Following histological analysis and thickness measurements (Table 4-1) the static electrospinning conditions were optimised in an effort to reduce the thickness of the construct. As the surface area of the collector plate was reduced (from 150 cm^2 to 84 cm^2) the duration of spinning was reduced (4 hours to 2 hours). The resulting scaffolds were roughly 50% thinner but the scaffolds still showed elements of heterogeneity in terms of their thickness across the entire scaffold. To further reduce the scaffold thickness and also ensure more consistency a rotating collector was employed for scaffold collection. The scaffolds had to be produced over a longer duration (4 hours opposed to 2 hours) to ensure the scaffolds could still be handled easily. As the drum surface area was greater than the static collector plates (237.6 cm^2) the resulting scaffolds

were thinner, demonstrated good thickness consistency across samples but as an added benefit resulted in the production of a greater amount of scaffold per run due to the larger surface area of the collector drum. No visible changes in morphological features were observed (e.g. fibre diameter) by SEM between static and rotating collection and the relatively slow rotational speed did not result in any fibre alignment (Figure 4.10).

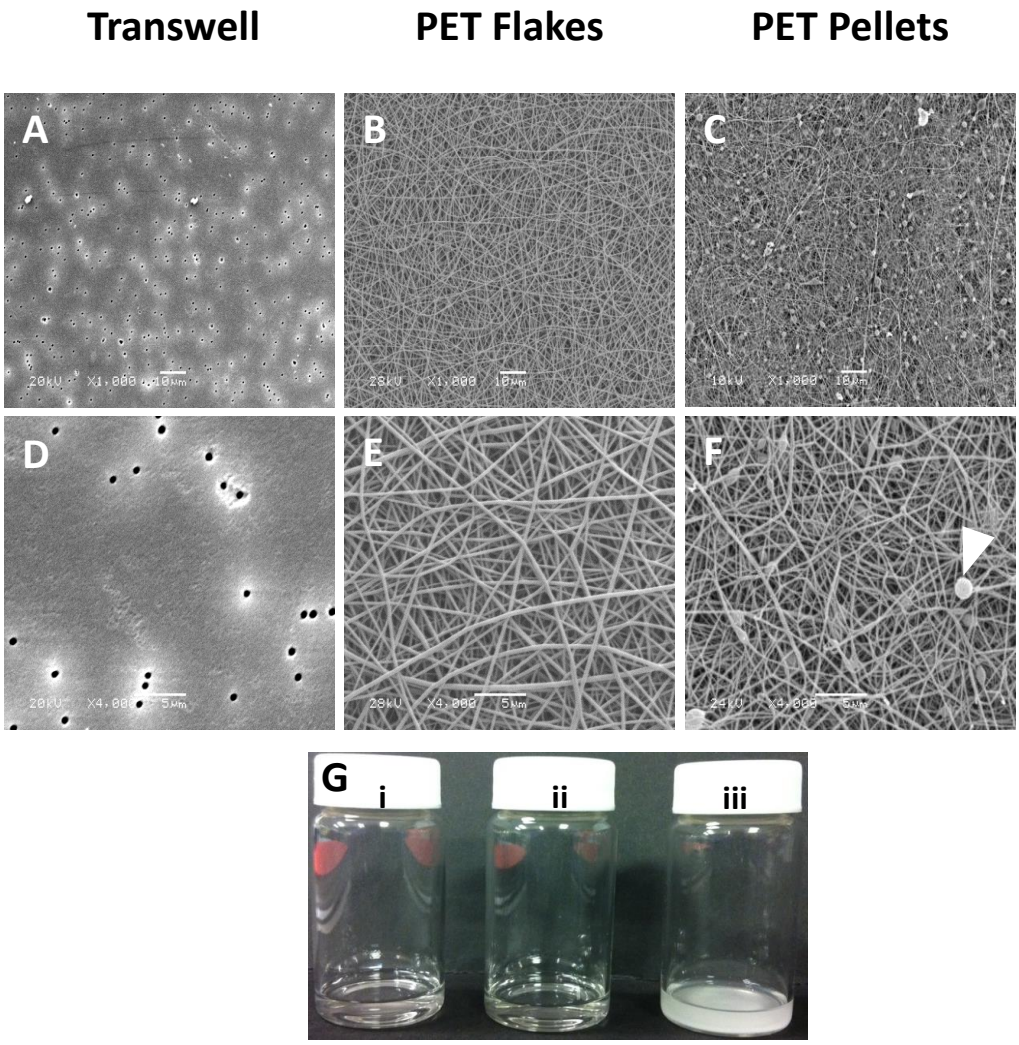

Figure 4.7. Analysis and comparison of conventional transwell inserts with fibre scaffolds. (A & D) High and low magnification scanning electron micrographs of conventional transwell PET membrane inserts (pore size 0.4 µm) and (B & E) nanofibre scaffolds produced by electrospinning using PET flakes and (C & F) commercially sourced PET pellets. Polymer beading can be observed in F (white arrow). Polymer solutions of (G-i) 10% (*w/v*) and (G-ii) 20% (*w/v*) PET.flakes, (G-iii) commercially available PET pellets dissolved in the same solvent solution at 10% (*w/v*) after 24 hours of dissolution.

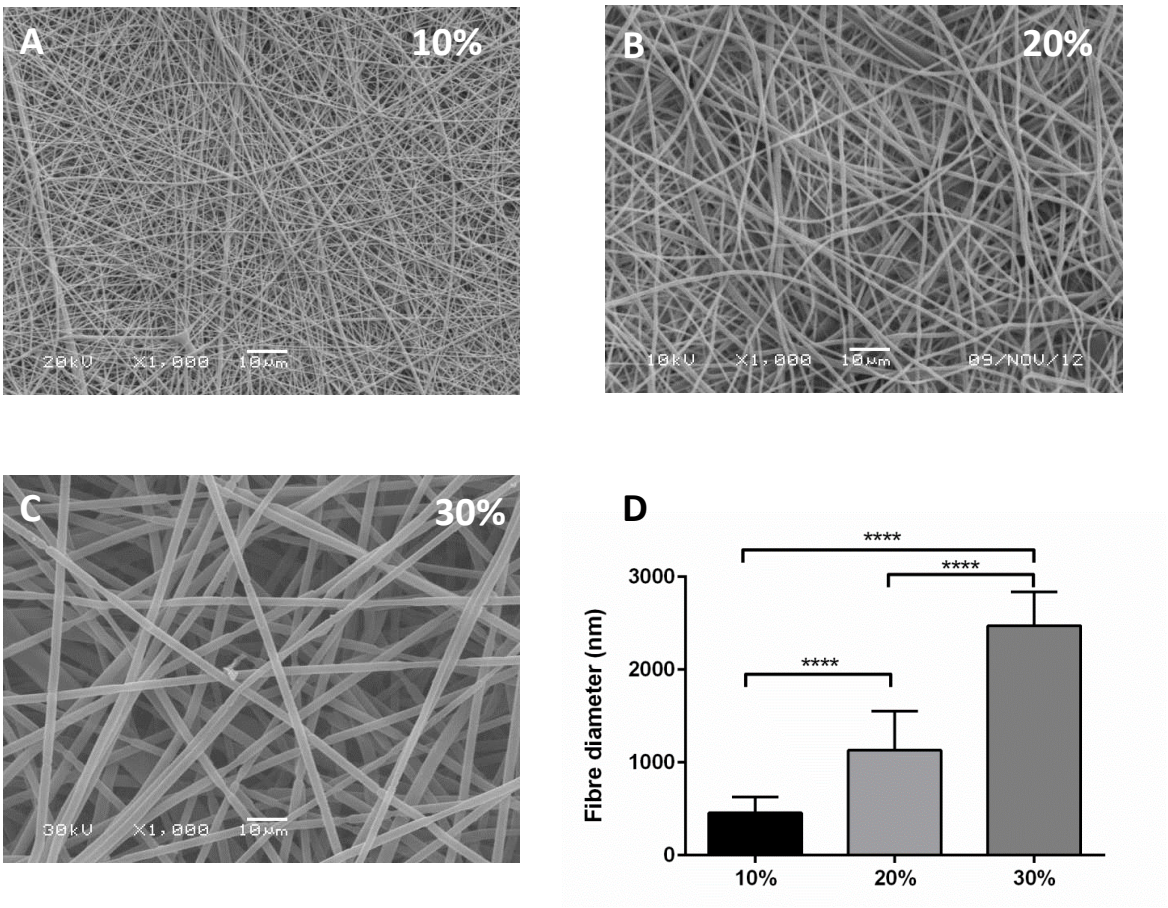

Figure 4.8. PET fibre scaffold morphology and diameter analysis. Representative scanning electron micrographs of PET fibre scaffolds produced with polymer solutions of increasing concentration; (A) 10% (*w/v*), (B) 20% (*w/v*) and (C) 30% (*w/v*). (D) Comparison of the average fibre diameters of the scaffolds at different polymer concentrations. Values are mean ± 1 SD. Statistical significance was determined by ANOVA with Tukey's multiple comparison, n=80 measurements from a minimum of 3 independently produced scaffolds. *** $p \leq 0.001$, **** $p \leq 0.000.1$.

Table 4-2. Electrospinning process parameters for PET nano and micro fibre production. The production of PET nano and microfibers with a 14 kV applied voltage, 15 cm tip-collector plate distance.

Polymer Concentration (% w/v)	Flow rate (ml/hr)	Average Fibre Diameter (nm)
10	0.5	457 ± 170
20	1	1131 ± 418
30	1	2473 ± 361

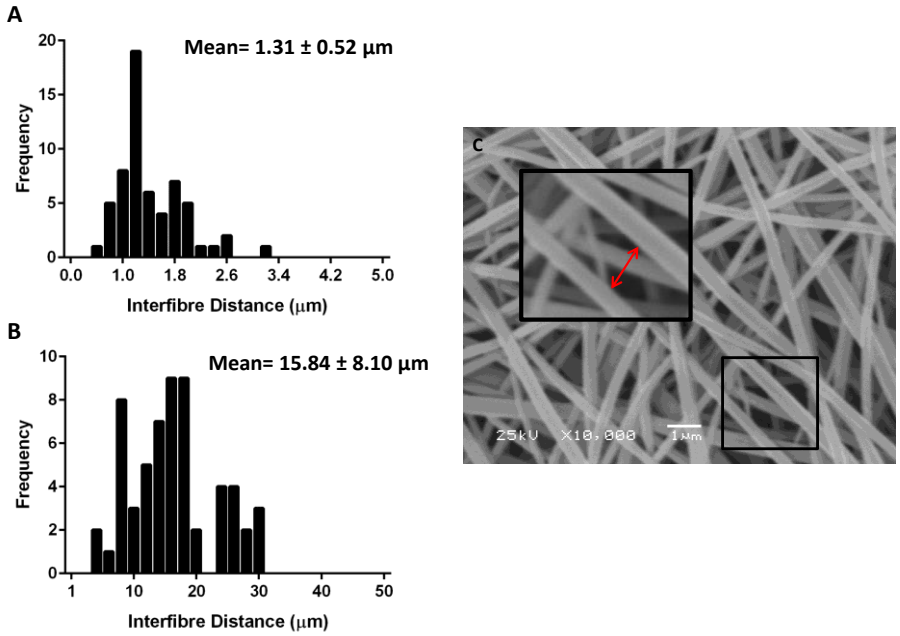

Figure 4.9. Inter-fibre distances in nano and microfibre scaffolds. (A & B) Frequency plot of interfibre distances for 10% and 30% (*v/v*) PET produced by electrospinning. (C) Scanning electron micrograph demonstrating methodology for measuring of interfibre distance. n=60 measurements from 3 independently produced scaffolds.

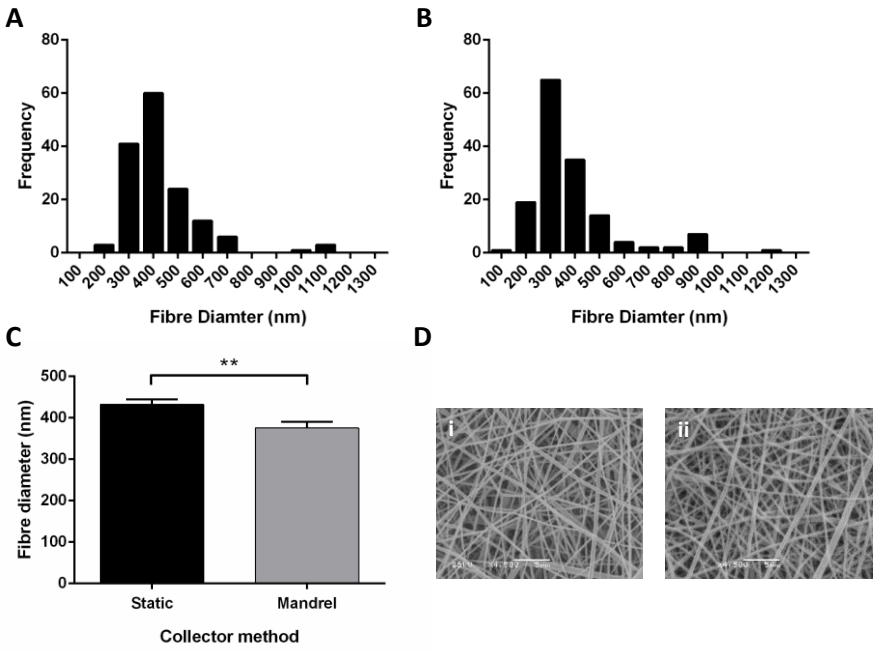

Figure 4.10. The effect of scaffold collection method on fibre diameter and morphology. Fibre diameters of scaffolds produced by (A) static collection and (B) rotating mandrel collection at 50 rpm. (C) Comparison of the average fibre diameters of the two collection methods. (D) Scanning electron micrographs of fibre scaffold morphology (D-i) Static collection, (D-ii) rotating mandrel. Values are mean ± SEM. Significance determined by two-tailed t test with Welch's correction, ** $p \leq 0.01$. n = 150 measurements, 50 measurements per scaffold from 3 independently produced scaffolds.

4.4.4 ToF-SIMS analysis of collagen type I adsorption to nanofibre scaffolds

The adsorption of collagen to the surface of the nanofibrous PET was investigated by ToF-SIMS. The extent of remaining collagen on the scaffolds after a wash step was studied as a measure of how resistant the adhered collagen layer was to the shear stress of liquid abrasion. The presence of nitrogen containing ion fragments, some of which have been attributed to specific amino acids based on literature reports of certain ion fragments[163], were used as indicators of the presence of collagen.

The secondary ion images of representative nitrogen containing ion fragments generated from spectral data demonstrate the collagen appears to coat the surface of the scaffold in a homogenous fashion for all the collagen treated samples (Figure 4.11). As expected the treatment at a high concentration (3.1 mg/mL) displays significantly more coverage of the surface with nitrogen containing ion fragments, specifically $C_4H_8N^+$, which is specifically attributed to the amino acid Proline (Table 4-3). Comparable surface coverage can be observed for all three representative ion fragments but at lesser intensities in all treated samples. The sample treated at the final working concentration solution (31µg/mL) that underwent a washing step (to simulate a physical interaction to the surface treatment with a liquid) still showed homogenous coating with regard to the ion fragment distribution albeit at a lower intensity. Some extremely low level intensity can be observed for all the ion fragments on the untreated PET sample which is likely to be artefacts of the surface topography (Figure 4.11).

In addition to the representative secondary ion images in Figure 4.11 other unique nitrogen containing peaks were identified and are listed in Table 4-3. Reference peaks and Ion peak fragment comparisons were also recorded (Figure A-3).

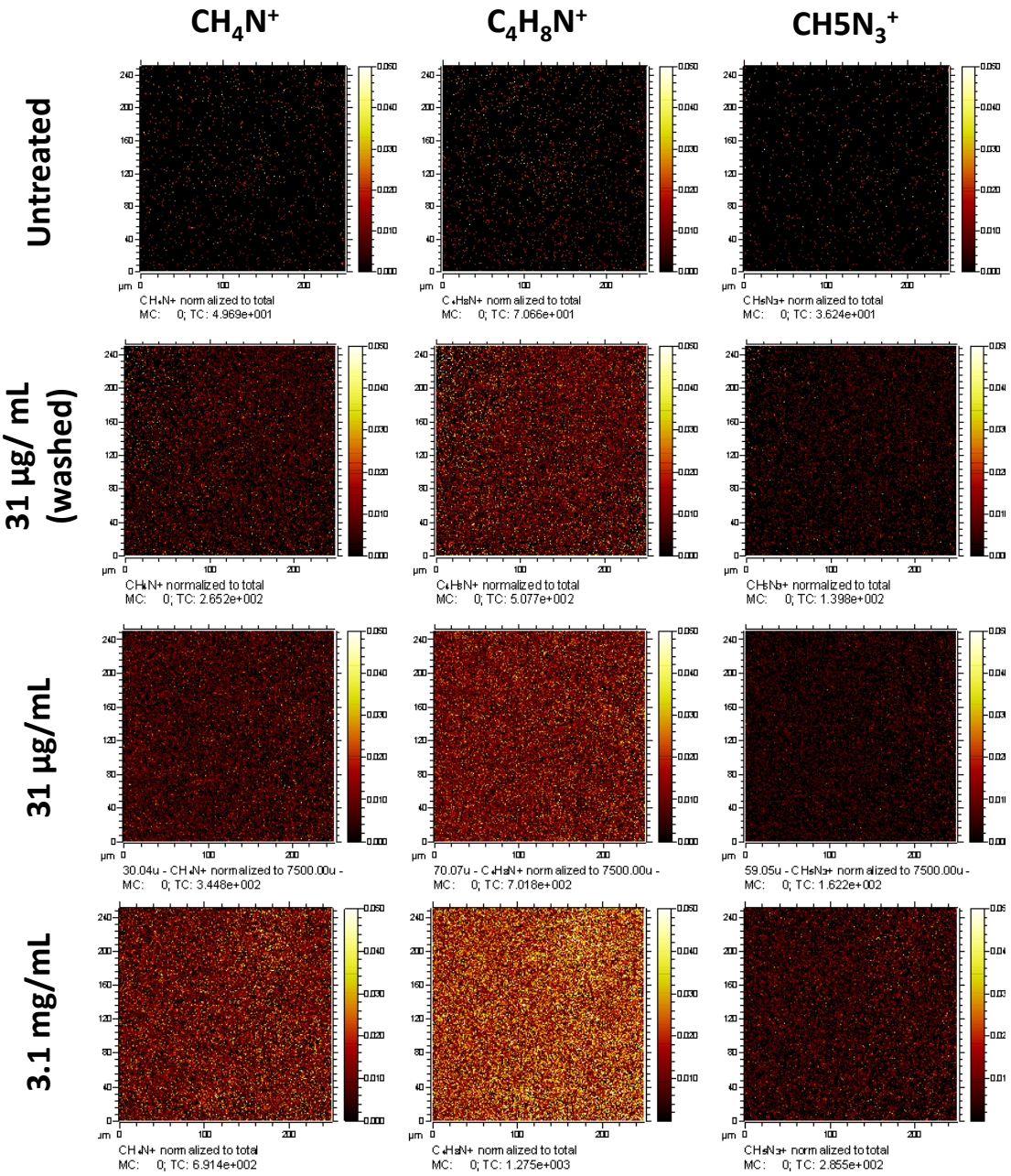

Figure 4.11. Normalised secondary ion images of untreated and collagen type I treated PET scaffolds. Ion images for unique nitrogen containing peaks in untreated and type I collagen treated nanofibre scaffolds. Images have been normalised to the total ion counts. Images are 250 x 250 µm

Table 4-3. Positive ion peaks identified from ToF SIMs analysis of nanofibre scaffolds. Unique nitrogen containing peaks were identified from spectra to analyse the extent of collage adsorption to the surface of the fibre scaffolds under different treatment conditions after a simulated 'wash' step.

Source	Ion	m/z	Sample	Deviation (ppm)
	NH_3^+	**17**	31 µg/ml (washed)	18.2
			31 µg/ml	-14.3
			3.1 mg/mL	12
Glycine	$C_2H_6N^+$	**30**	31 µg/ml (washed)	47.7
			31 µg/ml	48.6
			3.1 mg/mL	45.9
	CH_6N^+	**32**	31 µg/ml (washed)	38.9
			31 µg/ml	57.3
			3.1 mg/mL	44
	$C_2H_6N^+$	**44**	31 µg/ml (washed)	77.5
			31 µg/ml	71.4
			3.1 mg/mL	49.3
Arginine	$CH_5N_3^+$	**59**	31 µg/ml (washed)	35.3
			31 µg/ml	8.3
			3.1 mg/mL	18.8
	$CH_6N_3^+$	**60**	31 µg/ml (washed)	4.9
			31 µg/ml	18.8
			3.1 mg/mL	15.8
	$C_4H_6N^+$	**68**	31 µg/ml (washed)	78.9
			31 µg/ml	70.3
			3.1 mg/mL	44.8
Proline	$C_4H_8N^+$	**70**	31 µg/ml (washed)	81.5
			31 µg/ml	87
			3.1 mg/mL	79.2
Valine	$C_4H_{10}N^+$	**72**	31 µg/ml (washed)	-77.8
			31 µg/ml	88
			3.1 mg/mL	30
Arginine	$C_2H_7N_3^+$	**73**	31 µg/ml (washed)	-60.1
			31 µg/ml	-45.9
			3.1 mg/mL	-35.5
Glutamic acid	$C_4H_6NO^+$	**84**	31 µg/ml (washed)	29.6
			31 µg/ml	27.8
			3.1 mg/mL	30

Where ion fragment have been attributed a source this has been based on published characterisation of protein films by ToF-SIMS[163]

4.4.5 Examination of cell growth on nanofibrous PET and surface treatment of scaffolds

Initial culture of Caco-2 on nanofibre PET scaffolds revealed some inconsistent growth across the scaffolds surface and non-confluence of the epithelial cell layer. This was clearly visible to the naked eye after initial glutaraldehyde fixation (Figure 4.12 A & B). This finding was further corroborated by scanning electron microscopy where quite a significant section of a representative sample displayed no growth of Caco-2 cells (Figure 4.12 D). Following this finding, surface treatment of the nanofibre scaffolds was investigated to improve cell attachment and growth and to ensure complete confluence in epithelial cell growth. Simple coating of the scaffold with type I collagen and deposition of allylamine plasma coating were two methods investigated for alleviating the inconsistency in cell growth. Cell viability assessment of both surface treatments versus untreated controls with Caco-2, HT-29 and CCD-18co cells suggested that collagen type I treatment was superior to plasma allyl amine for all cell types compared to the untreated control. Initial assessment on day 1 (24 hours after seeding) seems to show that no real variability in viability across all scaffold types could be observed (with the exception of CCD-18co). This suggests that initial cell attachment was not particularly affected by either of the surface treatments (Figure 4.13). However in the following days of culture collagen type I treated scaffolds displayed increased cell viability compared with non-treated and ally amine treated scaffolds. Collagen treatment of the scaffolds was characterised further for surface wettability by measuring the water contact angle of the treated scaffold at different coating concentrations compared to untreated scaffolds. The untreated scaffolds were quite hydrophobic in nature before surface coating with collagen; the water contact angle for untreated nanofibre scaffolds was 95.3 (± 12.1) ° compared to 35.6 (± 26.2) ° and 21.1 (± 20.1) ° for collagen treatment at 31 µg/ mL (the final working concentration used) and 3.1 mg/mL (the stock concentration), respectively.

Collagen coating was employed for all subsequent cell culture experiments and cell attachment and growth was monitored. Representative images demonstrate clear improvement of confluence of the apical epithelial layer (Figure 4.14). Osmium and glutaraldehyde fixation did not show any areas devoid of cells and further examination by SEM showed a confluent well differentiated epithelium. The fissures appearing in low magnification view (Figure 4.14 C) are artefacts of the chemical drying process.

4.4.6 Analysis of CCD-18co morphology and intermediate filament marker expression on nanofibre scaffolds

Changes in CCD-18co morphology were observed when the cells were cultured on nanofibre scaffolds compared to traditional transwell cell supports. F-actin staining corroborated observations by electron microscopy that CCD-18co cells were much smaller in size when cultured on nanofibres (Figure 4.15). CCD-18co on transwell inserts by comparison show significant intracellular actin stress fibres whereas actin localisation appears to be localised mainly to the perimeter of the cell membrane when cultured on nanofibres. The cells were also re-examined for intermediate filament expression; similar expression profiles were observed to that seen on transwell inserts with positive expression of all 3 markers (Figure 4.16). Staining appeared more perinuclear in localisation with respect to vimentin and α-SMA when on nanofibres scaffolds and some joining of cells, almost forming together like a network (Figure 4.16 A - inset image). Similar to F-actin staining, changes in cell morphology with cells appearing more compact and rounded compared to those cultured on transwell inserts.

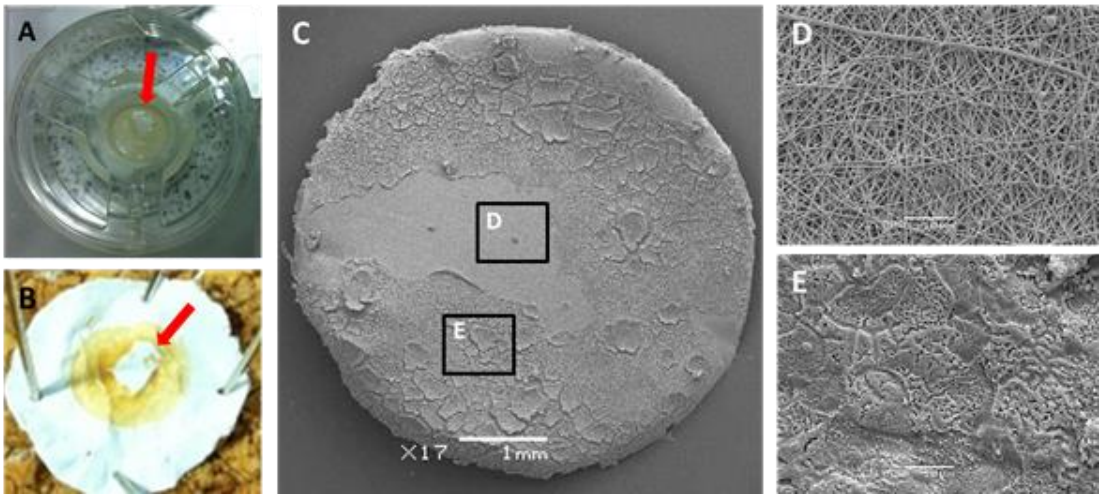

Figure 4.12. Examining the growth of Caco-2 cells on the surface of untreated nanofibre PET scaffolds. A-B) Samples were fixed 3% (*v/v*) glutaraldehyde whereby some patchiness of growth was observed on some scaffolds (red arrows). (C-E) Further SEM analysis of some of the scaffolds showed clear regions of the cell growth area devoid of cells (D) as well as areas covered by confluent epithelial sheets (E).

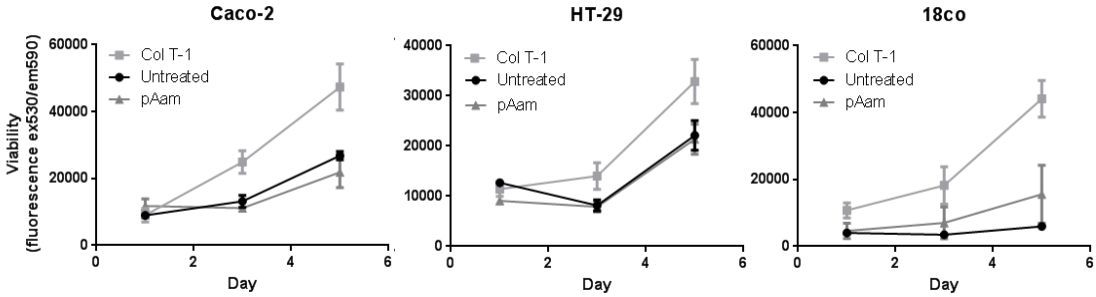

Figure 4.13.Cell viability assessment of nanofibre surface treatments.. Cell viability determined using the PrestoBlue assay of Caco-2, HT-29 and CCD-18co cells cultured on untreated, collagen type I treated (Col T-1) and plasma allylamine (pAam) treated nanofibre scaffolds. Values expressed as mean ± SD, n=3.

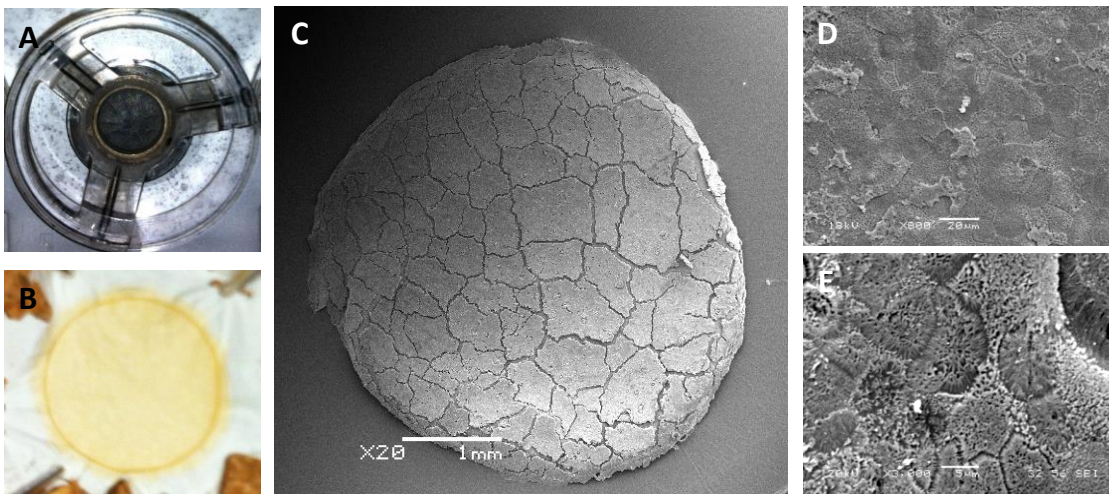

Figure 4.14. Examining the growth of Caco-2 cells on the surface of Collagen type I treated nanofibre PET scaffolds. (A-B) Samples were fixed in 3% (*v/v*) glutaraldehyde and post fixed with 1% (*v/v*) Osmium tetroxide. (A) Caco-2 coated nanofibre scaffold post osmium fixation. (B) Caco-2 coated nanofibre scaffold post glutaraldehyde fixation. (C-E) Further SEM analysis (at increasing magnification) of the scaffolds showed confluent coverage of the PET nanofibre scaffold by a sheet of Caco-2 cells.

4.4.7 Villi formers produced by Rapid Prototyping for villi-nanofibre scaffold production

Villi formers replicating physiological dimensions were designed and produced by rapid prototyping using a polymer resin. Two distinct designs were proposed; one where the villi protrude from base and also one where the structures intrude into a base (Figure 4.17). Representative former design arrangements and dimensions are shown in Figure A-4 and Table A-1, respectively. CAD designs of the two initial models were produced and the resulting formers were manufactured with high fidelity to the original designs (Figure 4.17 A, B, E & F). Following electrospinning, visual examination of the scaffolds (whilst still attached to the formers) demonstrated that both designs exhibited poor transfer of the intended villi geometry to the resulting scaffolds (Figure 4.17 C&D). For the extruded model the fibre scaffold formed a tent-like structure, suspended from the individual villi-like protrusions, without depositing significant fibres between the villi-base structures. This resulted in a poor resemblance to the intended nature of the scaffold following removal, as examined by scanning electron microscopy (Figure 4.17 D). The same was also true of the intruded model, fibres could be visualised covering the surface of the openings to each intruded villi structure (Figure 4.17.G). Furthermore this observation was verified by SEM where fibres meshes were observed to be covering the openings to intruded villi structures (Figure 4.17 H).

Following the initial poor results from the first former designs a retrospective approach was employed. Formers were designed to reflect individual villi at half the original proposed height (~300µm, depending on the build height quality) which were then used for electrospinning (Figure 4.18 A&B). The resulting fibre meshes appeared to show much greater homogeny with the individual structures than the physiologically relevant formers. Following this relative success in fidelity transfer from the former to the resulting scaffold, extruded formers were designed with double spacing between villi whilst keeping to the original former heights (180µm villi-base diameter and ~500µm villi height) (Figure 4.18

C). Intruded formers were designed with double the villi-base diameter with double spacing and original villi height (360µm villi-base and ~500µm villi height) (Figure 4.18 D). The formers were further augmented with the intruded model to display the same wide base whilst maintaining original villi height dimensions with original spacing (25 villi/ mm^2). For the extruded model the villi height was increased to 700µm whilst maintaining the optimised villi double spacing (i.e. villi base-to-villi base dimensions). For both models these dimensions showed considerable improvement upon the original geometries in terms of transference of the former shape onto the scaffold (Figure 4.18 E&F). The extruded model was superior to the intruded model, which suffered from the same initial shortcomings of the initial design in that the fibres did not penetrate into the intruded villi openings, even with the increased dimensions.

It is noteworthy that variation (which was sometimes quite dramatic) was detected between the designed villi dimensions and the actual final manufactured former dimensions for some of the formers. For the extruded models this often resulted in a shortfall upon the original dimensions where errors appeared to occur in the build process (Figure 4.18 A) resulting in a shortfall from the expected dimensions. With respect to the intruded model the dimensions were either fairly accurate or slightly in excess of the intended design dimensions.

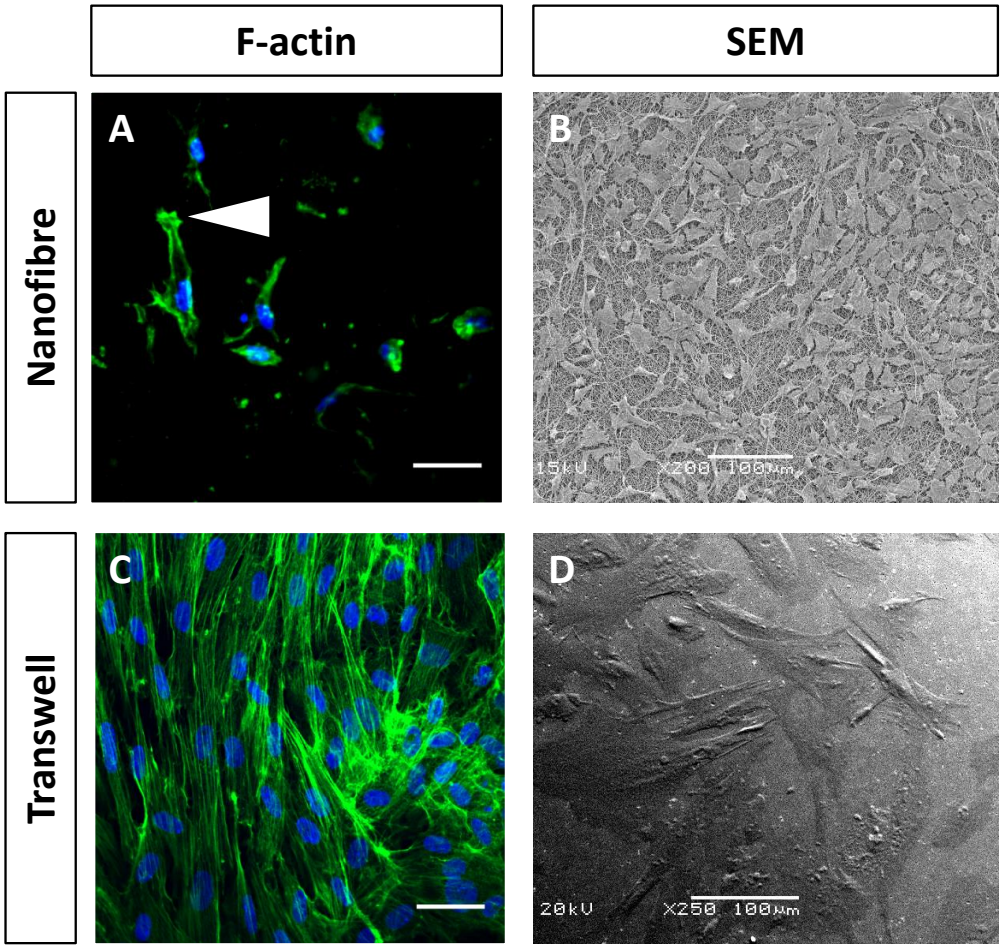

Figure 4.15. CCD-18co myofibroblast morphology assessment. (A&C) Immunostained F-actin CCD-18co myofibroblasts on nanofibre and transwell inserts respectively. Localisation of F-actin of CCD-18co appeared to be around the cell protrusions (white arrow) when cultured on nanofibres. Scale bars = 50 µm. (C&D) Representative scanning electron micrographs of CCD-18co myofibroblasts, scale bars = 100 µm.

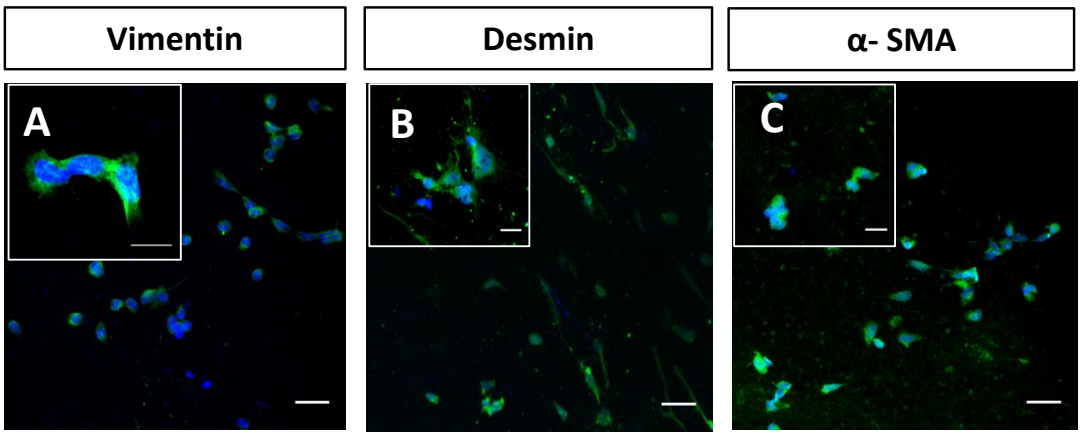

Figure 4.16. CCD-18co intermediate filament expression on nanofibre scaffolds. Immunocytochemistry characterisation of CCD-18co cells for key myofibroblast markers (A) Vimentin, (B) Desmin and (C) α-smooth muscle actin on nanofibre scaffolds. Scale bars = 20 µm, inset images scales bars = 10 µm.

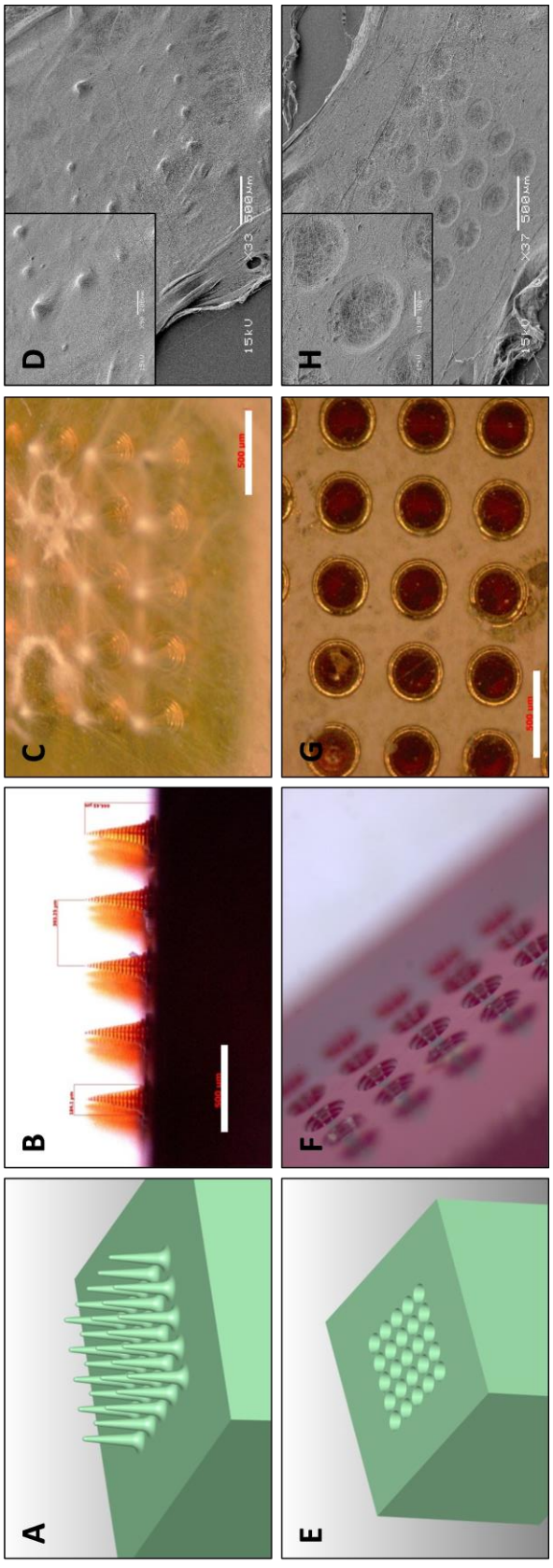

Figure 4.17. Villi like formers produced by additive manufacturing and the resulting fibre scaffolds. (A&E) Villi formers with accurate physiologically relevant dimensions were designed with CAD software and (B&F) produced by rapid prototyping. (C&G) Low magnification microscope images of the scaffolds, still attached to the formers, directly after electrospinning. (D&H) Representative scanning electron micrographs of the fibre scaffolds at low and high (inset images) magnification.

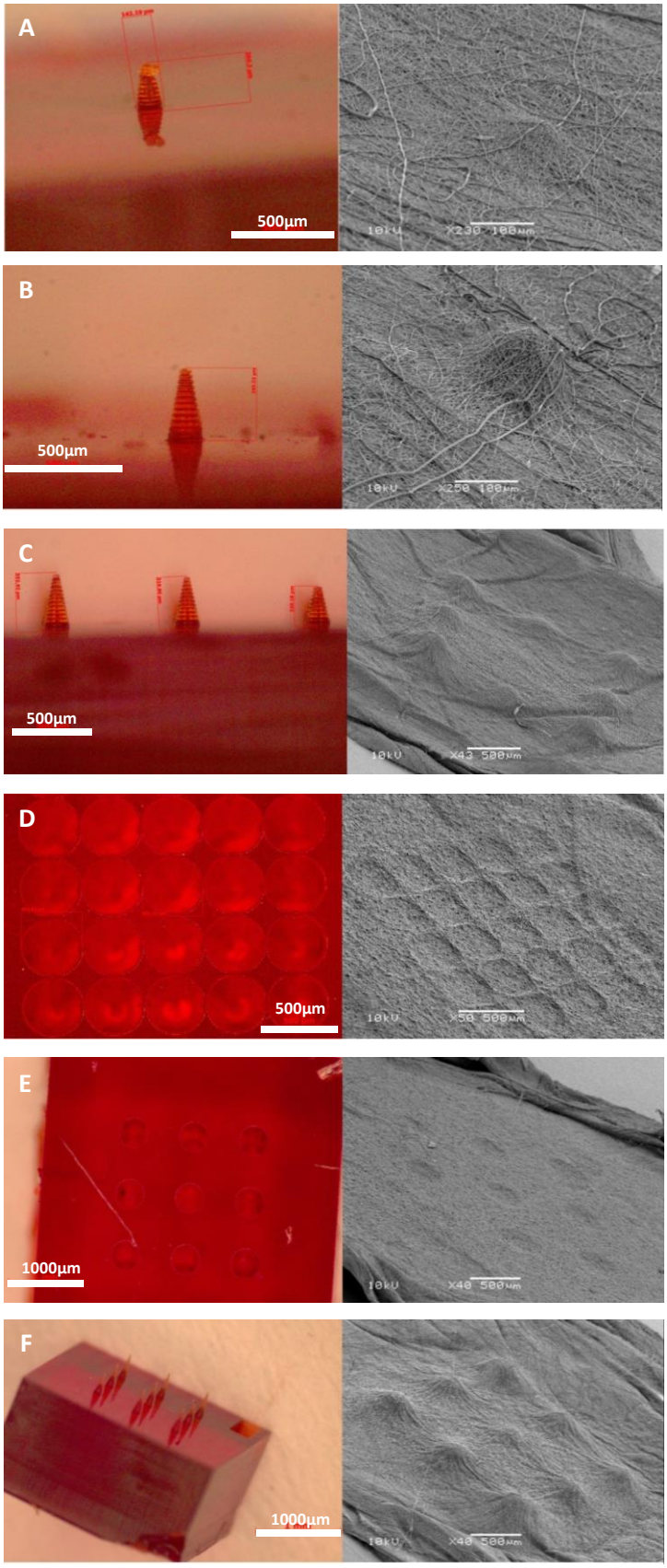

Figure 4.18. Representative microscope images and scanning electron micrographs of villi formers and the resulting fibre scaffolds. Former dimensions were adjusted in an attempt to make the structures more amenable to fibre deposition and result in fibre scaffolds with a higher fidelity to the villi architectures found in the intestine *in vivo*.

4.5 Discussion

Electrospinning can be used to produce fibre structures which mimic the physical architecture of the ECM and subsequently the technique has gained significant interest in the research community. The technique has been widely employed in the production of three-dimensional artificial cellular constructs to support cell growth. The rationale being that such matrices provide more faithful environments to those found *in vivo*, promoting more realistic cell behaviours and responses and for allowing the culture of multiple cell types more easily. Technology such as this facilitates the transition from simple cell monocultures towards simulating tissue function in the lab.

One of the reasons electrospinning has received such attention is partly a result of the fact it is an extremely flexible manufacturing process. A cheap and simple experimental set-up can be used for basic research-based investigations but the process can also be scaled up for high throughput production. Furthermore, a plethora of polymers can be used; in principle any soluble polymer can be used leading to many potential downstream applications.

With regard to initial investigations, the beaded morphology observed when using PET pellets is potentially a result of the glass stabiliser used in the pellet formulation. The apparent poor dissolution of the polymer in addition to the glass component of the pellets resulted in electrospraying, unstable jet formation or inconsistent fibre formation[155,165] (potentially all three simultaneously) resulting in undesirable fibre defects. Although this could be alleviated by altering processing conditions it was evident that PET pellets were not an ideal source of the polymer and PET flakes were used for all electrospinning.

Nanofibrous scaffolds reflect a more dense fibre structure, typical of the BM which supports epithelial tissues, compared to microfibrous meshes which, with regard to structure, could be perhaps be compared to interstitial ECM. As the BM structure is a supportive structure

which physically separates the epithelial cell layer from the underlying stroma it was important that any scaffold would be suitable for this task. Cell migration, whether it is active (i.e. as a result of cellular migration) or passive (i.e. as a result of large pores in the material that cells can physically fall through upon cell seeding) could allow the cells to mix with each other. Some groups have developed multi-phase/layered fibre scaffolds to recreate the various architectural milieus of consecutive layers of tissue, for example the epithelium and stromal elements alongside a smooth muscular/immunological element, for airway epithelium[72,115], skin[70,166] and soft-hard tissue constructs[167]. Given the bi-cellular nature of the intended myofibroblast-epithelial co-culture model a more simplistic nanofibrous scaffold was employed. This not only simplifies the production of the scaffold but also allows for closer proximity of the two cell types (~10-20µm for the nanofibre PET alone); this proximity can be limited by poor cellular infiltration into a microfiber stromal scaffold component, as was observed by Morris et al,[72].

Given that electrospinning is a multifactorial process the conditions for the production of specific fibre meshes varies considerably; changes in the morphology and nature of the scaffold (e.g. fibre diameter, porosity/inter-fibre distance) can be tuned by multiple processing conditions. As a result published literature on electrospinning shows considerable variation in parameter conditions in achieving a fibre construct. Hadjizadeh *et al*., report the production of PET nanofibres using rotating collection (300 rpm) with an average fibre diameter of 400 nm at a concentration of 7.7% (*w/v*) with a flow rate of 0.05 ml/hr and 700 nm at 9% (*w/v*) at 0.5 mL/hr (12-14 kV applied voltage, 15 cm TCD with a 22G spinneret)[160]. Morris *et al*., were able to produce fibres of 250 nm diameter using static collection at 8% (*w/v*) at 0.5 mL/hr (14 kV, 15 cm TCD, 23G spinneret)[116]. Data from this study suggest that rotating collection, even at low rotation speeds, causes a reduction in fibre diameter (this is most probably due to further narrowing of the fibre as it attaches to the moving collector). Therefore the reported nanofibre diameters from Hadjizdeh *et al*., do not correlate well with the results presented herein. When examined in comparison with other

literature, considering the low polymer concentration, flow rate and spinneret diameter, the nanofibre diameter reported by Hadjizadeh et al., is actually significantly greater by comparison. This may be a result of variation in the polymer properties (e.g. molecular weight of the polymer chains) rather than the conveyed processing parameters. As it is clear that each process variable has impact on the final morphology[148,155] published literature conditions serve only as a guide to in-house optimisation required for reproducible and defined fibre production.

Epithelial cell growth was quite variable on untreated PET scaffolds. Without complete confluence of an overlying epithelial layer then an *in vitro* model attempting to mimic the barrier properties of the *in vivo* tissue would be inherently flawed. Even during epithelial cell shedding neighbouring epithelial cells, in a concerted effort, orchestrate redistribution of tight junctions around the shredded cell to maintain barrier integrity[168,169]. Given many polymer plastics used in cell culture are generally coated or treated to improve cell attachment and growth a similar approach also had to be employed for this work. Transwell PET inserts are manufactured such that they are supplied culture treated (that is with a proprietary surface modification) to improve cell attachment and growth. This improvement is more likely a result of altering the surface chemistry of the scaffolds which improves the adsorption of serum proteins from the cell media (and also maintains the native protein structure) which promotes cell attachment and growth[170-172]. Although plasma deposition was investigated, a simple thin coating with type I collagen proved more successful in improving cell growth and confluence on the electrospun scaffolds. Analysis of surface wetting by contact angle measurements and coating adsorption to the surface by TOF-SIMS demonstrated increased surface wetting and homogenous distribution of collagen on the nanofibres respectively.

Although it could be argued epithelial tissue are two dimensional ‘sheets’ this is not strictly true, certainly in regard to the intestinal epithelium given the overall tissue

macroarchitecture. It is widely accepted that the crypt-villus axis exhibits an important physiological relevance and influences the overall barrier properties of intestinal tissue and as a result oral drug disposition[7,12]. Some of the most recent developments in intestinal tissue engineering are based in reconstituting full tissue architecture; specifically the villi structures[12,13,15] but also the crypts[16].

When attempting to mimic or recreate biology there are commonly two schools of thought; attempt to direct the self-assembly of an anatomical/physiological element or try to synthetically mimic it. Using formers produced from rapid prototyping an attempt was made to electrospin fibre meshes which would imitate the villi structure into nanofibre scaffolds as had previously been reported by this technique[153]. Thorough investigation and optimisation of the formers and the resulting scaffolds resulted in poor faithfulness to the structures found *in vivo*. It was possible to produce the former structures to the accurate dimensions although there were some issues regarding build consistency. This could have been a result of inefficient curing of the resin layers between each build layer resulting in unstable build foundations for the subsequent resin layers. Due to high aspect ratio of the individual villi and the layer-by-layer building approach any issues early in the build process greatly affect the structural integrity of each individual villus. The scaffolds themselves did not demonstrate significant integrity and removal of the scaffolds from the formers also resulted in some deformation of the structures. The extruded model, although improved in conformity using the wider spaced villi format, further highlighted a significant problem with the design. During the spinning process fibres collecting around the base of the villi ultimately reduce the height aspect of the villi structure itself. After spinning for longer to ensure the integrity and ease of handling of the scaffold, the deposition of fibres at the base of the villi structures broaden the final scaffold villi shape. The only foreseeable way to alleviate this would to be to achieve an ultra-thin fibre scaffold but with greater structural integrity.

Yu *et al*., and Weng-Chen *et al*., used a sacrificial hydrogel process[13,15] to produce villi gels which recapitulated the intestinal architectures with accurate fidelity. Both of the developed systems replicated the intended geometry however neither group thoroughly assessed the model functionally (e.g. extensive drug permeability screening). Yu *et al*., reported lower TEER and higher permeability of atenolol in their model than what had been reported for human excised tissue[173]. Despite this interesting finding the authors also reported that the hydrogels themselves limited the penetration of rapidly permeating drugs which limits the scope of the method if it does not allow the study of a wide range of drug molecules. This could perhaps be overcome through optimisation of the hydrogel porosity making it more suitable for permeation studies.

There are some examples of more sophisticated approaches to nanofibre scaffold functionalization than has been investigated. One such example, which focused on the grafting of peptide integrin binding sequences onto side chains of the polymer[151,152], may represent a more wholesome approach to direct future research utilising electrospun fibres for cell culture applications. Some groups have also investigated decellularised matrices for Caco-2 culture[11]. Whilst this is an interesting approach, a synthetic production method for biologically relevant scaffolds would be preferable as this would more likely provide a consistent and reproducible material. However the synthetic route may be at the cost of more physiologically relevance. This would definitely be true of stem and primary derived cell based models which present more significant challenges in maintained cell culture.

As the former work did not present a workable result in its current form and due to the constraints of time, simple nanofibre scaffolds were taken forward for further investigation for the epithelial-myofibroblast model.

The scaffolds produced in this chapter were taken forward with work from the previous chapter to develop *in vitro* epithelial-myofibroblast models which could be characterised and assessed for the permeability of some model compounds.

5. An epithelial myofibroblast in vitro co-culture model

5.1 Introduction

Since the inception of investigations into the Caco-2 cell line by *Pinto* et al.,[83] several iterations and developments have been proposed to improve the likeness of the model with the *in vivo* situation. Early work from the likes of Ronald Borchardt[84] and Per Artusson[6,107] were fundamental in developing the initial discovery of the cell line into an actual functioning model which enabled *in vitro* predictions which are translatable to human drug permeability. It was at this time that theoretical basis for a biopharmaceutic drug classification system was being developed[174] to which *in vitro* cell models now contribute significantly towards[82,175].

Despite all of the proposed developments and improvements over the 25 years from its origin the simple Caco-2 monoculture model, cultured on porous hanging inserts remains the most abundantly used *in vitro* cell assay for intestinal based investigations. What is the reason for this? Its longevity in this simple and original form can perhaps be a result of the fact that it has been quite useful without need to improve it further. It is regularly used in

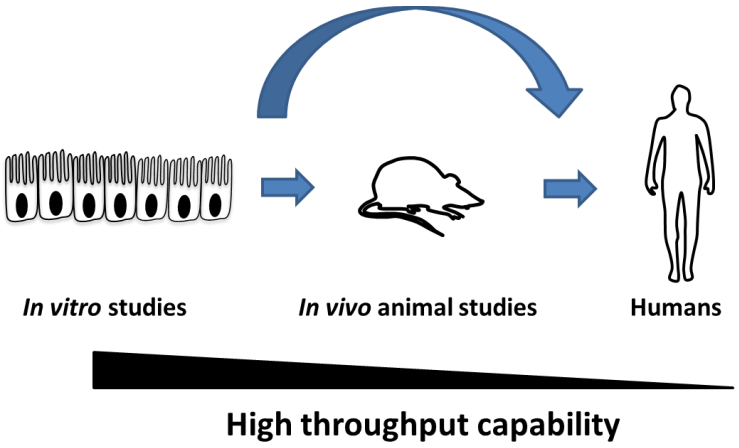

Figure 5.1. Bridging the gap from *in vitro* studies to humans. The aim of developing more sophisticated *in vitro* models for testing new drugs will enable more accurate prediction from the lab into humans, earlier in development.

conjunction with other pre-clinical models such as comparatively low throughput animal based *in vitro* methods like Ussing chambers and everted gut sacs to provide better insight into drug permeability[8,10]. Furthermore, as suggested by Balimane *et al*., combinations of the Caco-2 system alongside assays such as PAMPA (parallel artificial membrane permeability assay) can shed more light on pharmaceutically relevant drug interactions, such as with p-glycoprotein[9], earlier in drug development. New and more sophisticated *in vitro* tools will not only speed up the development of new drugs but will also enable more promising drug candidates to be prioritised earlier in the process. Bridging the gap between the *in vitro* and clinical evaluation of new drug candidates (Figure 5.1) could reduce early development costs but also reduce the number animal experiments necessary to move a drug compound into clinical evaluation. One main issue is that for many of the Caco-2 model 'improvements' remain under evaluated (for the purposes of drug screening) and most of which have not been approved by the main regulators (e.g. FDA and ECVAM[10,134]). Whilst important improvements have been investigated, more effort must be made to fully evaluate these models that are shown to predict human drug permeability *in vitro*.

With regard to the function of some of the emerging models of the intestine, many of the published models remain poorly characterised for drug permeability screening purposes. Kim *et al*., with the gut-on-a-chip model reported high TEER values (>3000 Ω cm^2), far beyond physiological relevance and to date have only tested the permeability of a single molecule, FITC-dextran 20kDa. Although an increase in permeability was observed over transwell cultures, considering the size of FD20, it is a poor choice of marker for paracellular permeability. It has previously been demonstrated human paracellular tight junctional pores have a diffusion pore radius of around 13 Å[68] and Caco-2 of 4.5 and ~7.5Å[65](a biphasic profile). FD20 has a Stokes (hydrodynamic) radii of 33Å (Sigma Aldrich product sheet data) and is therefore unlikely to be a useful indicator of paracellular permeability. Given the lack of extensive permeability data with this model it is very difficult to speculate on its immediate utility for drug permeability testing.

Another approach that displayed some interesting results is the work of Pusch *et al*., utilising decellularised porcine jejunal segments[11] with Caco-2 in co-culture with human microvascular endothelial cells (hMECs) in a perfused bioreactor system. Some notable changes in cell morphology and arrangement into multi-layered prismatic cell structures (later also observed by Kim *et al*., in their gut-on-a-chip model[17,18]) were observed for those cultured under bioreactor perfusion conditions. Again the system was under assessed in terms of drug permeability; only fluorescein, desmopressin and rhodamine 123 were investigated.

Possibly the most evaluated model is that of the aforementioned Caco-2/HT-29 (MTX) co-culture model. It was only briefly after the Caco-2 model was first proposed that researchers were looking to introduce a mucus element into the model. This was a result of the observation that HT-29 cells were not only goblet cell-like but also formed 'leakier' TJs than Caco-2[108]. On the discovery of the methotrexate treated HT-29 MTX line which displayed greater goblet cell homogeneity[135,136], a Caco-2/HT-29 MTX co-culture model and the HT-29 MTX line itself were characterised in detail[19,88,109,176]. Various ratios of Caco-2:HT-29 MTX were investigated with lower TEER and higher permeability reported as the HT-29 MTX component increased. It is understood that goblet cells constitute 10% of the exposed epithelium in the small intestine and up to 24% in the colon and thus represent a significant component of the epithelial barrier[109,177]. One caveat was that p-glycoprotein (p-gp - intestinal efflux transporter) expression in HT-29 MTX is considerably lower than Caco-2 (which in itself is believed to have lower p-gp expression than that found *in vivo*). Furthermore TEER readings and drug permeability, although closer to the *in vivo* situation, were still above human tissue values[19] even when non physiological cell ratios were used (e.g. 1:1 Caco-2 to HT-29 MTX). There is no doubt however that the Caco-2/HT-29 MTX co-cultures and the HT-29 MTX line are hugely important tools to investigate variety of permeability questions posed during the development of a new drug.

The previously mentioned paper from Pereira *et al*., potentially details one of the most complicated approaches to date to enhance the complexity of the existing Caco-2 and Caco-2/HT-29 MTX co-culture systems through the inclusion of CCD-18co myofibroblasts[14]. As discussed in chapter 3, myofibroblasts have become an interesting avenue of focus for epithelial cultures due to the growing recognition of the role they play in epithelial barrier integrity and function[14,34,36,46,114-116]. Familiar too many of the other investigated model improvements, the impact of myofibroblasts on epithelial permeability remain relatively under evaluated. The data presented herein represents an investigation into the permeability properties of Caco-2/CCD-18co co-cultures on conventional transwell inserts and also nanofibre scaffolds. The findings were validated by comparing our work with resected porcine tissue sections, a technique recently shown to be relevant to human drug permeability[110].

5.2 Aims

The aims of this chapter were to bring together the work from the previous two chapters and produce an epithelial-myofibroblast model using nanofibre scaffolds produced by electrospinning. To characterise this nanofibre based model using the techniques described previously and assess the permeability of paracellular permeants and some model drug compounds representing the major routes of adsorption across epithelial boundaries (Transcellular, paracellular and transporter mediated). The final goal was to develop an *ex vivo* model using resected porcine intestinal tissue and evaluate the same compounds to compare with data obtained from the *in vitro* models.

- Investigate the barrier performance of Caco-2 and Caco-2/18co co-cultures on nanofibres scaffolds in comparison with transwell equivalents
- Develop an *ex vivo* porcine tissue permeability system for comparison with the developed *in vitro* systems
- Investigate the permeability properties of all of the systems with fluorescent marker probes and model drug compounds atenolol and propranolol

5.3 Methods

5.3.1 Nanofibre cell culture set up

Commercially available snapwell inserts were adapted for housing nanofibre scaffolds. Using a scalpel, the existing polycarbonate membranes were removed from each of the individual hanging inserts (Figure 5.2 A-C). Sterile PET nanofibre scaffolds were placed over the insert and secured in place using the securing ring (Figure 5.2 C & E). Individual inserts were then placed in standard 6 well plates ready for use.

After mounting the scaffolds each one was coated with type I collagen (Section 4.3.3) and subsequently seeded with cells. Cells were seeded at the same seeding densities as per the previously mentioned protocol (Section 3.3.2). For snapwell based cultures the apical and basolateral volumes used were 0.5 mL and 6 mL respectively. During CCD-18co seeding on the underside of scaffolds, medium (150 µL) was carefully replenished every 30 minutes during the 4 hour attachment period to prevent the cells from drying out. Due to the high porosity of the scaffolds the original cell seeding volume perfused through the scaffold and

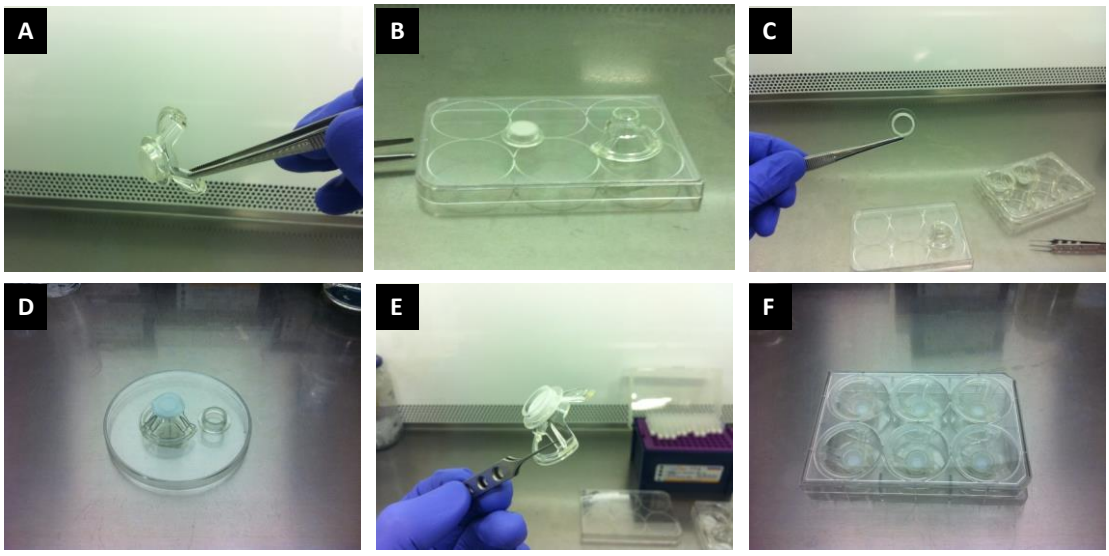

Figure 5.2. Flow schematic demonstrating the use of Snapwell cell inserts for housing nanofibre scaffolds produced by electrospinning. (A-C) The individual hanging inserts are removed from the plate, the removable cap is detached and the existing membrane removed using a scalpel. (D-F) Pre-cut and sterilised nanofibre sections are placed over the insert and fastened using the removable cap. The modified inserts are then placed into a conventional 6-well plate, ready for use.

down into the petri dish so medium had to be replaced to ensure effective attachment of the myofibroblasts.

5.3.2 Immunochemistry, histology & electron microscopy

Immunochemistry, histology and electron microscopy were conducted as per previously mentioned protocol (Section 2.2.6, 2.2.7 & 2.2.9). F-actin was visualised using alexa fluor-488 primary tagged phalloidin and tight junctions were stained with anti-ZO-1 primary tagged alexa fluor-488 (Section 3.3.3). Confocal imaging was conducted using a Leica SP2 confocal laser scanning microscope.

5.3.3 Porcine intestinal segment preparation

Pigs were not sacrificed solely for the purpose of this research in accordance with NC3R framework on the reduction and refinement of animals in research; samples were only obtained from healthy pig cadavers being used for the purposes of other research projects. The work was conducted according to strict UK Home Office guidelines (Animal Scientific Procedures Act 2010). Healthy pigs weighing approximately 40 kgs were sourced and maintained at the University of Nottingham. Slaughter was by overdose of intravenous barbiturate followed by exsanguination.

Regional sections from the duodenum (first 25 cm from the stomach), jejunum (150cm from the stomach) and ileum (first 50cm back from the ileocecal valve) were resected from pig cadavers. Tissue was stored in ice cold HBSS during transport to the laboratory. Intestinal segments were flushed with fresh ice cold HBSS to remove any remaining luminal contents and cut longitudinally to make rectangular shaped pieces. The tissue was pinned taut and the serosa and muscularis poropria were removed by gently peeling the layers off using forceps taking care to not damage the specimens (Figure 5.3). Inner sections of each segment were cut into small square sections and mounted into snapwell hanging inserts

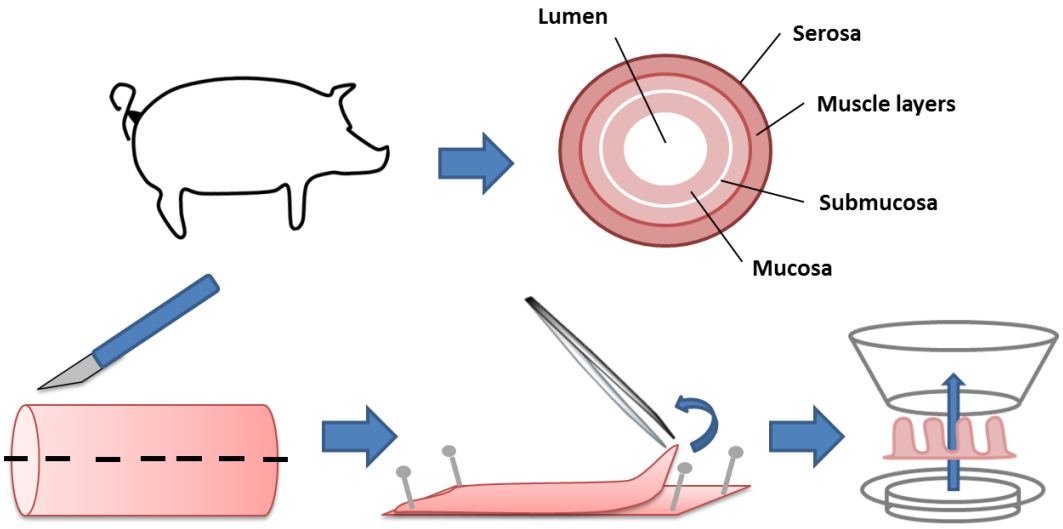

Figure 5.3. Isolation and preparation of porcine intestinal segments. Intestinal sections were taken from porcine cadavers and stored in ice cold HBSS. Individual pieces were sectioned lengthways and pinned serosa side facing upwards. Using tweezers the serosa and muscularis propria (muscle layers) were carefully peeled away leaving the mucosa. Sections were then cut appropriately to fit the snapwell inserts and used in 6-well plates.

(0.784 cm^2 exposed surface area). Samples were briefly rinsed in pre-warmed transport buffer to remove excessive mucus build up on the apical surface and fresh buffer added (0.5 mL/6 mL apical/basolateral volumes, respectively) and equilibrated for 45 minutes at 37° C, 5% CO_2 with shaking at 150 rpm. All tissue was kept on ice and used within a 24 hour time period, post-collection. For pig samples n = technical replicates and N = biological replicates (e.g. number of pig donors). Routine H&E cross sections were recorded for all tissue samples and are shown in Figure A-5.

5.3.4 Drug Permeability

Drug permeability in Caco-2, Caco-2/18co (transwell and snapwell) and porcine segments was conducted using the previously mentioned protocol (Section 2.2.10). Atenolol, propranolol and verapamil were dissolved in a minimal volume of DMSO before dilution into transport buffer. Final DMSO concentrations were less than 0.1 % (*v/v*) and donor drug/compound concentrations used for all experiments were; atenolol 1mM, propranolol and verapamil 0.5 mM, lucifer yellow 50 µM, FITC-dextran 4 and rhodamine 123 10µM.

Samples were quantified by reverse phase-HPLC with UV detection (atenolol, propranolol and verapamil) or using a plate reader (lucifer yellow, FITC-dextran 4000 and rhodamine 123). HPLC samples were filtered (0.2 µm) prior to analysis to remove any tissue, cell debris or mucus. All HPLC was performed using a Kinetix XB-C18 5 µm, 100 Å pore size, 150 x 4.56 mm^2 column (with a guard column) on an Agilent 1100 HPLC system. Atenolol and propranolol were analysed at 225 nm and 290 nm, respectively. Samples were analysed using gradient runs with Milli-Q dH_2O, 0.5 % TFA (eluent A) and acetonitrile, 0.5 % TFA (eluent B). Verapamil was analysed at 235nm on a gradient run of pH 3 potassium phosphate buffer (eluent A) and acetonitrile (eluent B).

TEER was used as an acceptance criterion before permeability experiments, the following values were determined based on average TEER values recorded for each set up. For transwell cultures Caco-2 monocultures only monolayers >500 Ω cm^2 were used and for Caco-2/18co >150 Ω cm^2; for nanofibres cultures TEER >200 Ω cm^2 for both mono and co-cultures and for porcine tissue TEER >60 Ω cm^2 were deemed acceptable.

A change in TEER (< 80% of the initial value - Equation 5-1) was set as an indicator of possible influence to barrier integrity/toxicity to the cell layer and test compound recoveries <70% (Equation 5-2) were carefully deliberated due to potentially erroneous permeability calculation assessment as a result of low compound recovery[5].

Equation 5-1

$$Barrier\ integrity\ (\%) = (TEER_{final}/TEER_{initial}) \times 100$$

Equation 5-2[5]

$$Recovery\ (\%) = (Cd\ fin \times Vd + \Sigma(Cs \times Vs) + Cr\ fin \times Vr\ fin) \times 100 / (Cd\ 0 \times Vd\ 0)$$

Where C_d is the final donor compartment concentration, V_d is the final donor compartment volume at t=0 or the end of the experiment. C_s and V_s denote the concentration and volumes of withdrawn samples at intermediate time points throughout the experiments.

5.4 Results

5.4.1 The influence of scaffold substrate on barrier integrity in Caco-2 and Caco-2/18co co-cultures

The barrier integrity of Caco-2 and Caco-2/18co co-cultures on nanofibre scaffold was assessed by measuring the increase in TEER over a 21 day culture differentiation period (Figure 5.4.). As discussed in Chapter 3 Caco-2 cells cultured on traditional transwell supports display high final TEER readings (>500 Ω cm^2 from day 15 onwards). In these cultures TEER begins to increase dramatically as early as 3 days after cell seeding (to around 200 Ω cm^2) and steadily increases throughout the culture period (Figure 5.4.A). TEER values in Caco-2 transwell cultures begin to plateau around 800 Ω cm^2 from day 21 onwards (data not shown). When Caco-2 cells were cultured on nanofibre scaffolds a different picture can be observed. Similar to transwell cultures TEER begins to rise early in culture however, this increase starts around day 6 with cultures displaying resistance readings of ~ 70 Ω cm^2. TEER steadily increases over the next 9 days to reach around 200 Ω cm^2 at day 15 of culture. From day 15 to day 21 Caco-2 cultures begin to plateau with final TEER readings stabilising above 220 Ω cm^2.

For Caco-2/18co co-cultures a similar trend was observed to that of Caco-2 monocultures when cultured on nanofibre scaffolds (Figure 5.4 B). The trends in TEER over the culture period were in fact almost indistinguishable from one another except for a slight non-significant deviation at day 15.

CCD-18co cells were also cultured in monoculture to see if the cells had any effect on TEER by themselves (Figure 5.4.C). When cultured on nanofibre scaffolds CCD-18co exhibited no real impact upon TEER, in some circumstances the measured TEER value was lower than that measured for a blank scaffold resulting in negative TEER values for a few days of the culture period.

5.4.2 Qualitative assessment of Caco-2 barrier formation

Caco-2 cultures (both transwell and nanofibre) were assessed by various techniques to confirm the formation of a complete cellular barrier across the nanofibres scaffolds and to identify key features of a functional epithelium. F-actin immunostained monocultures showed a confluent epithelial sheet in both transwell and nanofibre scenarios (Figure 5.5.). As expected a clear, flat single monolayer was observed for transwell cultures (Figure 5.5.A&B) whereas undulations could be observed in the surface actin staining of the Caco-2 cells cultured on nanofibre scaffold (Figure 5.5. D). Multi-layering of the Caco-2 epithelial cells could be observed in the nanofibre sample which, coupled with the scaffold surface topography, might explain the surface undulations in the epithelial cell layer.

Scanning electron micrographs of the surface of the epithelial layer in both circumstances revealed tightly packed epithelial layers with clear boundaries visible between neighbouring cells (Figure 5.6.). Higher magnification images demonstrate further the presence of apical surface features, like microvilli (Figure 5.6.C&D). Some discontinuities can be observed in all of the images which are most likely to be artefacts of the chemical drying process during the processing of the samples and not evidence of damage to the epithelial cell layer.

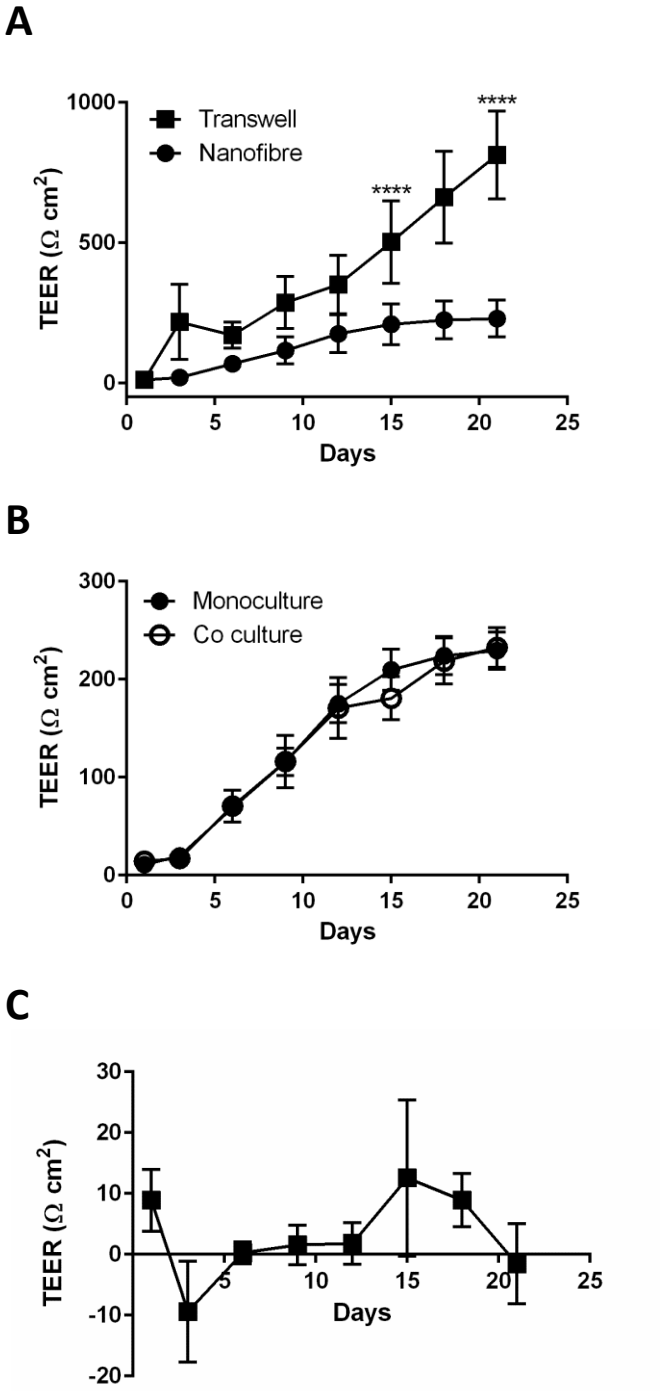

Figure 5.4. Trans-epithelial electrical resistance of Caco-2, Caco-2/18co co-cultures and CCD-18co on nanofibre scaffolds. (A) Comparison of caco-2 monocultures cultured on transwell and nanofibre scaffolds. (B) Comparison of caco-2 and caco-2/18co cultures both grown on nanofibre scaffolds. (C) CCD-18co myofibroblasts cultured on nanofibre scaffolds over an identical 21 day culture period. Values expressed as mean ± 1 SD. For (A) and (B) n= 9-15 inserts from a minimum of 3 independent experiments. Significance determined by student's t-test, ****$p<0.0001$.

Histological cross sections displayed comparable cellular arrangement and morphology of Caco-2 monocultures irrelevant of the culture substrate (Figure 5.7. A&B). Some difficulty was experienced in obtaining quality images of co-culture samples with the CCD-18co myofibroblasts layers often separating from the support (transwell) during processing (data not shown). Analysis of Caco-2/18co co-cultures revealed clear evidence of the presence of both Caco-2 and CCD-18co (white arrows) separated by the nanofibre scaffold (Figure 5.7.C). The epithelial layer appeared to have lifted away to some extent from the nanofibre scaffold surface but again this is most likely an artefact of the sample processing. It is noteworthy however that nanofibre cultured samples were more sensitive to this compared to transwell cultured cells. As seen before with immunostaining, cellular multi-layering was evident on nanofibre scaffolds and although some multilayers were observed in transwell cultures they were more abundant in nanofibre samples.

Comparative cross sectional TEM analysis of Caco-2 monocultures on the two different cell supports showed single-celled monolayers with all of the expected characteristic features such as microvilli (Figure 5.8.). Caco-2/18co nanofibre based co-cultures exhibited typical cellular morphology with microvilli and apical tight junction expression (Figure 5.9.A&C). CCD-18co can be clearly seen on the basolateral side of the scaffold and have not penetrated it at all (Figure 5.9. B&D). As per previous observations some stacking of cells was evident but a well differentiated enterocyte-like layer of cells was also observed (Figure 5.9.B).

To further investigate barrier formation and the expression of key tight junction protein ZO-1 was again also assessed (Figure 5.10.). Distinct apical staining (specific to apical tight junctions) can be visualised in the XZ cross section view for each sample as well as the typical cobblestone-like appearance of the epithelium.

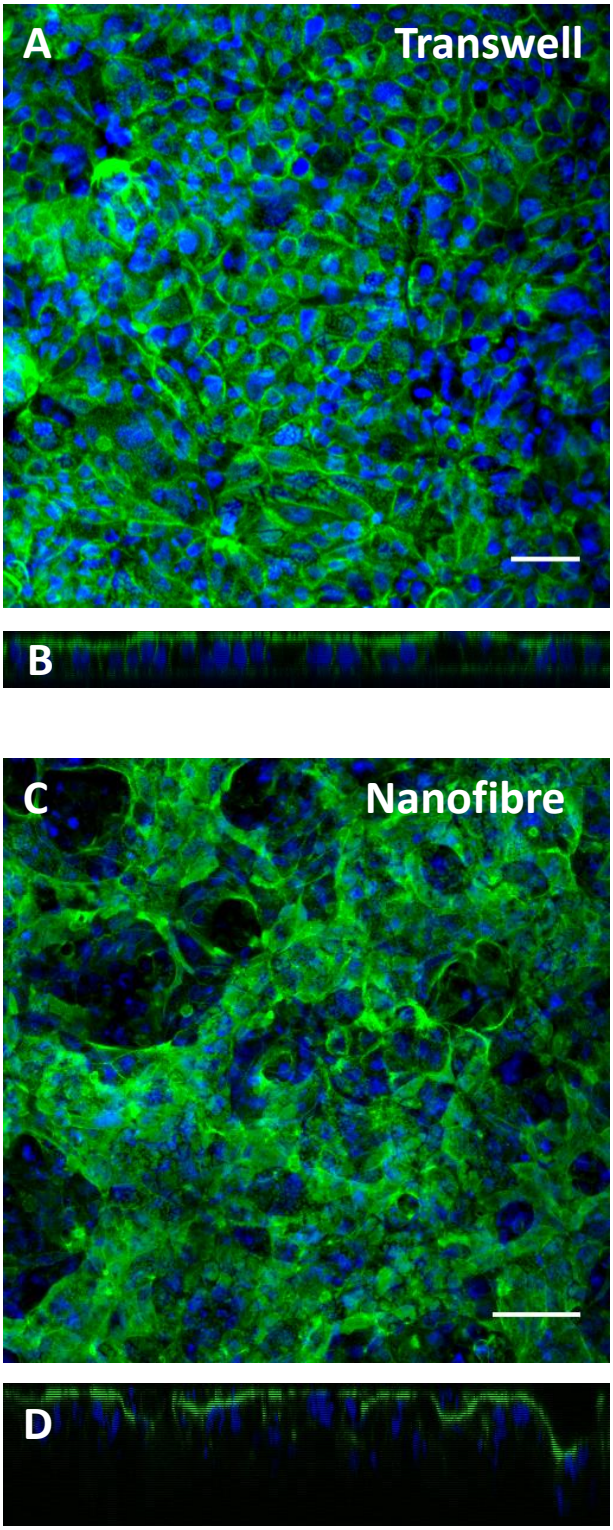

Figure 5.5. F-actin immunostaining of Caco-2 monocultures on transwell and nanofibre scaffolds. (A&C) Caco-2 monocultures on transwell and nanofibre supports respectively, stained for cytoskeletal filament F-actin (green) viewed top down and (B&D) respective XZ cross sectional views. Scale bars = 50 µm.

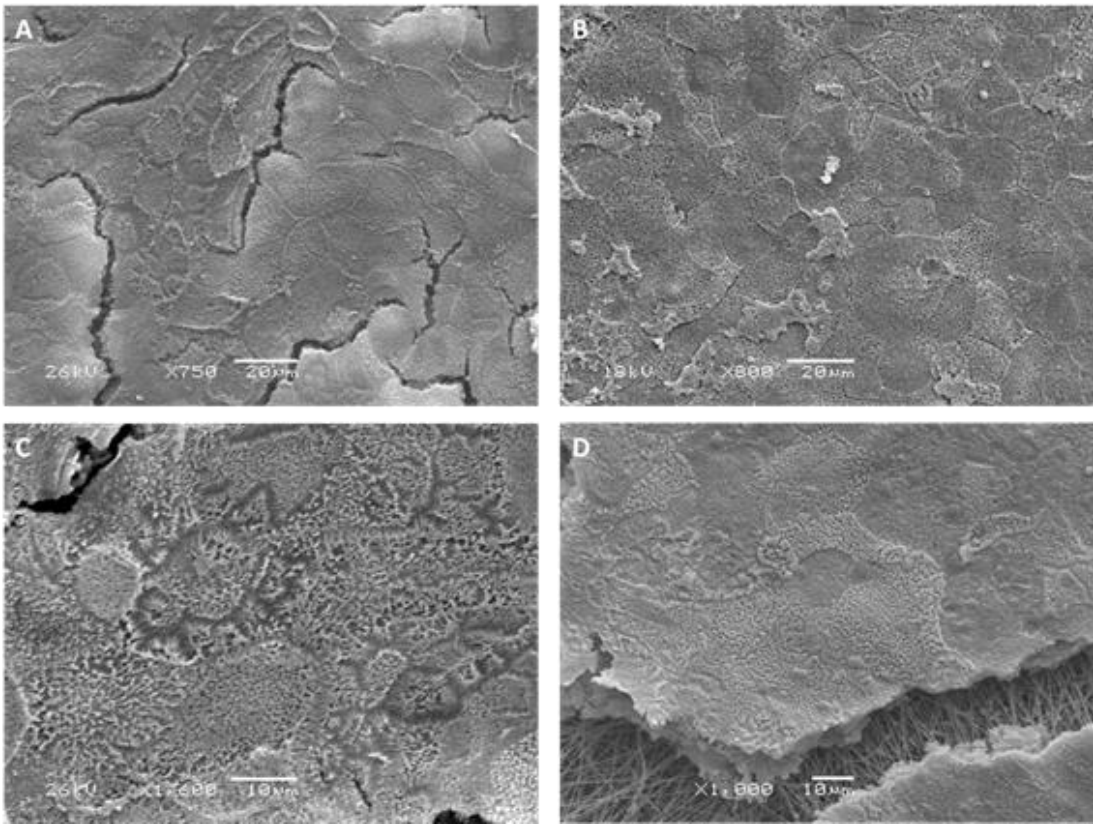

Figure 5.6. Representative scanning electron micrographs of Caco-2 epithelial cells on transwell and nanofibre scaffolds Representative images of Caco-2 cells cultured on (A&C) transwell surfaces and (B&D) nanofibre scaffolds. (C&D) Comparable apical morphology and microvilli expression can be observed at higher magnifications. (D) Nanofibres can be observed through a fracture in the epithelial layer (the fracture is an artefact of the procedure and can be observed in the other samples also).

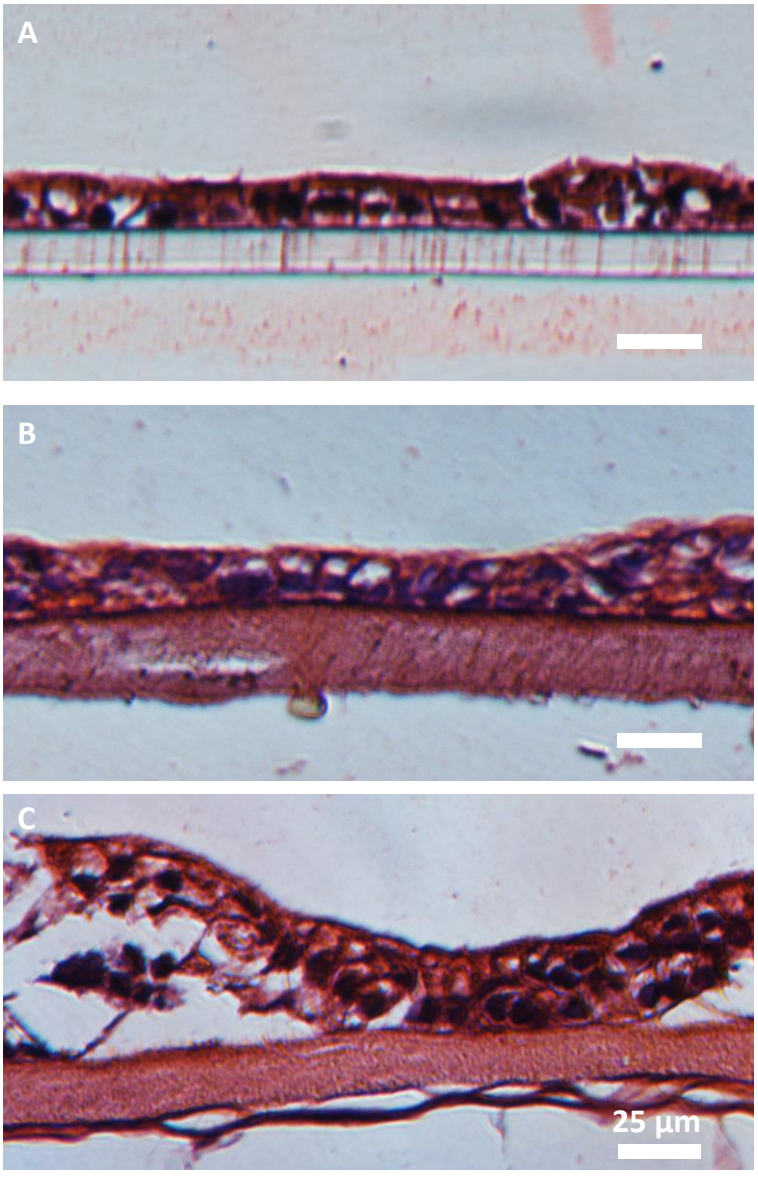

Figure 5.7. H&E stained Caco-2 and Caco-2/18co cross sections Caco-2 and Caco-2/18co samples were fixed and processed in paraffin wax and sectioned into 8µm thin sections. Samples were subsequently stained with haematoxylin (nuclear) and eosin (cytosol) to differentiate cellular regions. (A) Caco-2 on transwell inserts and (B&C) Caco-2 and Caco-2/18co nanofibre scaffolds, respectively.

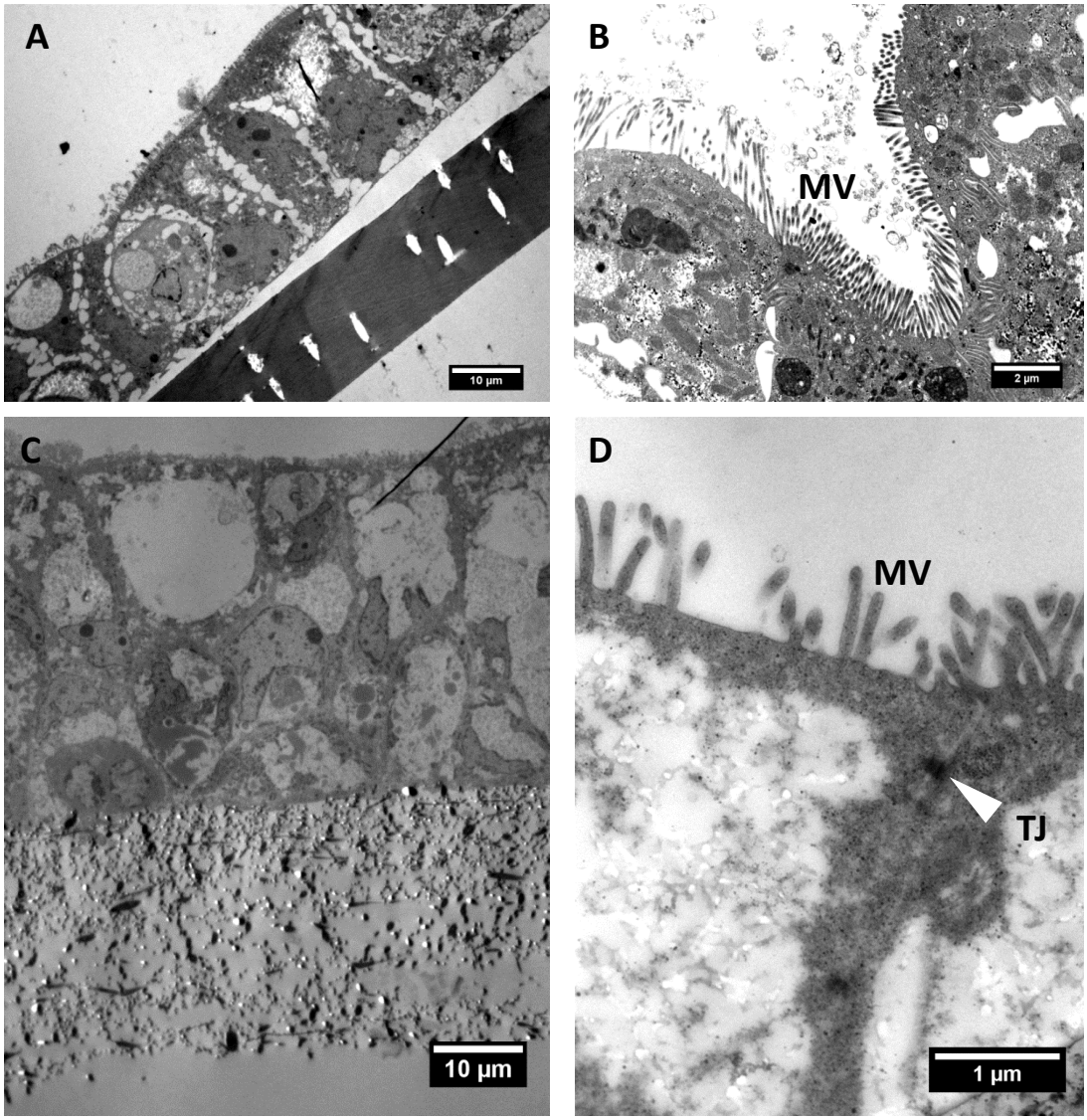

Figure 5.8. Representative transmission electron micrographs of Caco-2 monocultures. (A&B) Transwell Caco-2 cultures. (C&D) Nanofibre Caco-2 cultures. (A&C) Low and (B&D) high magnification micrographs of Caco-2 monocultures on transwell and nanofibre scaffolds, respectively. As before microvilli (MV) and apical tight junctions (TJ – white arrow) have been highlighted.

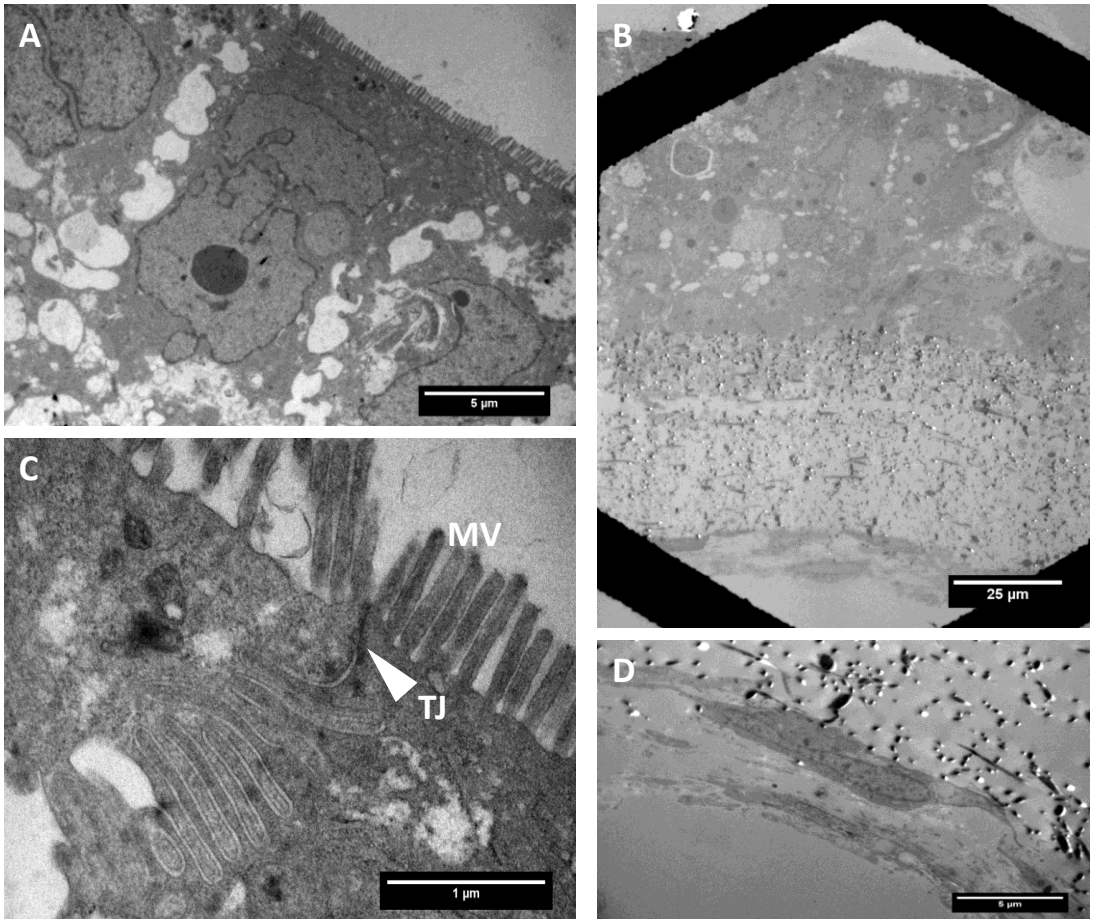

Figure 5.9 Representative transmission electron micrographs of Caco-2/18co cultures on nanofibre scaffolds. (A) An individual Caco-2 cell with distinct apical microvilli. Clear intercellular space can be seen between neighbouring Caco-2 cells. (B) Low magnification view of the entire construct wit hCaco-2 cells on the apical side of the nanofibre scaffold and CCD-18co cells on the underside (basolateral) side of the scaffold. (C) High magnification image of an apical connection between two adjoining Caco-2 cells, microvilli (MV) and an apical tight junction (TJ) are highlighted. (D) High magnification image of a CCD-18co myofibroblast on the underside of the nanofibre scaffold.

5.4.3 Electrical resistance of porcine intestinal segments

Porcine intestinal segments were evaluated for their trans-epithelial electrical resistance to examine whether any regional variation could be observed throughout the intestinal tract. Mean TEER values recorded for the duodenum, jejunum and ileum were 98 ±40, 145 ±80 and 113 ±63 Ω cm^2 (±SD) respectively with significant differences observed between the jejunum and both other regions (duodenum and ileum) (Figure 5.11.A).

Day 21 TEER readings from respective mono and co-culture set ups on both scaffold type were compared with the porcine intestinal segments (Figure 5.11.B). Caco-2 transwell cultures exhibit a comparatively high TEER compared to all the other set ups (both Caco-2 monocultures and Caco-2/18co co-cultures) which show electrical resistance values closer to the *ex vivo* porcine tissue sections. Despite demonstrating resistance values more closely aligned with the tissue section TEERs all of the developed *in vitro* models (with the exception of Caco-2/18co transwell cultures) had significantly higher TEER from the porcine tissue also.

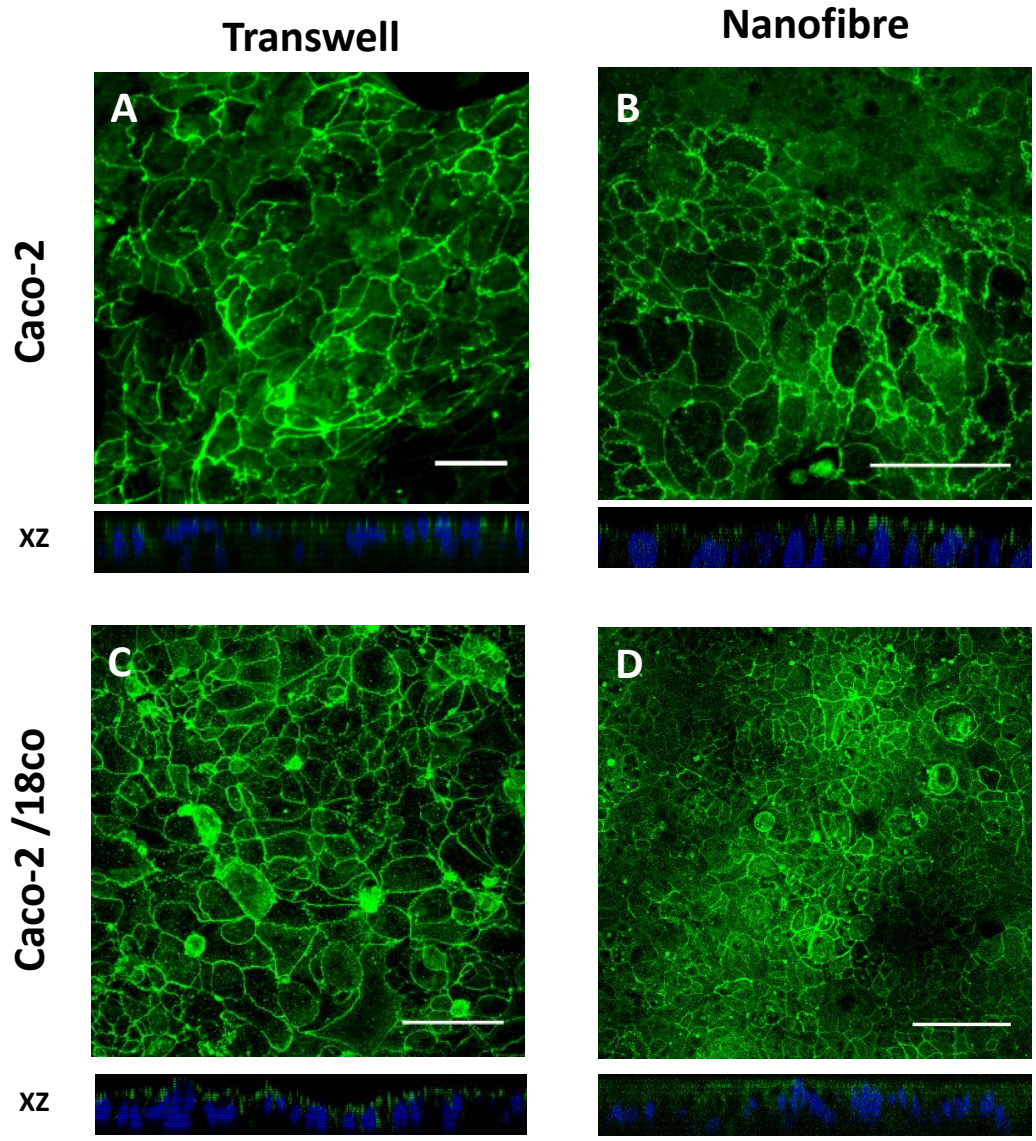

Figure 5.10. Tight junction expression in Caco-2 and Caco-2/18co transwell and nanofibre scaffolds. Expression of tight junction protein ZO-1 (green) was investigated in (A&C) monocultures and (B&D) co-cultures of Caco-2 and Caco-2/18co. Comparable apical staining was observed in all the samples. Cell nuclei were counterstained with Hoechst (blue). Scale bars equal 50 µm.

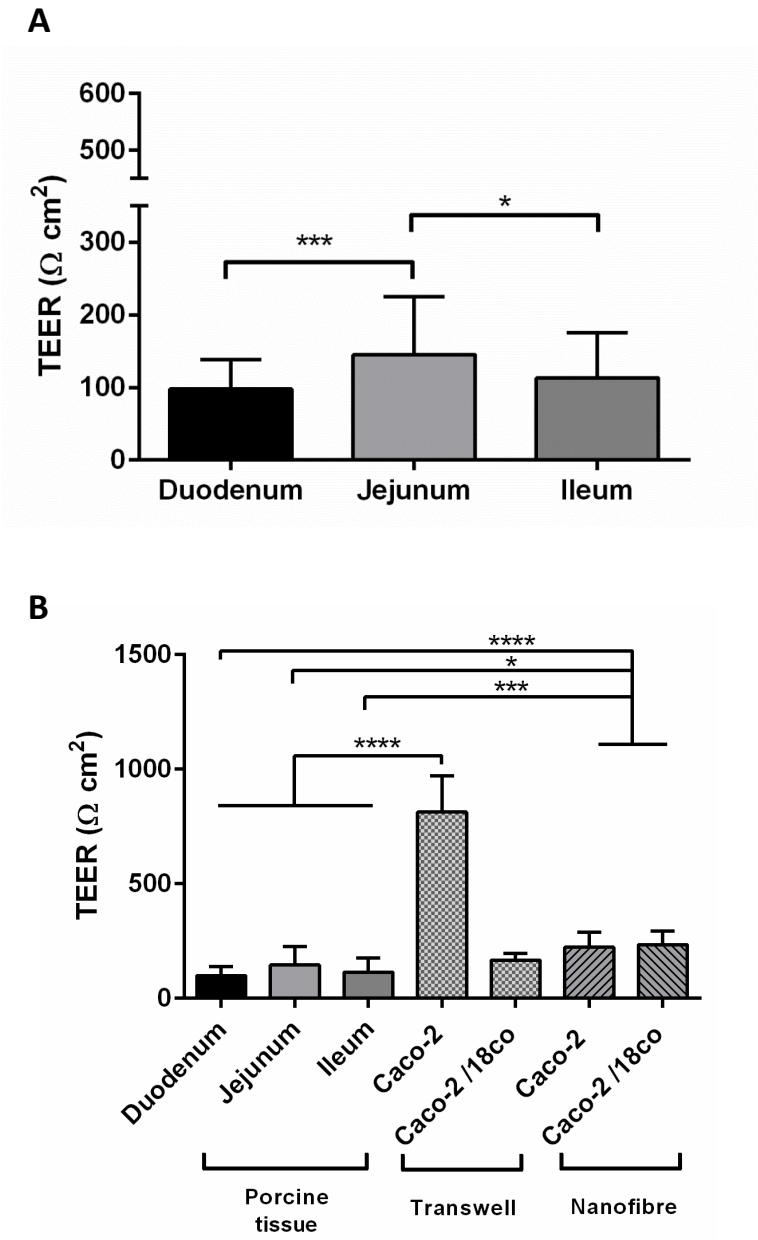

Figure 5.11. Electrical resistance of regional porcine segments in comparison with developed *in vitro* models. (A) Comparison of the regional differences in electrical resistance of resected porcine intestinal tissue. Values represent mean ± SD, n= 50-54, N=4-5. (B) Evaluation of the difference in porcine intestinal tissue sections with conventional transwell Caco-2 cultures and developed mono and co-culture systems on nanofibre scaffolds on day 21 of culture. Values represent mean ± SD, n=9-15 (inserts) from a minimum of two independent experiments. Significance determined by One-way ANOVA with Tukey's multiple comparison test, *$p \leq 0.05$, ***$p \leq 0.001$, ****$p \leq 0.0001$.

5.4.4 Permeability studies

5.4.4.1. Lucifer yellow (LY)

The permeability of lucifer yellow can be used as a method to evaluate the integrity of Caco-2 monolayers and is used as a low permeability marker of the paracellular route of absorption. Given the permeability is passive (i.e. not carrier/transporter mediated) then transport would be expected to be equal in both directions. Conventional Caco-2 monolayers display a low flux of LY with permeability values of 0.30 (±0.13)/0.66 (±0.23) x 10^{-6} cm s^{-1} (A to B/B to A) (Figure 5.12.). Interestingly this results in an efflux ratio (PappBA/PappAB) in excess of 2 which can suggest the compound is undergoing active efflux. However, given the very low permeability coefficients in both directions (<1 x 10^{-6} cm s^{-1}) and the fact that LY is not a reported efflux substrate this is not likely to be a true assertion. The permeability of LY increased in Caco-2/18co co-cultures in both transport directions (transwell) to 1.64 (±0.46)/1.40 (±0.51) although the increase was not significantly different (in either transport direction) from the Caco-2 monocultures (Table 5-1).

Nanofibre monocultures and co-cultures exhibited P_{app} values of 7.14 (±0.4.53)/8.51 (±6.61) and 10.22 (±6.60)/7.01 (±0.51) x 10^{-6} cm s^{-1} respectively which were significantly higher than transwell Caco-2 monocultures and Caco-2/18co co-cultures. The standard deviations for nanofibre based set ups were significantly larger than their transwell equivalents, but there was no valid reason to exclude the experimental P_{app} values (i.e observed changes in TEER or poor compound recovery). Some of values were above 1 x 10^{-5} cm s^{-1} (2- 3 inserts in each transport direction). Acellular nanofibre scaffolds did demonstrate much higher P_{app} for LY compared to acellular transwell inserts (Figure A-6).

Porcine intestinal segments displayed significantly higher permeability of LY than transwell-based Caco-2 equivalents (with the exception of duodenal sections in the BA

transport direction). LY P_{app} values for duodenal, jejunal and ileal sections were 4.66 (±1.19)/2.01 (±0.85), 5.71 (±1.50)/4.31 (±2.58) and 5.58 (±3.93)/3.80 (±3.46) x 10^{-6} cm s^{-1}, respectively. These permeability values were not significantly different from those obtained with nanofibre based Caco-2 and Caco-2/18co *in vitro* set ups. LY recovery for porcine intestinal segments was lower than that observed in transwell or nanofibre cultures and was in the range of 40-75%.

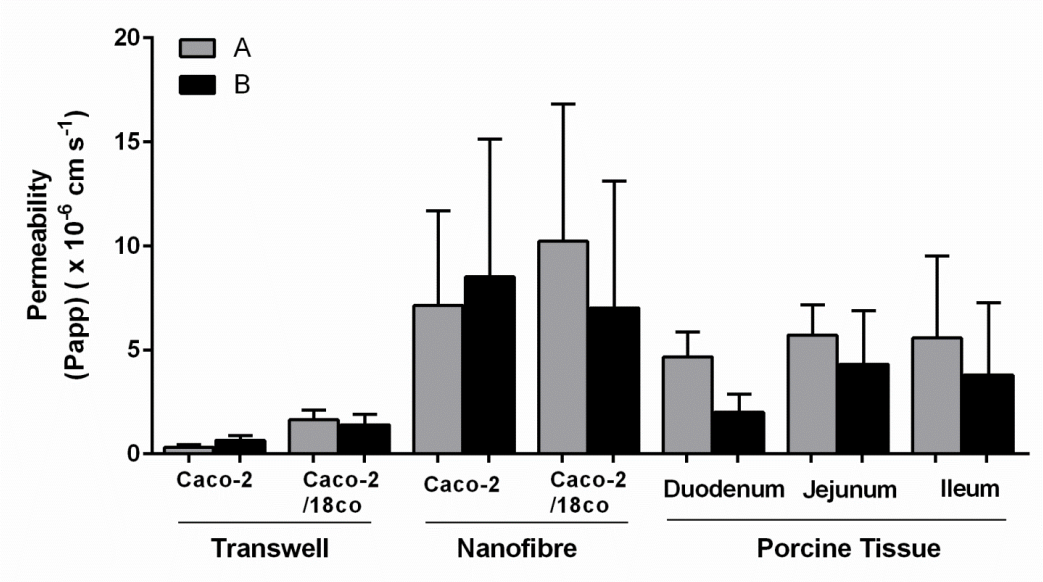

Figure 5.12. The bidirectional apparent permeability coefficients (Papp) of paracellular marker lucifer yellow. The permeability of lucifer yellow in absorptive and secretory transport directions was investigated in *in vitro* models and compared with *ex vivo* porcine tissue sections. Values represent mean ± SD, n=6-12 inserts from a minimum of two independent experiments for transwell/nanofibre set ups. n= 6-7 inserts, N=3-4 donor pigs with respect to porcine tissue samples.

Table 5-1. Summary of Tukey's multiple comparisons test (One-way ANOVA) showing the statistically significant results for lucifer yellow permeability. P-values= *p≤ 0.05, **p≤ 0.01, ***p ≤ 0.001, ****p≤0.0001.

AB		BA	
Caco-2 (T) vs. Caco-2 (N)	***	Caco-2 (T) vs. Caco-2 (N)	***
Caco-2 (T) vs. Caco-2/18co (N)	****	Caco-2/18co (T) vs. Caco-2 (N)	***
Caco-2/18co (T) vs. Caco-2 (N)	**	Caco-2 (N) vs. Jejunum	***
Caco-2/18co (T) vs. Caco-2/18co (N)	***	Caco-2 (N) vs. Ileum	**
Caco-2 (T) vs. Duodenum	***	Caco-2/18co (N) vs. Jejunum	*
Caco-2 (T) vs. Jejunum	****		
Caco-2 (T) vs. Ileum	****		
Caco-2/18co (T) vs. Duodenum	*		
Caco-2/18co (T) vs. Jejunum	***		
Caco-2/18co (T) vs. Ileum	***		

5.4.4.2. FITC-dextran 4000 (FD4)

FITC-dextran 4000 is a high molecular weight fluorescent molecule that, like lucifer yellow, can be used to quantifiably assess the integrity of *in vitro* cell monolayers and *ex vivo* tissue sections. Like LY, FD4 is thought to be a passively permeating compound because it is hydrophilic and has a Stoke's radii of 14 Å and in theory should be able to permeate via the paracellular route. As with LY, equal permeability of FD4 would be expected in both transport directions (Figure 5.13.). Transwell based Caco-2 monolayers again display a very low Papp for this type of molecule with permeability coefficients of 0.18 (±0.10)/0.51 (±0.25) x 10^{-6} cm s^{-1} (A to B/B to A). These values equate to a total molecular flux of less than 0.1%. By comparison, transwell Caco-2/18co co-cultures displayed elevated FD4 P_{app} of 1.15 (±0.91)/0.55 (±0.21) x 10^{-6} cm s^{-1}. Although these are significantly higher (AB direction only) than Caco-2 monocultures the flux still represents <1% total flux of the compound which is extremely low.

Caco-2 monocultures based on nanofibre scaffolds showed some evidence of directional transport bias with considerably increased permeability in the absorptive direction (i.e. A to B) over the secretory direction (i.e. B to A). Papp values for the nanofibre Caco-2 monocultures were 4.51 (±0.67)/0.75 (±0.74) x 10^{-6} cm s^{-1} with the absorptive permeability being significantly higher than that of both transwell based cultures.

Porcine segments all displayed P_{app} values between 2.5-4.8 x 10^{-6} cm s^{-1} (AB direction) and 1.85-5.00 x 10^{-6} cm s^{-1} (BA direction). The porcine permeability coefficients were comparable to the nanofibre Caco-2 cultures but significantly higher than transwell based cultures (Table 5-2). Interestingly FD4 permeability appeared to show some regional variation for A to B permeability, in a stepwise fashion with permeability decreasing along the intestinal tract; however the experimental differences between the tissue sections were not significant. The permeability in both AB and BA transport directions for porcine

intestinal segments were significantly higher than any of the transwell based cultures set ups. FD4 recovery for porcine tissues was similar to LY with recoveries ranging from 50-70%. Due to time constraints nanofibre Caco-2/18co co cultures could not be evaluated.

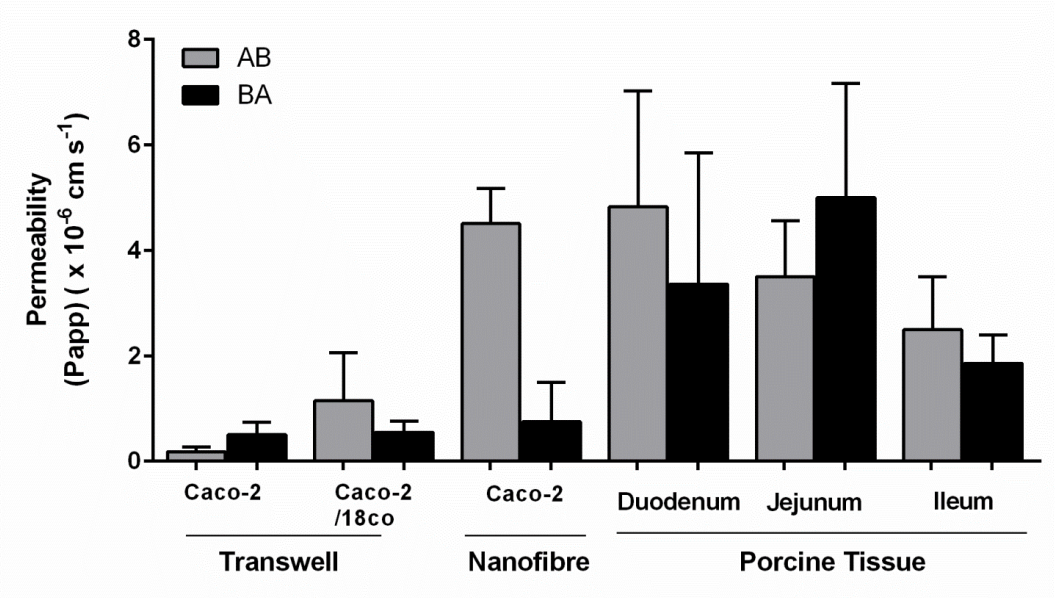

Figure 5.13. The bidirectional apparent permeability coefficients (Papp) of paracellular marker FITC-dextran 4000 (FD4). The permeability of fluorescently tagged dextran in absorptive and secretory transport directions in *in vitro* models and compared with *ex vivo* porcine tissue sections. Values represent mean ± SD, n=9-13 inserts from a minimum of two independent experiments for transwell/nanofibre set ups. n= 2-4 inserts, N=2 donor pigs with respect to porcine tissue samples.

Table 5-2. Summary of Tukey's multiple comparisons test (One-way ANOVA) showing the statistically significant results for FD4 permeability. P-values= *p≤ 0.05, **p≤ 0.01, ***p ≤ 0.001, ****p≤0.0001.

AB		BA	
Caco-2 (T) vs. Caco-2/18co (T)	**	Caco-2 (T) vs. Duodenum	**
Caco-2 (T) vs. Caco-2 (N)	****	Caco-2 (T) vs. Jejunum	****
Caco-2/18co (T) vs. Caco-2 (N)	****	Caco-2/18co (T) vs. Duodenum	**
Caco-2 (T) vs. Duodenum	****	Caco-2/18co (T) vs. Jejunum	****
Caco-2 (T) vs. Jejunum	****	Caco-2 (N) vs. Jejunum	***
Caco-2 (T) vs. Ileum	**		
Caco-2/18co (T) vs. Duodenum	****		
Caco-2/18co (T) vs. Jejunum	**		

5.4.4.3. Rhodamine 123 (Rho 123)

Rhodamine is a known substrate of p-glycoprotein (P-gp/MDR1) and as such displays active efflux which can be demonstrated *in vitro* with the Caco-2 model. Transwell Caco-2 cultures serve as evidence of this with Rho-123 P_{app} values of 0.82 (±0.51)/3.80 (±0.31) x 10^{-6} cm s^{-1} (A to B/B to A). These values give an efflux ratio of 4.6 (Table A-2) which, as alluded to previously, is indicative of active efflux. As Caco-2 is known to express P-gp the permeability of Rho-123 was used to investigate potential changes in p-gp activity in co-culture models and also in porcine tissue segments.

Transwell Caco-2/18co co-cultures demonstrated comparable permeability to Caco-2 monocultures with no significant differences observed in either transport direction although the efflux ratio was lower for the co-culture set up (2.8 compared to 4.6) (Figure 5.14). Despite being able to observe this efflux phenomenon in transwell cultures this was not detectable in nanofibre based cultures or in porcine tissue segments. Rho-123 Papp in porcine segments ranged from 5.6-7.6 x 10^{-6} cm s^{-1} for A to B transport and 1.8-3.6 x 10^{-6} cm s^{-1} for B to A permeability. Compound recovery was notably poor for Rho-123 with recoveries between 37-54% (4 tissue segments for each transport direction from two donor pigs).

Nanofibre based tissue constructs showed increased permeability over the porcine tissue segments and, similar to the porcine sections, did not demonstrate expected directional bias towards the efflux pathway but rather showed relatively equal permeability in both directions.

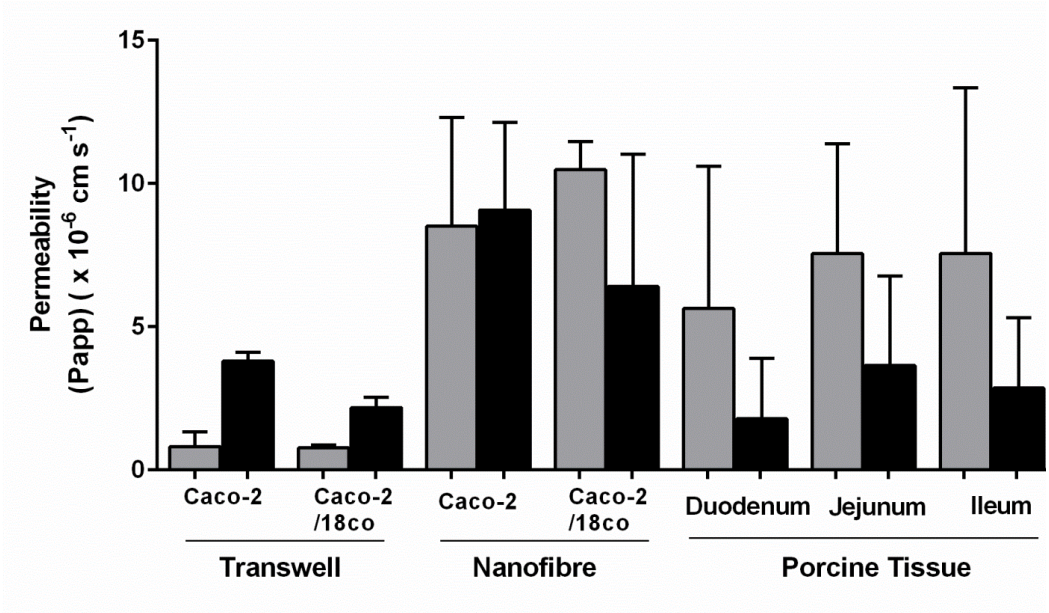

Figure 5.14. The bidirectional apparent permeability coefficients (Papp) of p-gp substrate rhodamine 123. The permeability of fluorescently tagged dextran in absorptive and secretory transport directions in *in vitro* models and compared with *ex vivo* porcine tissue sections. Values represent mean ± SD, n=3-12 inserts from a minimum of two independent experiments for transwell/nanofibre set ups. n= 2-4 inserts, N=2 donor pigs with respect to porcine tissue samples.

Table 5-3. Summary of Tukey's multiple comparisons test (One-way ANOVA) showing the statistically significant results for Rho-123 permeability. P-values= *p≤ 0.05, **p≤ 0.01, ***p ≤ 0.001, ****p≤0.0001.

AB		BA	
Caco-2 (T) vs. Caco-2 (N)	****	Caco-2 (T) vs. Caco-2 (N)	****
Caco-2 (T) vs. Caco-2/18co (N)	****	Caco-2/18co (T) vs. Caco-2 (N)	****
Caco-2/18co (T) vs. Caco-2 (N)	****	Caco-2/18co (T) vs. Caco-2/18co (N)	*
Caco-2/18co (T) vs. Caco-2/18co (N)	****	Caco-2 (N) vs. Duodenum	**
Caco-2 (T) vs. Duodenum	*	Caco-2 (N) vs. Ileum	*
Caco-2 (T) vs. Jejunum	**		
Caco-2 (T) vs. Ileum	**		
Caco-2/18co (T) vs. Duodenum	*		
Caco-2/18co (T) vs. Jejunum	**		
Caco-2/18co (T) vs. Ileum	**		

5.4.4.4. Atenolol (ATN)

Atenolol is a commonly utilised drug for Caco-2 based assessment of permeability due to the fact it has been widely used in *in vivo* studies and there is general agreement upon the fraction absorbed (%FA) being roughly 50% of the administered dose[95,178]. As such it helps serve as one of several compounds regularly used to provide a rank order of drugs with known FA values which enables permeability predictions to be made for novel compounds using the Caco-2 model.

Like LY and FD4, atenolol is reasoned to permeate mainly via the paracellular route of absorption. Typically low permeability was observed in Caco-2 monolayers, in this study baseline Caco-2 $P_{app's}$ (AB/BA) for ATN were 0.48 (±0.09)/0.67 (±0.21) x 10^{-6} cm s^{-1} (Figure 5.15.). Transwell Caco-2/18co co-cultures demonstrated increased permeability over the monoculture equivalent with significant difference in both transport directions with values of 2.94 (±2.13)/4.60 (±3.02) x 10^{-6} cm s^{-1} whilst still demonstrating relatively equal permeability for AB and BA directions (as would be expected for a passively permeating compound such as ATN).

Nanofibre based cultures both showed increased atenolol permeability over the conventional transwell Caco-2 system but the differences were not significantly different (Table 5-4). The Papps between the monoculture and co-culture however demonstrated no significant difference (1.48 (±1.32)/1.44 (±1.04) x 10^{-6} cm s^{-1} and 2.18 (±1.62)/1.74 (±1.37) x 10^{-6} cm s^{-1} for the Caco-2 monoculture and Caco-2/18co co-culture respectively).

Porcine intestinal segment permeability ranged from 3.71-5.58 (A/B) and 3.22-9.44 (B/A) x 10^{-6} cm s^{-1}. As with the majority of the other tested compounds no significant regional variation was observed in ATN permeability, in either transport direction. The P_{app} values were however significantly higher than Caco-2 transwell culture for jejunal and ileal segments in the AB direction but only for duodenal tissue in the BA direction (Table 5-4).

Unlike other compounds tested with porcine tissue, ATN recovery in porcine tissue was quite acceptable with an average recovery of 80% (range between 70-95%).

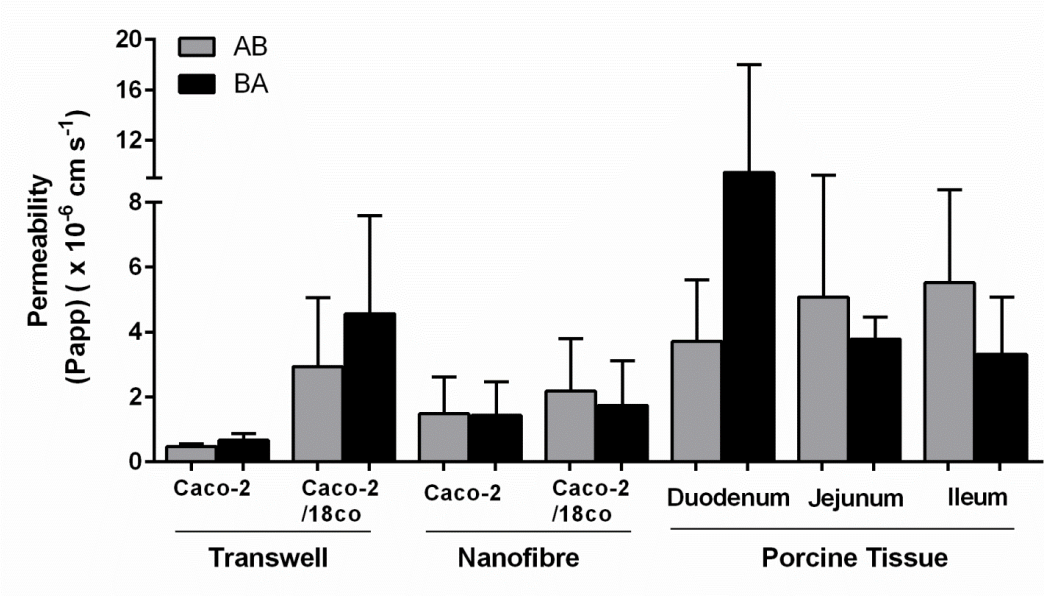

Figure 5.15. The bidirectional apparent permeability coefficients (Papp) of paracellular drug compound atenolol. The permeability of atenolol absorptive and secretory transport directions in *in vitro* models and compared with *ex vivo* porcine tissue sections. Values represent mean ± SD, n=6-9 inserts from a minimum of three independent experiments for transwell/nanofibre set ups. n= 2-4 inserts, N=2 donor pigs with respect to porcine tissue samples.

Table 5-4. Summary of Tukey's multiple comparisons test (One-way ANOVA) showing the statistically significant results for ATN permeability. P-values= *p≤ 0.05, **p≤ 0.01, ***p ≤ 0.001, ****p≤0.0001.

AB		BA	
Caco-2 (T) vs. Caco-2/18co (T)	**	Caco-2 (T) vs. Caco-2/18co (T)	***
Caco-2 (T) vs. Jejunum	*	Caco-2/18co (T) vs. Caco-2 (N)	*
Caco-2 (T) vs. Ileum	**	Caco-2/18co (T) vs. Caco-2/18co (N)	*
		Caco-2 (T) vs. Duodenum	**
		Caco-2 (N) vs. Duodenum	*
		Caco-2/18co (N) vs. Duodenum	*

5.4.4.5. Propranolol (PRN)

Propranolol, like atenolol, is a commonly used compound for with a well-known FA (>90%) and is therefore also very useful molecule to probe the permeability properties of *in vitro* models. Due to the lipophilic properties of PRN, passive transcellular permeability is likely to be the dominant mechanism of permeability across the epithelium.

Propranolol demonstrates high permeability in conventional Caco-2 cultures 30.67 (±6.32)/ 32.03 (±4.41) x 10^{-6} cm s^{-1} (AB/BA) with good agreement between both directional fluxes. Caco-2/18co transwell co-cultures demonstrate comparable PRN transport with P_{app} values of 31.49 (±7.64)/ 26.46(±7.72) x 10^{-6} cm s^{-1} for the absorptive and secretory transport directions, respectively. Nanofibre based set ups by comparison demonstrate vastly higher transport than their transwell counterparts demonstrating more than a two-fold increase in PRN by comparison (86.34(±12.14)/75.14(±14.23) x 10^{-6} cm $s^{-1}$for nanofibre Caco-2 cultures and 88.72(±12.22)/63.14(3.42) x 10^{-6} cm s^{-1} for Caco-2/18co co-cultures respectively (Figure 5.16.). Some directional transport bias was also observed for nanofibre based cultures in both Caco-2 and Caco-2/CCD-18co co-cultures.

Porcine tissue segments displayed very low permeability coefficients 7.76-9.6 x 10^{-6} cm s^{-1}in the A to B direction and 1.85-5.50 x 10^{-6} cm s^{-1}in the B to A direction. PRN demonstrated a lower recovery with an average of 58% (range between 35-75%).

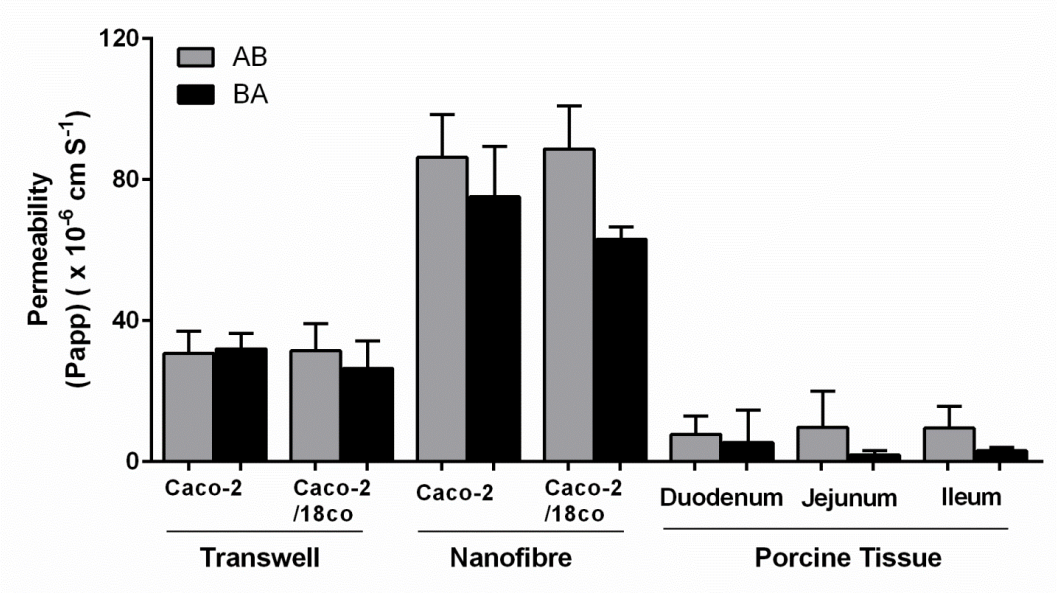

Figure 5.16. The bidirectional apparent permeability coefficients (Papp) of transcellular drug compound propranolol. Propranolol permeability was investigated in both absorptive and secretory transport directions in *in vitro* models and in comparison with *ex vivo* porcine tissue sections. Values represent mean ± SD, n=6-15 inserts from a minimum of two independent experiments for transwell/nanofibre set ups. n= 2-4 inserts, N=2 donor pigs with respect to porcine tissue samples.

Table 5-5. Summary of Tukey's multiple comparisons test (One-way ANOVA) showing the statistically significant results for PRN permeability. P-values= *p≤ 0.05, **p≤ 0.01, ***p ≤ 0.001, ****p≤0.0001.

AB		BA	
Caco-2 T vs. Caco-2 (N)	****	Caco-2 T vs. Caco-2 (N)	****
Caco-2 T vs. Caco-2/18co (N)	****	Caco-2 T vs. Caco-2/18co (N)	****
Caco-2/18co (T) vs. Caco-2 (N)	****	Caco-2/18co (T) vs. Caco-2 (N)	****
Caco-2/18co (T) vs. Caco-2/18co (N)	****	Caco-2/18co (T) vs. Caco-2/18co (N)	****
Caco-2 T vs. Duodenum	****	Caco-2 T vs. Duodenum	****
Caco-2 T vs. Jejunum	***	Caco-2 T vs. Jejunum	****
Caco-2 T vs. Ileum	****	Caco-2 T vs. Ileum	****
Caco-2/18co (T) vs. Duodenum	***	Caco-2/18co (T) vs. Duodenum	****
Caco-2/18co (T) vs. Jejunum	***	Caco-2/18co (T) vs. Jejunum	****
Caco-2/18co (T) vs. Ileum	***	Caco-2/18co (T) vs. Ileum	****
Caco-2 (N) vs. Duodenum	****	Caco-2 (N) vs. Duodenum	****
Caco-2 (N) vs. Jejunum	****	Caco-2 (N) vs. Jejunum	****
Caco-2 (N) vs. Ileum	****	Caco-2 (N) vs. Ileum	****
Caco-2/18co (N) vs. Duodenum	****	Caco-2/18co (N) vs. Duodenum	****
Caco-2/18co (N) vs. Jejunum	****	Caco-2/18co (N) vs. Jejunum	****
Caco-2/18co (N) vs. Ileum	****	Caco-2/18co (N) vs. Ileum	****

Table 5-6. Overview of apparent permeability (Papp) of selected compounds in different *in vitro* models and porcine intestinal tissue segments

	Permeability (Papp AB/BA ± SD x 10^{-6} cm s^{-1})						
Compound	**Transwell**		**Nanofibre**		**Porcine Tissue**		
	Caco-2	Caco-2/18co	Caco-2	Caco-2/18co	Duodenum	Jejunum	Ileum
Lucifer yellow	0.31 ± 0.13/0.66 ± 0.23	1.64 ± 0.46/1.40 ± 0.51	7.14 ± 4.53/8.51 ± 6.62	10.22 ± 6.60/7.01 ± 6.10	4.67 ± 1.19/2.02 ± 0.85	5.71 ± 1.46/4.31 ± 2.59	5.58 ± 3.93/3.80 ± 3.46
FD4	0.18 ± 0.09/0.51 ± 0.23	1.15 ± 0.91/0.55 ± 0.21	4.51 ±0.67/0.75 ± 0.74		4.83 ± 2.20/3.36 ± 2.49	3.50 ± 1.06/5.01 ± 2.16	2.50 ± 0.99/1.85 ± 0.54
Rho 123	0.82 ± 0.51/3.80 ± 0.31	0.77 ± 0.11/2.18 ± 0.36	8.51 ± 3.80/9.07 ± 3.07	10.48 ± 0.98/6.40 ± 4.63	5.64 ± 4.97/1.78 ± 2.11	7.55 ± 3.83/3.64 ± 3.13	7.56 ± 5.77/2.86 ± 2.46
Atenolol	0.48 ± 0.9/0.66 ± 0.21	2.94 ± 2.13/4.57 ± 3.02	1.48 ± 1.13/1.43 ±1.04	2.18 ± 1.62/1.74 ± 1.37	3.71 ± 1.89/9.44 ± 8.56	5.08 ± 4.12/3.79 ± 0.67	5.52 ± 2.97/3.32 ± 1.75
Propranolol	30.67 ± 6.32/32.03 ± 4.41	31.49 ± 7.64/26.46 ± 7.72	86.34 ± 12.14/75.14 ± 14.23	88.72 ± 12.22/63.14 ± 3.42	7.76 ± 5.12/5.50 ± 9.14	9.76 ± 10.25/1.85 ± 1.22	9.57 ± 6.09/3.09 ± 0.93
Verapamil	27.05 ± 11.51/33.73 ± 10.62		74.59 ± 14.77/55.67 ± 17.27				

5.5 Discussion

The focus of this chapter of work was to further investigate the influence of a myofibroblast cell line on Caco-2 barrier function when cultured on both a transwell and electrospun nanofibre based inserts. The focus was specifically on the contribution and effect myofibroblast cells exert upon the epithelial barrier. The effect upon drug permeability was investigated to highlight whether epithelial-myofibroblast co-cultures would be of further interest in the development of more sophisticated *in vitro* tools to improve existing pre-clinical cells models to study intestinal drug permeability. Additionally, nanofibre scaffolds produced by electrospinning, which attempt to mimic the physical structures cells interact with *in vivo*, were also integrated as a platform for the epithelial/myofibroblast cell cultures. The final aim was to rationalise the scientific observations of these *in vitro* models with comparable *ex vivo* porcine tissue sections, a method which has been demonstrated as a potentially powerful technique for assessing drug permeability *in vitro*[110].

The significance of myofibroblasts in epithelial barrier maintenance has become an increasing area of research focus. The role myofibroblasts play in regulating epithelial tissues is not completely understood and, from a handful of published studies, *in vitro* analysis of this relationship paints a complex and sometimes contradictory picture. This is perhaps because of the uncertainty surrounding the precise involvement of the different cells and their particular functions within the lamina propria[124], as discussed previously (Chapter 3). Beltinger *et al*., studied the relationship between primary myofibroblasts and HCA-7 colonic epithelial cells, mainly with regard to the electrical resistance and flux of mannitol. They noted myofibroblasts (and myofibroblast conditioned medium) increased TEER and delayed the flux of mannitol across the cell layer[34]. This work was based on earlier observations by Berschneider and Powell who conducted similar work in the T84 epithelial cells (colonic-airway metastases)[179]. Willemsen *et al*., proposed a co-culture model of T84 epithelial cells with CCD-18co myofibroblasts and noted no significant difference in TEER

between monocultures and co-cultures. They did however discover myofibroblasts exerted a protective role; helping maintain intestinal barrier integrity during immune related barrier disruption[114]. Other studies have simply investigated the developmental influences of myofibroblasts on T84 epithelial organisation and differentiation[180]. Clearly the varied origin of the cell types under investigation contributes towards the variability in reported data.

It is only very recently that significant research effort has started to focus on using myofibroblasts in an *in vitro* model for drug permeability assessment[14]. Pereira *et al*., observed similar responses of Caco-2 when co-cultured with CCD-18co myofibroblasts to that reported herein, that is a reduction in TEER and increased permeability to a permeability marker (in the case of Pereira *et al*., the drug studied was insulin). The picture is convoluted further given the authors tested a variety of co-cultures (Caco-2/CCD18co direct co-cultures – i.e. Caco-2 seeded directly atop of a CCD-18co layer and two 3D, matrigel based set ups. One where CCD-18co were imbedded within matrigel (a gelatinous protein mixture derived from mice cells), the other where CCD-18co and Caco-2 were physically separated by a matrigel layer). Although TEER was reduced in all co-cultures significant change in insulin transport was only observed in the 3D cultures and not in Caco-2/CCD-18co direct co-cultures, despite the significant changes in TEER.

The data presented herein is the first extensive investigation into the paracellular permeability properties of Caco-2/18co co-cultures and nanofibre based culture systems as alternative platforms for predicting drug permeability *in vitro.* Pereira *et al*., attributed CCD-18co induced changes in Caco-2 barrier integrity as a result of direct interspacing between the epithelial cells (given they cultured them in direct contact with one another). Given the findings presented with conditioned media in Chapter 3 and other published observations using conditioned media, these changes in barrier integrity are more likely to be mediated by a paracrine mechanism[34,179].

TEER induced changes observed from Caco-2 monocultures to Caco-2/18co co-cultures in transwell cultures were not observed when the cells were cultured on nanofibre scaffolds. Furthermore whilst nanofibre cultures demonstrated increased permeability over analogous transwell cultures for all the molecules tested, no considerable difference was observed between nanofibre Caco-2 and Caco-2/18co co-cultures. This could perhaps indicate cellular behavioural changes in CCD-18co, speculatively as a result of the culture substrate, given there is no perceived barrier to paracrine signalling in the nanofibre based culture systems. However, this could also be a result of a dilution of any perceived paracrine mediator (and hence the observed effect) given the larger basolateral volume required for nanofibre cultures compared to the conventional transwell system (6 mL versus 1.2 mL, respectively). Clearly the modulation that occurs in transwell based cultures does not readily transfer to the snapwell-based nanofibre insert system. The design of an in-house culture system which is comparable in size to the 12-well insert transwell or the direct manipulation of transwell inserts for use with the nanofibre scaffolds (and hence allow the use of same apical and basolateral volumes) would help identify any contribution of the experimental set up to the observations. Additionally, conditioned media experiments conducted on nanofibre cultures may shed further light on whether the change in TEER has merely been masked by the culture conditions or whether the effect is lost when the cells are cultured on nanofibre substrates.

It is notable that nanofibre based monocultures of Caco-2 displayed inherently lower TEER values than the transwell equivalents. This singularity has been observed for other epithelial cultures (namely air epithelial cell line Calu-3) cultured on nanofibre scaffolds[115,116]. The basis for this decrease in TEER has not been proven or evidenced in detail, seemingly it must be a result of the culture substrate; Morris *et al*., suggest that it is a direct result of the increased porosity of nanofibres over transwell inserts[116]. Given the structural topography of the nanofibre structures it is perhaps possible that the tight junctions formed between neighbouring cells are physically disrupted or altered resulting in lower TEER (perhaps also

explaining the increased molecular flux). Given that regular ZO-1 staining was observed, which is used as an indicator of functional tight junction expression[5], complete tight junction disruption seems implausible. Inconsistencies in epithelial layer confluence (i.e. break points in the cell layer) cannot be completely discounted as a potential cause for some of the experimental observations (decreased TEER/higher molecular permeability), despite extensive examination of the Caco-2 layer in all the developed systems which demonstrated confluent barrier formation.

The use of resected porcine tissue has recently been developed as a relatively powerful (and more predictive) tool in drug permeability assessment[110]. Westerhout *et al*., reported TEER values of jejunal segments of 58 ± 7 Ω cm^2 (generally ≤ 100 Ω cm^2 is in agreement with other literature papers[181]) which is in relatively good agreement with our findings if not slightly lower than is reported herein (reported porcine TEER, irrelevant of region, ranged from 97-145 Ω cm^2). The slightly elevated TEER readings observed could be indicative of incomplete removal of some of the muscle layers from the resected porcine tissue causing slight elevations in the recorded electrical resistance or simply a result of biological variation.

In terms of molecular permeability Westerhout *et al*., reported P_{app} for atenolol and propranolol (A to B permeability only) of 1.25/2.92 x 10^{-6} cm s^{-1} (in minipigs/ normal pigs) and 0.42/25.1 x 10^{-6} cm s^{-1} (that is P_{app}/P_{app}total), respectively. The low P_{app} value for propranolol was attributed to the poor compound recovery for which the authors corrected for by factoring in tissue accumulation after 90 minutes (P_{app}tissue)[110,182]. Tissue accumulation is likely to be significant for highly lipophilic compounds such as propranolol (see P_{app}total value for corrected value which is 60-fold higher than the P_{app}). Unfortunately due to the experimental design (experiment duration and sampling intervals) a similar correction could not be applied to our data set. It has been suggested however that generalised corrections of P_{app} are not advisable as the processes involved in the loss of

compound are often compound specific[5,183]. Even without attempting to correct the P_{app} values for poor compound recovery the calculated P_{app}'s for LY (or comparable paracellular marker, mannitol) and atenolol demonstrated good comparison with reported human jejunal P_{app} by Sjöberg *et al*.,[96] and Rozehnal *et al*.,[182] (4.02 ±2.20 and 5.56 ±2.21 x 10^{-6} cm s^{-1} for lucifer yellow and mannitol respectively and 4.11±1.32 and 2.82±0.65 x 10^{-6} for atenolol).

Upon reflection of the three developed models the Caco-2/18co transwell based system possibly represents the best as an *in vitro* permeability prediction tool, based upon our investigations. This model demonstrates permeability values closer to the human *ex vivo* tissue permeability coefficients which are higher than the conventional Caco-2 monoculture system. Caco-2 has been known to under predict the absorption of some compounds, namely those where paracellular transport is thought to be dominant[7,9,19,75,84,107-109,184]. There is however some concern that some sensitivity to p-gp substrates is diminished under co-culture conditions. Further investigations with using verapamil as an inhibitor of p-gp would help shed light on p-gp function in Caco-2/CCD-18co co-cultures.

Nanofibre based systems and porcine intestinal segments may demonstrate some closer similarity to the actual human permeability values but considering the loss of sensitivity to p-gp substrates the versatility and broad utility of these systems is perhaps questionable (based on this research). Additionally, given there is no proof to support or explain the observed differences in barrier integrity and molecular flux for nanofibre based cultures it is difficult to countenance a theory that the nanofibre system presented herein are truly more representative of the *in vivo* scenario. There can of course be cautious optimism on the same subject because there have been multiple observations of reduced TEER in epithelial nanofibre-based cultures reported elsewhere[115,116]. This suggests there is a logical explanation for the observed barrier phenotype when epithelial cells are cultured on nanofibre scaffolds.

6. General Discussion, Conclusions & Future Work

The aim of this thesis was to investigate co-cultures of intestinal epithelial cells with the CCD-18co cell line and explore the functional consequence of the co-cultures with respect to implications for *in vitro* cell models used to predict human *in vivo* drug permeability. The impact of cell culture substrate architecture was also examined to probe the important relationship between cell behaviour and the role of the cellular microenvironment and the response of cultured epithelial cell lines to these environmental cues. The results of these first two aims were compiled and applied into the development of an *in vitro* epithelial-myofibroblast model which was characterised and evaluated for the permeability of molecular tracers and typical drug compounds.

The intestinal epithelium itself is a continuously renewing tissue with a distinct architectural and cellular milieu. Cell culture models, as simple as they may be in comparison to the actual tissue, enable us to investigate the basic biology of the cells that compose the tissue. By investigating the complex cellular interactions between the various cell types within the intestine and attempting to decipher the cross talk mechanisms, which are crucial to the tissue function, we can improve our understanding of the fundamental aspects of this biological barrier. The importance of this knowledge should not be underestimated; the understanding of this tissue has far reaching influence, whether it is in the fields of developmental biology, nutrition, bacteriology, immunology, intestinal pathology or within pharmaceutical medicines development (as has been the focus of this thesis research).

In the first chapter of work CCD-18co cells were shown to express key markers of myofibroblasts; staining positive for α-SMA and vimentin but also for smooth muscle marker, desmin, which is not always usual for ISEMFs. In our initial studies using transwell inserts it was clear that CCD-18co cells did not physically contribute to changes in the

barrier integrity in monoculture. Under co-culture conditions with common epithelial cell lines (Caco-2, HT-29 and Calu-3) CCD-18co were able to modulate the function of the epithelial barrier in regards to TEER and drug disposition. This modulation to the barrier integrity could also, in part, be propagated through media conditioned by the CCD-18co cells postulating secreted factors as the harbingers of the observed epithelial changes. No visual changes were observed in ZO-1 tight junction protein expression under co-culture conditions. Preliminary investigations into the use of HT-29 for goblet-like cell co-cultures provided interesting insights into manipulating the barrier in a more direct fashion, however undesirable cell behaviour (such as multi-layering, cell detachment and variable barrier properties) resulted in the omission of this component from the final model.

The second chapter of work focused mainly on nanofibre scaffolds, which were produced by electrospinning the polymer poly ethylene terephthalate (PET) and investigated for use as cell culture substrates. Early work highlighted potential issues with cell attachment and growth on PET scaffolds and as a result surface treatment was investigated to achieve epithelial cell confluence. Surface coating of the nanofibre scaffolds with collagen resulted in a more hydrophilic surface chemistry which enhanced cell growth across the scaffolds. Rapid prototyping of resin formers was also explored as a technique to confer intestinal macroarchitectures into the nanofibre scaffolds. Although some progress was made towards imparting villi structures into the scaffolds simple nanofibre constructs were taken forward into the final epithelial-myofibroblast model.

The final chapter of experimental work focused on bringing together the work from each previous chapter for the development of an epithelial-myofibroblast model for drug permeability assessment. This permeability evaluation, using a series of compounds, was compared with the transport through resected porcine tissue sections for different regions of the small intestine. Caco-2/CCD-18co transwell co-cultures demonstrated increased flux to molecules permeating via the paracellular route (LY, FD4 and atenolol) over Caco-2

monolayers and comparable permeability with regards to transcellular marker propranolol and p-gp efflux substrate Rho-123. Nanofibre based cultures showed increased permeability coefficients to all of the molecules under investigation in comparison to Caco-2 transwell cultures. The permeability profile of nanofibre cultures was generally more closely aligned with P_{app}'s obtained from porcine tissue sections however there was some suggestion that the p-gp function was diminished or undetectable.

It is clear myofibroblasts have an important role in intestinal tissue function in both health and disease. Almost all current cell models of the intestine focus almost entirely on the cell types of the epithelium but it is becoming increasingly apparent that supportive cell types, such as the myofibroblasts, have a pivotal role. The contribution of myofibroblasts (and perhaps other supportive cells of the lamina propria) begins during organogenesis where they deliver important instructive signals along the villi-crypt axis, directing the fate of the intestinal stem cell niche as the cells migrate to the villus tips[33]. Following organogenesis it is clear myofibroblasts play a crucial role in continual tissue homeostasis; initiating and regulating immune responses[33,114,185], secreting ECM[32], providing structural support to the tissue architecture[46] and initiating repair[186]. Almost all of these functions derive from the ability of myofibroblasts to propagate chemical and physical signals from their environment which is crucial to maintenance of the entire intestinal microenvironment.

Given the uncertainty regarding the exact contribution of each specific α-SMA(+) cell type within the lamina propria to the overall tissue function[124], it is perhaps difficult to gauge exactly what path future research should take. With respect to CCD-18co, further investigation into their phenotype is essential. Immunostaining for validated pericyte markers (such as PDGFR-β[187], NG2[188], CD13[126]) would help characterise this cell type further and clear up any ambiguity about the CCD-cell phenotype reported in this thesis. The use of isolated primary human myofibroblasts would serve as a control for such

investigations and provide an excellent parallel for any new observations made using the CCD-18co cell line.

In vitro data on epithelial-myofibroblast interactions can lead to conflicting reports. Evidently myofibroblasts influence the barrier properties of cultured epithelial cells; however this can have different outcomes for the barrier properties of the epithelium. There are examples where myofibroblast co-culture increased the barrier integrity in both intestinal and airway epithelial cell lines[34,115,116]. In contrast, there are examples where the co-culture increased the 'leakiness' of the epithelium[14] and also where no effect on the epithelial barrier integrity was observed[114]. Unravelling the molecular mechanism of myofibroblast mediated barrier modulation will be important to understanding why different reports demonstrate different responses from the cultured epithelium. The different cell types used within each investigation is a likely factor in the observed experimental outcomes. Clearly the modulation of the epithelial barrier could have physiological importance, following injury or barrier disruption for example.

Any stimulation increasing the epithelial permeability could also serve to have important physiological, developmental or perhaps even pathological implications. The modulation of barrier integrity that is observed in epithelial-myofibroblast co-cultures is perhaps indicative that myofibroblast-secreted factors influence or regulate tight junctional composition. This is evidenced by the fact that differential expression of tight junctional proteins has been observed along the villi-crypt axis[61,69] and that the expression of specific tight junction proteins (i.e. the claudin composition of the TJ) which determine the pore size of the tight junction[58,61,189]. Myofibroblasts are themselves known to be involved in the differentiation and regulation of the epithelium by secreting paracrine mediators in various gradients along the very same axis[33,46]. It is therefore possible that they are directly involved in signalling that impacts tight junction expression in the epithelium. Beltinger *et al*., attributed the increase in TEER in HCA-7 monolayers to TGF- β as they were able to ablate the effect of

myofibroblast induced changes with a pan specific antibody against TGF- β[34]. Conversely, it has been demonstrated that myofibroblast induced changes in Calu-3 is attributed, in part, to interleukin-6[190]. It is very likely the modulation is not merely a result of a single mechanism but a complex cross talk of various mediators.

As Caco-2 cells are derived from colon tissue, which is widely known to have more restrictive TJs than the small intestinal epithelium, they most probably have a well-defined claudin composition that epitomises the barrier integrity of the colon tissue[61]. It is therefore possible that if the paracrine secretions CCD-18co could result in changes to the claudin composition of the tight junctions. This might result in the observed cell phenotype with the leakier epithelia, similar to upper intestinal tract. Although perhaps speculative this would explain observed changes in TEER and molecular permeability in Caco-2 monocultures vs Caco-2/CCD-18co co-cultures in our data and that of Pereira et al.,[14]. This could be investigated by directly studying the claudin composition of Caco-2 tight junctions in monoculture and myofibroblast co-cultures. Given that Calu-3 cells seem to demonstrate a wholly uniform response during co-culture they could provide an interesting parallel for such an investigation.

Advanced biomaterials and synthetic cell scaffolds which mimic the specific natural microenvironment are in high demand not only for their potential in therapeutic interventions but also in furthering the understanding of basic conceptual biology. Cell behaviour, tissue hierarchy and ultimately organ function rely on the fundamental interactions between cells themselves and their environment[145,191].

Fibrillar scaffolds produced by electrospinning are one of many techniques under investigation to meet the growing challenge for biomaterials in the modern age. In light of some emerging research in this area it is perhaps remiss, in retrospect, to have failed to integrate a chemical component into our fibre scaffolds other than simple coatings. There

are many barriers to using natural proteins in electrospinning however, the cost implications, increased difficulty of production and also degradation properties can be prohibitive. There is however some examples of research where chemical moieties, mimicking the binding motifs of natural polymers, are grafted to surrogate polymers to attempt to achieve both chemical and anatomical biomimicry in nanofibre culture substrates[151,152]. Despite this, there are perhaps some important lessons still to be learned from simple nanofibre substrates, namely the importance of simple microarchitecture.

The interesting observation from the use of nanofibre scaffolds in this research is the perceived reduction of barrier integrity when epithelial cells are cultured on nanofibre substrates[115,116]. It is often stated that planar culture surfaces, such as those offered by transwell inserts, offer an unrealistic platform for epithelial cell growth. The type of porous permeable support material (nitrocellulose, aluminium oxide, polycarbonate (plus collagen coated) , polyester and poly ethylene terephthalate) has been demonstrated to affect barrier integrity in terms of epithelial resistance, molecule permeability properties, morphology and even transporter expression (PepT1 and HPT1) in Caco-2[192,193]. Behrens and Kissel attributed changes observed between polycarbonate (PC), polyester (PE) and poly ethylene terephthalate (PET) membranes to altered tight junction organisation and different cell-support interactions[193]. Despite changes in TEER, almost two fold increase between PC (~450 Ω cm^2) and both PE (~950 Ω cm^2) and PET (~800 Ω cm^2) there was little variation in the observed permeability to FD4 (~0.5 x 10^{-6} cm s^{-1}). A similar situation where no direct correlation was drawn between TEER and paracellular flux in two clones of Caco-2 was observed by Artusson[75]. However on nanofibre scaffolds a change in TEER was also coupled with an increase in permeability (especially in paracellular permeants LY, FD4 and ATN). As mentioned previously, further investigation into the claudin composition of the TJ complexes might help shed light on the substrate induced changes observed in Caco-2.

Further work using nanofibre structures for cell culture should focus on screening more epithelial cell lines to see if the reduced barrier integrity (measured by TEER) is

synonymous for all epithelial cell types. The increased permeability of nanofibre based cultures could be investigated further by adopting the same approach as Artusson et al., and Watson et al.,; by using a series of structurally similar compounds with graded molecular weight which permeate via the paracellular route; from this the paracellular pore characteristics can be modelled extensively[65,75]. This would shed light on any functional changes to the intercellular tight junctional complexes and would supplement further research that examined the tight junction composition, as mentioned previously.

To be more definitive regarding the conclusions of the final drug permeability study a larger panel of compounds would need to be studied. Compounds which represent both passive transport mechanisms (transcellular and paracellular) and also drugs that undergo carrier mediated flux, both absorptive and secretory (Figure A-7), would enable a correlation of human bioavailability (% FA) with experimental P_{app} values. The expressions of the drug the transporters involved the carried mediated permeability studies could be quantified by quantitative polymerase chain reaction to get an idea of real time expression of the proteins and correlate this with observed permeability coefficients.

With specific respect to rhodamine 123 permeability, a known p-gp substrate[194,195], nanofibre cultures demonstrated a distinct lack of directional polarity unlike traditional permeable supports. Investigation into p-gp function in nanofibres cultures would elucidate this result. Using p-gp inhibitor substrates, such as verapamil[176,194], during Rho-123 permeability experiments would ascertain whether there is decreased p-gp activity in nanofibre cultures or whether the observed result is a consequence of increased apical to basolateral transport of Rho-123 due to the increased flux in the paracellular route (Figure A-8). Given the pharmaceutical relevance of p-gp, the apparent loss of function or sensitivity requires further investigations.

In the meantime some important decisions must be made about how helpful and realistic are current developments to the Caco-2 model. Will these changes be implemented and fed into the development process? Do they add significant predictive power over the simple Caco-2 system? Do they layers of complexity merely convolute and complicate factors such as assay robustness and inter-lab reproducibility? Proper evaluation and assessment of any significant advances in *in vitro* intestinal modelling by the appropriate regulatory bodies, such as the European Centre for the Validation of Alternative Methods (ECVAM)[10,134], can help add guarantees to researchers and regulators alike as to the utility of such new models. There is no doubt that work such as that presented in this thesis and the cited research papers will help form a body of work which will not only help answer complex biological questions regarding cell-cell and cell-matrix interactions but ultimately lead to more predictive *in vitro* tools. This will inevitably reduce the burden on animal based models but will also improve the efficiency of the drug development process.

7. References

1 Lipinski, C. A. Drug-like properties and the causes of poor solubility and poor permeability. *J Pharmacol Toxicol Methods* **44**, 235-249 (2000).

2 Weisman, R. in *Boston Globe* (Online, 2014).

3 FDA. Novel New Drugs 2014 Summary. (FDA Centre for Drug Evaluation and Research, 2015).

4 Artursson, P. & Borchardt, R. Intestinal drug absorption and metabolism in cell cultures: Caco-2 and beyond. *Pharm Res* **14**, 1655 - 1658 (1997).

5 Hubatsch, I., Ragnarsson, E. G. & Artursson, P. Determination of drug permeability and prediction of drug absorption in Caco-2 monolayers. *Nat Protoc* **2**, 2111-2119, doi:10.1038/nprot.2007.303 (2007).

6 Artursson, P. & Karlsson, J. Correlation between oral drug absorption in humans and apparent drug permeability coefficients in human intestinal epithelial (Caco-2) cells. *Biochemical and biophysical research communications* **175**, 880-885, doi:10.1016/0006-291x(91)91647-u (1991).

7 Artursson, P., Palm, K. & Luthman, K. Caco-2 monolayers in experimental and theoretical predictions of drug transport. *Advanced Drug Delivery Reviews* **46**, 27-43, doi:10.1016/s0169-409x(00)00128-9 (2001).

8 Balimane, P. V., Chong, S. & Morrison, R. A. Current methodologies used for evaluation of intestinal permeability and absorption. *Journal of Pharmacological and Toxicological Methods* **44**, 301-312, doi:10.1016/s1056-8719(00)00113-1 (2000).

9 Balimane, P. V., Han, Y.-H. & Chong, S. Current Industrial Practices of Assessing Permeability and p-glycoprotein interaction. *Aaps J* **8**, 1-13 (2006).

10 Le Ferrec, E. *et al.* In vitro models of the intestinal barrier. The report and recommendations of ECVAM Workshop 46. European Centre for the Validation of Alternative methods. *Alternatives to laboratory animals : ATLA* **29**, 649-668 (2001).

11 Pusch, J. *et al.* The physiological performance of a three-dimensional model that mimics the microenvironment of the small intestine. *Biomaterials* **32**, 7469-7478, doi:10.1016/j.biomaterials.2011.06.035 (2011).

12 Yu, J., Peng, S., Luo, D. & March, J. C. In vitro 3D human small intestinal villous model for drug permeability determination. *Biotechnol Bioeng* **109**, 2173-2178, doi:10.1002/bit.24518 (2012).

13 Wen-Cheng, Y. *et al.* Engineering a Biomimetic Villus Array for In Vitro Three-Dimensional Culture of Intestinal Epithelial Cells. *Microelectromechanical Systems, Journal of* **21**, 1418-1425, doi:10.1109/jmems.2012.2205902 (2012).

14 Pereira, C., Araújo, F., Barrias, C. C., Granja, P. L. & Sarmento, B. Dissecting stromal-epithelial interactions in a 3D in vitro cellularized intestinal model for permeability studies. *Biomaterials* **56**, 36-45, doi:http://dx.doi.org/10.1016/j.biomaterials.2015.03.054 (2015).

15 Sung, J. H., Yu, J., Luo, D., Shuler, M. L. & March, J. C. Microscale 3-D hydrogel scaffold for biomimetic gastrointestinal (GI) tract model. *Lab Chip* **11**, 389-392, doi:10.1039/c0lc00273a (2011).

16 Majani, R., Zelzer, M., Gadegaard, N., Rose, F. R. & Alexander, M. R. Preparation of Caco-2 cell sheets using plasma polymerised acrylic acid as a weak boundary layer. *Biomaterials* **31**, 6764-6771, doi:http://dx.doi.org/10.1016/j.biomaterials.2010.05.049 (2010).

17 Kim, H. J. & Ingber, D. E. Gut-on-a-Chip microenvironment induces human intestinal cells to undergo villus differentiation. *Integrative Biology*, doi:10.1039/c3ib40126j (2013).

18 Kim, H. J., Huh, D., Hamilton, G. & Ingber, D. E. Human gut-on-a-chip inhabited by microbial flora that experiences intestinal peristalsis-like motions and flow. *Lab Chip* **12**, 2165-2174, doi:10.1039/c2lc40074j (2012).

19 Hilgendorf, C. *et al.* Caco-2 versus Caco-2/HT29-MTX co-cultured cell lines: permeabilities via diffusion, inside- and outside-directed carrier-mediated transport. *J Pharm Sci* **89**, 63 - 75 (2000).

20 Tavelin S. *et al.* An improved cell culture model based on 2/4/A1 cell monolayers for studies of intestinal drug transport: characterization of transport routes. *Pharm Res* **20**, 373-381. (2003).

21 Yin, X. *et al.* Niche-independent high-purity cultures of Lgr5+ intestinal stem cells and their progeny. *Nat Meth* **11**, 106-112, doi:10.1038/nmeth.2737 http://www.nature.com/nmeth/journal/v11/n1/abs/nmeth.2737.html#supplementary-information (2014).

22 Takenaka, T. *et al.* Human small intestinal epithelial cells differentiated from adult intestinal stem cells as a novel system for predicting oral drug absorption in humans. *Drug metabolism and disposition: the biological fate of chemicals* **42**, 1947-1954, doi:10.1124/dmd.114.059493 (2014).

23 Aldhous, M. C., Shmakov, A. N., Bode, J. & Ghosh, S. Characterization of conditions for the primary culture of human small intestinal epithelial cells. *Clinical and Experimental Immunology* **125**, 32-40, doi:10.1046/j.1365-2249.2001.01522.x (2001).

24 Perreault, N. & Beaulieu, J.-F. Primary Cultures of Fully Differentiated and Pure Human Intestinal Epithelial Cells. *Experimental Cell Research* **245**, 34-42, doi:http://dx.doi.org/10.1006/excr.1998.4221 (1998).

25 Tannergren, C., Bergendal, A., Lennernas, H. & Abrahamsson, B. Toward an increased understanding of the barriers to colonic drug absorption in humans: implications for early controlled release candidate assessment. *Mol Pharm* **6**, 60-73, doi:10.1021/mp800261a (2009).

26 Pocock, G. & Richards, C. D. *Human Physiology: The Basis of Medicine*. (Oxford University Press, 2004).

27 Wright, N. & Alison, M. *The biology of epithelial cell populations*. Vol. 2 (Oxford University Press, 1984).

28 Snoeck, V., Goddeeris, B. & Cox, E. The role of enterocytes in the intestinal barrier function and antigen uptake. *Microbes and Infection* **7**, 997-1004, doi:http://dx.doi.org/10.1016/j.micinf.2005.04.003 (2005).

29 Abreu, M. T. Toll-like receptor signalling in the intestinal epithelium: how bacterial recognition shapes intestinal function. *Nat Rev Immunol* **11**, 215-215 (2010).

30 Powell, D. W. *et al.* Myofibroblasts. I. Paracrine cells important in health and disease. *American Journal of Physiology - Cell Physiology* **277**, C1-C19 (1999a).

31 Powell, D. W. *et al.* Myofibroblasts. II. Intestinal subepithelial myofibroblasts. *American Journal of Physiology - Cell Physiology* **277**, C183-C201 (1999b).

32 Powell, D. W., Adegboyega, P. A., Di Mari, J. F. & Mifflin, R. C. Epithelial Cells and Their Neighbors I. Role of intestinal myofibroblasts in development, repair, and cancer. *American Journal of Physiology - Gastrointestinal and Liver Physiology* **289**, G2-G7, doi:10.1152/ajpgi.00075.2005 (2005).

33 Powell, D. W., Pinchuk, I. V., Saada, J. I., Chen, X. & Mifflin, R. C. Mesenchymal cells of the intestinal lamina propria. *Annu Rev Physiol* **73**, 213-237, doi:10.1146/annurev.physiol.70.113006.100646 (2011).

34 Beltinger, J. *et al.* Human colonic subepithelial myofibroblasts modulate transepithelial resistance and secretory response. *American Journal of Physiology - Cell Physiology* **277**, C271-C279 (1999).

35 McKaig, B. C., Makh, S. S., Hawkey, C. J., Podolsky, D. K. & Mahida, Y. R. Normal human colonic subepithelial myofibroblasts enhance epithelial migration (restitution) via TGF-β3. *American Journal of Physiology - Gastrointestinal and Liver Physiology* **276**, G1087-G1093 (1999).

36 McKaig, B. C., Hughes, K., Tighe, P. J. & Mahida, Y. R. Differential expression of TGF-beta isoforms by normal and inflammatory bowel disease intestinal myofibroblasts. *Am J Physiol Cell Physiol* **282**, C172-182, doi:10.1152/ajpcell.00048.2001 (2002).

37 Crosnier, C., Stamataki, D. & Lewis, J. Organizing cell renewal in the intestine: stem cells, signals and combinatorial control. *Nat Rev Genet* **7**, 349-359 (2006).

38 Falk, P., Roth, K. A. & Gordon, J. I. *Lectins are sensitive tools for defining the differentiation programs of mouse gut epithelial cell lineages*. Vol. 266 (1994).

39 Johansson, M. V. *et al.* Composition and functional role of the mucus layers in the intestine. *Cell. Mol. Life Sci.* **68**, 3635-3641, doi:10.1007/s00018-011-0822-3 (2011).

40 Aoki, Y., Morishita, M. & Takayama, K. Role of the mucous/glycocalyx layers in insulin permeation across the rat ileal membrane. *International Journal of Pharmaceutics* **297**, 98-109, doi:http://dx.doi.org/10.1016/j.ijpharm.2005.03.004 (2005).

41 Gunawardene, A. R., Corfe, B. M. & Staton, C. A. Classification and functions of enteroendocrine cells of the lower gastrointestinal tract. *International Journal of Experimental Pathology* **92**, 219-231, doi:10.1111/j.1365-2613.2011.00767.x (2011).

42 Clevers, H. C. & Bevins, C. L. Paneth cells: maestros of the small intestinal crypts. *Annu Rev Physiol* **75**, 289-311, doi:10.1146/annurev-physiol-030212-183744 (2013).

43 Bevins, C. L. & Salzman, N. H. Paneth cells, antimicrobial peptides and maintenance of intestinal homeostasis. *Nat Rev Micro* **9**, 356-368 (2011).

44 Cheng, H. & Leblond, C. P. Origin, differentiation and renewal of the four main epithelial cell types in the mouse small intestine V. Unitarian theory of the origin of the four epithelial cell types. *American Journal of Anatomy* **141**, 537-561, doi:10.1002/aja.1001410407 (1974).

45 Hunyady, B., Mezey, E. & Palkovits, M. Gastrointestinal immunology: cell types in the lamina propria--a morphological review. *Acta physiologica Hungarica* **87**, 305-328 (2000).

46 Furuya, S. & Furuya, K. Subepithelial fibroblasts in intestinal villi: roles in intercellular communication. *International review of cytology* **264**, 165-223, doi:10.1016/s0074-7696(07)64004-2 (2007).

47 Lahar, N. *et al.* Intestinal Subepithelial Myofibroblasts Support in vitro and in vivo Growth of Human Small Intestinal Epithelium. *PLoS One* **6**, e26898, doi:10.1371/journal.pone.0026898 (2011).

48 Valentich, J. D., Popov, V., Saada, J. I. & Powell, D. W. Phenotypic characterization of an intestinal subepithelial myofibroblast cell line. *American Journal of Physiology - Cell Physiology* **272**, C1513-C1524 (1997).

49 Furuya, K., Sokabe, M. & Furuya, S. Characteristics of subepithelial fibroblasts as a mechano-sensor in the intestine: cell-shape-dependent ATP release and P2Y1 signaling. *Journal of Cell Science* **118**, 3289-3304, doi:10.1242/jcs.02453 (2005).

50 Krueger, M. & Bechmann, I. CNS pericytes: Concepts, misconceptions, and a way out. *Glia* **58**, 1-10, doi:10.1002/glia.20898 (2010).

51 Baglole CJ *et al.* (Landes Bioscience; 2000-, Madame Curie Bioscience Database [Internet]. , 2000).

52 Kell, D. B., Dobson, P. D. & Oliver, S. G. Pharmaceutical drug transport: the issues and the implications that it is essentially carrier-mediated only. *Drug Discovery Today* **16**, 704-714, doi:http://dx.doi.org/10.1016/j.drudis.2011.05.010 (2011).

53 Kell, D. B., Dobson, P. D., Bilsland, E. & Oliver, S. G. The promiscuous binding of pharmaceutical drugs and their transporter-mediated uptake into cells: what we (need to) know and how we can do so. *Drug Discovery Today* **18**, 218-239, doi:http://dx.doi.org/10.1016/j.drudis.2012.11.008 (2013).

54 Dobson, P. D. & Kell, D. B. Carrier-mediated cellular uptake of pharmaceutical drugs: an exception or the rule? *Nat Rev Drug Discov* **7**, 205-220, doi:http://www.nature.com/nrd/journal/v7/n3/suppinfo/nrd2438_S1.html (2008).

55 Dobson, P. D., Patel, Y. & Kell, D. B. 'Metabolite-likeness' as a criterion in the design and selection of pharmaceutical drug libraries. *Drug Discovery Today* **14**, 31-40, doi:http://dx.doi.org/10.1016/j.drudis.2008.10.011 (2009).

56 Sugano, K. *et al.* Coexistence of passive and carrier-mediated processes in drug transport. *Nat Rev Drug Discov* **9**, 597-614, doi:10.1038/nrd3187 (2010).

57 Di, L. *et al.* Evidence-based approach to assess passive diffusion and carrier-mediated drug transport. *Drug Discovery Today* **17**, 905-912, doi:http://dx.doi.org/10.1016/j.drudis.2012.03.015 (2012).

58 Günzel, D. & Yu, A. S. L. *Claudins and the Modulation of Tight Junction Permeability*. Vol. 93 (2013).

59 Hartsock, A. & Nelson, W. J. Adherens and tight junctions: structure, function and connections to the actin cytoskeleton. *Biochimica et Biophysica Acta (BBA)-Biomembranes* **1778**, 660-669 (2008).

60 González-Mariscal, L., Betanzos, A., Nava, P. & Jaramillo, B. E. Tight junction proteins. *Progress in Biophysics and Molecular Biology* **81**, 1-44, doi:http://dx.doi.org/10.1016/S0079-6107(02)00037-8 (2003).

61 Chiba, H., Osanai, M., Murata, M., Kojima, T. & Sawada, N. Transmembrane proteins of tight junctions. *Biochimica et Biophysica Acta (BBA) - Biomembranes* **1778**, 588-600, doi:http://dx.doi.org/10.1016/j.bbamem.2007.08.017 (2008).

62 Claude, P. Morphological factors influencing transepithelial permeability: A model for the resistance of theZonula Occludens. *J. Membrain Biol.* **39**, 219-232, doi:10.1007/bf01870332 (1978).

63 Claude, P. & Goodenough, D. A. Fracture faces of zonaulae occuldentes from 'tight' and 'leaky' epithelia. *The Journal of Cell Biology* **58**, 390-400 (1973).

64 McNeil, E., Capaldo, C. T. & Macara, I. G. Zonula Occludens-1 Function in the Assembly of Tight Junctions in Madin-Darby Canine Kidney Epithelial Cells. *Molecular Biology of the Cell* **17**, 1922-1932, doi:10.1091/mbc.E05-07-0650 (2006).

65 Watson, C. J., Rowland, M. & Warhurst, G. *Functional modeling of tight junctions in intestinal cell monolayers using polyethylene glycol oligomers*. Vol. 281 (2001).

66 Madara, J. L. & Dharmsathaphorn, K. Occluding junction structure-function relationships in a cultured epithelial monolayer. *J Cell Biol* **101**, 2124-2133 (1985).

67 Ma, T. Y. *et al.* Mechanism of colonic permeation of inulin: is rat colon more permeable than small intestine? *Gastroenterology* **108**, 12-20 (1995).

68 Fine, K. D., Santa Ana, C. A., Porter, J. L. & Fordtran, J. S. Effect of changing intestinal flow rate on a measurement of intestinal permeability. *Gastroenterology* **108**, 983-989 (1995).

69 Fihn, B. M., Sjoqvist, A. & Jodal, M. Permeability of the rat small intestinal epithelium along the villus-crypt axis: effects of glucose transport. *Gastroenterology* **119**, 1029-1036 (2000).

70 Chau, D. Y., Johnson, C., MacNeil, S., Haycock, J. W. & Ghaemmaghami, A. M. The development of a 3D immunocompetent model of human skin. *Biofabrication* **5**, 035011, doi:10.1088/1758-5082/5/3/035011 (2013).

71 Petrova, A. *et al.* 3D In Vitro Model of a Functional Epidermal Permeability Barrier from Human Embryonic Stem Cells and Induced Pluripotent Stem Cells. *Stem Cell Reports* **2**, 675-689, doi:10.1016/j.stemcr.2014.03.009 (2014).

72 E., M. G. *et al. Human airway smooth muscle maintain in situ cell orientation and phenotype when cultured on aligned electrospun scaffolds*. Vol. 307 (2014).

73 Lippmann, E. S., Al-Ahmad, A., Azarin, S. M., Palecek, S. P. & Shusta, E. V. A retinoic acid-enhanced, multicellular human blood-brain barrier model derived from stem cell sources. *Scientific Reports* **4**, 4160, doi:10.1038/srep04160 http://www.nature.com/articles/srep04160#supplementary-information (2014).

74 Srinivasan, B. *et al.* TEER measurement techniques for in vitro barrier model systems. *J Lab Autom* **20**, 107-126, doi:10.1177/2211068214561025 (2015).

75 Artursson, P., Ungell, A. L. & Lofroth, J. E. Selective paracellular permeability in two models of intestinal absorption: cultured monolayers of human intestinal epithelial cells and rat intestinal segments. *Pharm Res* **10**, 1123-1129 (1993).

76 Amidon, G. L., Lennernas, H., Shah, V. P. & Crison, J. R. A theoretical basis for a biopharmaceutic drug classification: the correlation of in vitro drug product dissolution and in vivo bioavailability. *Pharm Res* **12**, 413-420 (1995).

77 Amidon, G. L., Kou, J., Elliott, R. L. & Lightfoot, E. N. Analysis of models for determining intestinal wall permeabilities. *J Pharm Sci* **69**, 1369-1373 (1980).

78 Elliott, R. L., Amidon, G. L. & Lightfoot, E. N. A convective mass transfer model for determining intestinal wall permeabilities: laminar flow in a circular tube. *J Theor Biol* **87**, 757-771 (1980).

79 Lennernas, H. *et al.* Regional jejunal perfusion, a new in vivo approach to study oral drug absorption in man. *Pharm Res* **9**, 1243-1251 (1992).

80 Lennernas, H. *et al.* The effect of L-leucine on the absorption of levodopa, studied by regional jejunal perfusion in man. *Br J Clin Pharmacol* **35**, 243-250 (1993).

81 Shah, V. P. & Amidon, G. L. G.L. Amidon, H. Lennernas, V.P. Shah, and J.R. Crison. A theoretical basis for a biopharmaceutic drug classification: the correlation of in vitro drug product dissolution and in vivo bioavailability, Pharm Res 12, 413-420, 1995--backstory of BCS. *AAPS J* **16**, 894-898, doi:10.1208/s12248-014-9620-9 (2014).

82 U.S. Department of Health and Human Services, F. D. A. Guidance for Industry: Waiver of In Vitro Bioavailability and Bioequivalence Studies for Immediate-Release Solid Oral

Dosage Forms Based on a Biopharmaceutics Classification System. (Center for Drug Evaluation and Research (CDER), 2000).

83 Pinto, M. *et al.* Enterocyte-like differentiation and polarization of the human colon carcinoma cell line Caco-2 in culture. *Biol Cell* **47**, 323 - 330 (1983).

84 Hidalgo, I. J., Raub, T. J. & Borchardt, R. T. Characterization of the human colon carcinoma cell line (Caco-2) as a model system for intestinal epithelial permeability. *Gastroenterology* **96**, 736-749 (1989).

85 Tavelin, S., Milovic, V., Ocklind, G., Olsson, S. & Artursson, P. A Conditionally Immortalized Epithelial Cell Line for Studies of Intestinal Drug Transport. *Journal of Pharmacology and Experimental Therapeutics* **290**, 1212-1221 (1999).

86 Taipalensuu, J. *et al.* Correlation of Gene Expression of Ten Drug Efflux Proteins of the ATP-Binding Cassette Transporter Family in Normal Human Jejunum and in Human Intestinal Epithelial Caco-2 Cell Monolayers. *Journal of Pharmacology and Experimental Therapeutics* **299**, 164-170 (2001).

87 Wikman, A., Karlsson, J., Carlstedt, I. & Artursson, P. A drug absorption model based on the mucus layer producing human intestinal goblet cell line HT29-H. *Pharm Res* **10**, 843-852 (1993).

88 Behrens, I., Stenberg, P., Artursson, P. & Kissel, T. Transport of lipophilic drug molecules in a new mucus-secreting cell culture model based on HT29-MTX cells. *Pharm Res* **18**, 1138-1145 (2001).

89 Buisine, M. P. *et al.* Mucin gene expression in human embryonic and fetal intestine. *Gut* **43**, 519-524 (1998).

90 Cereijido, M., Robbins, E. S., Dolan, W. J., Rotunno, C. A. & Sabatini, D. D. Polarized monolayers formed by epithelial cells on a permeable and translucent support. *J Cell Biol* **77**, 853-880 (1978).

91 Irvine, J. D. *et al.* MDCK (Madin–Darby canine kidney) cells: A tool for membrane permeability screening. *Journal of Pharmaceutical Sciences* **88**, 28-33, doi:10.1021/js9803205 (1999).

92 Mizutani, T. *et al.* Real-time analysis of P-glycoprotein-mediated drug transport across primary intestinal epithelium three-dimensionally cultured in vitro. *Biochemical and biophysical research communications* **419**, 238-243, doi:10.1016/j.bbrc.2012.01.155 (2012).

93 Kauffman, A. L. *et al.* Alternative functional in vitro models of human intestinal epithelia. *Frontiers in Pharmacology* **4**, 79, doi:10.3389/fphar.2013.00079 (2013).

94 Lennernas, H., Ahrenstedt, O. & Ungell, A. L. Intestinal drug absorption during induced net water absorption in man; a mechanistic study using antipyrine, atenolol and enalaprilat. *Br J Clin Pharmacol* **37**, 589-596 (1994).

95 Lennernäs, H. Human intestinal permeability. *Journal of Pharmaceutical Sciences* **87**, 403-410, doi:10.1021/js970332a (1998).

96 Sjöberg, Å. *et al.* Comprehensive study on regional human intestinal permeability and prediction of fraction absorbed of drugs using the Ussing chamber technique. *European Journal of Pharmaceutical Sciences* **48**, 166-180, doi:http://dx.doi.org/10.1016/j.ejps.2012.10.007 (2013).

97 Huh, D., Torisawa, Y.-s., Hamilton, G. A., Kim, H. J. & Ingber, D. E. Microengineered physiological biomimicry: Organs-on-Chips. *Lab Chip* **12**, 2156-2164, doi:10.1039/c2lc40089h (2012).

98 Kirkland, S. C. Dome formation by a human colonic adenocarcinoma cell line (HCA-7). *Cancer Res* **45**, 3790-3795 (1985).

99 Ramond, M. J., Martinot-Peignoux, M. & Erlinger, S. Dome formation in the human colon carcinoma cell line Caco-2 in culture. Influence of ouabain and permeable supports. *Biol Cell* **54**, 89-92 (1985).

100 Rothen-Rutishauser, B., Braun, A., Günthert, M. & Wunderli-Allenspach, H. Formation of Multilayers in the Caco-2 Cell Culture Model: A Confocal Laser Scanning Microscopy Study. *Pharm Res* **17**, 460-465, doi:10.1023/A:1007585105753 (2000).

101 Costello, C. M. *et al.* Synthetic small intestinal scaffolds for improved studies of intestinal differentiation. *Biotechnol Bioeng* **111**, 1222-1232, doi:10.1002/bit.25180 (2014).

102 Costello, C. M. *et al.* 3-D Intestinal Scaffolds for Evaluating the Therapeutic Potential of Probiotics. *Molecular Pharmaceutics* **11**, 2030-2039, doi:10.1021/mp5001422 (2014).

103 Kim, S. H. *et al.* Three-dimensional intestinal villi epithelium enhances protection of human intestinal cells from bacterial infection by inducing mucin expression. *Integrative biology : quantitative biosciences from nano to macro* **6**, 1122-1131, doi:10.1039/c4ib00157e (2014).

104 Bancroft, J. D. & Gamble, M. *Theory and Practive of Histological Techniques*. (Elsevier, 2008).

105 Hackam, D. G. & Redelmeier, D. A. Translation of research evidence from animals to humans. *Jama* **296**, 1731-1732, doi:10.1001/jama.296.14.1731 (2006).

106 Pound, P., Ebrahim, S., Sandercock, P., Bracken, M. B. & Roberts, I. Where is the evidence that animal research benefits humans? *BMJ* **328**, 514-517, doi:10.1136/bmj.328.7438.514 (2004).

107 Artursson, P. Epithelial transport of drugs in cell culture. I: A model for studying the passive diffusion of drugs over intestinal absorptive (Caco-2) cells. *J Pharm Sci* **79**, 476-482 (1990).

108 Wikman-Larhed, A. & Artursson, P. Co-cultures of human intestinal goblet (HT29-H) and absorptive (Caco-2) cells for studies of drug and peptide absorption. *European Journal of Pharmaceutical Sciences* **3**, 171-183, doi:http://dx.doi.org/10.1016/0928-0987(95)00007-Z (1995).

109 Walter, E., Janich, S., Roessler, B. J., Hilfinger, J. M. & Amidon, G. L. HT29-MTX/Caco-2 cocultures as an in vitro model for the intestinal epithelium: In vitro–in vivo correlation with permeability data from rats and humans. *Journal of Pharmaceutical Sciences* **85**, 1070-1076, doi:10.1021/js960110x (1996).

110 Westerhout, J. *et al.* A new approach to predict human intestinal absorption using porcine intestinal tissue and biorelevant matrices. *Eur J Pharm Sci* **63**, 167-177, doi:10.1016/j.ejps.2014.07.003 (2014).

111 Leonard, F., Collnot, E. M. & Lehr, C. M. A Three-Dimensional Coculture of Enterocytes, Monocytes and Dendritic Cells To Model Inflamed Intestinal Mucosa in Vitro. *Molecular Pharmaceutics* **7**, 2103-2119, doi:10.1021/mp1000795 (2010).

112 Raymond, M. *et al. IL-1β stimulation of CCD-18co myofibroblasts enhances repair of epithelial monolayers through Wnt-5a*. Vol. 303 (2012).

113 Joyce, N. C., Haire, M. F. & Palade, G. E. Morphologic and biochemical evidence for a contractile cell network within the rat intestinal mucosa. *Gastroenterology* **92**, 68-81 (1987).

114 Willemsen, L. E. *et al.* A coculture model mimicking the intestinal mucosa reveals a regulatory role for myofibroblasts in immune-mediated barrier disruption. *Dig Dis Sci* **47**, 2316-2324 (2002).

115 Harrington, H. *et al.* Immunocompetent 3D Model of Human Upper Airway for Disease Modeling and In Vitro Drug Evaluation. *Molecular Pharmaceutics*, doi:10.1021/mp5000295 (2014).

116 Morris, G. E. *et al.* A novel electrospun biphasic scaffold provides optimal three-dimensional topography for in vitro co-culture of airway epithelial and fibroblast cells. *Biofabrication* **6**, 035014, doi:10.1088/1758-5082/6/3/035014 (2014).

117 Lahar, N. *et al.* Intestinal subepithelial myofibroblasts support in vitro and in vivo growth of human small intestinal epithelium. *PLoS One* **6**, e26898, doi:10.1371/journal.pone.0026898 (2011).

118 Eyden, B. Fibroblast phenotype plasticity: relevance for understanding heterogeneity in "fibroblastic" tumors. *Ultrastructural pathology* **28**, 307-319, doi:10.1080/019131290882204 (2004).

119 Eyden, B., Curry, A. & Wang, G. Stromal cells in the human gut show ultrastructural features of fibroblasts and smooth muscle cells but not myofibroblasts. *Journal of cellular and molecular medicine* **15**, 1483-1491, doi:10.1111/j.1582-4934.2010.01132.x (2011).

120 Madison, B. B. *et al.* Epithelial hedgehog signals pattern the intestinal crypt-villus axis. *Development (Cambridge, England)* **132**, 279-289, doi:10.1242/dev.01576 (2005).

121 Ma, B., Von Wasielewski, R., Lindenmaier, W. & Dittmar, K. E. J. Immmunohistochemical Study of the Blood and Lymphatic Vasculature and the Innervation of Mouse Gut and Gut-Associated Lymphoid Tissue. *Anatomia, Histologia, Embryologia* **36**, 62-74, doi:10.1111/j.1439-0264.2006.00741.x (2007).

122 Adegboyega, P. A., Mifflin, R. C., DiMari, J. F., Saada, J. I. & Powell, D. W. Immunohistochemical study of myofibroblasts in normal colonic mucosa, hyperplastic polyps, and adenomatous colorectal polyps. *Archives of pathology & laboratory medicine* **126**, 829-836, doi:10.1043/0003-9985(2002)126<0829:isomin>2.0.co;2 (2002).

123 Simmons, J. G., Pucilowska, J. B., Keku, T. O. & Lund, P. K. IGF-I and TGF-β1 have distinct effects on phenotype and proliferation of intestinal fibroblasts. *American Journal of Physiology - Gastrointestinal and Liver Physiology* **283**, G809-G818, doi:10.1152/ajpgi.00057.2002 (2002).

124 Mifflin, R. C., Pinchuk, I. V., Saada, J. I. & Powell, D. W. Intestinal myofibroblasts: targets for stem cell therapy. *American Journal of Physiology - Gastrointestinal and Liver Physiology* **300**, G684-G696, doi:10.1152/ajpgi.00474.2010 (2011).

125 Armulik, A., Genové, G. & Betsholtz, C. Pericytes: Developmental, Physiological, and Pathological Perspectives, Problems, and Promises. *Developmental Cell* **21**, 193-215, doi:http://dx.doi.org/10.1016/j.devcel.2011.07.001 (2011).

126 Kunz, J., Krause, D., Kremer, M. & Dermietzel, R. The 140-kDa protein of blood-brain barrier-associated pericytes is identical to aminopeptidase N. *Journal of neurochemistry* **62**, 2375-2386 (1994).

127 Alliot, F., Rutin, J., Leenen, P. J. & Pessac, B. Pericytes and periendothelial cells of brain parenchyma vessels co-express aminopeptidase N, aminopeptidase A, and nestin. *Journal of neuroscience research* **58**, 367-378 (1999).

128 Dente, C. J., Steffes, C. P., Speyer, C. & Tyburski, J. G. Pericytes augment the capillary barrier in in vitro cocultures. *J Surg Res* **97**, 85-91, doi:10.1006/jsre.2001.6117 (2001).

129 Dohgu, S. *et al.* Brain pericytes contribute to the induction and up-regulation of blood-brain barrier functions through transforming growth factor-beta production. *Brain research* **1038**, 208-215, doi:10.1016/j.brainres.2005.01.027 (2005).

130 Nakagawa, S. *et al.* A new blood-brain barrier model using primary rat brain endothelial cells, pericytes and astrocytes. *Neurochemistry international* **54**, 253-263, doi:10.1016/j.neuint.2008.12.002 (2009).

131 Hori, S., Ohtsuki, S., Hosoya, K., Nakashima, E. & Terasaki, T. A pericyte-derived angiopoietin-1 multimeric complex induces occludin gene expression in brain capillary endothelial cells through Tie-2 activation in vitro. *Journal of neurochemistry* **89**, 503-513, doi:10.1111/j.1471-4159.2004.02343.x (2004).

132 Luca, A. C. *et al.* Impact of the 3D microenvironment on phenotype, gene expression, and EGFR inhibition of colorectal cancer cell lines. *PLoS One* **8**, e59689, doi:10.1371/journal.pone.0059689 (2013).

133 Anderson, J. M. & Van Itallie, C. M. Physiology and Function of the Tight Junction. *Cold Spring Harbor Perspectives in Biology* **1**, doi:10.1101/cshperspect.a002584 (2009).

134 Flavia Zucco *et al.* An Inter-laboratory Study to Evaluate the Effects of Medium Composition on the Differentiation and Barrier Function of Caco-2 Cell Lines. *ATLA* **33.6** (2005).

135 Lesuffleur, T. *et al.* Dihydrofolate reductase gene amplification-associated shift of differentiation in methotrexate-adapted HT-29 cells. *J Cell Biol* **115**, 1409 - 1418 (1991).

136 Lesuffleur, T., Barbat, A., Dussaulx, E. & Zweibaum, A. Growth adaptation to methotrexate of HT-29 human colon carcinoma cells is associated with their ability to differentiate into columnar absorptive and mucus-secreting cells. *Cancer Res* **50**, 6334-6343 (1990).

137 Menard, S., Cerf-Bensussan, N. & Heyman, M. Multiple facets of intestinal permeability and epithelial handling of dietary antigens. *Mucosal Immunol* **3**, 247-259, doi:10.1038/mi.2010.5 (2010).

138 Park, J. E. *et al.* Fibroblast activation protein, a dual specificity serine protease expressed in reactive human tumor stromal fibroblasts. *The Journal of biological chemistry* **274**, 36505-36512 (1999).

139 Scanlan, M. J. *et al.* Molecular cloning of fibroblast activation protein alpha, a member of the serine protease family selectively expressed in stromal fibroblasts of epithelial cancers. *Proceedings of the National Academy of Sciences of the United States of America* **91**, 5657-5661 (1994).

140 Kourtidis, A. *et al.* Distinct E-cadherin-based complexes regulate cell behaviour through miRNA processing or Src and p120 catenin activity. *Nat Cell Biol* **17**, 1145-1157, doi:10.1038/ncb3227 (2015).

141 Schwarzbauer, J. Basement membrane: Putting up the barriers. *Current Biology* **9**, R242-R244, doi:http://dx.doi.org/10.1016/S0960-9822(99)80153-5 (1999).

142 Tanjore, H. & Kalluri, R. The Role of Type IV Collagen and Basement Membranes in Cancer Progression and Metastasis. *The American Journal of Pathology* **168**, 715-717, doi:10.2353/ajpath.2006.051321 (2006).

143 Osawa, T., Onodera, M., Feng, X. Y. & Nozaka, Y. Comparison of the thickness of basement membranes in various tissues of the rat. *Journal of Electron Microscopy* **52**, 435-440, doi:10.1093/jmicro/52.4.435 (2003).

144 Kalluri, R. Basement membranes: structure, assembly and role in tumour angiogenesis. *Nat Rev Cancer* **3**, 422-433 (2003).

145 Stevens, M. M. & George, J. H. Exploring and Engineering the Cell Surface Interface. *Science* **310**, 1135-1138, doi:10.1126/science.1106587 (2005).

146 Baker, S. C. *et al.* Characterisation of electrospun polystyrene scaffolds for three-dimensional in vitro biological studies. *Biomaterials* **27**, 3136-3146, doi:http://dx.doi.org/10.1016/j.biomaterials.2006.01.026 (2006).

147 Sun, T. *et al.* Development of a 3D cell culture system for investigating cell interactions with electrospun fibers. *Biotechnol Bioeng* **97**, 1318-1328, doi:10.1002/bit.21309 (2007).

148 Agarwal, S., Wendorff, J. H. & Greiner, A. Use of electrospinning technique for biomedical applications. *Polymer* **49**, 5603-5621, doi:http://dx.doi.org/10.1016/j.polymer.2008.09.014 (2008).

149 Ma, Z., Kotaki, M., Yong, T., He, W. & Ramakrishna, S. Surface engineering of electrospun polyethylene terephthalate (PET) nanofibers towards development of a new material for blood vessel engineering. *Biomaterials* **26**, 2527-2536, doi:http://dx.doi.org/10.1016/j.biomaterials.2004.07.026 (2005).

150 Liang, D., Hsiao, B. S. & Chu, B. Functional electrospun nanofibrous scaffolds for biomedical applications. *Advanced Drug Delivery Reviews* **59**, 1392-1412, doi:10.1016/j.addr.2007.04.021 (2007).

151 Biltresse, S., Attolini, M. & Marchand-Brynaert, J. Cell adhesive PET membranes by surface grafting of RGD peptidomimetics. *Biomaterials* **26**, 4576-4587, doi:10.1016/j.biomaterials.2004.11.042 (2005).

152 Grafahrend, D. *et al.* Degradable polyester scaffolds with controlled surface chemistry combining minimal protein adsorption with specific bioactivation. *Nat Mater* **10**, 67-73, doi:http://www.nature.com/nmat/journal/v10/n1/abs/nmat2904.html#supplementary-information (2011).

153 Rogers, C. M. *et al.* A novel technique for the production of electrospun scaffolds with tailored three-dimensional micro-patterns employing additive manufacturing. *Biofabrication* **6**, 035003 (2014).

154 Wang, C., Lee, M.-F. & Wu, Y.-J. Solution-Electrospun Poly(ethylene terephthalate) Fibers: Processing and Characterization. *Macromolecules* **45**, 7939-7947, doi:10.1021/ma300121k (2012).

155 Greiner, A. & Wendorff, J. H. Electrospinning: A Fascinating Method for the Preparation of Ultrathin Fibers. *Angewandte Chemie International Edition* **46**, 5670-5703, doi:10.1002/anie.200604646 (2007).

156 Han, D. & Gouma, P. I. Electrospun bioscaffolds that mimic the topology of extracellular matrix. *Nanomedicine : nanotechnology, biology, and medicine* **2**, 37-41, doi:10.1016/j.nano.2006.01.002 (2006).

157 Nezarati, R. M., Eifert, M. B. & Cosgriff-Hernandez, E. Effects of humidity and solution viscosity on electrospun fiber morphology. *Tissue engineering. Part C, Methods* **19**, 810-819, doi:10.1089/ten.TEC.2012.0671 (2013).

158 De Schoenmaker, B. *et al.* Effect of the relative humidity on the fibre morphology of polyamide 4.6 and polyamide 6.9 nanofibres. *J Mater Sci* **48**, 1746-1754, doi:10.1007/s10853-012-6934-9 (2013).

159 Moreno, M. J. *et al.* Development of a compliant and cytocompatible micro-fibrous polyethylene terephthalate vascular scaffold. *Journal of biomedical materials research. Part B, Applied biomaterials* **97**, 201-214, doi:10.1002/jbm.b.31774 (2011).

160 Hadjizadeh, A., Ajji, A. & Bureau, M. N. Nano/micro electro-spun polyethylene terephthalate fibrous mat preparation and characterization. *J Mech Behav Biomed Mater* **4**, 340-351, doi:10.1016/j.jmbbm.2010.10.014 (2011).

161 Michelmore, A., Steele, D. A., Whittle, J. D., Bradley, J. W. & Short, R. D. Nanoscale deposition of chemically functionalised films via plasma polymerisation. *RSC Advances* **3**, 13540-13557, doi:10.1039/C3RA41563E (2013).

162 Kumar, G. & Prabhu, K. N. Review of non-reactive and reactive wetting of liquids on surfaces. *Advances in Colloid and Interface Science* **133**, 61-89, doi:http://dx.doi.org/10.1016/j.cis.2007.04.009 (2007).

163 Wagner, M. S. & Castner, D. G. Characterization of Adsorbed Protein Films by Time-of-Flight Secondary Ion Mass Spectrometry with Principal Component Analysis. *Langmuir* **17**, 4649-4660, doi:10.1021/la001209t (2001).

164 GJ, T. & SR, G. *Principles of anatomy and physiology*. (Harper Collins College., 1993).

165 Li, Z. & Wang, C. *One-Dimensional nanostructures: Electrospinning Technique and Unique Nanofibers*. (2013).

166 Bye, F. J. *et al.* Development of a Basement Membrane Substitute Incorporated Into an Electrospun Scaffold for 3D Skin Tissue Engineering. *Journal of Biomaterials and Tissue Engineering* **4** (2014).

167 Bye, F. J. *et al.* Development of bilayer and trilayer nanofibrous/microfibrous scaffolds for regenerative medicine. *Biomaterials Science* **1**, 942-951, doi:10.1039/C3BM60074B (2013).

168 Guan, Y. *et al.* Redistribution of the tight junction protein ZO-1 during physiological shedding of mouse intestinal epithelial cells. *Am J Physiol Cell Physiol* **300**, C1404-1414, doi:10.1152/ajpcell.00270.2010 (2011).

169 Williams, J. M. *et al.* Epithelial Cell Shedding and Barrier Function: A Matter of Life and Death at the Small Intestinal Villus Tip. *Veterinary Pathology*, doi:10.1177/0300985814559404 (2014).

170 Tamada, Y. & Ikada, Y. Cell adhesion to plasma-treated polymer surfaces. *Polymer* **34**, 2208-2212, doi:http://dx.doi.org/10.1016/0032-3861(93)90752-V (1993).

171 Bhattacharyya, D., Xu, H., Deshmukh, R. R., Timmons, R. B. & Nguyen, K. T. Surface chemistry and polymer film thickness effects on endothelial cell adhesion and proliferation. *Journal of biomedical materials research. Part A* **94**, 640-648, doi:10.1002/jbm.a.32713 (2010).

172 Colley, H. E., Mishra, G., Scutt, A. M. & McArthur, S. L. Plasma Polymer Coatings to Support Mesenchymal Stem Cell Adhesion, Growth and Differentiation on Variable Stiffness Silicone Elastomers. *Plasma Processes and Polymers* **6**, 831-839, doi:10.1002/ppap.200900040 (2009).

173 Lennernäs, H., Palm, K., Fagerholm, U. & Artursson, P. Comparison between active and passive drug transport in human intestinal epithelial (caco-2) cells in vitro and human jejunum in vivo. *International Journal of Pharmaceutics* **127**, 103-107, doi:http://dx.doi.org/10.1016/0378-5173(95)04204-0 (1996).

174 Amidon, G., Lennernäs, H., Shah, V. & Crison, J. A Theoretical Basis for a Biopharmaceutic Drug Classification: The Correlation of in Vitro Drug Product Dissolution and in Vivo Bioavailability. *Pharm Res* **12**, 413-420, doi:10.1023/a:1016212804288 (1995).

175 U.S. Department of Health and Human Services, F. D. A. Waiver of In Vivo Bioavailability and Bioequivalence Studies for Immediate-Release Solid Oral Dosage Forms Based on a Biopharmaceutics Classification System Guidance for Industry. (Center for Drug Evaluation and Research (CDER), 2015).

176 Pontier, C., Pachot, J., Botham, R., Lenfant, B. & Arnaud, P. HT29-MTX and Caco-2/TC7 monolayers as predictive models for human intestinal absorption: role of the mucus layer. *J Pharm Sci* **90**, 1608-1619 (2001).

177 Forstner, J. F. F., G. G. . in *Gastrointestinal mucus* (ed L. R. Johnson) 1255-1283 (Raven Press: New York, 1994).

178 Lennernas, H. Intestinal permeability and its relevance for absorption and elimination. *Xenobiotica; the fate of foreign compounds in biological systems* **37**, 1015-1051, doi:10.1080/00498250701704819 (2007).

179 Berschneider, H. M. & Powell, D. W. Fibroblasts modulate intestinal secretory responses to inflammatory mediators. *Journal of Clinical Investigation* **89**, 484-489 (1992).

180 Halttunen, T., Marttinen, A., Rantala, I., Kainulainen, H. & Maki, M. Fibroblasts and transforming growth factor beta induce organization and differentiation of T84 human epithelial cells. *Gastroenterology* **111**, 1252-1262, doi:http://dx.doi.org/10.1053/gast.1996.v111.pm8898639 (1996).

181 Moeser, A. J. *et al.* Stress signaling pathways activated by weaning mediate intestinal dysfunction in the pig. *American journal of physiology. Gastrointestinal and liver physiology* **292**, G173-181, doi:10.1152/ajpgi.00197.2006 (2007).

182 Rozehnal, V. *et al.* Human small intestinal and colonic tissue mounted in the Ussing chamber as a tool for characterizing the intestinal absorption of drugs. *European Journal of Pharmaceutical Sciences* **46**, 367-373, doi:http://dx.doi.org/10.1016/j.ejps.2012.02.025 (2012).

183 Östh, K., Gråsjö, J. & Björk, E. A new method for drug transport studies on pig nasal mucosa using a horizontal Ussing chamber. *Journal of Pharmaceutical Sciences* **91**, 1259-1273, doi:10.1002/jps.10123 (2002).

184 Sun, H., Chow, E. C., Liu, S., Du, Y. & Pang, K. S. The Caco-2 cell monolayer: usefulness and limitations. *Expert opinion on drug metabolism & toxicology* **4**, 395-411, doi:10.1517/17425255.4.4.395 (2008).

185 Saada, J. I. *et al.* Subepithelial Myofibroblasts are Novel Nonprofessional APCs in the Human Colonic Mucosa. *The Journal of Immunology* **177**, 5968-5979 (2006).

186 Desmouliere, A., Chaponnier, C. & Gabbiani, G. Tissue repair, contraction, and the myofibroblast. *Wound repair and regeneration : official publication of the Wound Healing Society [and] the European Tissue Repair Society* **13**, 7-12, doi:10.1111/j.1067-1927.2005.130102.x (2005).

187 Winkler, E. A., Bell, R. D. & Zlokovic, B. V. Pericyte-specific expression of PDGF beta receptor in mouse models with normal and deficient PDGF beta receptor signaling. *Molecular neurodegeneration* **5**, 32, doi:10.1186/1750-1326-5-32 (2010).

188 Ozerdem, U., Grako, K. A., Dahlin-Huppe, K., Monosov, E. & Stallcup, W. B. NG2 proteoglycan is expressed exclusively by mural cells during vascular morphogenesis. *Developmental dynamics : an official publication of the American Association of Anatomists* **222**, 218-227, doi:10.1002/dvdy.1200 (2001).

189 Itallie, C. M. V. & Anderson, J. M. Claudins and epithelial paracellular transport. *Annual Review of Physiology* **68**, 403-429, doi:doi:10.1146/annurev.physiol.68.040104.131404 (2006).

190 Cato, P. *Development of an in vitro human 3D immunocompetent upper respiratory tract model* PhD thesis, University of Nottingham, (2014).

191 Hagios, C., Lochter, A. & Bissell, M. J. Tissue architecture: the ultimate regulator of epithelial function? *Philos Trans R Soc Lond B Biol Sci* **353**, 857-870, doi:10.1098/rstb.1998.0250 (1998).

192 Nicklin, P., Irwin, B., Hassan, I., Williamson, I. & Mackay, M. Permeable support type influences the transport of compounds across Caco-2 cells. *International Journal of Pharmaceutics* **83**, 197-209, doi:http://dx.doi.org/10.1016/0378-5173(82)90023-0 (1982).

193 Behrens, I. & Kissel, T. Do cell culture conditions influence the carrier-mediated transport of peptides in Caco-2 cell monolayers? *European Journal of Pharmaceutical Sciences* **19**, 433-442, doi:http://dx.doi.org/10.1016/S0928-0987(03)00146-5 (2003).

194 Yumoto, R. *et al.* Transport of rhodamine 123, a P-glycoprotein substrate, across rat intestine and Caco-2 cell monolayers in the presence of cytochrome P-450 3A-related compounds. *J Pharmacol Exp Ther* **289**, 149-155 (1999).

195 Oga, E. F., Sekine, S., Shitara, Y. & Horie, T. Potential P-glycoprotein-mediated drug-drug interactions of antimalarial agents in Caco-2 cells. *The American journal of tropical medicine and hygiene* **87**, 64-69, doi:10.4269/ajtmh.2012.11-0817 (2012).

8. Appendix

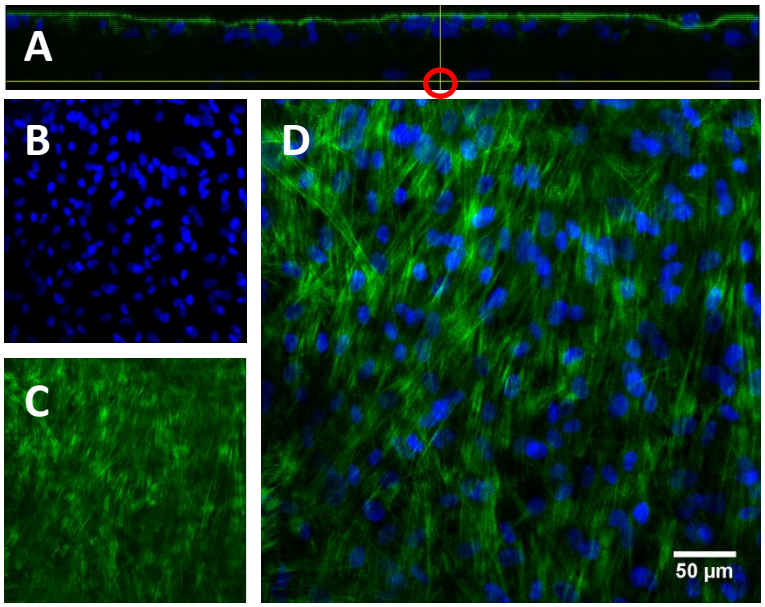

Figure A-1. Confocal cross section of Caco-2/18co transwell culture. (A) XZ cross section stack of Caco-2/18co transwell co-culture. Red circle indicates confocal cross section represented in (B-D). (B-D) Composite immunostained images showing cell nuclei (blue) and F-actin (green) of CCD-18co. (D) Merged image demonstrating CCD-18co presence on the underside of transwell co-cultures.

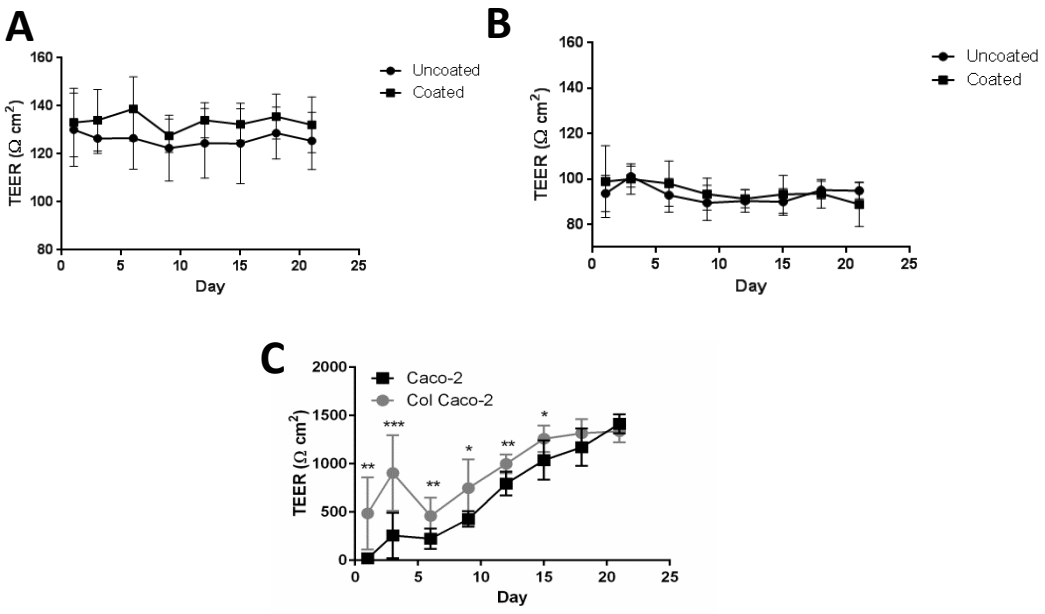

Figure A-2. The effect of collagen coating on TEER. (A) Collagen type I coated and uncoated acellular transwell inserts over a 21 day culture period. (B) Collagen type I coated and uncoated acellular nanofibre inserts over a 21 day culture period. (C) Comparison of Caco-2 TEER over 21 days on collagen coated and non-collagen coated transwell inserts. n=6-9 from a minimum of two independent experiments.

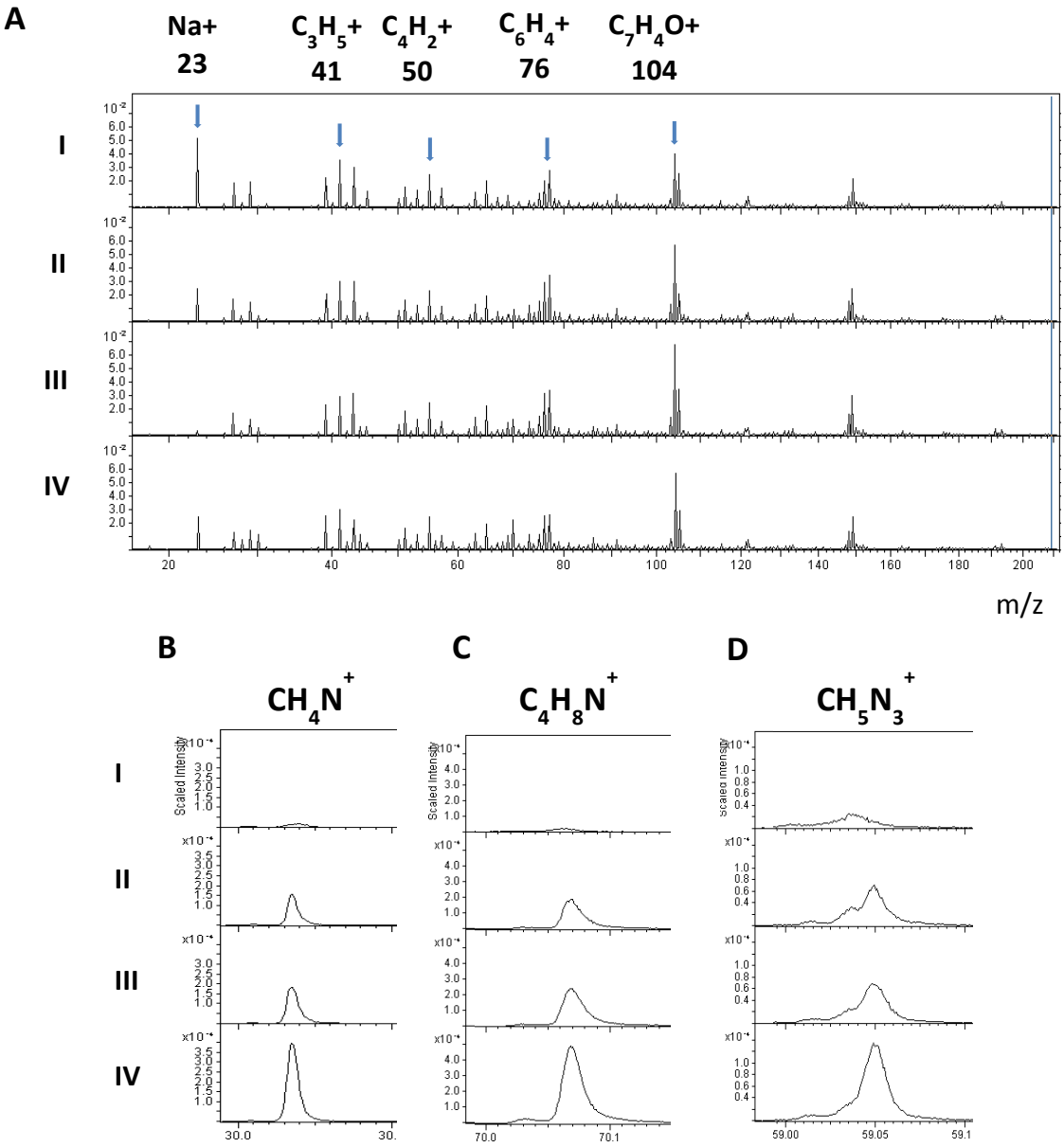

Figure A-3. ToF-SIMS spectral data and representative nitrogen contain fragments of collagen surface treatment of nanofibre scaffolds.. (A) Survey spectra of (A-I) untreated nanofibre, (A-II) 31µg/ mL treated nanofbre scaffold (washed), (A-III) 31µg/ mL treated nanofbre scaffold and (A-IV) 3. 1 mg/ mL treated nanofibre scaffold. (B-D) Comparison of nitrogen containing positive ion fragment peaks. (B-I) untreated nanofibre, (B-II) 31µg/ mL treated nanofibre scaffold (washed), (B-III) 31µg/ mL treated nanofibre scaffold and (B-IV) 3. 1 mg/ mL treated nanofibre scaffold

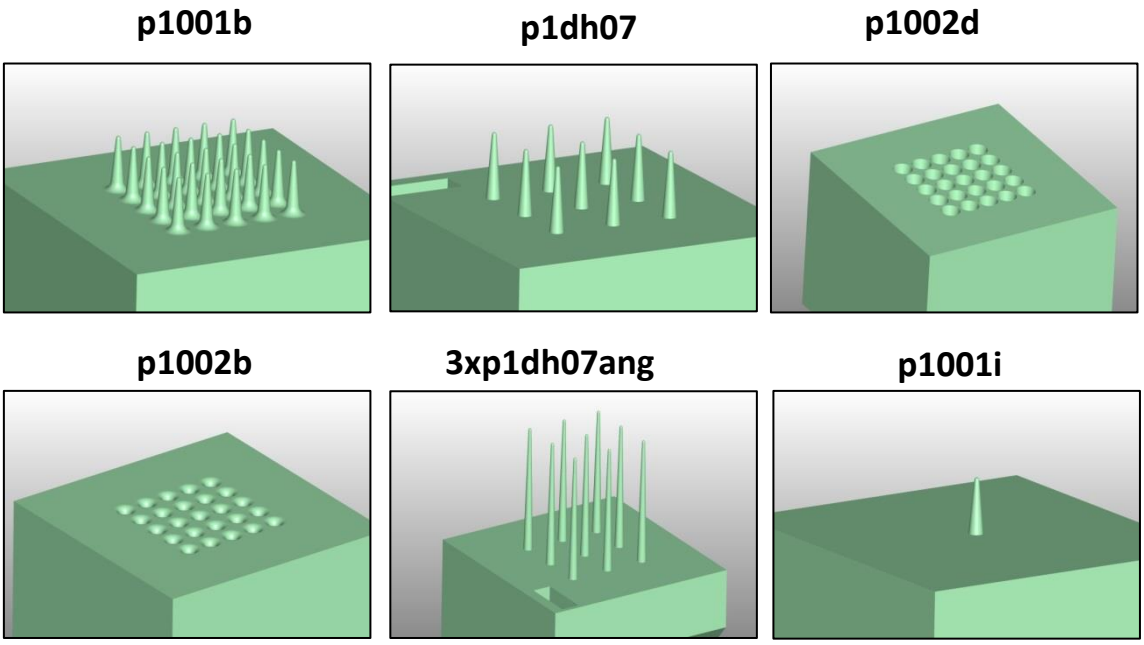

Figure A-4. Representative 3D reproductions of villi former designs.

Table A-1. Villi former dimensions

	Villi dimensions (mm)				
Model Reference	tip to tip	base to base	height	Array	Notes
p1dh07	0.8	0.6	0.7	3 x 3	
3xp1dh07ang	0.8	0.6	2	3x3	
3xp1ih07ang	n/a	n/a	2	1	
p1ih07	n/a	n/a	0.7	1	
p2ed036	0.8	0.3	0.7	3	
p1001a	0.4	0.04	0.6	5x5	
p1001b	0.4	0.04	0.6	5x5	
p1001c	0.4	0.2	0.6	5x5	
p1001c	0.4	0.2	0.6	5x5	Flat topped
p1001d	0.8	0.6	0.7	3x3	
p1001ix2				1	single villi
p1001i	n/a	n/a	0.6	1	single villi
p1002d	0.4	0.04	0.6	5x5	inverted array
p1002d2	0.8	0.45	0.6	3x3	double spaced inverted array
p1002b	0.4	0.04	0.6	5x5	inverted array graduated base

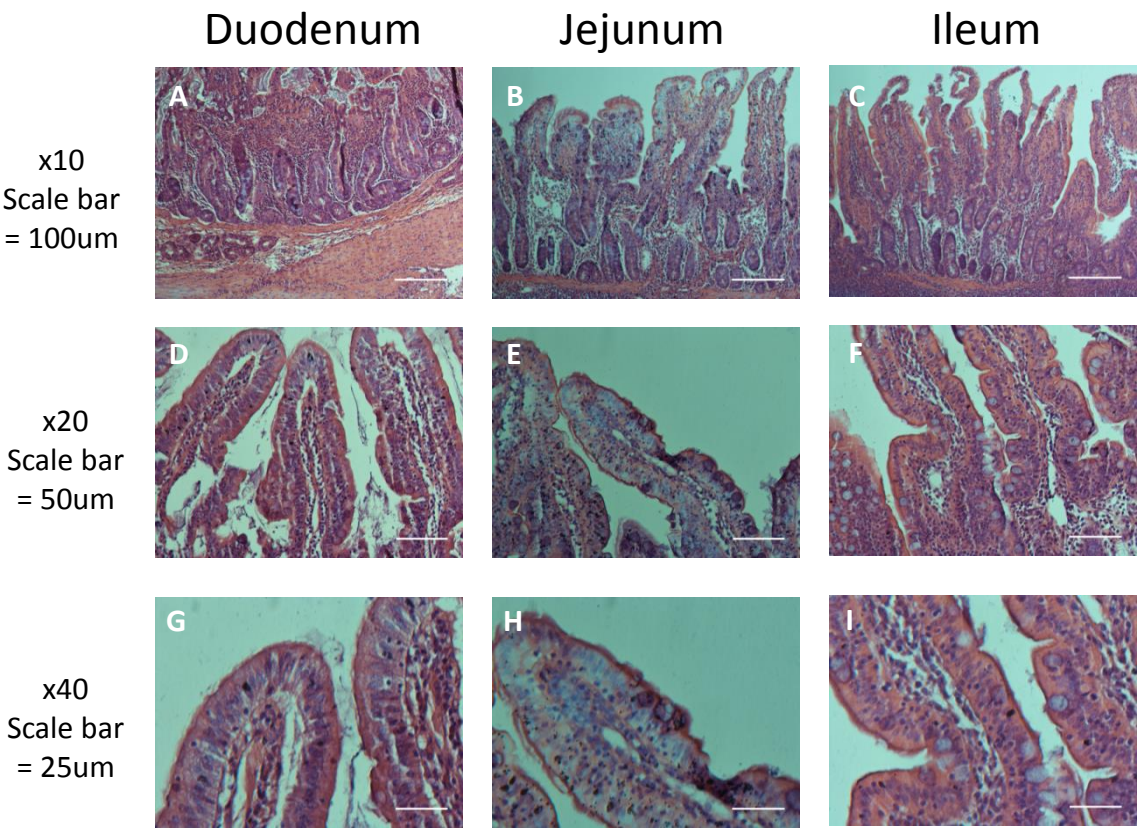

Figure A-5. Routine H&E staining of porcine intestinal segments at various magnifications.

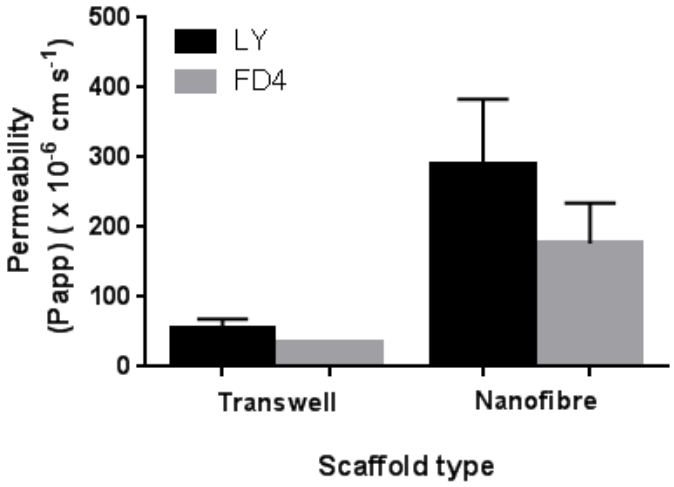

Figure A-6. Lucifer yellow and FD4 permeability of acellular transwell and nanofibre scaffolds. Values represent mean (± SD), n=2-3.

Table A-2. Efflux ratios for Rhodamine 123 permeability for *in vitro* models and porcine intestinal segments.

Substrate	Model	Efflux Ratio
Trans	Caco-2	4.6
	Caco-2/18co	2.8
Nano	Caco-2	1.1
	Caco-2/18co	0.6
Porcine	Duodenum	0.3
	Jejunum	0.5
	Ileum	0.4

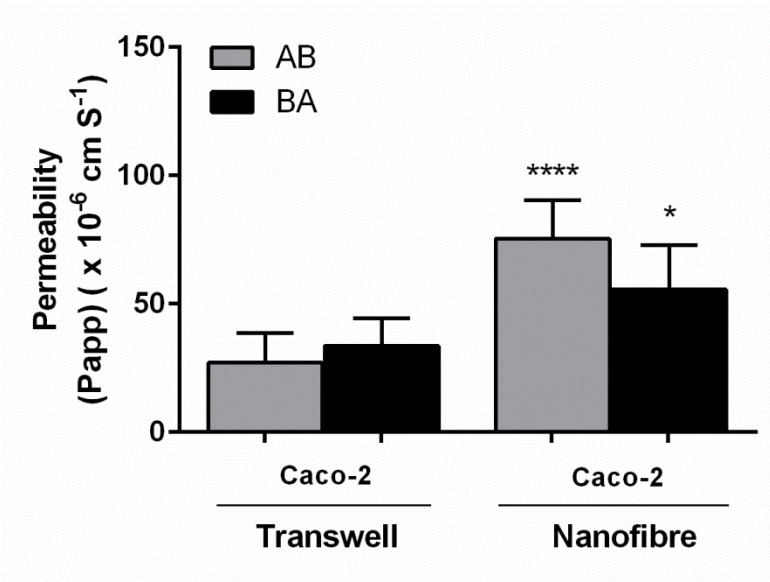

Figure A-7. Bidirectional verapamil permeability (active transport) in Caco-2 transwell and nanofibre monocultures. Values represent mean (± SD), n=4-6 from 2-3 independent experiments. Significance determined by One-Way ANOVA with Sidaks multiple comparisons. *p≤0.05, ****p≤0.0001.

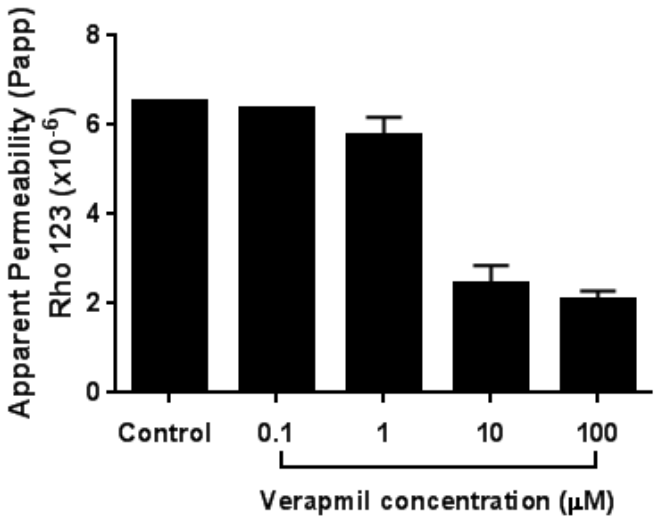

Figure A-8. Basolateral to apical (BA) permeability of Rhodamine 123 with co incubation with p-gp inhibitor verapamil. Values represent mean (± SD), n=1-3 from a singlet experiment.